Scaling Studies for Advanced High Temperature Reactor Concepts
Nuclear Energy University Program, Project 14-6794

Final Technical Report: October 2014—December 2017

Submitted to:	US Department of Energy
Date Submitted:	March 26, 2018
Project Start Date:	October 1, 2014
Project End Date:	December 31, 2017
Award Number:	DE-NE0008294
Collaborators:	Oregon State University General Atomics

School of Nuclear Science and Engineering
Oregon State University; DUNS: 053599908
116 Radiation Center
Corvallis, OR 97331-5902

Principal Investigator:
Brian Woods, Professor
brian.woods@oregonstate.edu
541-737-6335

CONTENTS

Page

EXECUTIVE SUMMARY

Computer simulations of nuclear reactor thermal-hydraulic phenomena are often used in the design and licensing of nuclear reactor systems. In order to assess the accuracy of these computer simulations, computer codes and methods are often validated against experimental data. This experimental data must be of sufficiently high quality in order to conduct a robust validation exercise. In addition, this experimental data is generally collected at experimental facilities that are of a smaller scale than the reactor systems that are being simulated due to cost considerations. Therefore, smaller scale test facilities must be designed and constructed in such a fashion to ensure that the prototypical behavior of a particular nuclear reactor system is preserved.

The work completed through this project has resulted in scaling analyses and conceptual design development for a test facility capable of collecting code validation data for the following high temperature gas reactor systems and events—

1. Passive natural circulation core cooling system,
2. pebble bed gas reactor concept,
3. General Atomics Energy Multiplier Module reactor, and
4. prismatic block design steam-water ingress event.

In the event that code validation data for these systems or events is needed in the future, significant progress in the design of an appropriate integral-type test facility has already been completed as a result of this project. Where applicable, the next step would be to begin the detailed design development and material procurement.

As part of this project applicable scaling analyses were completed and test facility design requirements developed. Conceptual designs were developed for the implementation of these design requirements at the Oregon State University (OSU) High Temperature Test Facility (HTTF). The original HTTF is based on a ¼-scale model of a high temperature gas reactor concept with the capability for both forced and natural circulation flow through a prismatic core with an electrical heat source. The peak core region temperature capability is 1400°C.

As part of this project, an inventory of test facilities that could be used for these experimental programs was completed. Several of these facilities showed some promise, however, upon further investigation it became clear that only the OSU HTTF had the power and/or peak temperature limits that would allow for the experimental programs envisioned herein. Thus the conceptual design and feasibility study development focused on examining the feasibility of configuring the current HTTF to collect validation data for these experimental programs.

In addition to the scaling analyses and conceptual design development, a test plan was developed for the envisioned modified test facility. This test plan included a discussion on an appropriate shakedown test program as well as the specific matrix tests. Finally, a feasibility study was completed to determine the cost and schedule considerations that would be important to any test program developed to investigate these designs and events.

1. INTRODUCTION

The scope of this project was to expand the utilization of the Oregon State University (OSU) High Temperature Test Facility (HTTF) to the validation of design and safety thermal-hydraulics methods developed for a broader range of advanced high temperature reactors and events. While the HTTF was originally built for a prismatic block High Temperature Gas Reactor (HTGR), it can be expanded to other advanced gas-cooled reactors as well as key safety aspects of other high temperature reactors such as molten salt and even sodium cooled reactors.

The original HTTF is based on a ¼-scale model of an HTGR with the capability for both forced and natural circulation flow through the prismatic core with an electrical heat source. The peak core region temperature capability is 1400°C. The facility could be modified to simulate safety-related passive natural circulation core cooling with heat rejection to air as well as passive containment cooling. Both these features are essential to several advanced high temperature reactor concepts including advanced gas-cooled fast reactors, molten salt reactors and sodium cooled reactors. Although the fluids may be different, the computation methods for flow distribution, coupled natural circulation loops and direct heat rejection to air are similar. This later aspect is an important safety feature of advanced high temperature reactors in that their safety cooling systems reject heat to air through a heat exchanger rather than by evaporative cooling which requires water replenishment within 72 hrs.

In addition, there are several advanced gas reactor designs that are radically different in both geometry and operation from the prismatic block HTGR. Two such examples include the pebble bed core type gas reactor and the General Atomics Energy Multiplier Module (EM^2) reactor. The existing test facility could be modified to model these gas reactor types. Also, there were several accident scenarios identified in the DOE and NRC gas reactor Phenomenon Identification and Ranking Tables (PIRT) that were not addressed in the original scaling analysis for this test facility. These include steam-water ingress events and process plant coupling events, each of which could be explored using the current test facility, if modified.

The purpose of this project was to revise the scaling analyses of the OSU HTTF to add a detailed scaling analysis of (1) a passive natural circulation core cooling system, (2) a pebble bed gas reactor concept, (3) the General Atomics Energy Multiplier Module (EM^2) reactor, as well as (4) the utilization of the test facility for transients that were not included in the original scaling analyses. The test facility will not be able to provide high-quality data for these designs and transients as currently configured and thus this work also included the development of a set of design requirements, required modifications and a feasibility study for each of these different scaling sets.

2. ACCOMPLISHMENTS

This project was divided into four separate objectives. The accomplishments for each are summarized below. Over the course of this project seven graduate and seven undergraduate students have contributed to its progression. The work has directly supported two Master's Theses and one full conference paper.

2.1. Scaling and Design Requirements

This objective included the following tasks:

1. Review of existing test facilities available to meet the data needs for the applicable scenarios.
2. Completion of preliminary PIRTs for the EM^2 type reactor and the steam-water ingress events for all gas reactor types.
3. Completion of scaling analyses for the (1) passive natural circulation cooling system, (2) pebble bed core type gas reactor, (3) EM^2 type reactor, and (4) steam-water ingress events. These scaling analyses were intended to be general enough that they could be applied to any integral level test facility to investigate each of these scenarios, and would not just be test facility specific. The scaling analyses included the development of system level and computational fluid dynamics (CFD) thermal fluid models to be used to inform the scaling process as needed.
4. Development of design requirements that translate the scaling analyses into specific design recommendations for the test facility.

Completion of this objective and associated tasks were documented in the *Scaling and Design Requirements Technical Report* deliverable completed on January 29, 2016. This report included discussion of scaling methodologies used, a description of method application and scaling results obtained. Design requirements were outlined and discussed.

General Atomics completed a review of the *Scaling and Design Requirements Technical Report* in 2017. A revised version of the *Scaling and Design Requirements Technical Report* was submitted in December of 2017, incorporating the comments from General Atomics and revisions as a result of completion of the *Feasibility Study*.

2.2. Design of Test Facility

This objective included the following tasks:

1. Develop a conceptual design of the experimental apparatus including hardware, software and data acquisition systems that would be required to meet the design requirements developed under this work.
2. Develop a conceptual instrumentation plan for each of the systems or events covered under this work.

Completion of this objective was documented in the *Test Facility Description Technical Report* deliverable completed on February 28, 2017. General Atomics completed a review of the *Test Facility Description Technical Report* during 2017. A revised version of the *Test Facility Description Technical Report* was submitted on December 22, 2017, incorporating the comments from General Atomics and revisions as a result of completion of the *Feasibility Study*.

2.3. Test Plan

This objective included the development of both the shakedown test plan and the matrix test plan. The shakedown test plan included a description of tests required to prepare and condition the experimental apparatus to conduct quality matrix tests. The matrix test plan included documentation of the experiment design and rationale. General initial and transient conditions were included.

Completion of this objective was documented in the *Test Plan Technical Report* deliverable completed on May 12, 2017. General Atomics completed a review of the *Test Plan Technical Report* during the fall of 2017 with no comment.

2.4. Feasibility Study

The feasibility study included anticipated budgets and schedules required to complete the work outlined in objectives 2.2 and 2.3 at the OSU HTTF. In order to develop these budgets and schedules additional detail on the conceptual designs for the facility and instrumentation packages originally outlined in objective 2.2 was provided.

Completion of this objective was documented in the *Feasibility Study Technical Report* deliverable completed on December 21, 2017. The *Feasibility Study Technical Report* covered three major areas—the Pebble Bed Reactor, the EM^2 with a Passive Natural Circulation Cooling System, and the Steam Water Ingress Event. The feasibility study examined the ability of the OSU HTTF to serve as an experimental test facility to explore these systems and events.

In the *Scaling and Design Requirements Technical Report* an inventory of test facilities that could be used for these experimental programs, other than the OSU HTTF, was completed. Several of these facilities showed some promise, however, upon further investigation it became clear that none of these facilities had the power and/or peak temperature limits that would allow for the experimental programs envisioned herein. Therefore, the *Feasibility Study Technical Report* focused on examining the feasibility of configuring the current HTTF to collect validation data for these experimental programs.

In the *Feasibility Study Technical Report* it was noted that all test programs completed at the HTTF will be conducted under the OSU *HTTF Program Quality Plan* (PQP). The HTTF PQP establishes the general requirements to assure the quality of test data collected at the HTTF by controlling all aspects of maintenance and operations that affect the integrity of matrix test data. The latest revisions of the following documents constitute PQP requirements to the extent specified in the PQP.

1. 10CFR21, Reporting of Defects and Noncompliance.
2. 10CFR50, Appendix B, Quality Assurance Criteria for Nuclear Power Plants and Fuel Reprocessing Plants.
3. ANSI/ASME NQA-1a-2009, Addendum to ASME NQA-1-2008, Quality Assurance Requirements for Nuclear Facility Applications.
4. ANSI/ASME NQA-1-2008, Quality Assurance Requirements for Nuclear Facility Applications.
5. OSU Safety Policy and Procedure Manual.

Any modifications to the HTTF and the maintenance and operation of any modified test facility would be conducted under the OSU HTTF Program Quality Program.

The *Feasibility Study Technical Report* is the culmination of the work for this project and is thus included in Appendix A to document project outcomes.

3. PRODUCTS

This project has resulted in the development of following four Oregon State University internal technical reports—

1. *Scaling Studies for Advanced High Temperature Reactor Concepts, Scaling and Design Requirements Technical Report,* Revision 1, December 22, 2017,
2. *Scaling Studies for Advanced High Temperature Reactor Concepts, Test Facility Description Technical Report,* Revision 2, December 22, 2017,
3. *Scaling Studies for Advanced High Temperature Reactor Concepts, Test Plan Technical Report,* Revision 1, May 12, 2017, and
4. *Scaling Studies for Advanced High Temperature Reactor Concepts, Feasibility Study Technical Report,* December 21, 2017.

This project has resulted in the following full paper conference publication—

1. Gutowska, I., Coddington, T. N., and Woods, B. G., Feasibility Study Of The Pebble Bed High Temperature Test Facility, *Proceedings 2018 International Congress on Advances in Nuclear Power Plants (ICAPP 18)*, April 2018. (accepted) (attached as Appendix A)

In addition, the following two Master's Theses were developed in support of this work—

1. Cox, J., *Scaling of the Chinese HTR-PM Reactor Design for Licensing and Testing at the Oregon State University High Temperature Test Facility*, M.S. Thesis, Oregon State University, 2015, and
2. Blake, G., *Scaling Analysis of the Direct Reactor Auxiliary Cooling System for Gas-cooled Fast Reactors during a Depressurized Loss of Forced Convection Event*, M.S. Thesis, Oregon State University, 2016.

4. IMPACT

Computer simulations of nuclear reactor thermal-hydraulic phenomena are often used in the design and licensing of nuclear reactor systems. In order to assess the accuracy of these computer simulations, computer codes and methods are often validated against experimental data. This experimental data must be of sufficiently high quality in order to conduct a robust validation exercise. In addition, this experimental data is generally collected at experimental facilities that are of a smaller scale than the reactor systems that are being simulated due to cost considerations. Therefore, smaller scale test facilities must be designed and constructed in such a fashion to ensure that the prototypical behavior of a particular nuclear reactor system is preserved.

The work completed through this project has resulted in scaling analyses and conceptual design development for a test facility capable of collecting code validation data for the following high temperature gas reactor systems and events—

1. Passive natural circulation core cooling system,
2. pebble bed gas reactor concept,
3. General Atomics Energy Multiplier Module reactor, and
4. prismatic block design steam-water ingress event.

In the event that code validation data for these systems or events is needed in the future, significant progress in the design of an appropriate integral-type test facility has already been completed as a result of this project. Where applicable, the next step would be to begin the detailed design development and material procurement.

This work also potentially impacts other disciplines in the sense that the computer simulations that are used to model the fluid dynamics and heat transfer phenomena occurring in a high temperature gas reactor can also be used to model fluid dynamics and heat transfer in other situations. Thus the tools that are developed and validated using the data collected under any facility that results from this work could potentially be used in any discipline where the computer modeling of fluid dynamics and heat transfer is important.

This project provided valuable research experience for seven graduate and seven undergraduate students over the course of the project. It is anticipated that these student will eventually be able to take away what they learned on this project as they move on in their nuclear engineering careers.

APPENDIX A

Scaling Studies for Advanced High Temperature Reactor Concepts
Feasibility Study Technical Report

Date Published: December 21, 2017

Prepared by:
Izabela Gutowska
Taylor Coddington
Stephen Louria
Brian Woods

School of Nuclear Science and Engineering
Oregon State University
116 Radiation Center
Corvallis, OR 97331-5902

Prepared for:
NEUP

Contents

ABBREVIATIONS

ANSEL	Advanced Nuclear System Engineering Laboratory
D-LOFC	Depressurized loss of forced convection
DHX	Direct Heat Exchanger
DOE	Department of Energy
DPT	Differential pressure transmitter
DRACS	Direct Reactor Auxiliary Cooling Systems
EM^2	Energy Multiplier Module
GCI	Gas Concentration Instruments
HTGR	High Temperature Gas Reactor
HTTF	High Temperature Test Facility
LAS	Laser absorption spectroscopy
MCSS	Metallic Core Support Structure
MEMS	Micro-Electro-Mechanical Systems
MHC	Molybdenum-Hafnium-Carbon
MHTGR	Modular High Temperature Gas Reactor
NDHX	Natural Draft Heat Exchanger
NIR	Near-infrared
NRC	Nuclear Regulatory Commission
OSU	Oregon State University
PB-HTTF	Pebble Bed—High Temperature Test Facility
PIRT	Phenomenon Identification and Ranking Tables
P-LOFC	Pressurized loss of forced convection
PQP	Program Quality Plan
RCSS	Reactor Cavity Simulation System
RPV	Reactor Pressure Vessel
SCR	Silicon Controlled Rectifier
SWI	Steam Water Ingress
TDLAS	Tunable diode laser absorption spectroscopy
UHMW	Ultra High Molecular Weight Polyethylene

1. INTRODUCTION AND GENERAL CONSIDERATIONS

This report has been prepared as part of a Department of Energy (DOE) Nuclear Energy University Program grant. The purpose of this project is to expand the utilization of the Oregon State University (OSU) High Temperature Test Facility (HTTF) to the validation of design and safety thermal-hydraulics methods developed for a broader range of advanced high temperature reactors and events. While the HTTF was originally built for a prismatic block High Temperature Gas Reactor (HTGR), it can be expanded to other advanced gas-cooled reactors as well as key safety aspects of other high temperature reactors such as molten salt and even sodium cooled reactors.

The original HTTF is based on a ¼-scale model of an HTGR with the capability for both forced and natural circulation flow through the prismatic core with an electrical heat source. The peak core region temperature capability is 1400°C. The facility could be modified to simulate safety-related passive natural circulation core cooling with heat rejection to air as well as passive containment cooling. Both these features are essential to several advanced high temperature reactor concepts including advanced gas-cooled fast reactors (e.g. EM^2), molten salt reactors (e.g. AHTR and FHR) and sodium cooled reactors (e.g. PRISM). Although the fluids may be different, the computation methods for flow distribution, coupled natural circulation loops and direct heat rejection to air are similar. This later aspect is an important safety feature of advanced high temperature reactors in that their safety cooling systems reject heat to air through a heat exchanger rather than by evaporative cooling which requires water replenishment within 72 hrs. (e.g. AP1000).

In addition, there are several advanced gas reactor designs that are radically different in both geometry and operation from the prismatic block HTGR. Two such examples include the pebble bed core type gas reactor and the General Atomics Energy Multiplier Module (EM^2) reactor. The existing test facility could be modified to model these gas reactor types. Also, there were several accident scenarios identified in the DOE and Nuclear Regulatory Commission (NRC) gas reactor Phenomenon Identification and Ranking Tables (PIRT) that were not addressed in the original scaling analysis for this test facility. These include steam-water ingress events and process plant coupling events, each of which could be explored using the current test facility, if modified.

The purpose of this report is to analyze the feasibility of developing an experimental test program to collect high-quality data for (1) a passive natural circulation core cooling system, (2) the EM^2 reactor concept, (3) a pebble bed gas reactor concept, and (4), the steam water ingress event.

In the *Scaling and Design Requirements Technical Report* (Woods, 2017, 1), an inventory of test facilities that could be used for these experimental programs was completed. Several of these facilities showed some promise, however, upon further investigation it became clear that none of these facilities had the power and/or peak temperature limits that would allow for the experimental programs envisioned herein. (INL, 2007) (INL, 2009) Therefore, this report will focus on examining the feasibility of configuring the current HTTF to collect validation data for these experimental programs.

Information on the currently configured HTTF system including its instrumentation system is included in the *Test Facility Description Technical Report* (Woods, 2017, 2).

All test programs completed at the HTTF will be conducted under the OSU *HTTF Program Quality Plan* (PQP) (Woods, 2017, 3). The HTTF PQP establishes the general requirements to assure the quality of test data collected at the HTTF by controlling all aspects of maintenance and operations that affect the integrity of matrix test data. The latest revisions of the following documents constitute PQP requirements to the extent specified in the PQP.

1. 10CFR21, Reporting of Defects and Noncompliance.
2. 10CFR50, Appendix B, Quality Assurance Criteria for Nuclear Power Plants and Fuel Reprocessing Plants.
3. ANSI/ASME NQA-1a-2009, Addendum to ASME NQA-1-2008, Quality Assurance Requirements for Nuclear Facility Applications.

4. ANSI/ASME NQA-1-2008, Quality Assurance Requirements for Nuclear Facility Applications.
5. OSU Safety Policy and Procedure Manual.

Any modifications to the HTTF and the maintenance and operation of any modified test facility would be conducted under the OSU HTTF Program Quality Program.

2. PEBBLE BED TYPE REACTOR

To support the development of the scientific and technical bases that could lead to the commercialization of a Pebble Bed High Temperature Gas Cooled Reactor, Oregon State University is in the process of developing a conceptual pebble bed experimental test program. This program would focus on the collection of data that could be used for the validation of simulation codes that potentially apply to such system's physical phenomena and system components modeling. The specific objective of this section is to examine the feasibility of converting the current HTTF design into a design that is capable of meeting the needs of a pebble bed reactor system integral test program. For the purpose of this work, the Chinese HTR-PM reactor has been selected as the prototype against which the HTTF will be redesigned. A brief description of the HTR-PM is given in the *Test Facility Description Technical Report* (Woods, 2017, 2). A general pebble bed reactor scaling analysis has been completed and is documented in the *Scaling and Design Requirements Technical Report* (Woods, 2017, 1). A scaling analysis implemented for the HTR-PM is included in the *Test Facility Description Technical Report* (Woods, 2017, 2).

2.1. Pebble Bed-High Temperature Test Facility (PB-HTTF) Design Details

While addressing the OSU HTTF reconfiguration to a pebble bed core, it is important to understand that the new test facility should represent a scaled model of the actual reactor, not only an assortment of representative pebble bed core sections. A major design reconfiguration has to be undertaken to accommodate the currently existing prismatic block facility to the prototype pebble bed reactor design specifications. The primary purpose of introducing major design changes is to reflect, to the greatest possible extent, the coolant flow passages, pressure drop and heat transfer characteristics of the HTR-PM reactor.

This part of the Feasibility Study aims at laying out the structure and placement of PB-HTTF RPV internal components. The goal is to use existing OSU HTTF components to the greatest possible extent, as long as it does not severely interfere with the PB-HTTF reference reactor layout. Conceptual designs with detailed drawings will be prepared in the conceptual design project phase.

2.1.1. Pebble Diameter and Wall Effect

The packing structure in pebble beds affects local fluid, heat, and mass transport, which in turn influences macroscopic thermal hydraulic and heat transfer core characteristics. To capture flow similarity, it is important to analyze the effects of changing the size and number of pebbles and effectively the porosity of the core. The porosity is defined as the ratio of gas volume (voids between the pebbles) to the total core volume (voids and pebbles). It can be estimated using correlations developed by (du Toit, 2008). The average porosity of the HTR-PM is 0.39 (Ximing, 2014).

This value can change significantly due to the effects of stacking spheres next to walls—called the wall effect. Strong oscillatory behavior of the porosity near the core barrel extends up to 0.5 m from the core barrel wall (Figure 2-1). In Figure 2-2, it can be observed that in the PB-HTTF, the same pebble diameter as in HTR-PM (6 cm) will result in an oscillatory porosity region throughout the entire core cross section. The smaller the pebble diameter is the less wall effect can be observed. It is necessary to select a pebble diameter in the model that will allow for a region free of pebble porosity wall effects, and will sustain the core to pebble diameter ratio and similitude between effective core flow area in the model and prototype. This will push the pebble diameter to scale as the facility diameter scales. However, the practical consideration of sphere manufacture will tend to push in the opposite direction because the larger the pebble, the easier and cheaper they will be to construct. If the pebble diameter scaling ratio is equal to 1:4 (and scaled pebble diameter equals 1.5 cm) then a similar oscillatory behavior of pebble distribution will be present in the test facility with around 300,000 pebbles being installed.

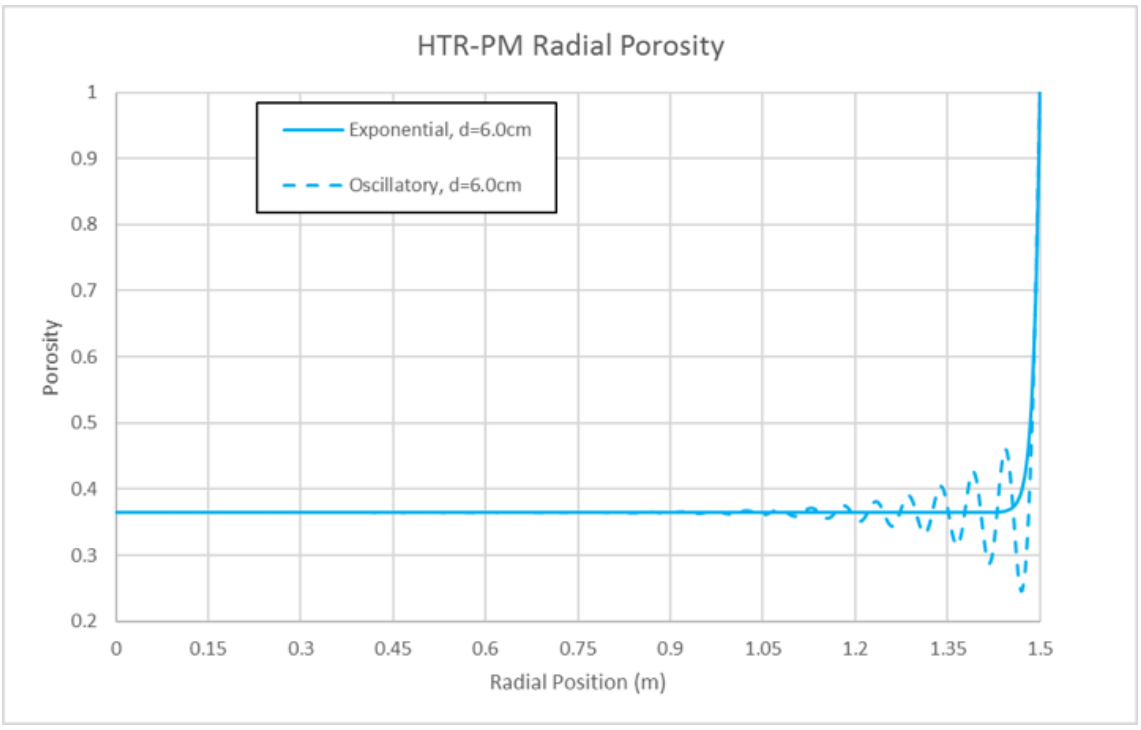

Figure 2-1. HTR-PM porosity distribution across the core width.

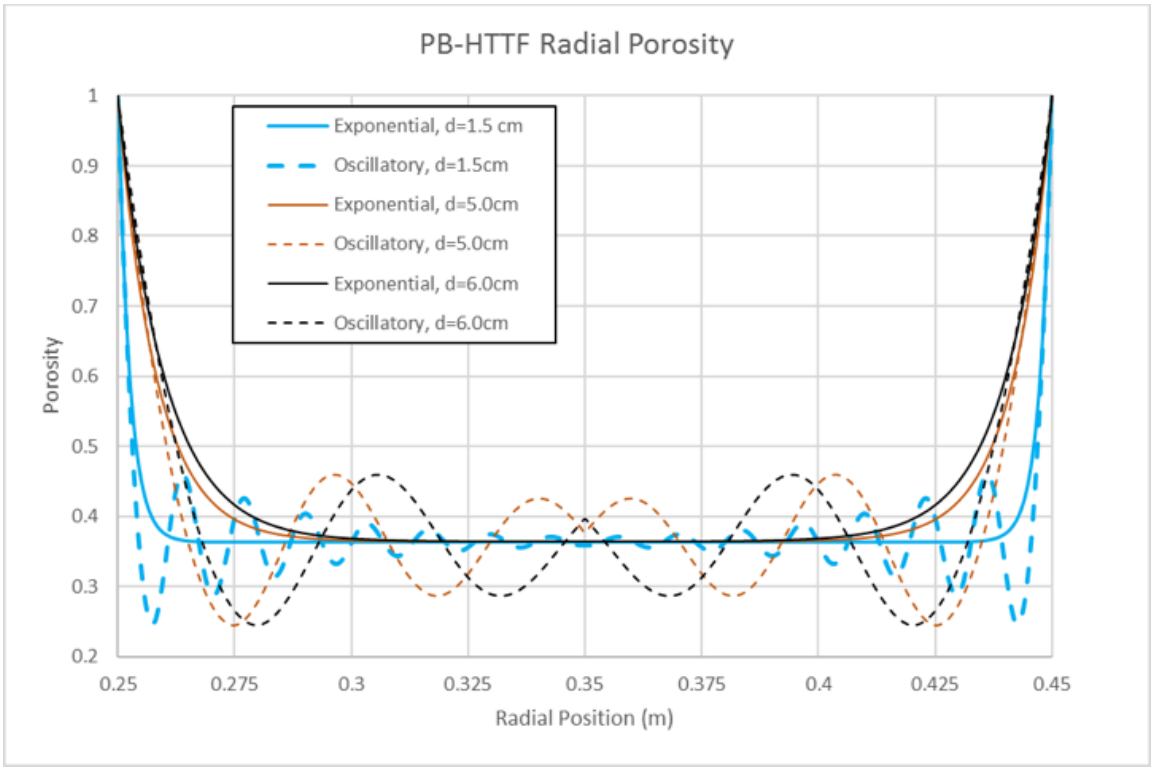

Figure 2-2. HTTF porosity distribution across the core width.

2.1.2. RPV Internal Components

None of the systems beyond the RPV will be changed or updated in the existing test facility to meet the pebble bed core characteristics. Regarding HTTF RPV internal components, the main redesign needs will concentrate on the core and reflector structure replacement and lower plenum redesign.

The following parts will be re-used in the PB-HTTF:

1. Lower and upper liner shells (core barrel),
2. Lower and upper head assembly (upper plenum),
3. Metallic Core Support Structure (MCSS) and bottom insulation, and
4. Cross duct (connecting part within the RPV structure).

One of the main redesign aspects refers to the core heater installation. As discussed in Section 2.2.3, a central graphite heating column was identified as the most feasible heating system for the pebble bed core. Graphite sleeves and heating rods will be installed in place of the central reflector that is currently a part of the OSU HTTF prismatic core blocks.

Above the bottom insulation (placed between the MCSS and lower plenum floor in the OSU HTTF), and in the core barrel area, all OSU HTTF ceramic parts will be replaced. A conceptual layout of the redesigned test facility is shown in Figure 2-3. The bottom reflectors, hot helium header and top reflector with flow passage are schematically shown in order to locate them in the RPV structure. The design details of those parts are owned by reactor vendors and are not commonly available. The HTR-PM bounding dimensions were taken from (Zhou, 2013). A comparison of horizontal and vertical dimensions of particular RPV segments between the PB-HTTF and ¼ scaled HTR-PM is presented in Figures 2-4 and 2-5. Cumulative dimensions shown on the horizontal axis refers to the top of the bottom insulation (H=0.0 m).

The following design constraints had to be addressed to accommodate the currently existing prismatic block facility to the HTR-PM reactor design specifications:

1. Model and prototype geometrical similarity choice: 1:4 (Woods, 2017, 1).
2. Upper plenum slot placement—bounding horizontal dimension (H=342 cm from the OSU HTTF bottom insulation).
3. Cross duct location—bounding horizontal dimension for the hot helium header. Determines thickness of the bottom carbon brick.
4. Core barrel diameter—bounding radial dimension (D=151.5 cm).
5. Central heater dimensions—affects pebble bed core diameter and subsequently side reflector thickness.
6. Upper plenum shell and instrumentation rods—affects flexibility to mimic HTR-PM top carbon brick, metal plate and helium gap. Those system parts will not be designed in the PB-HTTF.

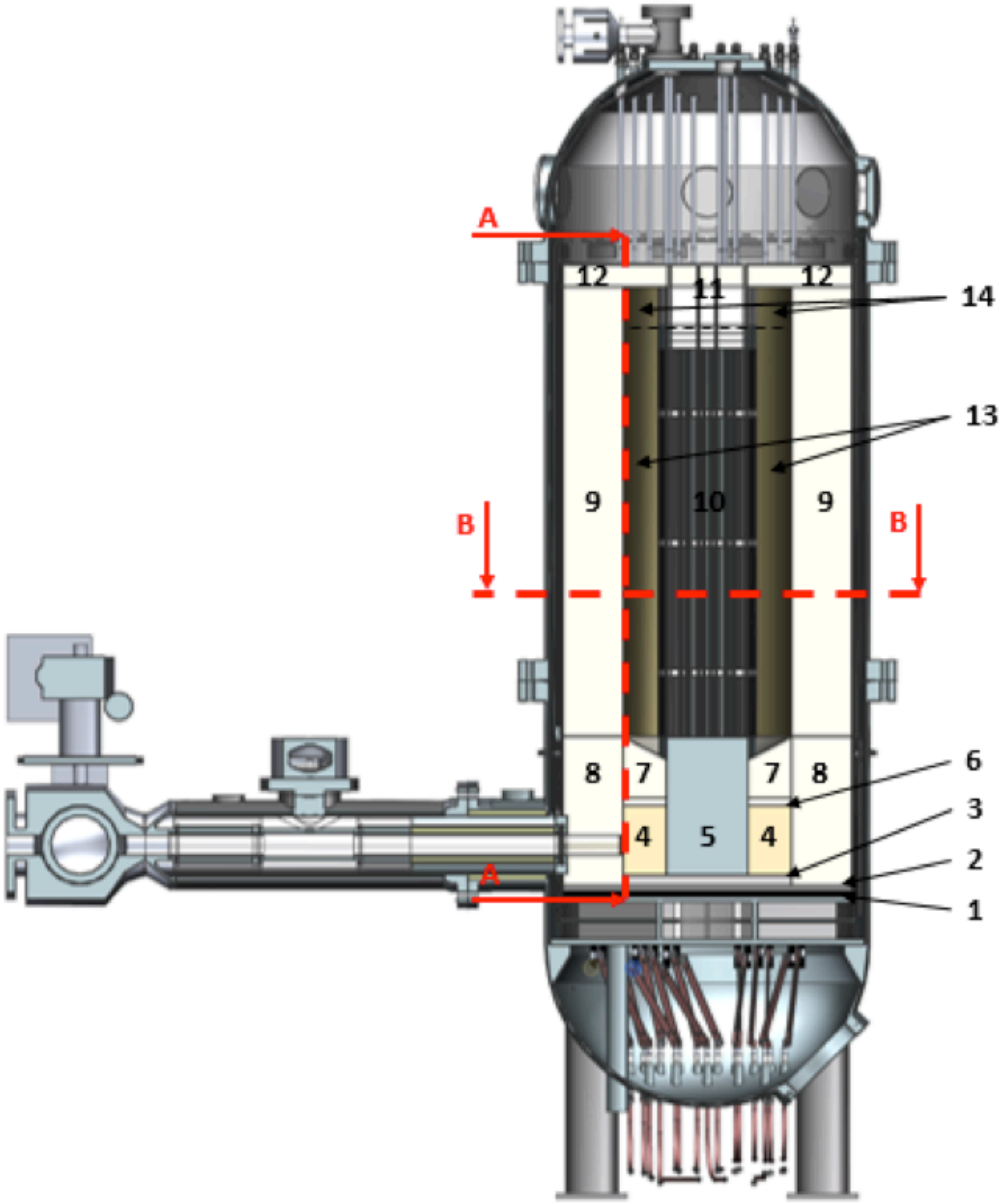

Figure 2-3. Cross section of the PB-HTTF conceptual 3-D model. 1- Bottom Insulation, 2-Bottom Carbon Brick, 3-Bottom Graphite Reflector, 4- Hot Helium Header, 5-Bottom Heater Support Structure, 6-Bottom Reflector 1, 7-Bottom Reflector 2, 8- Lower Side Reflector, 9-Side Reflector, 10-Central Graphite Heating Column, 11- Upper Heater Support Structure, 12- Top Reflector with Flow Passage, 13-Pebble Bed Core, 14-Cavity Over the Core.

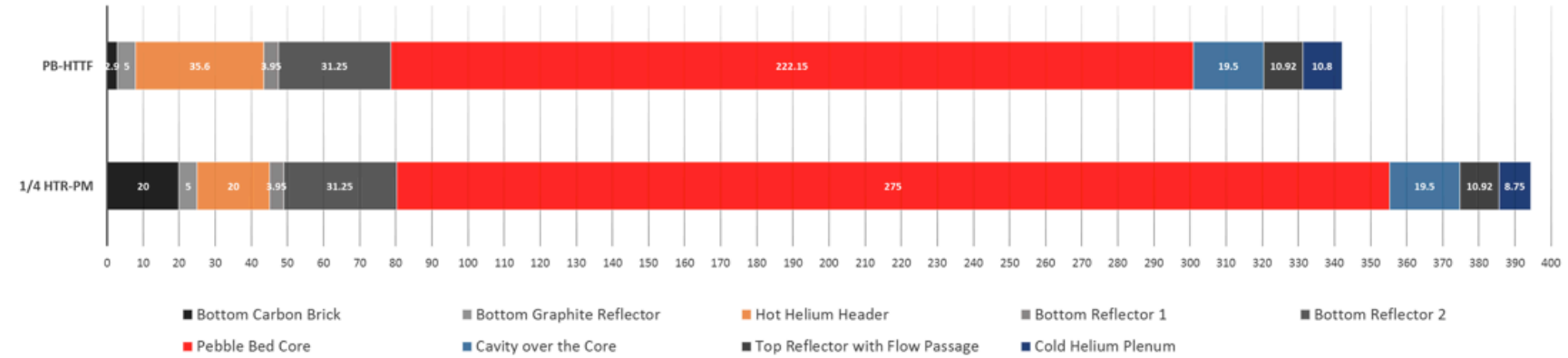

Figure 2-4. Comparison of vertical dimensions at Cross Section #A (cm).

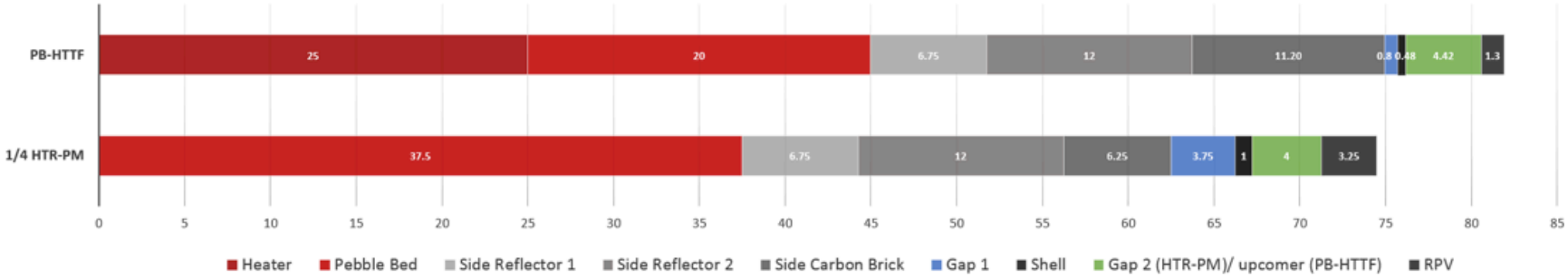

Figure 2-5. Comparison of horizontal dimensions at Cross Section #B (cm).

2.1.3. OSU HTTF Redesign Summary and Cost

The OSU-HTTF structural redesign requirements can be summarized as follows:

1. Replacement of 10 prismatic core blocks with pebble bed and central heating column (~300,000 pebbles, diameter equal to 1.5 cm).
2. Removal of 3 upper, 3 lower and side reflectors, lower plenum floor and roof, and graphite plate. Installation of side, bottom and top reflectors that are in line with the scaled HTR-PM components dimensions.
3. Removal of existing heating structure (210 graphite heating rods).
4. Lower plenum reconfiguration to meet HTR-PM hot helium header design.

The following parts of the HTR-PM RPV system will not be taken into account when reconfiguring the existing test facility:

1. Bottom metal support.
2. Pebble discharge and refueling pipes.
3. The control channels in the side reflectors.
4. The rise flow passage of cold helium in the side reflector—cold helium will enter the core flowing through the upcomer (space between the RPV and core barrel), as it was designed in the OSU HTTF.
5. The structure of the cavity cooler, air gaps, metal baffle outside the cavity cooler and concrete wall that are outside the RPV.
6. The top reflector, carbon brick, metal plate over the core and helium gap above the upper reflector with flow Passage.

The total cost for the proposed RPV internal design, excluding the heaters, is given in the Table 2-1. Please note that this budget is partially estimated on the basis of quotes received for the OSU HTTF components (for flexible joints) and online given prices. Some of the remaining costs are engineering estimates (i.e. support plates). Only components that will have to be replaced in the redesigned facility are listed. Since the described heater concept is still preliminary, inclusion of a contingency factor in the price estimate is necessary and allows for margin of error in given estimates.

Table 2-1. Cost estimate for the PB-HTTF core internal structures.

	Unit Cost $	Quantity	Total Cost $
Powder			
Al_2O_3	0.7	16,200	11,340
ShotTech (Thor 80 Castable)	0.61	9,125	5,566
Manufacturing			
Bottom Carbon Brick	4,500	1	4,500
Bottom Graphite Reflector	4,500	1	4,500
Hot Helium Header	12,500	1	12,500
Bottom Reflector 1	10,000	1	10,000
Bottom Reflector 2	12,500	1	12,500
Side Reflectors	750	36	27,000
Top Reflector with Flow Passage	12,500	1	12,500
Side Carbon Brick	750	36	27,000
Contingency		25%	31,852
Total			**159,258**

2.2. Heating Element Design

The primary objective of this section is to investigate potentially feasible pebble bed core heating design concepts and to work through any potential manufacturing issues.

There are a few mid-to-large scale high-temperature heating sources capable of delivering precise power distribution to a targeted location in a compact space. Steam or gas fired heating systems are options, although are challenging to integrate into surrounding systems and require complex installation and support infrastructures. Discrete electric heating elements are characterized by relative ease of design and installation. They are well suited for application to the PB-HTTF. Nevertheless several design aspects have to be accounted for while selecting the most suitable electric heating element:

1. Maximum operating temperature
2. Wattage capabilities, performance, resistance/resistivity
3. Heating method (conduction, convection or radiation)
4. Process temperatures of the media being heated
5. Available voltage and current draw required for the heating system
6. Temperature uniformity/distribution requirements
7. Temperature, power controls and sensor requirements

8. Manufacturability and availability
9. Compactness and integration with system specification
10. Localized stress/strain
11. Corrosion/oxidation risk
12. Service life and repairability
13. Cost

Figure 2-6 presents the anticipated steady state power density profile in the HTR-PM reactor core (Zheng, 2012). In the ideally designed reduced scale research facility, the prototypical axial and radial core heat distribution will be reproduced. However, since a designed non-nuclear system is a close but not an exact representation of the real facility, power profile distortion will most likely be present. Section 4-3 of the *Test Facility Description Technical Report* (Woods, 2017, 2) summarizes a number of potential pebble bed core electric heating methods. Those methods differ in terms of complexity, ease of fabrication and modeling, and ability to closely mimic heat from fission. Table 2-2 summarizes the main characteristics of these electrical heater concepts.

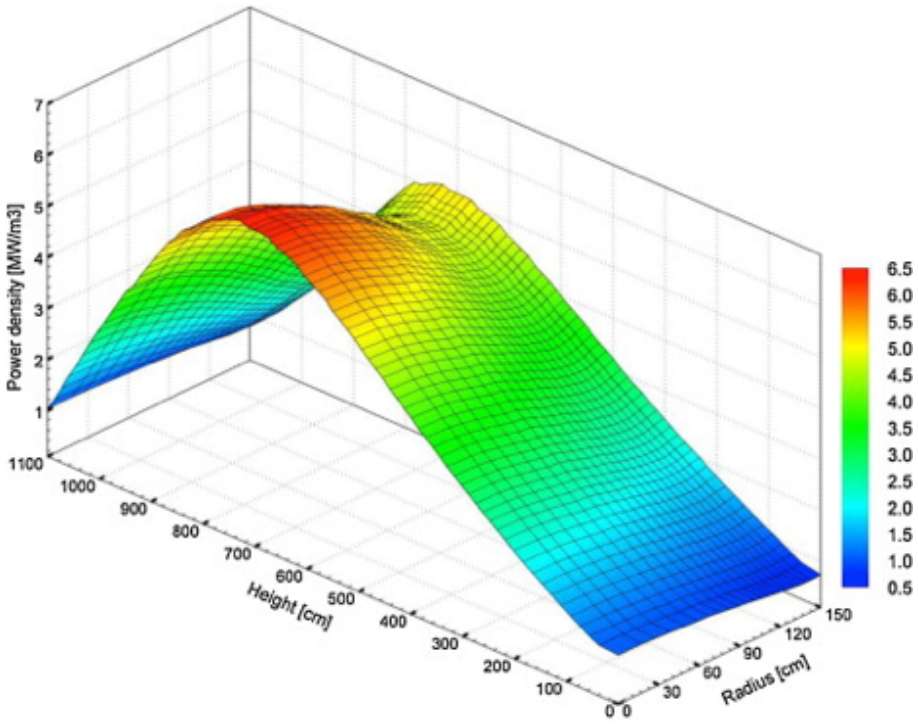

Figure 2-6. Steady state power density profile in HTR-PM normal condition (100% FP). Taken from (Zheng, 2012) with no changes.

Table 2-2. Heating methods screening survey.

Heating method	Electrical Resistance				Induction
Design	**Vertical**	**Horizontal**	**Profiled**	**Net of pebbles**	**Coil**
Material/type	Graphite	Graphite	Graphite	Cartridge heater (Kanthal)	Metallic pebbles
Temperature limit	2700°C	2700°C	2700°C	1700°C	1350°C
Cost	medium	medium	high	high	High
Complexity	medium	high	high	high	high
Other	Can inherit a significant part of the currently existing HTTF power distribution system	High complexity due to severe redesign needs of HTTF to accommodate terminations	Challenging manufacturing, variety of bench top testing required	Challenging termination of the heater within the core region	Negative impact of magnetic field on instrumentation

The critical design challenge of the PB-HTTF resistive heater is to configure the geometry to reach the desired power level while achieving uniform and efficient heat transfer in the core. To achieve a compact arrangement, the heating elements are bundled into the smallest possible diameter. While shrinking the heater dimensions, a component's surface heat flux and thermo-mechanical properties at elevated temperature present pertinent design challenges. Besides the heat transfer and geometrical constraints, properties such as heater chemical resistance, durability, power control and supply, support systems, wiring, and installation must be considered. The designed system should ensure the provision for a reliable physical contact between heaters and electrodes supplying the current accounting for thermal expansion of material during heat-up and steady state operation.

2.2.1. Heater Candidate Materials

Factors affecting material selection for the heater include the melting point, temperature coefficient of resistance, creep resistance, atmosphere of use, thermal and mechanical shock resistance and need for high electrical resistivity. (Omega Engineering, Inc. 2000)

In the case of the PB-HTTF and its extreme operating conditions—temperature becomes a key discriminator. Above 1600°C (maximum PB-HTTF design temperature) only molybdenum, tungsten and graphite heating elements are suitable candidates and, then only in a vacuum or protective atmosphere. The maximum temperature of use for these metals and the graphite are usually given as follows:

1. Molybdenum : 1870°C,
2. Tungsten: 2040°C,
3. Graphite: 2700°C.

These maximum temperatures do not consider the problem of supporting the molybdenum and tungsten heating elements and their leads which tend to creep under their own weight at relatively high temperatures. Moreover, molybdenum and tungsten become brittle with exposure to oxygen or water vapor.

Graphite, in addition to being more refractory is about one-fifth as dense as the metals. Hence, graphite does not have the same tendency to creep at elevated temperatures, and thus is the leading candidate for the very high temperature heating elements. The low resistivity of graphite means it requires high current power supplies and correspondingly large feedthroughs and cables. As temperature rises, the electrical resistance decreases in the range of 0-900˚C, but it increases in a higher temperature range. Heating elements can be supplied in rod, tube, bar, plate, and circular shapes or cloth form.

Additionally, graphite components do not diffuse, bond, or weld together. As such, it is a suitable material for easily replaceable heating elements. Furthermore, as the temperature of a graphite element increases, its compressive strength also increases up to about 2500˚C (depending on the graphite grade: by 15-50% over its room temperature value). (Poco Graphite, Inc. 2015)

Considering different material properties at elevated temperatures, graphite is the most reasonable choice for the structural heater material to be applied in the PB-HTTF. A broad spectrum of different graphite grades is available on the market.

2.2.2. Existing HTTF Power System

In terms of capital cost, familiarity with operation, in place/installed wiring and control systems, utilizing the existing HTTF power supply system in the pebble bed design is advantageous. The current HTTF design incorporates custom made graphite. There are 210 heater rods arranged in 10 heater banks, with 3 heater legs per heater bank. Each heater leg consists of 7 heater rods. For each heater bank, three heater legs enter the HTTF core. Each leg carries one phase of the three phase power. Vertical graphite heater bus bars carry power through the MCSS, the structural insulation, and into the lower plenum side reflectors. At the level of upper reflector #2, the vertical graphite heater bus bars connect to horizontal graphite bus bars which connect to the first heater rod. The first heater rod is then connected to the second heater rod through a graphite upper junction piece located in core block #10. The second heater rod is connected to the third heater rod through a graphite lower junction piece located in lower reflector #3. Each subsequent heater rod connects to the previous one in a similar fashion until the seventh heater rod. The seventh heater rod terminates in a graphite wye junction located in upper reflector #1. All three phases (heater legs) for a heater bank terminate in the same wye junction. A rendering of the OSU HTTF heating system is presented in Figure 2-7.

Each heater rod is actually composed of a series of graphite rodlets. The rodlets sit inside the channels cast in the ceramic core blocks.

Each heater bank is powered by a silicon controlled rectifier (SCR). An SCR is a semiconductor rectifier that has the added feature of controllability. The SCR is capable of conducting or blocking current in the forward direction, depending upon the gate signal. The SCR, like the diode, will always block current flow in the negative or reverse direction.

The SCRs are fed from the 4000A switchgear. The 4000A switchgear provides 480 V, 3-phase power to the SCRs. The SCRs control the power to the HTTF heaters. Currently each SCR has a rated load of 220 kW for a total rated core power of 2200 kW. Copper insulated lines attach each phase of each SCR with a corresponding heater leg. The copper lines enter the RPV through penetrations in the lower head. Once in the lower head region, the copper lines are attached to the vertical graphite bus bars via braided copper cable. In addition, a power meter is attached to each SCR.

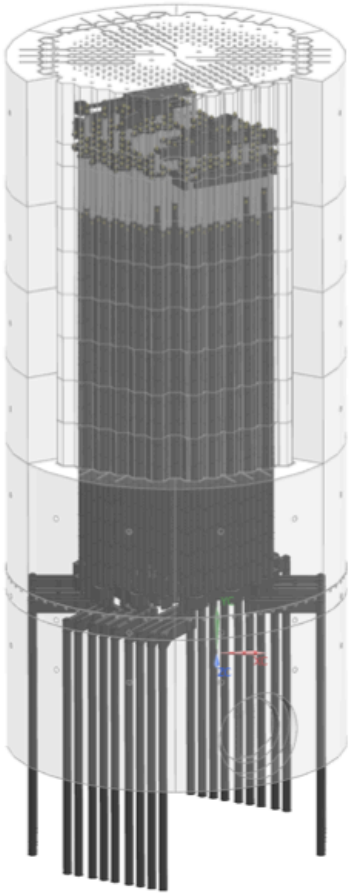

Figure 2-7. Render of the HTTF heating system.

2.2.3. Heating Rods, Enclosure and Support Plates

The existing arrangement of graphite rods is not applicable for use in the pebble bed core design. The random distribution of pebbles in the core will not provide sufficient support to the stack of 10 rodlets in each of the 210 heating rods within the core. This is why the new resistive heater layout must not only allow for connection to the exiting power supply, but at the same time comply with core dimensional and structural characteristics. A centrally located graphite heating column will result in the least disruption to the pebble arrangement (it will be also the most straightforward in terms of analytical or numerical modeling) as opposed to several heating columns redistributed throughout the core. A central heater of diameter equal to 50 cm is selected as a reference baseline to accommodate a total number of graphite heaters that will deliver 2.2 MW.

Since graphite heaters should be used in the near-vacuum or inert conditions to protect the material from oxidation, and to prevent the heater components from mechanical stresses caused by the differential thermal expansion of core internals, heaters will be placed in a graphite enclosure (sleeve). The enclosure acts as a thermal radiation receptor. The exterior of the sleeve transfers heat via convection, radiation and conduction (points of contact between ceramic pebbles and sleeve). The thickness of the enclosure equals 1 cm. High thermal conductivity for the enclosure structural material is necessary to efficiently transfer the heat to the pebble bed. GH030 graphite is selected as the material for the graphite enclosure. A summary of graphite GH030 properties is given in Appendix A.

There are 150 graphite rods placed inside the graphite enclosure and bundled into a close packed array. Each rod has an OD equal to 1.905 cm, an ID equal to 1.27 cm and a length of 182.88 cm (Purified Graphite Tube, 0.75"OD x 0.5"ID x 72"L, available at graphitestore.com). The sleeve wraps the heater rods creating 10 baffles (of 1 cm thickness) between every 15 rods. The role of the baffles is to create additional helium flow paths through the heater space and enhance heat transfer from the enclosure to the coolant and subsequently to the ceramic pebbles. A conceptual view of heater placement in the RPV and geometry of the sleeve along with arrangement of the heater rods is presented in Figure 2-8.

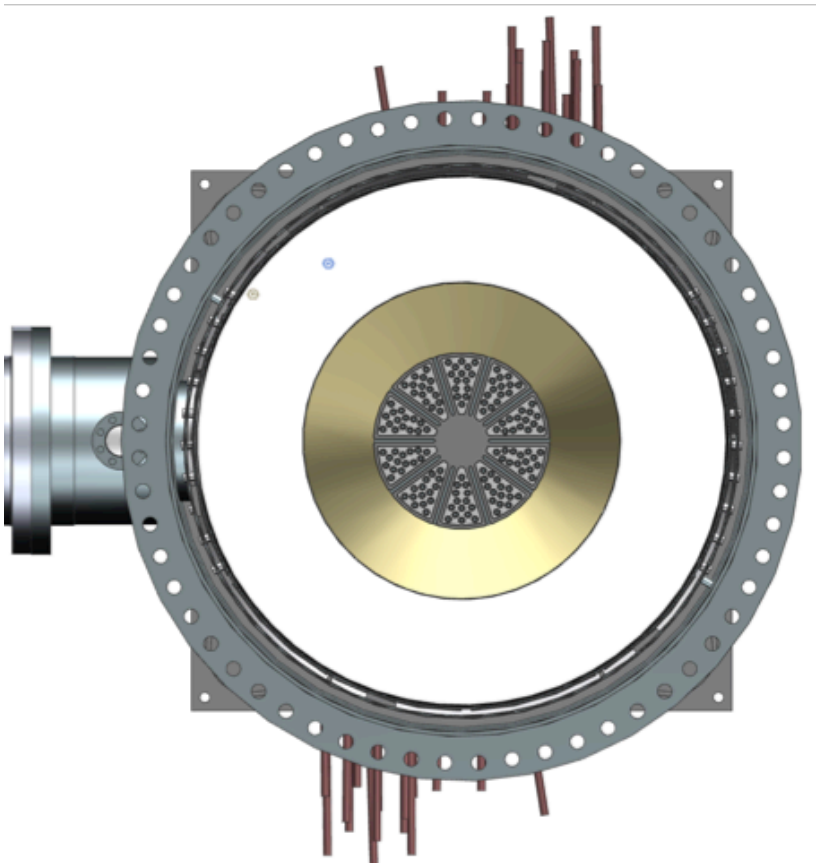

Figure 2-8. Conceptual view of heater placement in the RPV and geometry of the sleeve along with arrangement of the heater rods.

Graphite heating rods shall be passed through electrically non-conductive spacers. The role of the spacers is to separate rods lengthwise and support them from flexural deformation which should help to provide a considerable degree of stability. Those support plates can be composed of high purity Alumina for temperatures up to about 1700°C, Boron Nitride for temperatures up to 1900°C or Zirconium Oxide for temperatures of a range of 2000°C and higher. It is important that the structural material of the supporting plates be of high purity to reduce strength-limiting flaws caused by inclusions and pores (Dyson, 1989). A conceptual view of the heater with support plates is presented in Figure 2-9.

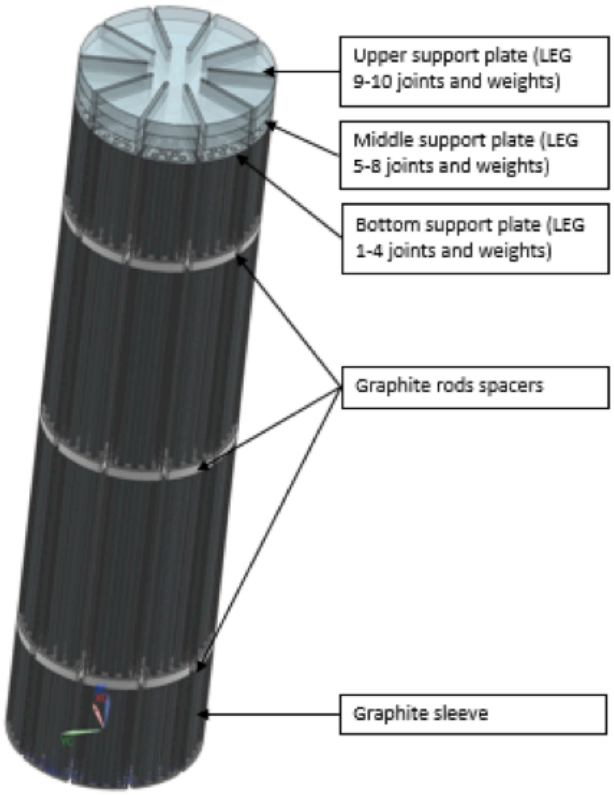

Figure 2-9. Structure of the graphite central heater.

The rods are joined at the top of the heater into a ten Wye series circuits. Each circuit of graphite heating rods defines a separately controllable heating zone. Analogous to the HTTF circuit arrangement —there are 10 individually controllable and energized heating zones composed of 1 heating bank per zone and 15 rods per bank. Rods are grouped into 5 rods per leg and there are 3 legs per heating bank. Rods are arranged into legs radially in a way that allows operation of a reduced number of circuits while sustaining uniformity of heat distribution within the thermal shield. A schematic showing rod connections is presented in Figure 2-10.

The gap distance between rods is limited by arcing. Arcing is an electrical breakdown of gas which results in plasma discharge. The well-known relationship between the breakdown voltage V_B, the gas pressure, and gap width between electrodes is described by Paschen's Law (Lieberman, 2005):

$$V_B = \frac{Bpd}{\ln\left(A'pd\right) - \ln\left(\ln\left(1+\frac{1}{\gamma_{SE}}\right)\right)} \tag{2-1}$$

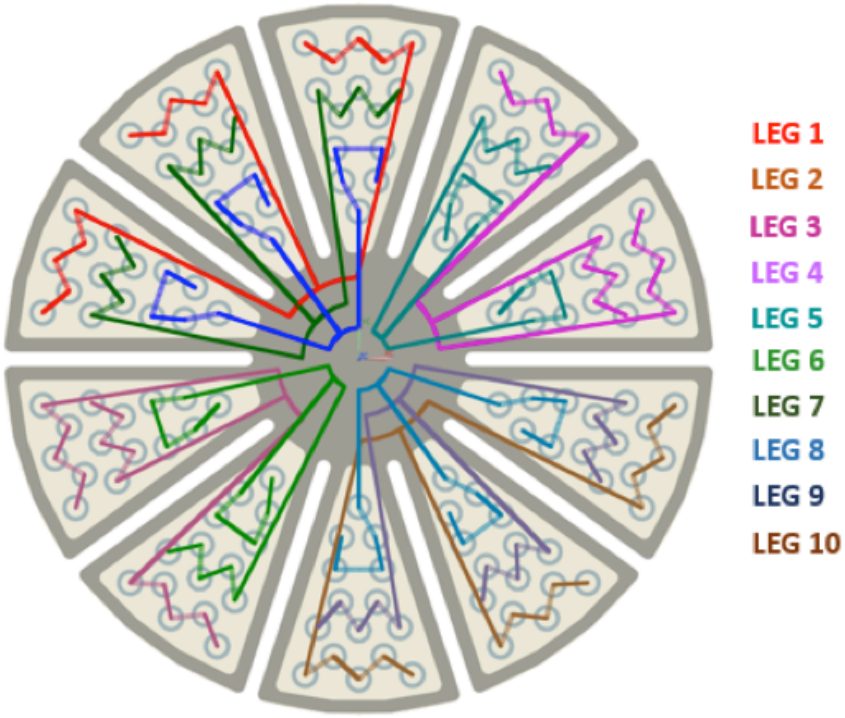

Figure 2-10. Rods arrangement and connections in the upper ceramic plates.

where:

V_B—gas breakdown Voltage [V],
p—gas pressure [Pa],
d—gap distance between electrodes [m],
γ_{SE}—secondary electron emission coefficient,
A'—constant, saturation ionization in the gas at particular ratio of electric field to pressure,
B—constant, refers to excitation and ionization energies.

A typical Paschen's curve for helium and air is shown in Figure 2-11. The distance between rods at the most narrow location equals 4 mm. Two operating pressure modes are considered: 100.325 kPa and 800 kPa. Regardless of the type of filling gas, for the given void among rods and pressure range, the breakdown voltage should not be reached (instantaneous, maximum expected circuit voltage equals 678.8 V). The parameters for which electrical breakdown is most probable to occur are: helium as a graphite sleeve filling gas, p=101.325 kPa and gap spacing equal to 0.3 mm. This scenario is possible, considering manufacturing curvature of the graphite rods. According to the specification for 72" long graphite tube available at the Graphite Store, the typical curvature is equal to +/- 0.5% arc to cord. Currently the proposed rod spacing is not able to accommodate this level of curvature. This means that supporting plates are required not only to separate and support graphite rods but also to help prevent electrical breakdown.

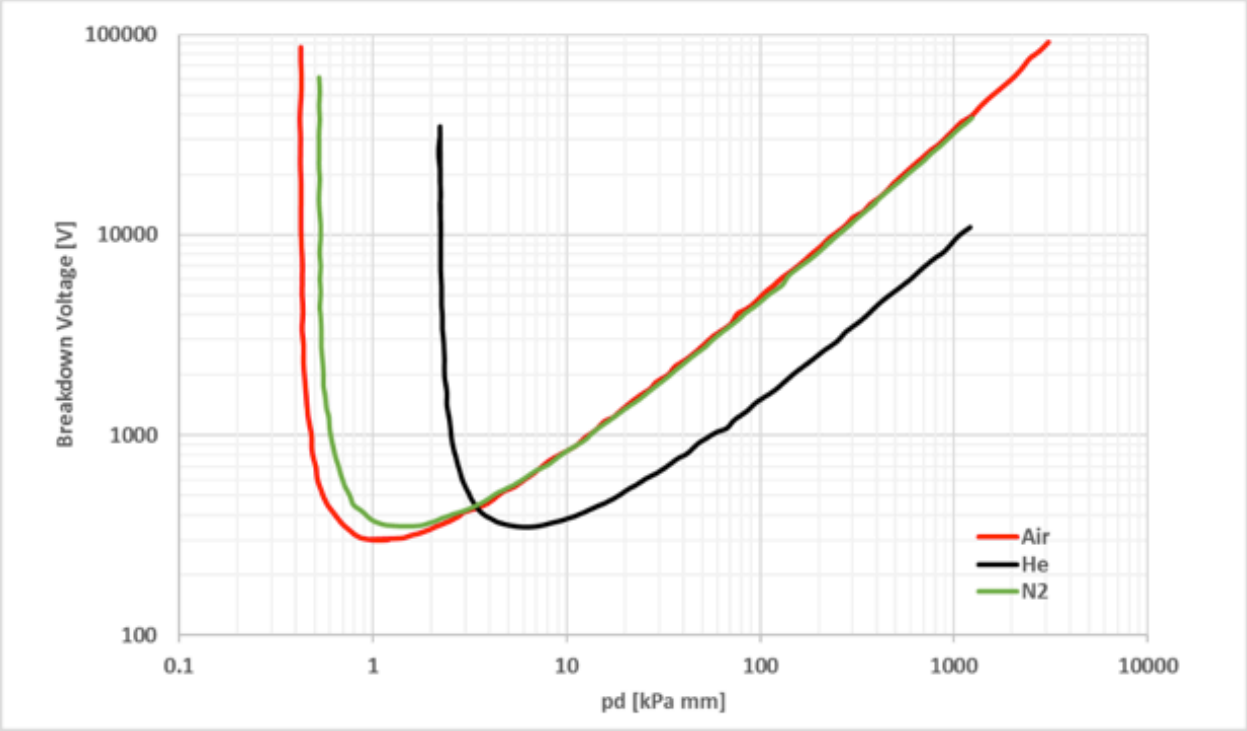

Figure 2-11. Pashen's curve for Air and Helium.

2.2.4. Electrical Joints

In most resistive heating applications, contacts through which current is transferred cause major design challenges. An essential requirement is the assurance of reliable physical contact between the graphite rods and the electrodes supplying the current. Reduced contact area is characterized by high resistance and gives rise to local overheating along with power losses (Omega Engineering, Inc. 2000). Moreover, connections should not only provide a continuous electrical resistance path between heating rods, but should also suppress excessive exertion of mechanical stresses and accommodate the thermal expansion of the heaters at elevated temperatures (Hegbom, 1997). Finally, the joining resistor should be designed in such a way that the temperature at the joint is low enough to avoid oxidation or mechanical degradation.

HTTF heating rod connections consist of flexible molybdenum bands, lids, molybdenum ring shims, tension bolts and tungsten rodlet compression weights (Figure 2-12). The bands' role is to accommodate eventual graphite rod displacement caused by core block differential thermal expansion. It was demonstrated in the HTTF that molybdenum joints are sufficiently flexible to withstand deflections of different magnitudes and in different directions. Moreover, they can be arranged into straight or angled junctions. The junctions consist of 7 stacked molybdenum bands. The configuration of the remaining pieces is relatively straightforward, with a tension bolt running through the center of the rodlet weight and providing compression for the flexible bus stack and the graphite contactor connections at the top and bottom of the assembly respectively.

In the locations where elongated connection is necessary (for instance between legs), graphite buses are incorporated along with flexible bands—see Figure 2-12.

Figure 2-12. Joints assembly: Flexible molybdenum bands—straight and angled, tungsten weights, graphite bus (on the right).

In the case of the PB-HTTF, on each heating leg there will be 2 upper and two lower joints between rods. To mechanically integrate the wye-connected system, additional joints are necessary between the legs within a particular heating bank. Altogether, there will be 120 junctions between graphite rods (named 'short'), 30 joints between the 5th rod in the leg and the leg-to-leg wye connection (named 'long'), and 30 angled joints that connect legs in the center of the upper ceramic plate. This results in 300 electrical contact locations between graphite heating rods and tungsten-molybdenum joints, and 30 connections among metallic and graphite buses in the designed heating system.

Three ceramic plates with a thickness of 5 cm are placed at the top of the heater sleeve to provide mechanical fastening for the heater rods joints. Connections for banks 1-4 will be placed in the bottom plate, for banks 5-7 in the middle plate and remaining ones in the upper plate. Tungsten weights will be used as well, although the compression weight will be reduced compared to the HTTF design (1.864 kg). Weights of 0.15, 0.3 and 0.46 kg will be placed respectively in the lower, middle and upper plates (calculated for tungsten density = 19320 kg/m^3).

The described arrangement causes the heating bars to be firmly coupled at both ends of the heater although rods are still allowed to expand linearly, lifting the compression weights (rods are not pinned at the ends). It should be stated that thermal linear expansion of graphite tubes can potentially cause breakage in the system's ohmic continuity. This failure mode should be further investigated through benchmark testing of the new heating system and the strategy towards management of differential thermal expansion between heating elements, support structures, terminations and joints should be evaluated. Although the details have not yet been finalized, this design will allow for easy removal and replacement of individual graphite rods from the top part of the heater, after fastening ceramic plates are removed from the top of the heater sleeve.

2.2.5. Terminals

The electrical terminals constitute the connection between the 10 graphite banks and copper wiring. Design limitations with regard to terminals refer mostly to the maximum operational temperature. This temperature should be low enough to avoid oxidation of the copper leads, destruction of its insulation, or excessive dimensional change due to thermal expansion leading to loosened connections. The OSU HTTF heater bank terminals are shown in Figure 2-13.

In the current HTTF design, all the graphite rods are supported from the bottom by the lower reflector. Therefore, graphite bus bars connected to terminals are free to expand and contract without developing additional compressive stresses. Details of the bottom structure of the pebble bed core, including bottom reflectors and the hot helium header are not determined. Further, specification of the geometry and placement of electrical terminals and their support structure will be established once reference system design specifications are available.

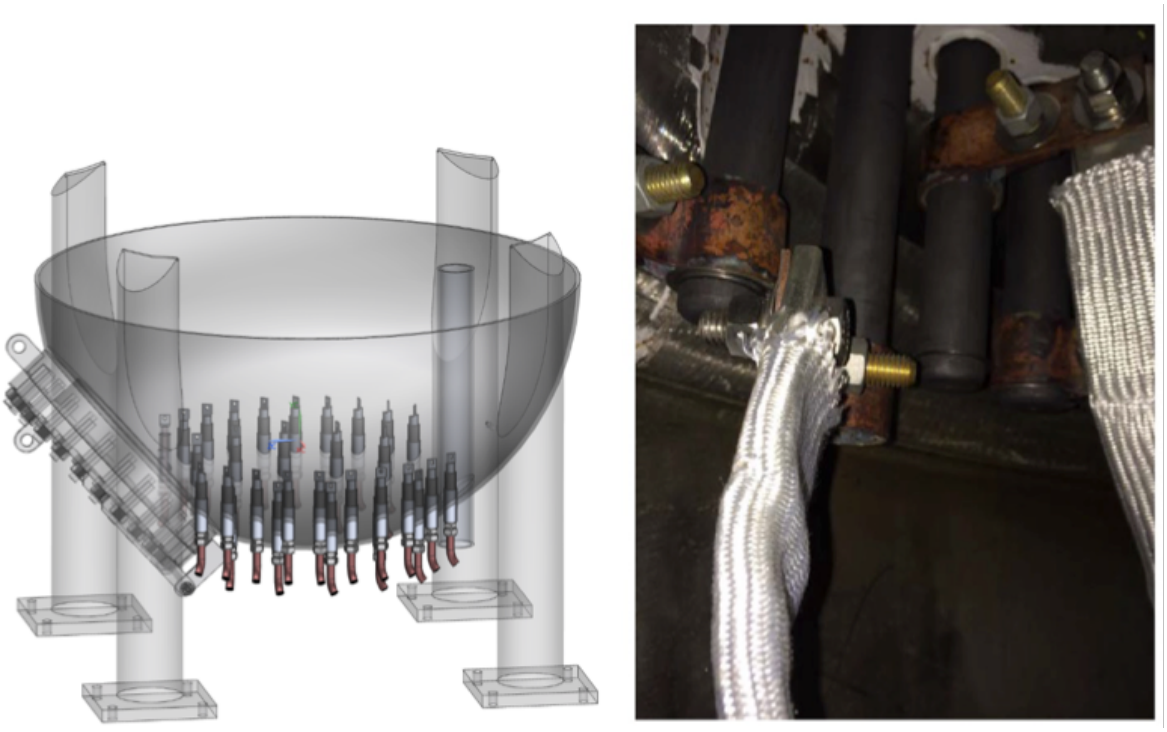

Figure 2-13. OSU HTTF terminals.

If details of the reference design are not available, then the most feasible path forward is to utilize the existing HTTF components in the PB-HTTF design. Particularly the MCSS, with its opening for graphite bus bars, can be used in the redesigned facility. Electrical leads can be passed through the existing openings in the MCSS, side reflector and then horizontally through bottom reflector #1. Flexible joints should be used to join horizontal leads with the graphite heater rods in the central column. Copper insulated lines that attach each phase of each SCR with a corresponding heater leg in the HTTF will be utilized in the PB-HTTF as well. Copper leads should deliver current through the RPV without the risk of shorting the circuit which requires installation of electrical insulator. Copper wires are then connected to the graphite heaters directly by wire clamps. A rendering of the bottom part of the heating system with bus bars and electrical leads is shown in Figure 2-14. The section of the render highlighted in red shows the location of the bottom flexible joints. This part of the heating system will be designed in detail during the Conceptual Design phase.

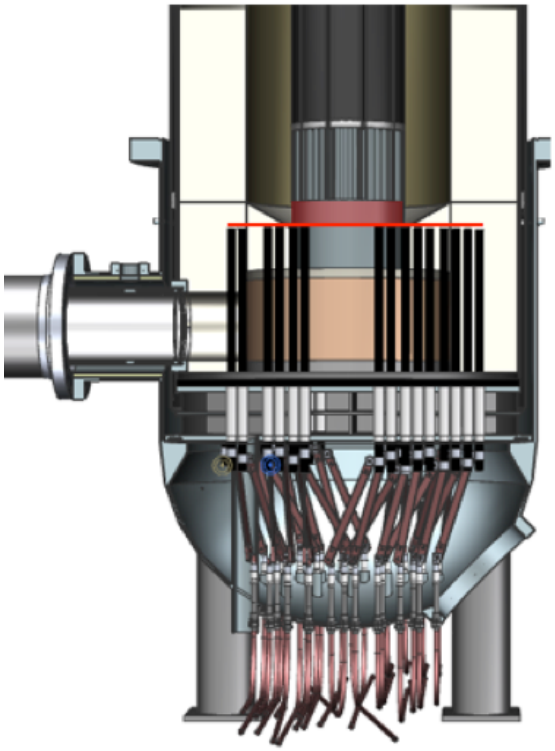

Figure 2-14. Electrical leads and graphite bus bars in the PB-HTTF (the same as in the HTTF). The red part of the render indicates location of bus bar flexible connections to the graphite rods in the central heater.

2.2.6. Power Calculations

As mentioned, the facility heating system is supplied with 480 V, three phase power. The ANSEL switchgear is rated to 4000 A although currently installed SCRs are rated to 300 A. In a three-phase wye, the leg current is calculated using the following equation:

$$I_{leg} = \frac{V_{line-to-line}}{\sqrt{3}R_{leg}} \tag{2-2}$$

In order to remain below the system current rating, leg resistance must remain above 0.92 Ω. Heater power is calculated using the following equation.

$$P_{heater} = 3I_{leg}^2 R_{leg} = \frac{V_{line-to-line}^2}{R_{leg}} \tag{2-3}$$

The design power of one heater is 220 kW (73 kW/leg). In order to achieve this heater power, the leg resistance must be no larger than 1.05 Ω. Power can be adjusted down using the SCRs in the case of leg resistance smaller than this. Thus the leg resistance must range between 0.92 Ω and 1.05 Ω over the expected range of operation.

The power delivered increases as the resistance drops. Resistance can be calculated using heater material properties and dimensions with the following equation.

$$R_{leg} = \frac{\rho L}{A} \tag{2-4}$$

In this equation ρ is the graphite electrical resistivity, L is the heater leg length and A is the graphite tube cross sectional area.

Each heater rod has a cross sectional area of 1.583 cm^2 and height of 182.88 cm. With five heater rods per heater leg, the length of the heater leg is 914.4 cm. This means that the resistivity of graphite should be in the range of 15.923 to 18.174 μΩm. Tokai Carbon specialty graphite can fulfill this criteria. The possible candidates are graphite G535 (ρ=17.0 μΩm) or G540 (ρ=15.0 μΩm)—both isotropic, fine grade graphite (offered by Electro-Tech Machining). Also, an iso-molded graphite R7660 (offered by SGL Carbon), with resistivity equal to 23 μΩm can be used. Graphite products specification sheets are given in Appendix A.

The resistivity of graphite tubes offered by the Graphite Store equals 8.128 μΩm (grade GR008GP manufactured by Graphtek LLC). Using this type of graphite, leg resistivity will equal to 0.47 Ω and effective leg current would exceed the rated current by 290 A. To meet the rated current requirements in a system with graphite grade of reduced resistivity, the following system changes should be introduced:

1. Increase the number of heating rods (at the same time the size of the graphite sleeve will increase).
2. Add contact locations between graphite rods (in the HTTF it was measured that 30% of system resistivity was generated at contact locations between graphite rodlets). This can generate an additional risk of arcing.
3. Reduce the cross section of the graphite rods (currently selected rods were of the smallest cross section and the longest among products available commercially on the market).

2.2.7. Application Contraints

Variable resistivity

The resistivity of graphite changes significantly with temperature. It decreases between room temperature and 400-600°C (depending on graphite type) by as much as 30%, but then slightly increases above this temperature range. According to Tokai Carbon, the resistivity of graphite can be controlled by modifying raw materials and the manufacturing process to meet broad requirements. Nevertheless, design constraints must be placed on the power system to assure required power level s and current rates at the temperatures range, where graphite resistivity is the lowest.

In the case of graphite G535, resistivity at ~500°C is reduced by 30%, equaling 11.9 μΩm. The resulting leg current in the PB-HTTF system would reach 436 A. This value is above currently installed SCR's rated current of 300 A. However, the maximum design current for the SCR is 400 A RMS. With a 400 A RMS current, the peak current is 566 A, which means that it is possible to operate at increased

amperage as long as the total current in the system does not exceed ANSEL switchgear amperage limit (4000 A). At the decreased resistivity range this can be achieved by varying power distribution among graphite legs. Other solutions include the installation of a phase-angle fired control system in the SCRs. This system would allow the voltage and power to be reduced during facility heat-up until the graphite reaches temperatures above those with reduced resistivity values where resistivity is once again within the acceptable range. Once resistivity returns to its reference level at elevated temperatures (~1200°C), full voltage/power can be applied.

Arcing

If the PB-HTTF heating system is not composed of continuous graphite rods it will contain a number of electrical contact locations. Contacts can fail even in the absence of differential expansion. When two conductors come in contact, the actual contact area is not the same as the apparent contact area due to surface roughness and imperfections at the contact surfaces. This actual contact area may be much smaller than the apparent contact area. The current flowing through the conductors must flow through the actual contact spots. Thus the current lines get distorted in the conductors as current flows through the reduced cross sectional area at the contact. This constriction resistance is a major contributor to the resistance across a contact. (Slade, 2014)

Heat is generated at the contacts due to the resistance across the contacts. The heat generated can be calculated using the following equation.

$$P_c = \frac{V_c^2}{R_c} \tag{2-5}$$

P_c is the heat generated at the contact, V_c is the voltage drop across the contact and R_c is the resistance across the contact. This heat is generated at the actual contact spots and is not distributed equally over the apparent contact area. To a first approximation, this heat is deposited locally at the actual contact spots where heat conduction through the electrical conductor is the only means of heat removal. The following equation can be used to estimate the temperature at the contact spots based on the average bulk temperature of the contacts.

$$T_c^2 - T_b^2 = \frac{V_c^2}{4L_{WFL}} \tag{2-6}$$

In this case T_c is the temperature of the actual contact spot, T_b is the average bulk temperature of the conductor, V_c is the voltage drop across the contact and L_{WFL} is the Wiedemann-Franz Lorenz number which is equal to 2.45×10^{-8} ($V^2/K^{2)}$. If the contact temperature for graphite reaches the sublimation temperature of graphite (approximately 4000 K), the contact will start to vaporize. This vaporization causes pressure at the contacts which pushes the two conductors apart. The carbon vapor also serves as an arcing medium between the separated conductors which will lead to interruption of the circuit and contact damage. (Woods, 2016, 1) (Slade, 2014)

There are several commercial means to improve electrical contacts. One of them includes application of flexible graphite foils, for instance Mineral Seal Corporation Premium Grade Graphite Foil (Grade 2010A, available at: http://minseal.com/flexible-graphite/premium-grade-graphite-foil/). It is designed to be used in applications where material purity is strictly required, such as in nuclear power plants. Foil is made from compressed high purity exfoliated mineral graphite. Its maximum working temperature in a non-oxidizing environment is 3000°C. Moreover, in cases of vertical heaters constrained from the bottom, additional weights or springs can be added at the top of them to enhance contact pressure. Bench top testing is required to verify the most feasible path forward to increase efficiency of electrical contacts.

Differential Thermal Expansion of Core Components

One of the major challenges for the heater design is the differential thermal expansion of the pebble bed, heater sleeve, power leads and graphite rods themselves. The temperatures experienced by these core components are expected to be between 30°C and 1735°C. Therefore, significant thermal expansion will occur during the PB-HTTF's operational cycle. The coefficient of thermal expansion for the different core and heater structural materials will vary and thus will experience different magnitudes of thermal expansion. Allowances for these differences must be incorporated into the PB-HTTF core design. Heater design must allow for misalignment of heating rods according to radial and axial movement at elevated temperatures.

The heater rods will be made of graphite, most likely G535, which has a different coefficient of thermal expansion than the copper leads and ceramic support plates. Once the core starts to heat up, ceramic components and the heaters start to expand. Differences in temperature between the ceramic components and the individual heater rods will determine the magnitude and direction of linear thermal expansion.

Because individual heater rods will also likely be at different temperatures, the height of adjacent heater rods will also vary even though they are made of the same material. In cases where adjacent heater rods are connected by an upper junction, this upper junction must allow for variable heights between the rods it connects.

The temperature range of the pebble bed is expected to be between 30°C and 1600°C. From the maximum expected pebble bed temperature of 1600°C, the maximum expected heater temperature can be determined. The total outside surface area, *A*, of the heater rods is calculated by the following equation.

$$A = N\pi dh = (150)\pi(0.019m)(1.829m) = 16.37m^2 \tag{2-7}$$

In this equation, *N* is the number of heater rods in the core, *d* is the outside diameter of the heater rods and *h* is the heated length of an individual heater (from lower junction to wye connection). The highest average heat flux is estimated by the following equation.

$$q'' = \frac{P}{A} = \frac{(2.2x10^6 W)}{(16.37m^2)} = 134.4kW/m^2 \tag{2-8}$$

In this equation, *P* is core power (full power), *q"* is the heat flux and *A* is the total surface area of the heaters.

Since the heater rods are placed in a sleeve that separates rods from the coolant flowing through the core, and from ceramic pebbles, radiation heat transfer will be the principal heat removal mechanisms from the rods. Radiation heat flux can be determined using the following equation.

$$q'' = \varepsilon\sigma(T_{heaters}^4 - T_{pebbles}^4) \tag{2-9}$$

ε is the emissivity of the material and σ is the Stefan-Boltzmann Constant (5.67×10^{-8} W/(m^{2}K^4)). The emissivity of graphite varies depending on graphite grade (0.7-0.9). For the purpose of this calculation it is conservatively assumed to be equal to 0.6. The emissivity of the ceramic is between 0.86 and 0.93. The emissivity for the ceramic was measured at low temperatures and showed a pattern of decreasing emissivity with increasing temperature. Thus, for conservatism, an emissivity of 0.6 will be used in the following calculation. Note that in the equation above, $T_{pebbles}$ in practice refers to the sleeve temperature. From the sleeve, heat will be transferred through conduction, convection and radiation to the pebbles. To simplify calculations, it is assumed that the pebble temperature equals the graphite sleeve temperature.

$$T_{heater} = \left(\frac{q''}{\varepsilon\sigma} + T_{ceramic}^4\right)^{0.25} = \left(\frac{13.44x10^4 \frac{W}{m^2}}{(0.6)\left(5.67x10^{-8}\frac{W}{m^2K^4}\right)} + (1873K)^4\right)^{0.25} = 2008K \tag{2-10}$$

Given that the maximum temperature of the ceramic core block is 1600°C, the maximum temperature of the heater rods is expected to be 1735°C.

The added value of the central heater design placed in a graphite sleeve is that it is separated from the thermal expansion of the ceramic pebbles. Nevertheless, it is necessary to consider differential thermal expansion between adjacent heater rods, between ceramic support plates, and graphite components. An estimation of heater components thermal displacement is required in order to design graphite rods joints, support plates, and sleeve fastenings that will accommodate eventual dimensional changes.

From Appendix D, the coefficient of linear thermal expansion (α) for G535 graphite is $5.5\text{x}10^{-6}$ K^{-1} (to 1000°C). Assuming the conservative case of a temperature rise from room temperature to the calculated maximum heater rod temperature (1735°C), the linear thermal expansion can be calculated for G535 graphite using the following equation:

$$\Delta h = \alpha h(\Delta T) = \left(5.5x10^{-6}K^{-1}\right)(1.829m)(2008-293)K = 0.0173m = 1.73cm \tag{2-11}$$

The linear thermal expansion coefficient for the Zirconia FBD ceramics equals $10.7x10^{-6}$ C^{-1} (to 1425℃). To simplify the calculation, the support plate is idealized as a circle without cooling fins. Using the equation above and conservatively assuming that plate temperatures will be uniform and equal to the maximum heating rod temperature, the linear thermal expansion equals:

$$\Delta d = \alpha d(\Delta T) = \left(10.7x10^{-6}C^{-1}\right)(0.5m)(1735-20)C = 0.0092m \cong 0.92cm \quad (2\text{-}12)$$

Radial thermal expansion of graphite heating tubes will be significantly smaller than expansion of Zirconia plate, and range around ~0.2 mm. This means that at higher temperatures, more clearance will be left among tubes and opening walls which will leave space for rod displacement due to eventual flexural bending and deflection.

It should be noted that ceramic materials are prone to permanent changes in material dimensions at elevated temperatures. This was observed while testing HTTF ceramics samples (Greencast 94F). Once the samples were heated to 1500°C, a permanent linear change of +1.17% was present when cooled back to 30°. This behavior can be avoided if the ceramic is heated/sintered at the temperatures expected in the core prior to installation. In the case of the PB-HTTF, ceramic pebbles should be cured at about 1735°C, which is the maximum expected heater temperature.

2.2.8. Estimated Budget

The total cost for the proposed heater design is given in Table 2-3. Please note that this budget is partially estimated on the basis of quotes received for the HTTF components (for flexible joints) and online given prices. Some of the remaining costs are engineering estimates (i.e. supports plates). Only components that will have to be replaced in the redesigned facility are listed. Since the described heater concept is a preliminary design, inclusion of a contingency factor in the pricing estimate is necessary and allows for a margin of error in given estimates.

Table 2-3. Heater design estimated cost.

	Material	Unit Cost $	Quantity	Total Cost $
Graphite Rod[1] (L=45.72 cm)	G540	167.48	600	100,488
Support plate (t=3 cm)	Al_2O_3	12,000	3	36,000
Support plate (t=4 cm)	Al_2O_3	12,000	3	36,000
Electrical joints[2]	Tungsten/ Molybdenum	200,000	1	200,000
Heater sleeve (t=31.5 cm)	GH030	2,450	2	4,900
Heater sleeve (t=63.0 cm)	GH030	4,180	2	8,360
Contingency			25%	96,437
Total				**482,185**

[1] Unit cost given for the highest price quoted (G540). Unit price for G535 tube is $114.33 (300 tubes, L=91.42 cm). Unit price for GR008GP equals $173.4 (150 tubes, L=182.88 cm).
[2] Price provided with reference to the ELMET Technologies quote for the complete OSU HTTF heater design

2.2.9. Heating System Summary

The proposed heating system rearrangement allows for the utilization of the currently existing HTTF electrical service (480 VAC and 4000 A switchgear) along with feed-throughs up to the connection with the new graphite rods. Beyond this connection point a new heating system is proposed. This system borrows heavily from the existing HTTF heating system concept. Several alternative approaches to heat up the pebble bed were considered, but it was concluded that regardless of a number of technical challenges, resistive heating is the most promising method to meet the pebble bed design criteria and operating conditions. Depending on the heater design, it allows for prototypic core power profile generation and does not affect instrumentation operation.

One challenge associated with the proposed heater configuration comes from the close-packing of graphite rods. There is little margin left for extensive bending or displacement of rods that can arise from elevated temperatures. It can be also challenging to manufacture ceramic spacers with densely allocated openings. Moreover, after graphite supplier's product screening, there are reduced possibilities to manufacture a continuous rod (of L=182.88 cm) made of graphite G535 or G540 (maximum height of block size is respectively 48" and 18"). For the iso-molded graphite offered by SGL Carbon (R7660), two graphite tubes will be needed for the required heating length as well. In case the proposed system is unable to be implemented, an analogous system with only 3 rods per leg can be installed. This will reduce the claimed 2.2 MW (to ~1.00 MW) power rating but will still allow to reach desired operational temperatures. If it is decided to derate the core power, heater design principles, placement, connection method and geometry of graphite sleeve will be kept. Nevertheless, in such case, the Scaling Report for PB-HTTF should be revised.

As experience with the current HTTF design has shown, the application of axial heater joints in an environment of radial thermal expansion can present serious engineering challenges. It is anticipated that any multi-tube heater design will have to undergo significant development and testing prior to implementation in the PB-HTTF.

More generally, one should keep in mind that first of a kind test facilities developed to meet high temperature conditions with complicated designs, carry high risk in terms of project schedule and budget, and are prone to future technical complications. Previous lessons learned from operating and troubleshooting the existing HTTF heating system can be directly transferred to the redesigned facility project development, implementation and execution.

2.3. Core Material Selection

2.3.1. Selection Criteria

The High Temperature Test Facility at Oregon State University is designed to replicate conditions expected during various accident scenarios in gas reactors and generate data. The test facility is a scaled version and the data can be used to inform and predict the accident behavior in prototypical reactors (Woods, 2015, 1). As such, whatever material selected for the core internals must be able to withstand extended exposure to temperatures expected during the accident scenarios at or above 1600°C (Woods, 2015, 2). The pebbles at the base of the bed will be responsible for supporting the load of the pebbles above them, and must maintain mechanical integrity under all exposed conditions. Additionally, excess water in the core can damage electronics and degrade materials. Therefore, the material selected for the core should have minimal hygroscopicity. The material during its life in the core will be exposed to periods of atmospheric conditions, and should not degrade in these periods. Several materials may be capable of satisfying the physical requirements listed above. In that scenario, the final material selection will be based on ease of procurement and optimization of the scaling ratios deemed most critical.

2.3.2. Candidate Materials Evaluation

The materials that were deemed most likely to satisfy the requirements listed above were Graphite, Aluminum Nitride (AlN), Aluminum Oxide (Al_2O_3), Silicon Carbide (SiC), and Silicon Nitride (Si3N4). These materials, barring graphite, are known as refractories or structural ceramics. They are frequently used in harsh environments such as high temperature ovens or combustion chambers. They were selected for investigation as they are readily available, and are known to maintain their mechanical strength at elevated temperatures. Graphite is also a natural choice for investigation as it has historically been utilized in gas reactor designs as moderator and reflector in the core (Zheng, 2009). The materials listed will be analyzed with respect to their thermal expansion characteristics, hygroscopicity, distortions from ideal scaling, and ease of procurement.

Thermal Expansion

Due to the high temperatures experienced in the facility, the thermal expansion of the materials is a significant concern. The core must be designed to accommodate the expansion of the selected materials.

The pebble bed core is still in the preliminary design phase and the dimensions are still not finalized. For the purpose of the thermal expansion analysis core height is approximated to 1.98 m (height of the core blocks currently in the HTTF Prismatic Block core configuration). The current proposal is to have an annular pebble bed with an inner radius of 0.25 m and an outer radius of 0.45 m. For the purpose of this analysis the core has been idealized to be a cylinder with a radius of 0.375 m. This simplification maintains the same cross sectional area as the annulus. For the purposes of determining material appropriateness, this simplified geometry should provide sufficient information to decide on material suitability with respect to thermal expansion properties.

The proposed HTTF core temperature profiles during Normal Operation, DCC, and PCC accident scenarios are listed in Table 2-4. The average core temperatures selected were found in literature for these accident progressions simulated in the HTR-PM (Zheng, 2009). The thermal expansion calculations were performed for each material and accident scenario, and compared to the nominal

geometry at room temperature. The calculations were performed in MatLab, and the code is included in Appendix C.

Table 2-4. Core Average Temperature during Varying Core Conditions.

Scenario	Average Core Temperature ˚C
Normal Operation	600
DCC Air Ingress	600
DCC Natural Circulation	975
PCC Natural Circulation	775

The calculations performed are dependent on the assumption that the pebble bed behaves as if it were a block of material linearly expanding in the axial and radial directions. The justification for treating the pebble bed as a solid is based on research of Lithium Titanate. The thermal expansion coefficient of solid Lithium Titanate was reported to be $1.8E^{-5}$ K^{-1} for the temperature range of 20–700˚C (Tanigawa, 2007). Additionally, Lithium Titanate has been studied to examine how it expands in a pebble bed. At temperatures of 20–700˚C, and packing factors of 0.655–0.685, the thermal expansion coefficient is 1.4 +/- 0.2E-5 K^{-1} (Tanigawa, 2009). This research suggests that the pebble bed expands slightly less than the solid Lithium Titanate. By analyzing the PB-HTTF as a solid, the calculations are conservative. Furthermore, the porosity, temperature, and pressure of the investigated pebble bed closely resembles conditions expected in the PB-HTTF.

Graphite has many traits that suggest it would be a suitable core material in the HTTF. Graphite has excellent mechanical behavior in high temperature environments, and typically remains in a solid phase up to temperatures around 4000K (Poco Graphite, 2015). Graphite does not absorb appreciable atmospheric water and is not hygroscopic. Graphite is known to oxidize, however this behavior only becomes prevalent at temperatures above 350˚C (Poco Graphite, 2015). During operation the primary fluid of the HTTF is an inert mixture of Helium and Nitrogen. Therefore, oxidation is not a concern during operation due to an inert environment, and it is not a concern during maintenance as the temperature is below the threshold for oxidation. Graphite has historically been used in high temperature reactors, and is intended to be the core material for the HTR-PM in the near future. It has demonstrated abilities to withstand the conditions in a high temperature gas reactor environment. The thermal expansion calculations were performed following a methodology found in literature for grade G-348 graphite (McEligot et al., 2017). The calculations were performed in MatLab, and the code is included in Appendix C.

Aluminum Nitride was selected as a material for investigation as it is capable of reaching temperatures of approximately 2800˚C. However, the chemical decomposition of AlN into Aluminum and Nitrogen gas occurs appreciably at temperatures above 1800˚C depending on the environment it is exposed to (Liu and Edgar, 2002). While the HTTF core is only designed to operate at a maximum temperature of 1600˚C, it is likely that a different material with a greater margin for error in temperature range would be preferred. Aluminum Nitride does oxidize slightly under atmospheric conditions, but the effect is negligible as a microscopic passivation layer forms that prevents bulk oxidation up to temperatures approaching 900˚C (Lee, 2002). Prior to sintering the AlN powder is hygroscopic and contact with water adversely affects the powder (Panchula, 1999). However, once the material is sintered, hydrolyzation by water is less of a concern as the effective surface area exposed to the water is drastically reduced. So long as extended exposure to liquid water can be prevented, the final sintered product should be stable. The thermal expansion coefficient was determined from Table 4 of (Bruls, 2001). The values used in

calculations are corroborated by similar values found in additional sources of literature (Slack and Batrum, 1975). The calculations were performed in MatLab, and the code is included in Appendix C.

Aluminum Oxide is likely the most ubiquitous refractory ceramic. It has a melting temperature of approximately 2050˚C (International Chemical Safety Cards (ICSC), 2000). Alumina in powder form is frequently used as a desiccant, and is a strong absorber of atmospheric water vapor. If selected as the material of choice, special procedures would need to be in place to accommodate excess water from the Alumina being released when the facility is heated. However, the HTTF has previously developed these procedures for the current core configuration. The thermal expansion coefficient for Alumina was determined from experiments performed on Greencast-94, which is 94% Alumina, reported in (Woods, 2015, 2). The calculations were performed in MatLab, and the code is included in Appendix C.

Silicon Carbide is a common structural ceramic. Depending on the phase of material that is procured for the PB-HTTF, the suitable range of operation can change. If it is necessary for the SiC to be in the Beta phase, then the upper temperature limit would be 1800°C. Above that temperature, the material undergoes a phase change to Alpha phase (Rohm, 2000). In Alpha phase, the material has an upper temperature limit of approximately 2700˚C above which it sublimates (International Chemical Safety Cards (ICSC), 2004). For the purposes of this analysis, the material was assumed to be sintered Alpha phase. The maximum temperature of the material is well above the designed operational conditions of the HTTF. However, SiC is a brittle material and its mechanical strength further degrades as it is heated (Munro, 1997). The propensity for cracking suggests Silicon Carbide is not suitable as a core material in the pebble bed. SiC is not hygroscopic, and is chemically stable under atmospheric conditions along with heated conditions in an inert environment (Ceramic Industry, 2015). The thermal expansion coefficient of Silicon Carbide was determined from equation 4b of (Munro, 1997). The calculations were performed in MatLab, and the code is included in Appendix C.

Silicon Nitride is an exceptionally strong ceramic at atmospheric conditions. However, many of the ceramic manufacturers list a maximum operating temperature of Si_3N_4 at 1000–1400˚C. This is due to a reduction in mechanical strength with increasing temperature. Additionally, Si_3N_4 decomposes to Silicon and Nitrogen gas at a temperature of 1850-1900˚C (Mori, 1984). The core is designed to reach temperatures of 1600˚C, and the degradation of mechanical strength along with the relatively small margins for decomposition temperature suggest that Si_3N_4 would not be a suitable material for the core of the pebble bed. Silicon Nitride is not hygroscopic (Ceramic Industry, 2015). The thermal expansion coefficient was determined from Table 5 of (Bruls, 2001). The values recorded are additionally supported by those included in (Slack and Huseby, 1982). The calculations were performed in MatLab, and the code is included in Appendix C.

A summary of the maximum radial and axial expansion is illustrated in Figure 2-15 and Figure 2-16 respectively. The values are also listed in Table 2-5 and Table 2-6. Thermal expansion will play a minimal role in the material selection process as of all potential materials Alumina experiences the maximum dimensional change at a value of approximately 0.6 %.

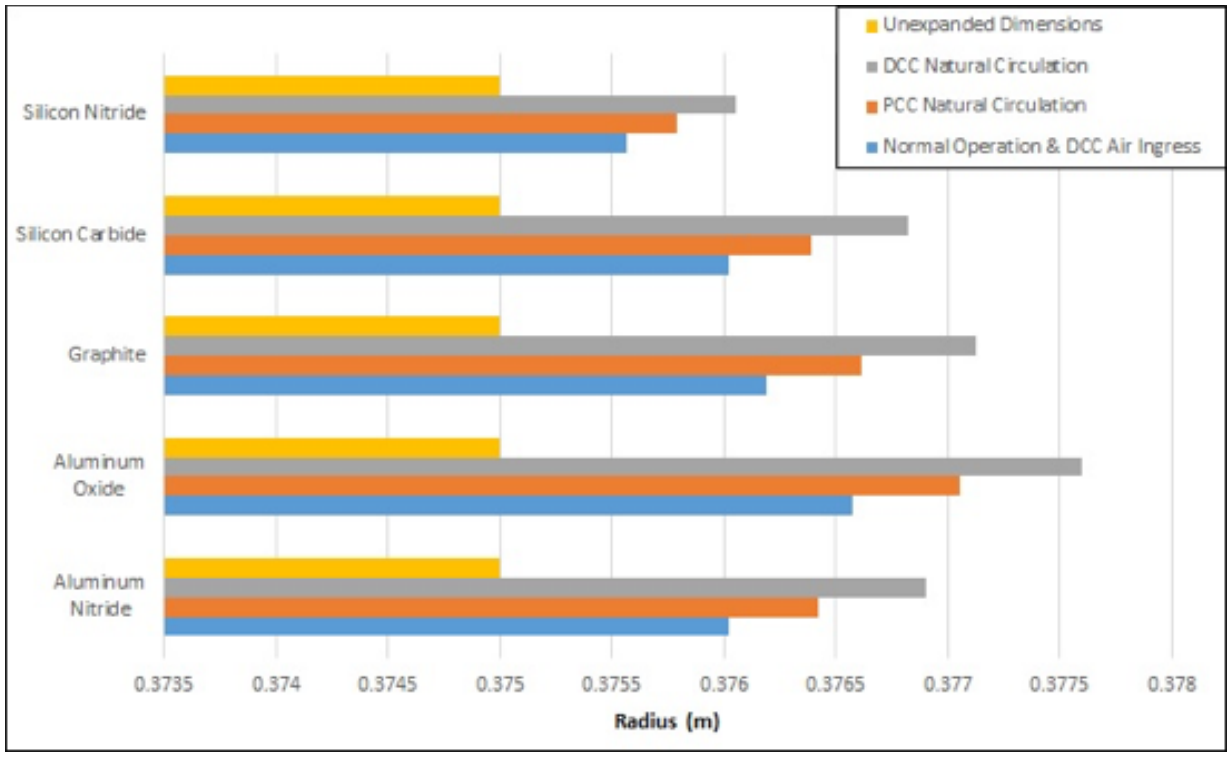

Figure 2-15. Radial Thermal Expansion.

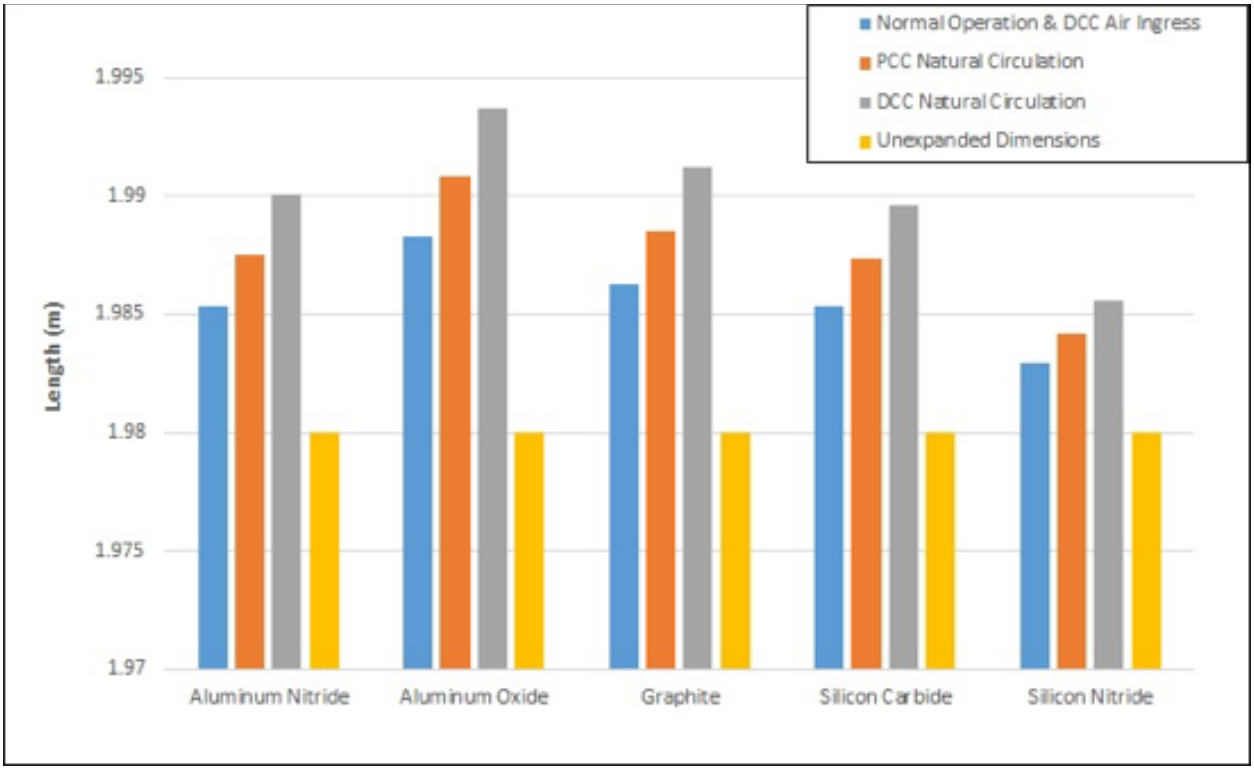

Figure 2-16. Axial Thermal Expansion.

Table 2-5. Radial Expansion Dimensions (m).

	Graphite	AlN	Al_2O_3	SiC	Si_3N_4
Normal Operation	0.3762	0.3760	0.3766	0.3760	0.3756
DCC Air Ingress	0.3762	0.3760	0.3766	0.3760	0.3756
DCC Natural Circulation	0.3771	0.3769	0.3776	0.3768	0.3761
PCC Natural Circulation	0.3766	0.3764	0.3771	0.3764	0.3758

Table 2-6. Axial Expansion Dimensions (m).

	Graphite	AlN	Al_2O_3	SiC	Si_3N_4
Normal Operation	1.9863	1.9854	1.9883	1.9854	1.9830
DCC Air Ingress	1.9863	1.9854	1.9883	1.9854	1.9830
DCC Natural Circulation	1.9912	1.9900	1.9937	1.9896	1.9856
PCC Natural Circulation	1.9885	1.9875	1.9908	1.9873	1.9842

2.3.3. Materials Scaling Analysis

Scaling analyses have been performed to characterize the relevant scaling groups that would be applicable in the HTTF were it to convert to a pebble bed core (Woods, 2016, 1). The various scaling groups were calculated and analyzed to determine the groups that would most likely be affected by changing the materials comprising the core. The groups that were affected were those that were dependent on material density, thermal conductivity, specific heat, and emissivity. The properties for the proposed PB-HTTF materials along with the HTR-PM material in the different accident phases were analyzed to calculate the relevant scaling Pi groups.

In the scaling analysis the emissivity of the material is considered multiple times in the different accident phases. For this analysis, the radiation exchange between surfaces was considered with the simplifying assumption that the pebbles behave as opaque diffuse surfaces at thermal equilibrium. With this assumption, the absorption of a material is equal to the emissivity of the material, and the scattering is equal to the reflectivity or one minus the absorptivity (Bergman, 2011). The spectral radiation distribution was calculated for an emitting black body at the average temperature of each accident phase using Planck's Law for spectral emissive power (Bergman, 2011). The spectrum was then integrated and a normalized distribution of the emitted energy at a given wavelength was produced for each accident phase.

Figures 2-17 and 2-18 illustrate the radiation spectrum and the normalized spectrum respectively. Note that the radiation intensity and spectrum is different for the different accident phases. The temperature during the accident phases used in calculations are tabulated in Table 2-7. The resultant emissivity values were calculated by summing the normalized radiation spectrum multiplied by the temperature and spectrum dependent emissivity. The emissivities for Al_2O_3 (Auerkari, 1996), SiC (Cagran, 2007), and Si_3N_4 (Abedrabbo, 1998) were calculated with this method. The Matlab codes for the aforementioned materials emissivity calculations are included in Appendices D, E, and F. The appropriate emissivity

values for Graphite (Thorn and Simpson, 1953) and AlN (Riou et al., 2013) were found in literature. Table 2-8 contains the resultant emissivity used for calculation in each accident scenario.

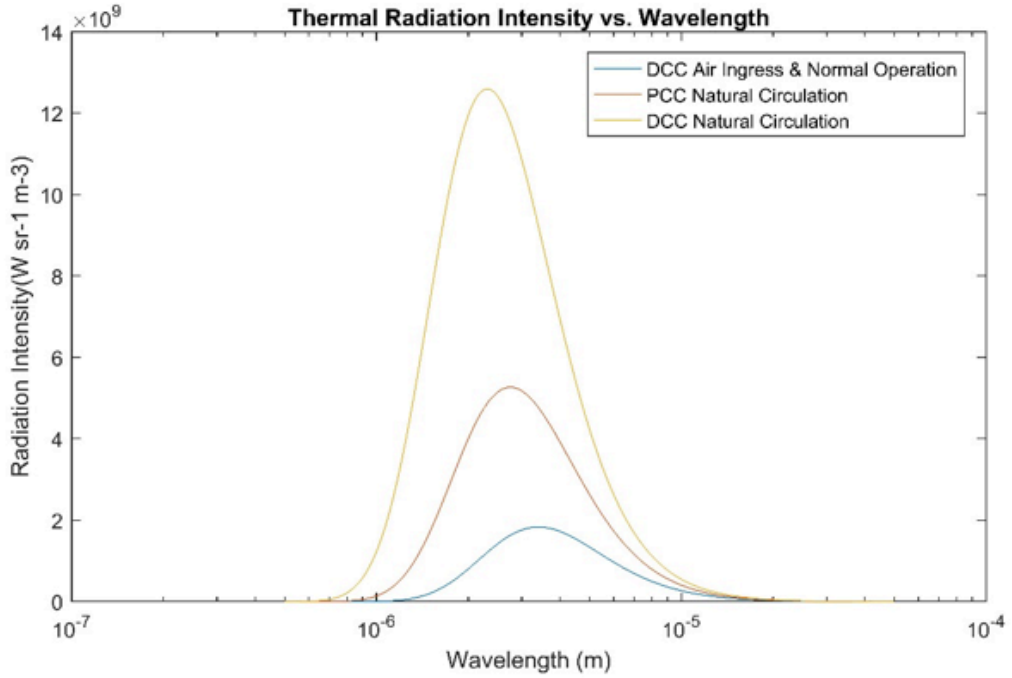

Figure 2-17. Planck Spectral Radiation Distribution.

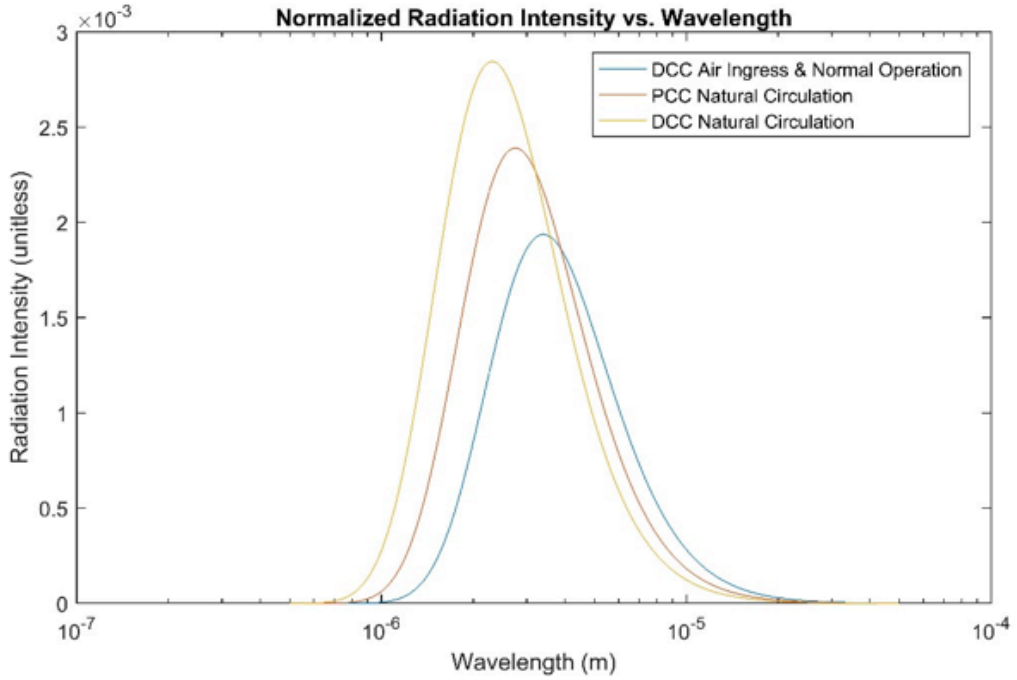

Figure 2-18. Normalized Radiation Spectrum.

Table 2-7. Material Emissivity Values.

	Graphite	AlN	Al_2O_3	SiC	Si_3N_4
Normal Operation	0.8	0.96	0.558	0.804	0.867
DCC Air Ingress	0.8	0.96	0.558	0.804	0.867
DCC Natural Circulation	0.8	0.96	0.434	0.818	0.888
PCC Natural Circulation	0.8	0.96	0.496	0.813	0.881

For the calculation of the scaling ratios, some of the Pi groups use the density of the material. Since the expansion of the material is exceedingly small as discussed previously, it was determined that density values at room temperature would be sufficient for the scaling calculations. The densities for Graphite (McEligot, 2017), Al_2O_3 (Bruls, 2001), SiC (International Chemical Safety Cards (ICSC), 2004), AlN (Bruls, 2001), and Si_3N_4 (Bruls, 2001) were found from literature and are summarized in Table 2-8.

Table 2-8. Material Density Values (g cm^{-3}).

Graphite	AlN	Al_2O_3	SiC	Si_3N_4
1.895	3.256	3.986	3.200	3.202

Many of the Pi groups are dependent on the material thermal conductivity. Thermal conductivity is known to have strong temperature dependence in some materials, and as such the material values were found for the average core temperatures for the various core accident progressions listed in Table 2-9. The thermal conductivities for graphite (McEligot, 2017), Al_2O_3 (de Faoite, 2011), SiC (Munro, 1997), AlN (Slack, 1987), and Si_3N_4 (de Faoite, 2011) were found from literature and are summarized in Table 2-9.

Table 2-9. Core Average Thermal Conductivity ($Wm^{-1}K^{-1}$).

	Graphite	AlN	Al_2O_3	SiC	Si_3N_4
Normal Operation	83	96	11	50	17
DCC Air Ingress	83	96	11	50	17
DCC Natural Circulation	66	51	7.5	37	14
PCC Natural Circulation	73	75	9	42	16

Various Pi groups are dependent on the material specific heat. Specific heat displays temperature dependence in materials, and as such the material values were found for the average core temperatures for the various core accident progressions listed in Table 2-10. The specific heat for Graphite (McEligot, 2017), Al_2O_3 (de Faoite, 2011), SiC (Munro, 1997), AlN (de Faoite, 2011), and Si_3N_4 (de Faoite, 2011) were found from literature and are summarized in Table 2-10.

Table 2-10. Core Average Specific Heat (J $kg^{-1}K^{-1}$).

	Graphite	AlN	Al_2O_3	SiC	Si_3N_4
Normal Operation	1700	1210	1200	1130	1140
DCC Air Ingress	1700	1210	1200	1130	1140
DCC Natural Circulation	1920	1300	1275	1230	1250
PCC Natural Circulation	1820	1260	1240	1180	1200

Given the material properties listed previously in Tables 2-7 through 2-10 along with facility dimensions for the HTTF (Woods, 2017, 1) and the HTR-PM, the scaling analysis outlined in (Woods, 2016, 1) was completed for Al_2O_3 and Graphite. The scaling analysis was limited to these materials as the mechanical properties of the other materials effectively excluded them from successful installation and operation within the PB-HTTF. The resulting scaling ratios and distortions for Pi groups that changed with the selected materials have been included in Tables 2-11 through 2-14. The equations are labeled corresponding with their equation number in (Woods, 2017, 1).

Table 2-11. DCC Air Ingress Scaling Analysis.

Equation	Graphite Ratio	Graphite Distortion	Al_2O_3 Ratio	Al_2O_3 Distortion
(3-56)	2.52	-1.52	0.23	0.77
(3-57)	3.75	-2.75	0.34	0.66
(3-60)	0.29	0.71	0.06	0.94
(3-62)	0.88	0.12	0.50	0.50

Table 2-12. DCC Natural Circulation Scaling Analysis.

Equation	Graphite Ratio	Graphite Distortion	Al_2O_3 Ratio	Al_2O_3 Distortion
(3-90)	36.2	-35.2	0.12	0.88
(3-91)	27.6	-26.6	2.26	-1.26
(3-92)	4.54	-3.54	3.25	-2.25
(3-96)	4.41	-3.41	3.16	-2.16
(3-95)	2.51	-1.51	0.34	0.66
(3-101)	7.60	-6.60	4.17	-3.17
(3-120)	0.13	0.87	0.60	0.40

Table 2-13. PCC Natural Circulation Scaling Analysis.

Equation	Graphite Ratio	Graphite Distortion	Al_2O_3 Ratio	Al_2O_3 Distortion
(3-139)	19.9	-18.9	1.75	-0.75
(3-140)	29.7	-28.7	2.61	-1.61
(3-141)	10.5	-9.5	7.31	-6.31
(3-144)	2.62	-1.62	0.45	0.55
(3-146)	7.95	-6.95	4.42	-3.42
(3-155)	0.11	0.89	0.56	0.44

Table 2-14. Normal operation Scaling Analysis.

Equation	Graphite Ratio	Graphite Distortion	Al_2O_3 Ratio	Al_2O_3 Distortion
(3-180)	0.01	0.99	0.10	0.90
(3-184)	0.10	0.90	0.24	0.76
(3-185)	0.20	0.80	1.51	-0.51
(3-186)	0.35	0.65	2.17	-1.17
(3-191)	0.10	0.90	0.52	0.48

2.3.4. Pebble Bed Procurement

The pebbles in a pebble bed are randomly distributed with variations in the packing primarily based on installation method and the ratio of the diameters. The porosity of the pebble bed is a primary concern as it directly influences the thermal behavior of the pebble bed (Kerntechnischer Ausschuss, KTA, 1983). The average porosity of the HTR-PM is 0.39 (Ximing, 2014), and the PB-HTTF should have the pebbles arranged in such a way to match this value. To ensure the PB-HTTF has this porosity, calculations were performed following methods suggested from literature (du Toit, 2008) and the relevant Matlab code is included in Appendix G. The resulting average porosity calculated for the PB-HTTF is approximately 0.38. This porosity matches extraordinarily well with that of the HTR-PM. To achieve this value the pebbles should be poured individually or as a stream into the core area (de Klerk, 2003). The need to pour the pebbles into the core simplifies installation, as PB-HTTF employees can easily pour pebbles into the core from the top.

Central to the feasibility of installing the PB-HTTF is the rough cost estimation for the pebble bed core. A cost estimate has been identified for procuring each material listed barring Aluminum Nitride balls as there are no commercial vendors that returned requests for quotes. It is worth noting that for all of the procured materials, the detailed thermal and mechanical properties are not available online and in reality it is unlikely the vendor has the information. The previous analysis was performed using referenced values for each generic material, but it would prudent to acquire and test samples to characterize the material properties before procuring and installing the material in the whole core.

Graphite

Graphite is one of the primary candidate materials for the pebble bed core. Graphite is commercially available in many grades, and it is expected that several different grades would adequately handle the core environment. One of the commercially available grades is BTG-5 which was quoted at a price of $0.63 for each 1.5 cm diameter sphere from Beijing North Xinyuan Electrical Carbon Products. Previous analyses were performed using the thermal properties for G-348 graphite which likely differs to some degree from those of the BTG-5.

Aluminum Nitride

Aluminum Nitride is readily available in powders, and can be cast and sintered. However, the properties of Aluminum Nitride are highly dependent on the sintering process. The purity of the materials, the sintering aids, and the length of the sintering process all affect the final product (Franco-Junior and Shanafield, 2004). This is problematic from a design and procurement process as values for analysis can be drastically different from those of the actual material received. The property that embodies the uncertainty the most is the thermal conductivity which can vary from 17–285 W $m^{-1}K^{-1}$ (Franco Junior and Shanafield, 2004). Several companies sell powders and some, such as Surmet, sell custom fabrication and sintering services. Additionally, 1.5 cm diameter Aluminum Nitride balls are advertised on Alibaba by Haihang Industry (Jinan) but the pricing was not available and quote requests have gone unanswered. This is of minor importance as the material was largely disqualified as a core material in previous sections.

Aluminum Oxide

Numerous companies sell Alumina spheres with a wide range of prices depending on material, sintering, and surface finish. Ortech Ceramics sell 1.5 cm diameter ball bearings for $9.50 each. Whereas, Guangzhou Chemxin Environmental Material sell 1 kg bags for $1.16 or $0.007 per ball. Both values discussed were commercially available on the internet and no specific quote was received. Similar to Aluminum Nitride discussed previously, the material properties of Alumina are highly dependent on surface and internal defects along with material composition and sintering procedure.

Silicon Carbide

The price for Silicon Carbide varies widely by vendor. 1.5 cm diameter balls were quoted from Zhejiang Jienaier New Material Co. on Alibaba for a price of $0.156 per ball, and on the other end of the

spectrum, balls of the same dimensions are available from Ortech Ceramics for $16.50 per ball. The wide varying cost in this material and others is in large part due to variations in surface finish and polishing. Highly polished balls from Zhejiang Jienaier New Material Co. were quoted at $4.36 per ball.

Silicon Nitride

Silicon Nitride balls are readily available, if albeit relatively expensive. 1.5 cm diameter balls are available from Ortech Ceramics for $16.50 per ball. Alternatively, a supplier found on Alibaba, Porei group based out of Jinan, China, quoted the 1.5 cm Silicon Nitride balls at $0.94 each.

Procurement Cost Summary

Using the dimensions for the proposed PB-HTTF annular core (L = 1.98 m, ID = 0.5 m, OD = 0.9 m), and the estimated void fraction, the total volume of core material was estimated to be 0.54 m^3. Dividing the total material volume by the volume of a single pebble produced an estimate of approximately 300,000 pebbles expected in the core. The cheapest cost estimate received for each material is summarized in Table 2-15.

Table 2-15. Pebble Bed Cost Summary.

	Graphite	AlN	Al_2O_3	SiC	Si_3N_4
$ / Pebble	0.63	-	0.007	0.16	0.94
$ / Core	193,000	-	2,200	47,000	283,000

2.3.5. Core Material Selection Summary

Five materials were examined for use as the core material within the PB-HTTF. The materials were analyzed for their appropriateness based on thermal expansion behavior, hygroscopicity, thermo-mechanical behavior, and distortions to the ideal scaling. None of the materials displayed adverse thermal expansion behavior. Aluminum Oxide and Aluminum Nitride were the only materials with hygroscopic tendencies, and it was determined that the test facility can take steps to mitigate this behavior.

It was determined that the thermo-mechanical behavior of SiC, AlN, and Si_3N_4 disqualified these materials from use in the PB-HTTF. Silicon Carbide is excessively fragile and the propensity to fracture makes it an undesirable core material. Aluminum Nitride has a decomposition temperature close to the operating temperature of the PB-HTTF, and a material with a greater margin for failure is preferred. Silicon Nitride, similar to Aluminum Nitride, decomposes at temperatures close to the operational temperature of the PB-HTTF. Additionally, it has dramatic reductions in mechanical strength with increasing temperature, and many vendors and manufacturers list a maximum operational temperature below the expected core temperatures in the PB-HTTF.

The remaining materials not excluded are Al_2O_3 and Graphite. Both materials were analyzed with respect to their effects on the Pi scaling groups. Clearly, neither are ideal in terms of scaling, and ultimately the perfect material in terms of scaling likely does not exist. The PB-HTTF is best suited for a DCC test facility and Alumina is best suited to reduce the scaling distortions. However, as distortions are inevitably present, the test facility is most likely to be used to validate systems codes. As such, either material is potentially suitable as a core material. As summarized in Table 2-15, the cost of procurement for a graphite core is $193,000 compared to the cost of an Alumina core at $2,200. Since it minimizes scaling distortions and cost, it is recommended that the core be composed of Aluminum Oxide.

2.4. Core Instrumentation

This part of the report outlines a brief description of the instrumentation to be used in the PB-HTTF. As stated in (Woods, 2015, 3) a correctly scaled integral facility can be used to examine the thermal hydraulic system behavior of the design basis and beyond design basis transients is of significant value. The experimental results obtained in such a program could be used to validate analytical tools and methods being proposed for use with the reference reactor design. Therefore, it is of importance that the PB-HTTF is instrumented in such a way that the required data is collected to meet its overall goals of phenomena examination and code validation.

In addition to the instrumentation used to collect data to achieve the overall goals of the PB-HTTF test program, there will be instrumentation in the PB-HTTF, which is primarily used to ensure the safe operation of the test facility. This type of instrumentation shall be termed “Control Instrumentation” and will be discussed in this section. This section will also discuss the DACS, which is a personal computer controlled system that is used to control both the collection and storage of the test matrix and control system data as well as electrical and mechanical operation of the test facility.

2.4.1. Instrumentation Layout

It is unlikely that the sensors outside of the core will change appreciably between the pebble bed and prismatic block core configuration. Likely the most drastic differences between the current and proposed core configurations are the changing of the outer core reflector dimensions. This would cause the thermocouples in the reflector to be modified or moved.

Sensor Rod Array Design

The core sensor rod design currently being considered is half a horizontal rod cut lengthwise extending from the outer core reflector into the pebble annulus of the core. The innermost part of the core is the heater/central reflector with a diameter of 50.0 cm. The pebble bed annulus has an outer diameter of 90.0 cm and a thickness of 20.0 cm. The outer reflector has a diameter of 150.0 cm and a thickness of 30.0 cm. The nominal instrumentation rod resembles 3 6.0 cm diameter spheres linearly connected with a 30.0 cm straight portion attached that passes through the outer reflector.

Figure 2-19 is a drawing of the rod, and the relevant dimensions are included in cm. Notably, the rod has a 1.0 cm diameter bore for sensor wires, and a minimum of 1.0 cm thick ceramic annulus around the bore to provide mechanical support. The rod was shaped this way in an effort to reduce the wall effect on the pebbles in the core in the region near the sensors on the rod. It is difficult to quantify the wall effect on the irregular geometry. If it is determined in the future that the shaped rods are not feasible, an alternative rod of identical lengths and diameters without the spherical features would be considered.

For the pebble bed core, sensor rods are to be placed in the pebble bed to provide support and housing for the necessary core sensors. The sensor rod is to be created as two halves that are secured together by the portion that passes through the outer reflector. There is to be a top half and a bottom half with the middle plane orthogonal to gravity. The rod was designed this way to facilitate an easier manufacturing process, allow easier installation of sensors and wiring through the bore, and allow the top and bottom pieces to differ geometrically depending on the sensors present. It is intended for the rods be composed of 90%+ Al_2O_3 and cast into the required shape. The rod was halved to simplify the casting and sintering in the production of the rods. Many of the half rods will have penetrations normal to the lengthwise axis where sensors are to be placed, and constructing molds with the penetrations already in place was deemed preferable to machining each rod individually. The necessary penetrations differ for the top and bottom halves of the rods, along with dependencies on the specific instrument placed at each sphere.

The rods are to be arranged such that 4 of them are on an axial plane each offset 90°. There are 5 axial planes all equally spaced 0.4 m from one another. The planes are to be at heights 0.2, 0.6, 1.0, 1.4, and 1.8 m from the lower plenum roof. Each axial plane will be rotated by 45° from the plane below such that

the rods between two axial planes are not directly above one another. Each sphere will have a sensor location present on it for a total of 3 per rod, 12 per axial plane, and 60 in the core. A cross section illustrating the rod layout has been included in Figure 2-20. Detailed instrumentation location is summarized in Appendix B.

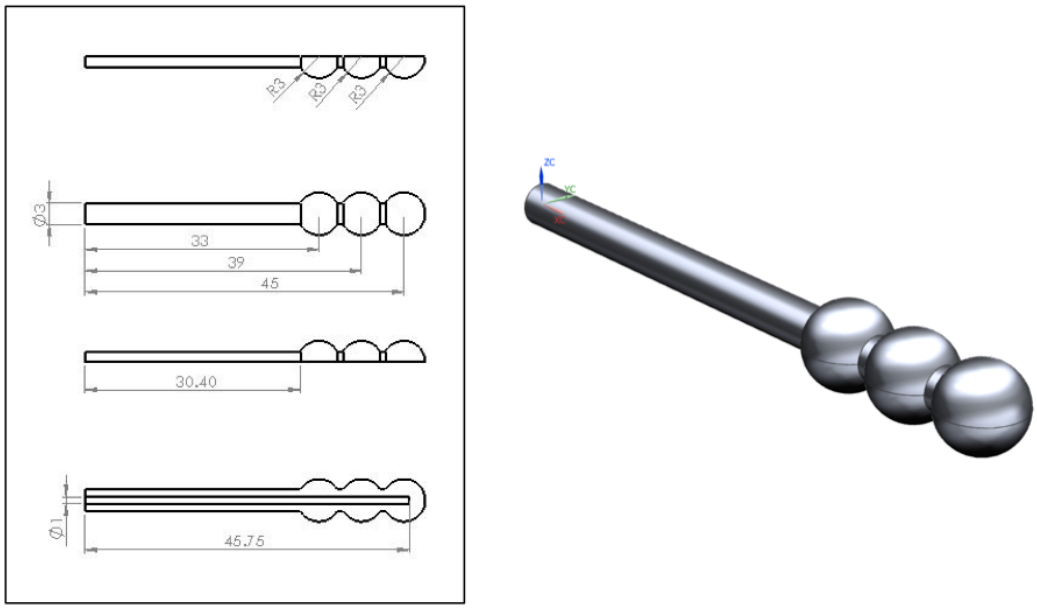

Figure 2-19. Shaped Instrumentation Rod.

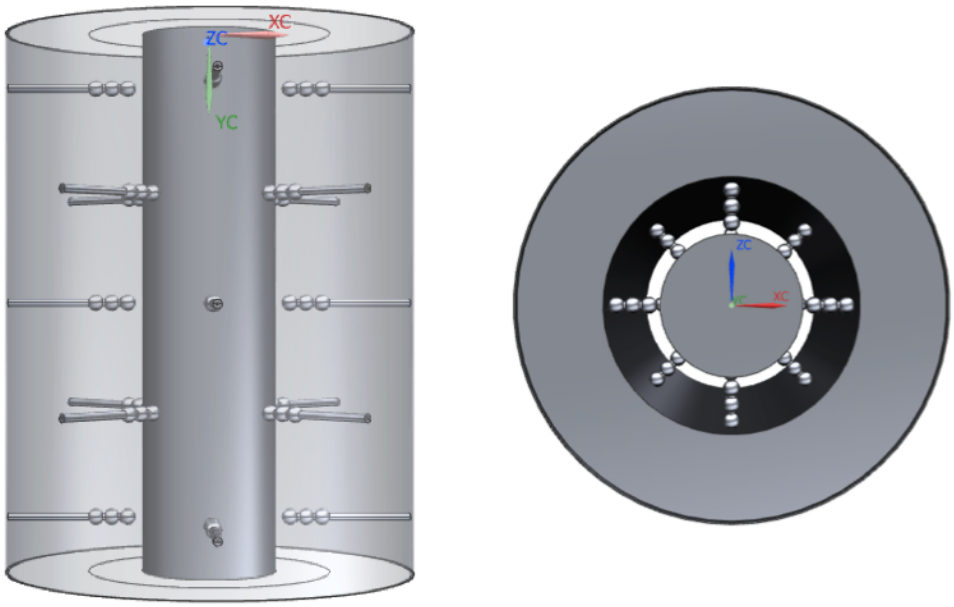

Figure 2-20. PB-HTTF Cross Section Instrumentation Rod layout.

Core Thermocouples

Thermocouples will be used to measure radial and axial core thermal profiles for coolant gas temperatures. On the sensor rods, there are three spheres each with a potential radial location to place a thermocouple. The temperature profile of the flow area during accident scenarios has not been calculated for the annular pebble bed configuration. However, for the prismatic core radial positions within 0.6 of the normalized radius were expected to reach temperatures above 1250°C (Woods, 2015, 3). For the annular pebble bed, the inner 0.6 of the radius includes the middle, and innermost sensor locations on the instrumentation rod. Therefore, thermocouples placed in these locations must be thermocouples that can withstand the high temperature conditions.

B-type thermocouples are capable of handling extended exposure to temperatures of 1700°C. However, they have a low output voltage to temperature ratio. This causes readings during low temperature operations to be problematic. R-Type thermocouples are capable of continuous operation temperatures of 1450°C, and their higher output voltage to temperature ratio than their B-Type counterparts allows increased performance at lower temperatures. However, as the core is designed to have regions of extended temperature exposure of 1600°C (Woods, 2015, 3), the R-Type thermocouple may not be suitable. C-Type thermocouples have been problematic in the HTTF current prismatic block core configuration, but they offer the widest range of continuous operational temperature. Additionally, they have the strongest output voltage to temperature ratio of the three high operating temperature thermocouples. K-type thermocouples have an operable range up to 1250°C and are widely used and significantly cheaper than the three high temperature thermocouples listed previously.

The choice of thermocouple for the middle and innermost radial locations shall be determined by the requirements of the testing matrix. The simplest apparent solution would be to limit the maximum extended exposure temperature of the thermocouples to 1450°C, and place R-Type thermocouples in the middle and innermost radial locations on the sensor rods, with K-Type for the outermost locations. If it is imperative that the core have extended temperatures above 1450°C, then the middle and innermost locations would be C-Type, and the rest would be K-Type.

The rod arrangement is designed to feature a total of 30 thermocouples with 2 inner, middle, and outer thermocouple locations on each axial level. Therefore, it is expected 20 thermocouples will be R or C-Type, and 10 of them will be K-type in the core.

The thermocouples are to be installed into a plug, and the plug installed into a generic slot in the sensor rod. This method was chosen to simplify the installation of instruments, and the production of the rods. The thermocouple plug is shown in Figure 2-21 below. The dimensions for the figure are in mm. The thermocouples are intended to have a 1/16th inch outer diameter on the protective sheath, and as such the hole through the plug is meant to fit the TC snugly.

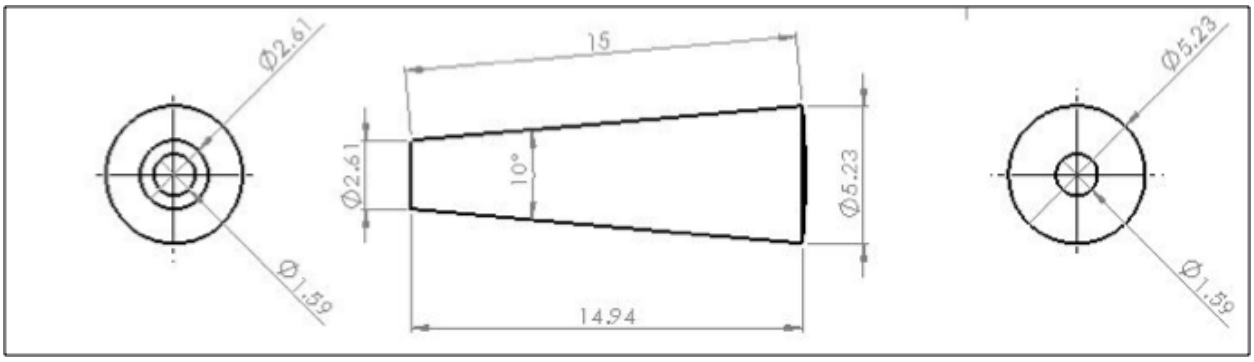

Figure 2-21. Thermocouple Plug.

The sensor rods are intended to have the plugs inserted in the top half rod. A half rod with all generic plug slots on the top is shown in Figure 2-22. Note that all the dimensions are in mm, and the rod is the same as the generic rod shown in Figure 2-19 with the exception that three holes are present in which the plugs from Figure 2-21 would sit. The bottom half accompanying the top half is the generic rod from Figure 2-19.

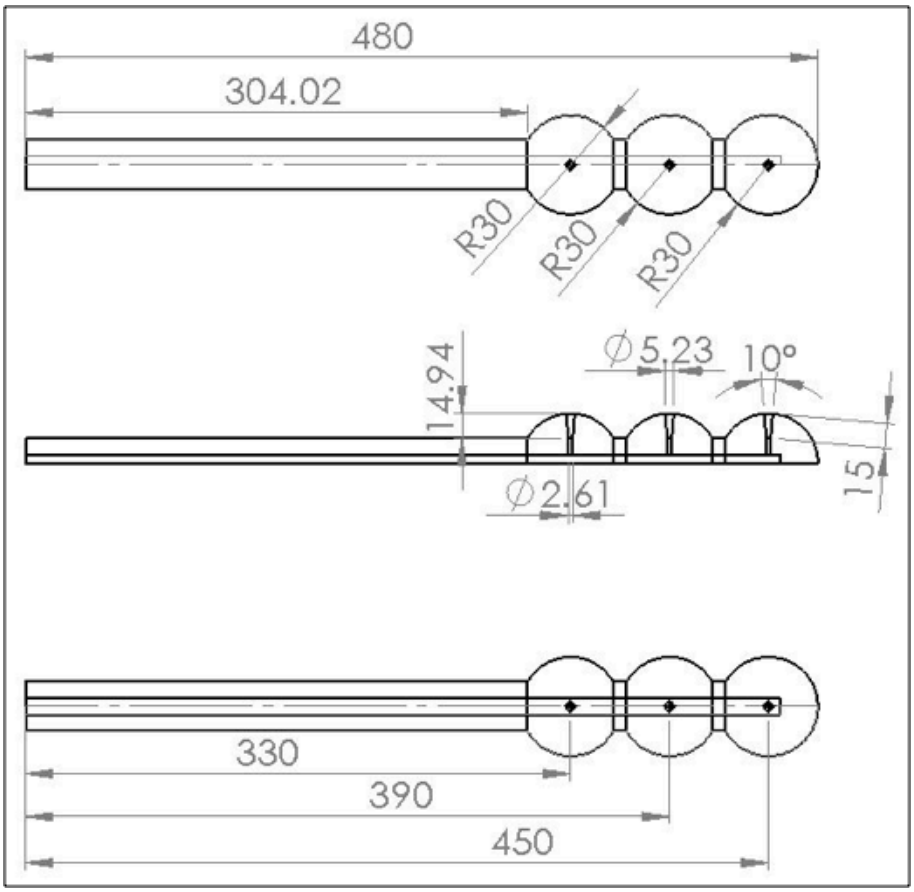

Figure 2-22. Instrumentation Rod Top Half with three Generic Slots.

MEMS Anemometers

The role of the core anemometers is to measure the local flow field in the region near the anemometer array. To generate a more complete flow field at a location, 3 anemometers are to be clustered together. The three velocity readings can be combined to generate a more accurate velocity profile at the given location. Each axial level is to have an anemometer cluster placed at each of the three radial locations of the spheres. This results in a total of 9 anemometers per axial level and 45 anemometers overall in the core.

The anemometer sensors are two-dimensional hot-wire probes which were created specifically for this application. The probes are produced using Micro-Electro-Mechanical Systems (MEMS) fabrication techniques, consisting of photo-lithography for masking and a variety of deposition and etching processes to build up the tungsten or platinum sensing elements. The fabrication technique allows for the creation of complex sensor geometry. The sensor and its housing are shown in Figure 2-23.

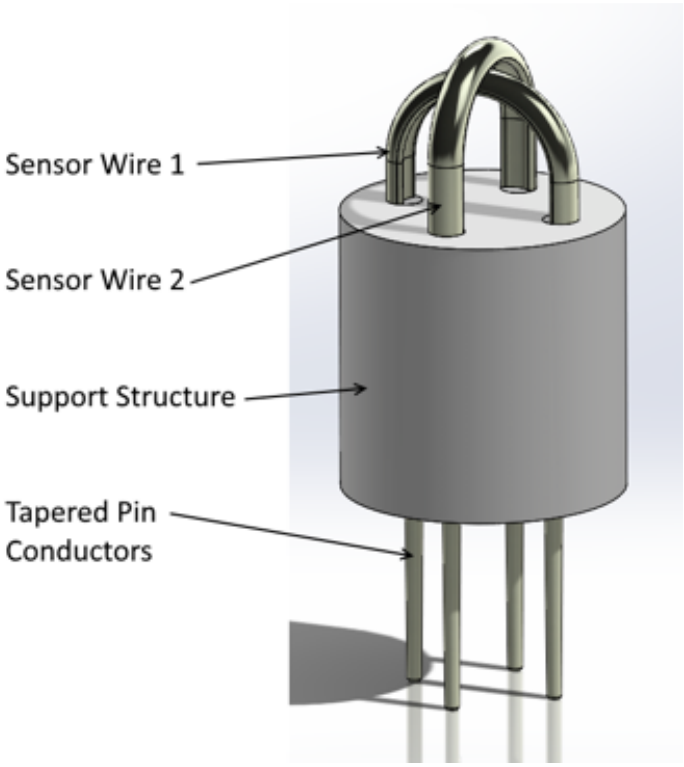

Figure 2-23. Render of the Anemometer Sensor.

The sensor wires are connected to two legs of a Wheatstone bridge circuit, with the differential voltage indicating the two-dimensional flow velocity of the local fluid. The response of the sensor can be adjusted by varying the sensor wire diameter and shape. The measurement location distance from the surface of the pebble can be adjusted by increasing the length of the support structure to allow the sensor wires to protrude further into the flow field. The tapered pin conductors allow the sensors to be installed into the dedicated instrument ports. The anemometers and their assemblies are intended to fit into an anemometer plug that will fit in the generic plug ports on the top half of the instrumentation rod shown in Figure 2-22. The anemometer plug is shown in Figure 2-24 below. The plug has three holes on top for the anemometer assemblies, of which Figure 2-23 is only the top portion. Figure 2-23 plugs into the rest of the anemometer assembly to provide power to the sensor without the need to solder the wires.

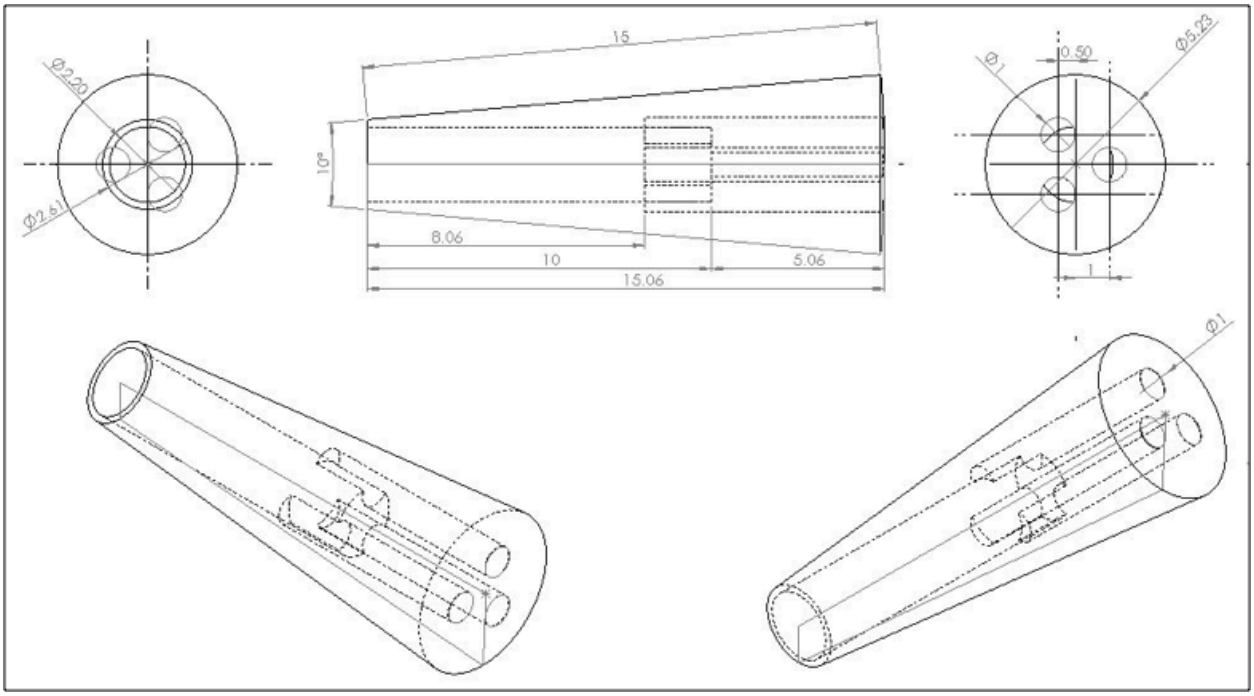

Figure 2-24. Anemometer Plug.

Core Pressure Instruments

A differential pressure transmitter (DPT) corresponding to upper and lower position pressure taps will be used to measure pressure drop across the core. Two vertical positions will be used for these instruments. The high position corresponds to above the orifice plate immediately below the upper plenum floor. The low position will be at the bottom of the core. This arrangement allows the overall pressure drop across the core to be easily calculated. The core pressure instruments are intended to remain mostly unchanged from the current prismatic block OSU HTTF configuration.

Core Gas Concentration Instruments

The GCI used in the core uses two plates to make a capacitive reading of the gas between the plates. New gases introduced in an accident scenario have a different capacitance than the nominal Helium, and the change in the detected capacitance between the plates can be used to calculate the composition of the gas (Cadell, 2012).

A new GCI was conceptualized that would fit in between the top and bottom halves of the sensor rod normal to the lengthwise axis. The top sensor rod would still have the generic plug slots present on the other two instrumentation sites. There are instrumentation rod designs for the GCI slot to be located at each radial position. The top half of the instrumentation rod with a GCI slot for the innermost radial position is show in Figure 2-25. Note that the dimensions are in mm, and that the generic ports have not been dimensioned to reduce clutter. The GCI will fit in the 5.0 mm diameter slot on the last sphere. The bottom half of the instrumentation rod is identical to the top half except it does not have the generic plug slots at the other two radial positions.

The GCI itself is show in Figure 2-26. It consists of two cylinders held in place by 4 posts with an annulus for gas to flow through. Note that all dimensions are in mm.

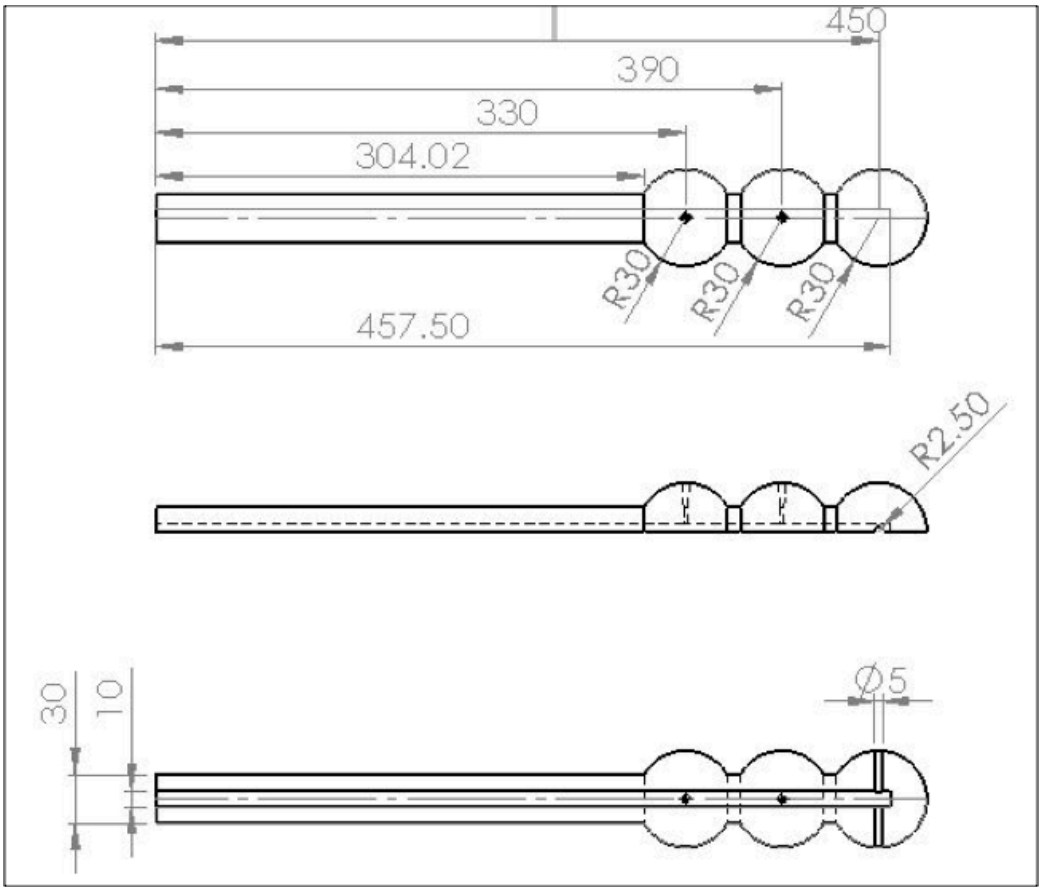

Figure 2-25. Instrumentation Rod with GCI Top Half.

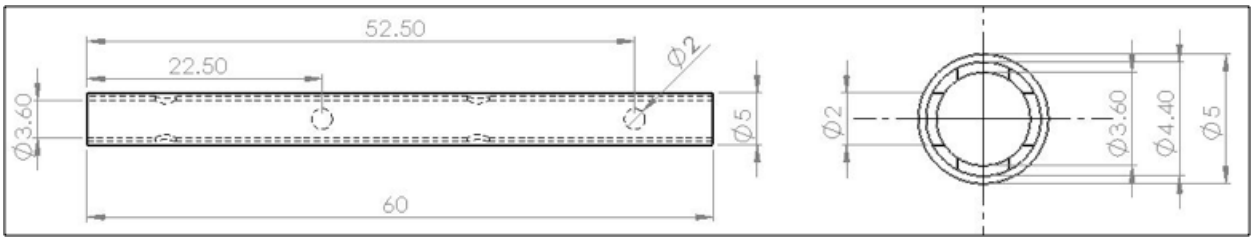

Figure 2-26. Gas Concentration Instrument Drawing.

The GCI is still in the conceptual phase and it is difficult to estimate the feasibility of the design without knowing how the GCIs in the current core perform. The GCI was designed as small as possible so that the wiring from the instruments can pass around it in the central bore hole. However, it may be necessary to enlarge the bore further to allow more clearance for the wiring around the GCI. It is intended to have one GCI at each radial location on each axial level for a total of 15 GCIs.

2.4.2. Instrumentation Hardware

R Type Thermocouples

Nordic Sensors quoted $95 for each metal sheathed and mineral insulated 1/16“ x 7’ strand of R-Type thermocouple. It is assumed the 7’ strand is long enough on average to get the thermocouple out of the pressure vessel. This would result in an overall cost of approximately $10,000 for the 20 thermocouples required.

C Type Thermocouples

The current OSU HTTF facility utilizes Type-C thermocouples in the core, and problems have arisen from the bare wire thermocouples. To address this issue, sheathed and mineral insulated C-Type thermocouples capable of withstanding the expected 1600 °C were identified from OMEGE Engineering. The 1/16” x 7’ C-Type thermocouple was quoted at approximately $1600. Assuming no discounts, the thermocouples would cost approximately $32,000 for the 20 thermocouples required. Note that if the R/B Type thermocouples are purchased Type-C would not be necessary.

K Type Thermocouples

The K-Type thermocouple would be purchased from OMEGA Engineering. The cost for each sheathed, mineral insulated 1/16’ x 7’ strand of K-Type thermocouple is $45.80. The core is expected to have 10 K-Type thermocouples in it for a total of $458. The wiring for the thermocouple is relatively insignificant as the thermocouple is assumed to escape the RPV allowing wiring that needs to withstand a much milder environment to be used.

Signal Processing

The thermocouples will terminate in a NI9214 module. As the pebble bed design consists of many fewer thermocouples than the current prismatic block configuration no additional modules would need to be purchased.

MEMS Hardware

The MEMS require 4 wires each to function optimally. Currently 4 lead mineral Insulated cable is being examined to supply the power to each MEMS. The MI cable is necessary to reduce noise from the power supply to the heaters. The MI cable costs around $5 per foot. With this assumption, the wiring leading to each MEMS cluster is approximately $100 (7ft x $5/ft x 3 MEMS/cluster). The MEMS have yet to be produced, but the designer is convinced the MEMS would cost between $50-100 apiece. For each MEMS sensor cluster it is between $250 and $400. There are 15 clusters overall in the core resulting in a cost of $3,750-$6,000.

Additionally, the MEMS are currently designed such that a NI9327 module would be required for data input. Each module can hold 4 MEMS requiring a total of 12 modules as 45 MEMS are present in the core. The NI9327 modules are retailing for approximately $1,100 meaning an additional $13,200 would be required for the sensors to be functional. These quotes will become more definitive during FY2018 when MEMS are going to be fabricated and tested at OSU.

Gas Concentration Instrument Hardware

The construction costs of the GCI’s remain to be seen, and is largely dependent on the final design geometry and materials. However, in terms of signal processing the GCI’s would require a NI9205 module. The current facility has more gas concentration instruments in the core than the proposed pebble bed facility, and as such no additional modules would need to be purchased.

Instrumentation Rod Hardware

A number of manufacturing processes were considered for procuring the rods, and it was decided that casting the rods would be the most efficient path forward. The rods must be capable of withstanding the conditions present in the core. Because of the stresses and temperatures it will be exposed to, the instrumentation rod will be constructed of primarily Aluminum Oxide (Al_2O_3). The material Greencast 94

will be used as the material for the rods. The product sheet provided by the supplier is included in Appendix A.

Greencast 94 was used as the casting material for the current HTTF core blocks, and has demonstrated that it can withstand the expected conditions in the core. In the proposed design, 40 of the half instrumentation rods shown in Figure 2-19 would be installed. Each half rod has a material volume of 261.18 cm^3. This results in 1.44472 E^{-2} m^3 of castable ceramic required for the instrumentation rods. The material has an advertised density of 2500 kg m^{-3} resulting in 26.1 kg or 57.5 lbs. of ceramic. Hard Luck Forge Supply has 20 lb bags of Greencast 94 available for $80.

The rods would need to be cast in a mold, and previous experience has shown that Ultra High Molecular Weight Polyethylene (UHMW) works well as the mold material. The molds would be constructed of two 1"x24"x24" machined UHMW sheets. Each of these molds would be capable of forming 8 of the half rods at a time. The sheets are available from McMaster Carr at a price of $129.30 each. Additional costs may arise in the machining process if it is not possible to machine them in house.

The rods after casting must be fired, and it is likely that they will be fired at Western Industrial Ceramics. The casting and firing at Western Industrial Ceramics was quoted at $232 per half rod for a total cost of $9,280. It will likely be cheaper to procure a second mold and have more of the half rods fired at a single time at WIC—i.e. 3 batches of 16 half rods instead of 5 batches of 8.

During installation in the core the half rods will be sealed together using Ceramic Structural Adhesives available on McMaster Carr. The adhesive has a maximum temperature of 2200 °C and is sold in 32 oz. cans for $109. It is unknown how many cans would be necessary. Assuming that one can will be able to seal two rods, then it would cost approximately $1100 for the adhesives.

In all, the raw material would cost $240 for the Greencast 94 powder, approximately $500 for the UHMW plastic, and $1,100 for the adhesives. The labor costs would be $9,280 for the casting and firing of the rods, with potential additional costs for machining the UHMW.

As an additional note, the shaped instrumentation rods have been noted as relatively difficult to manufacture. In the case that their manufacturing becomes too problematic or the wall effect benefits are determined to not be worth the additional effort, cylindrical rods of the same dimensions without the spherical features would likely be considered. The simpler rods would need to be manufactured in a similar manner, and the cost is likely comparable to that of the shaped rods. The dimensions of the instrumentation holes and plugs would differ slightly, and the GCI design would need to be reconsidered.

2.5. Project Management, Schedule and Cost Estimate

2.5.1. Program Management

The OSU HTTF will be reconfigured and managed according to the OSU High Temperature Test Facility Quality Program Plan. The funding source is not yet defined. Overall responsibility for executing Sponsor's project requirements will be held by the OSU Program Manager.

2.5.2. Schedule

If sufficient funding is available, design efforts can be initiated in 2018 with conceptual design work starting in Q1-2018 and completion of Final Design in Q2-2019. Construction activities should start after Final Design Review (2 months), acceptance of the Project Execution Plan (3 months) and components delivery (~3–4 months). If this timeline is met, facility startup should occur at the end of Q1-2021 and matrix testing at the beginning of Q4-2021. These dates will become more definitive during the Conceptual Design Phase. If the project Sponsor decides that the test facility should be built with reference to a different prototype pebble bed reactor design, then the timeline showed in Figure 2-27 will have to be updated with a revision to the scaling analyses and the project total time will be extended to ~5 years.

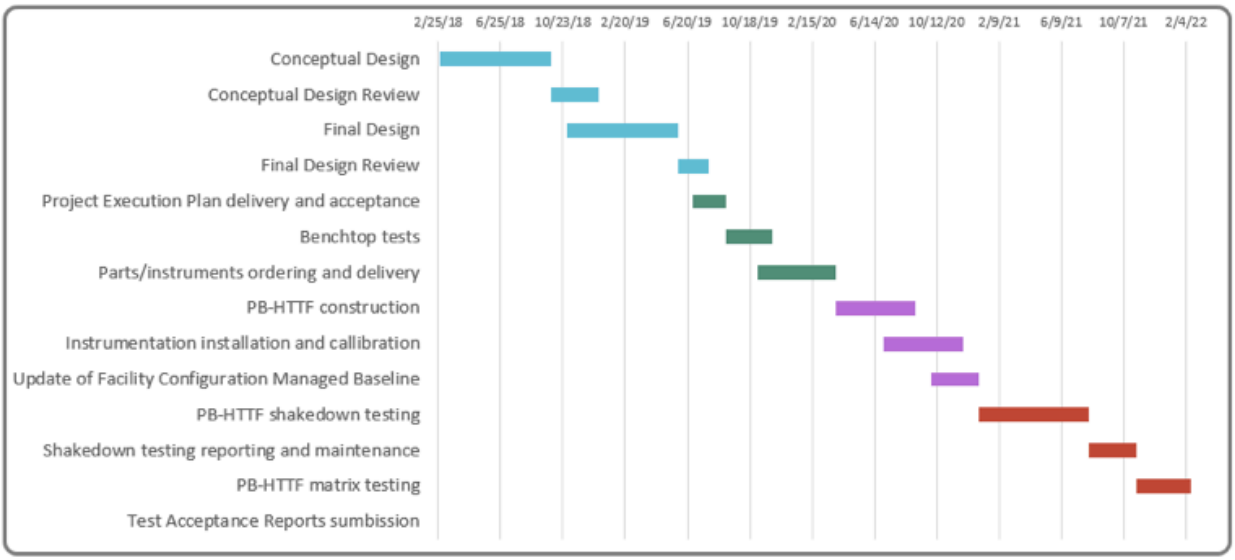

Figure 2-27. PB-HTTF project Gantt chart.

2.5.3. Cost Estimate

Summing up the partial costs detailed in previous sections, it is estimated that the design, construction, commissioning equipment, and salaries during the project lifecycle and for the OSU PB-HTTF procurement could be in the vicinity of $2,840,000. Table 2-16 and Table 2-17 summarize details of the cost estimate. This estimation does not include software, project meetings/travels and service (electricity) costs. Additional funding will be required for the matrix testing phase. The envisaged duration of the matrix testing phase is on the order of 1.5 year.

Table 2-16. Salaries and wages during PB-HTTF project lifecycle.

SALARIES AND WAGES	Year 1	Year 2	Year 3	Year 4
Principal Investigator	1 FTE-month	2 FTE-months	3 FTE-months	3 FTE-months
Salary	$14,667	$30,214	$46,680	$48,081
Fringe Benefits Rate	52.0%	54.0%	54.0%	54.0%
Fringe Benefits	$7,627	$16,316	$25,207	$25,964
Research Associate	10 FTE-months	12-FTE-months	12 FTE-months	12 FTE-months
Salary	$83,333	$103,000	$106,090	$109,273
Fringe Benefits Rate	52.0%	54.0%	54.0%	54.0%
Fringe Benefits	$43,333	$55,620	$57,289	$59,007
Graduate Research Assistants	2@3 terms	4@4 terms	4@4 terms	4@4 terms
Salary	$39,600	$108,768	$112,031	$115,392
Fringe Benefits	$10,200	$10,506	$10,821	$11,146
Tuition	$32,082	$89,830	$94,321	$99,037
Total Salary	$137,600	$241,982	$264,801	$272,746
Total Fringe Benefits & Tuition	$93,242	$172,272	$187,638	$195,154
Total Salary & Fringe Benefits	**$230,842**	**$414,254**	**$452,439**	**$467,900**
Overhead	**$93,417**	**$152,479**	**$168,315**	**$173,365**
			Total	**$2,153,011**

Table 2-17. Total PB-HTTF estimated procurement cost.

	Cost [$]
Heater	$482,185
Core reflectors	$159,258
Pebbles	$2,200
Instrumentation rods	$11,120
Thermocouples (C and K-Type)	$32,458
MEMS	$19,200
Total	**$685,288**

2.5.4. Risk

Given the first-of-a-kind characteristics of the proposed test facility, it is necessary to identify high technology risks early to avoid cost overruns and schedule delays later in the project's lifecycle.

One concern is about the central heater performance at elevated temperatures (thermal expansion, arcing). The central column shall be ordered as a custom designed heater from a company specialized in advanced heating systems design and procurement. The best case scenario is to obtain liability on the vendor end. The PB-HTTF heater is a complicated system and OSU needs a guarantee that eventual defects discovered late in the design process or during facility operation can be addressed by the producer. Thus, the central heater procurement should utilize prequalified vendor teams to develop pre-conceptual design and technical recommendations.

Moreover, bench top testing is necessary to prove the performance of the central heating column and core structural materials prior to installation. Separate components testing as well as integrated testing of core components is required.

Test facility reconfiguration provides an opportunity to transfer the experience and know-how gained through working with the OSU HTTF. Procedures, reports and QA plan developed for the HTTF reduces the risk of encountering problems during construction and commissioning of pebble bed test facility.

3. EM^2 TYPE REACTOR AND PASSIVE NATURAL CIRCULATION COOLING SYSTEM

This section considers the expansion of the utilization of the HTTF to the collection of validation data for design and safety thermal hydraulics methods employed in support of the Energy Multiplier Module (EM^2) reactor. With a properly designed re-configuration, the HTTF could provide integral effects thermal hydraulic data for code validation pertaining to the EM^2 and associated Direct Reactor Auxiliary Cooling Systems (DRACS) primarily during a D-LOFC event, with limited exploration into the P-LOFC event and normal operations.

A general scaling methodology for application to the EM^2 and DRACS is discussed in the *Scaling and Design Requirements Technical Report* (Woods, 2017, 1). An overview of the HTTF, the prototypical EM^2 and the prototypical DRACS designs is included in the *Test Facility Description Technical Report* (Woods, 2017, 2). The *Test Facility Description Technical Report* also includes a preliminary application of the scaling methodology outlined in the *Scaling and Design Requirements Technical Report*.

3.1. Facility Redevelopment Needs

The EM^2 design is very different from the MHTGR design from which the HTTF is modeled, and significant changes are necessary in order to configure the HTTF for EM^2-related testing. Despite this, the modular form in which the HTTF was designed will make feasible the proposed facility redevelopment. The primary system will require the most modifications, while the secondary and auxiliary systems currently in place at the HTTF will be able to be used with minimal reconfiguration.

A volume scaling ratio of 1:64 leads to an EM^2 model active core volume of 0.133 m^3, with a 0.56 m diameter and 0.54 m core height. A core of this size is considerably smaller than the existing prismatic block core, and to use the existing RPV to house the 1:4 scaled EM^2 core would result in significant distortions due to a lack of proportion between the outer plenum, outer annulus, and core.

The proposed solution is to house the core within a new properly scaled and configured pressure vessel, itself being housed within the existing pressure vessel. In doing so, the existing pressure vessel can serve as a simulated reactor cavity, allowing for a more realistic simulation of the D-LOFC event and blowdown into the cavity than the existing reactor cavity simulation system (RCSS). Thermal hydraulic measurements within the cavity itself would be valuable to fully understanding the D-LOFC event, and would be feasible under the proposed HTTF configuration. Implementing a new RPV would also relieve constraints that would have been imposed on the design of the DRACS integration with the upper vessel head, and priority can be placed on preserving thermal hydraulic conditions present in the prototypical core-DRACS configuration.

By placing the scaled vessel inside the current HTTF RPV, the reactor cavity cooling system used in the current HTTF configuration would no longer be useful. This does not present a problem since with the EM^2 reactor, the DRACS is used for passive decay heat removal during accident scenarios.

The following sections address design developments in core materials, heater concepts, and instrumentation.

3.1.1. Core Materials

The potential materials that reflect the required thermal properties have been narrowed on the basis of the following aspects:

1. high temperature behavior: has to withstand certain structural and thermal loads
2. low oxidation degradation potential
3. fabrication process: ease of machining/welding/casting, etc
4. material purity after processing
5. total material cost (material and manufacturing) and availability

Important thermal properties of interest are density, specific heat, thermal conductivity and emissivity. These properties define the majority of scaling ratios among the test facility and the EM^2.

The EM^2 is currently designed to operate at a higher temperature than the HTTF, as seen in Table 3-1. During accident scenarios such as the D-LOFC, the peak temperatures in the EM^2 core will also be higher, potentially reaching upwards of 2000˚C. (Schleicher 2013). Pressure vessel internals, including the heaters and reflectors, will be required to withstand operation at 2000˚C if we were to maintain temperature similarity in the core. The EM^2 uses beryllium carbide for the inner reflector, graphite for the outer reflector, SiC/SiC composite cladding, and UC fuel pellets. The cladding is postulated to operate at a peak temperature of 1100˚C during normal operation. (Schleicher, 2011)

Table 3-1. Geometric data for HTTF and EM^2 reactor. (Schleicher, 2014)

Parameter	Value	
	EM^2	**HTTF (Current)**
Power	500 MW	2.2 MW
Active core height	216.0 cm	198.0 cm
Active core diameter	224.0 cm	151.4 cm
Primary coolant pressure	13.3 MPa	0.8 MPa
Core inlet temperature	550˚C	259˚C
Core outlet temperature	850˚C	687˚C
Coolant	Helium	Helium

For the HTTF, silicon carbide and graphite have been considered as the most feasible heater rod materials. While graphite has the ability to perform at 2000˚C for the heater elements, a structural material for the reflector region capable of operating at 2000˚C and with appropriate thermal diffusivity was not found. Most high temperature monolithic ceramic candidates such as SiC and $MoSi_2$ have maximum operational temperatures below 2000˚C. Boron Nitride Grade AX05, may have the ability to withstand 2000˚C, but cannot be used as structural material due to its brittle nature and low mechanical strength.

The selected solution is to reduce the temperature scaling to 3:4 between the HTTF and EM^2, such that maximum temperatures would not exceed 1430˚C in the HTTF during the natural circulation phase of the D-LOFC event. This allows for the use of commercially available ceramic materials in the core and reflector region and more freedom to choose materials that better match the scaled thermal properties of the prototypical EM^2. The relevant natural circulation processes will still be captured at the reduced test facility maximum temperature.

With the reduced maximum temperature required, SiC heaters which are commercially available, can be used. Thus, the heater rod material has been chosen to be silicon carbide due to its ability to generate the target resistance per heater leg in a simple configuration, its commercial availability, and heat transfer properties.

60 heater rods will be employed in the revised configuration. 557 “dummy” rods will be included in the core region to properly simulate the EM^2 core geometry and flow conditions. Refractory metals have been considered for these rods. Molybdenum-Hafnium-Carbon alloy (MHC) is a viable material for the dummy rods in the core due to its high strength and hardness, good thermal conductivity, and ability to withstand 1430°C. MHC has a a thermal conductivity of 142 W/mK, and a maximum service temperature of 1550°C. (MatWeb)

For connecting the heater elements, molybdenum and tungsten alloys have been considered due to their high melting point and low coefficient of thermal expansion. Tungsten-rhenium alloys are capable of performing at over 1430°C and are commercially available, but are avoided due to cost considerations. There are a number of molybdenum alloys which have been considered for the terminal connection material. Molybdenum-Lanthana (MoLa) has been chosen as the most apt for the heater rod connection material due to its dimensional stability and strength at temperatures above the capabilities of either pure molybdenum or molybdenum TZM alloy. (HC Starck) The maximum advisable temperature for MoLa is 1900°C, which meets the design requirement of withstanding 1430°C.

For the reflector surrounding the core, the goal is to choose a commercially available ceramic that properly mimics heat conduction and heat capacity properties such that similarity of the reflector natural circulation axial and radial Fourier Number ratios is achieved. This results in a thermal diffusivity scaling of 1:4. The prototypical EM^2 employs a Be_2C inner reflector and graphite outer reflector. With a thermal conductivity of graphite of 21.50 W/mK at high temperature (Woods, 2015, 2), a density of 2.5E3 kg/m^3 and a specific heat capacity of 720 J/kgK, the thermal diffusivity of graphite is approximately 1.2E-5 m^2/s.

Be_2C properties will be assumed to be similar to that of graphite for the purposes of this study, to be revisited when necessary, considering that the addition of graphite to Be_2C does not significantly effect the thermal conductivity to the extent that a 50%/50% mixture of Be_2C and graphite has properties similar to that of graphite. (Kosolapova, 1971) With 1:4 scaling, the model reflector shall have a lower thermal diffusivity, approximately 3.0E-6 m^2/s, to properly insulate the core during the natural circulation phase of the D-LOFC event.

The ceramic materials being considered for the reflector region are KAST-O-LITE 30 LI PLUS and KAST-O-LITE 97 L PLUS by Harrison Walker International. These high-alumina materials have maximum service temperatures of 1650°C and 1815°C respectively, are lightweight, and have a significantly lower thermal conductivity than graphite. A major difference between them is that KAST-O-LITE 30 LI PLUS has about 35.3% silica, while the KAST-O-LITE 97 L PLUS has very little silica added, at about 0.3%.

3.1.2. Core Heating Concept

The primary purpose and function of the proposed core design will be to mimic radial and axial power profiles, match heat transfer properties of the EM^2 core, and to withstand structural and thermal loads present during test facility operation. As discussed in the *Test Facility Description Technical Report* (Woods, 2017, 2), the EM^2 core consists of 85 hexagonal fuel assemblies, 79 of which have 91 cylindrical rods, and 6 having 84 fuel rods and a single shutdown guide tube. The diameter of the guide tubes is not known, but their radial area occupied is assumed to be equivalent to 7 times that of the fuel rods,

since each guide tube replaces 7 fuel rods. These assemblies form a hexagonal active core region of height 2.16 m and diameter of 2.24 m. The fuel assemblies are surrounded by an inner reflector, an outer reflector, control drums, a neutron shield, and a core barrel as seen in Figure 3-1.

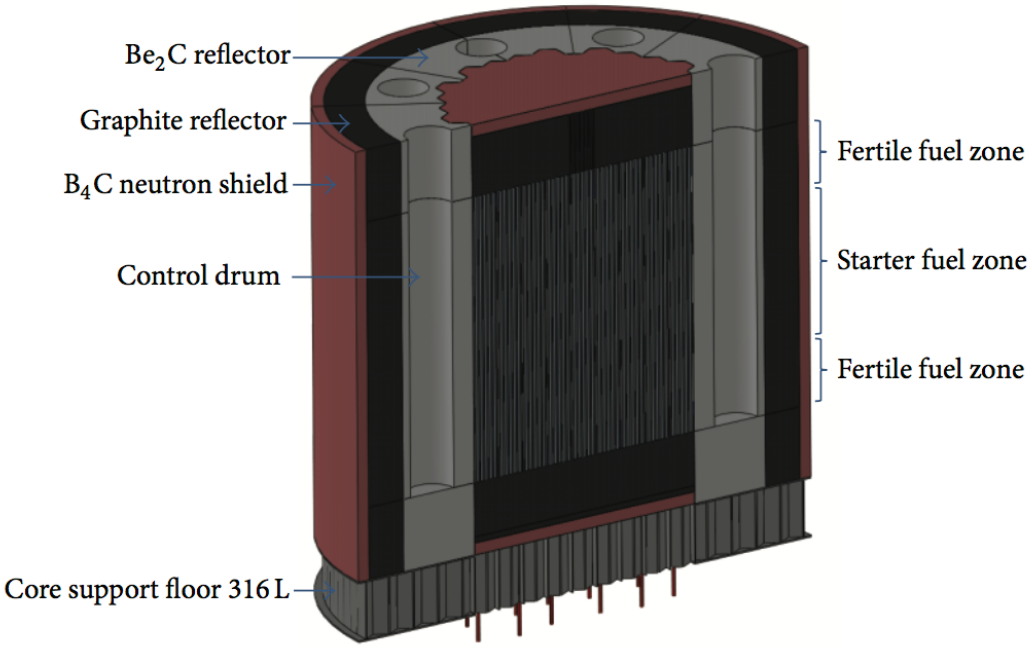

Figure 3-1. EM2 core region. (Choi, 2013)

The 1:4 scaled core will have a 0.56 m active core diameter and 0.54 m active core height. To ensure similarity in natural circulation heat transfer in the core during the D-LOFC natural circulation phase, the rod diameter shall scale as 1:1.1, resulting in a heater rod diameter of about 19 mm. It is important to note that the EM^2 is in the design phase of its development, and these calculations are approximate and subject to change as more information regarding the exact geometry of the EM^2 core is obtained.

SiC heater rods of 19 mm diameter are commercially available (I Squared R), and have an electrical resistance of 3.41E-3 Ω/mm, such that each rod of 0.54 m active length will have a nominal resistance of 1.84 Ω. The resistance will be higher during the D-LOFC conditions by approximately 15%-20%, resulting in a resistance of approximately 2.1 Ω per rod.

There are 10 heater banks installed in the HTTF, with each bank having 3 heater legs. Each heater bank is powered by a silicon controlled rectifier. The SCRs are fed from the 4000A switchgear which provides 480 V, 3-phase power. The phase voltage of the 3-phase wye system is 277 V. If each heater leg contains two rods in parallel, the total resistance per leg would be 1.05Ω. This leads to 263.8A of current, and a power output of 73.075 kW per heater leg. With three heater legs per heater bank, each SCR has a rated load of 219.2 kW per heater bank, for a total rated core power of 2,192 kW.

The EM^2 has a total of 7,699 rods and guide tubes, resulting in a radial area of 2.821 m^2. Given that the active core is hexagonal with a diameter of 2.24 m and the total radial area is 3.94 m^2, the core porosity is approximately 28%. With 60 SiC heater rods proposed for the model HTTF, additional “dummy” rods must be included in the core to match the porosity between the model and prototype. Matching the porosity is important for maintaining similarity of natural convection heat transfer during the D-LOFC event.

The HTTF core will have a radial area of 0.246 m^2. To match the core average effective porosity of 28%, 0.175 m^2 of the radial area must be occupied by the heater rods. Since the rod diameter scales 1:1.1 between the HTTF and EM^2, 617 19 mm rods will be needed. Since only 60 rods will be used as heaters, a total of 557 "dummy" rods will be needed to match the porosity. The core rods will be arranged vertically in a hexagonal prism to match the geometry of the actual EM^2 core, with a hexagonal side length of 28 cm. A diagram of the heater rod configuration is shown in Figure 3-2. Since the heater rods will be mounted vertically, they will be supported on the lower end by electrically insulated supports.

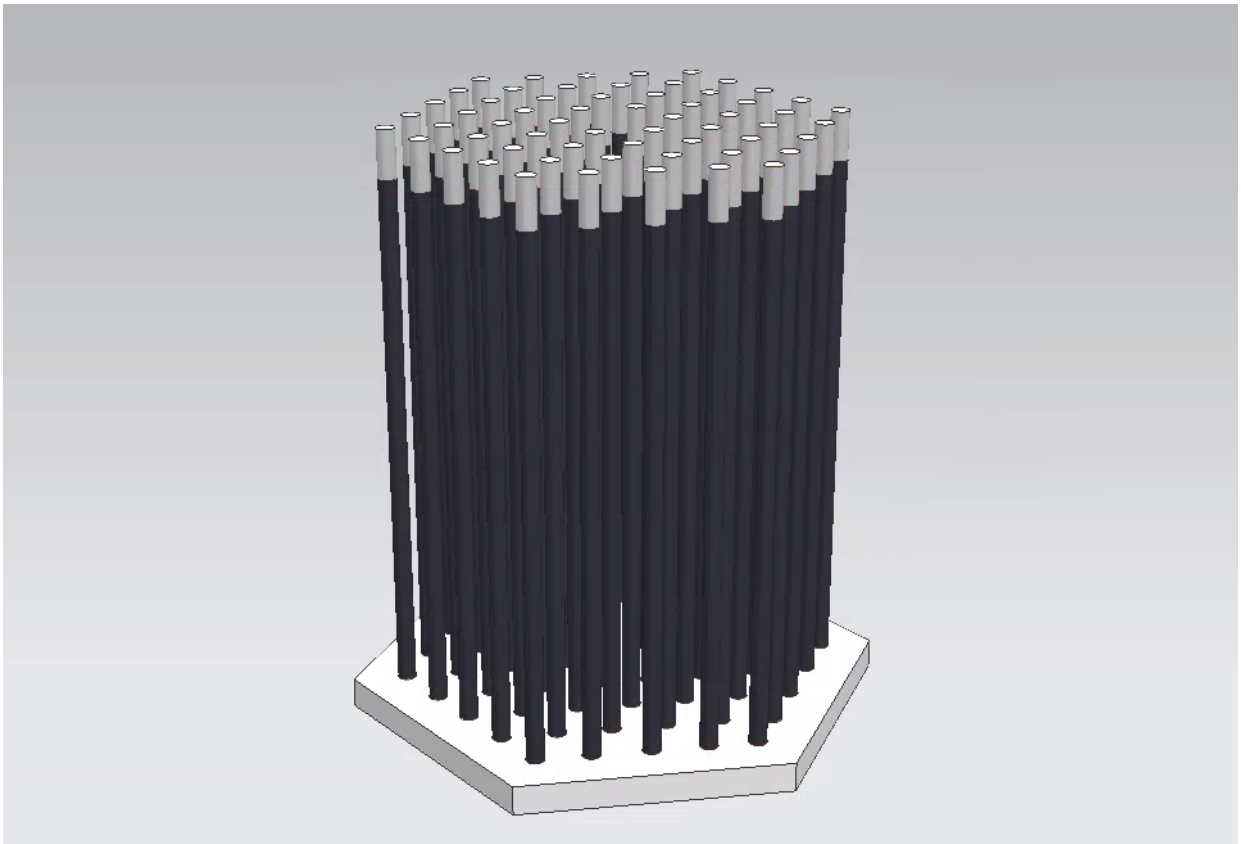

Figure 3-2. Radial heater rod configuration for the HTTF.

The heater rods can be connected using terminal straps and spring clamps. Due to the high operating current in the circuit, custom-made terminal straps and clamps made of molybdenum alloy will be necessary. There are vendors that have the capability to produce braided molybdenum wiring, and molybdenum-alloy wiring which may be feasible as well.

It is proposed that the core instrumentation be routed through the "dummy" rods. In order for the thermocouples to give meaningful data with regard to the location of the temperature measurement along the rod, the inner annulus must be kept in a cooled state, ensuring that the highest temperature along the thermocouple wire is at the end-point, where the measurement is intended. If the annulus is not cooled, the temperature throughout the rod will equalize and the thermocouple measurements will not be location-specific.

To accomplish this, coolant will be pumped in through the core support floor, and upward through the lower reflector into a dummy-rod annuli inlet manifold. The hotter coolant exiting above the core will be directed into the outlet manifold and through the upper reflector, where it is then directed radially

outward, and down through the side reflector region, before returning to below the core support floor. The inlet piping will connect to a circulator that will sit next to the pressure vessel via an instrumentation port on the lower head of the RPV. The dummy-rod cooling system will draw gas from the cold leg of the primary system, and reject hotter gas into the hot leg, which flows into the steam generator for heat removal. A basic image showing an upper and lower manifold with connections through the heater rods can be seen in figure 3-3.

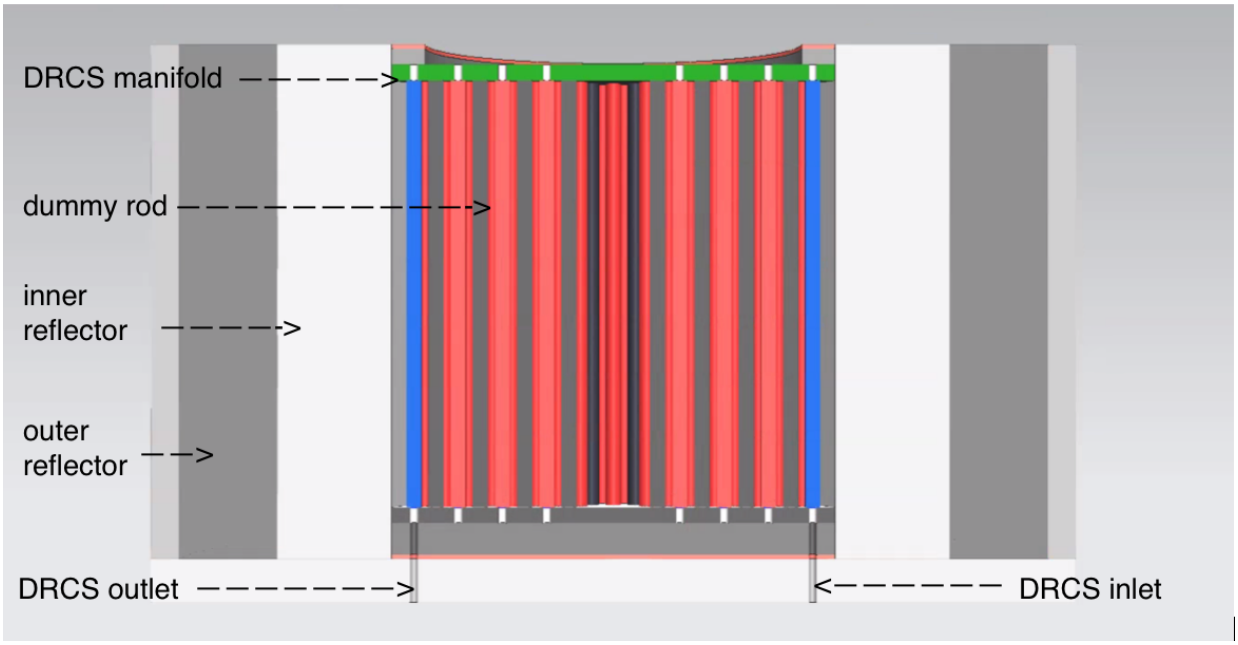

Figure 3-3. Dummy rod cooling system channels.

3.1.3. Instrumentation System

The HTTF will be instrumented to capture the behavior of the system during both steady-state and transient operation. The following types of instrumentation can be installed at the EM^2-modeled HTTF.

- Thermocouples to measure gas, heater, wall and ceramic temperatures. C-type thermocouples are capable of extended operation above the expected maximum temperature (1430˚C) at the HTTF.
- Pressure transducers to measure the static pressure in tanks and vessels.
- Differential pressure transducers to measure flow induced pressure drops as well as liquid levels in tanks, vessels and piping.
- Gas concentration instruments to measure the concentration of helium in a binary gas mixture. The GCIs measure the capacitance of a subject gas mixture and can use the measure of capacitance to determine the proportions of each gas in the mixture. The GCIs provide real-time measurement at high temperatures without the need for taking batch samples. These devices are being developed at OSU in support of the HTTF project.
- Power meters to measure the core power and provide feedback for core power control.

Overall, the HTTF will contain 190 sensors which can be used for matrix testing. The locations to be instrumented are the core, upper plenum, lower plenum, outer cylinder, inlet/outlet ducts, DRACS, and RCST. The DRACS instrumentation is described in a separate section in this report.

The core region will consist of separate instrumentation quadrants, with 4 axial levels, each divided into 6 azimuthal sectors. Only 3 of the 6 azimuthal sectors will be instrumented, which are deemed the primary (1), secondary (2), and tertiary (3) sectors. The primary sector will be opposite the inlet/outlet duct and the most heavily instrumented, with the secondary and tertiary sector progressively less instrumented. Figure 3-4 shows the axial levels and azimuthal regions.

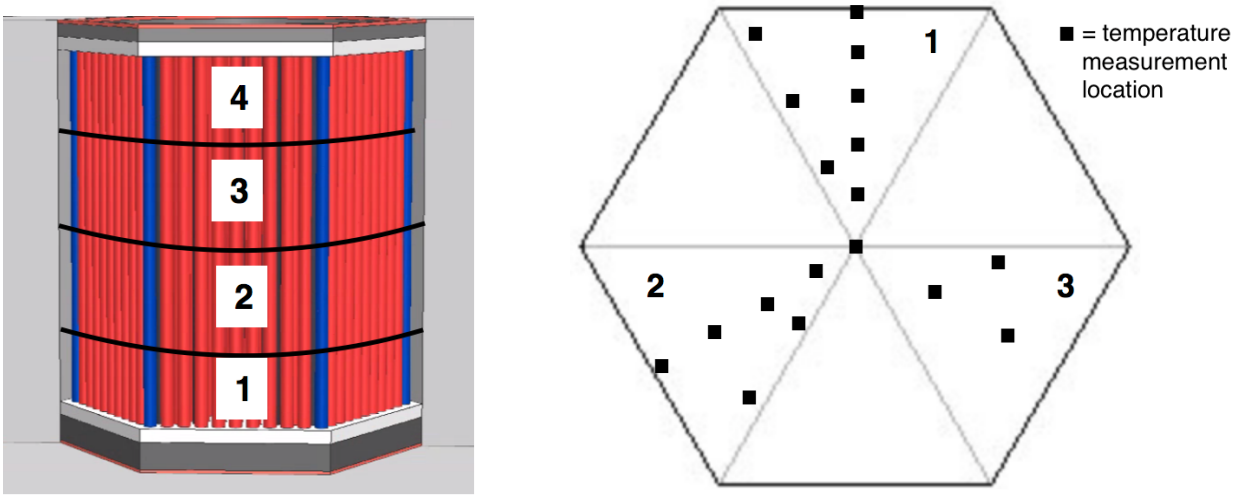

Figure 3-4. Proposed HTTF core configuration.

Frequent axial and radial thermocouple measurements are needed to adequately determine the core temperature profile and to monitor localized core hot spots. For the prototype EM^2, the coolant inlet/outlet temperature is 550˚C/850˚C, and the peak cladding temperature during normal operation is 1100 ˚C. (Schleicher, 2011) With a 3:4 temperature scaling, the HTTF will operate with a 344˚C/569˚C coolant inlet/outlet temperature during normal operation, and ideally with a peak heater rod temperature of 757 ˚C.

During a D-LOFC event, peak cladding temperatures in the EM^2 may reach as high as 2000 ˚C, corresponding to a HTTF peak heater rod temperature of 1430˚C. Thus the thermocouples in the core must sustain temperatures in excess of 1430˚C, warranting the use of C-type thermocouples, or other high temperature thermocouple. The coolant mixture at core outlet will achieve similar temperatures. Although the temperature decreases as a function of radial distance from the core's axial center, rods in the outer region will still be exposed to temperatures in excess of 1300˚C, justifying the use of C-type thermocouples throughout the active core instead of considering a mix of C-type and K-type as is implemented in the HTTF currently, where temperatures in the outer radial half of the core are limited to a maximum of 1250˚C.

To instrument these radial and axial measurement locations, thermocouples will be placed in a subset of dummy-rods, deemed the core instrumentation rods. These rods will have four axial measurement locations along their length, and will be connected to the dummy-rod cooling system inlet and outlet manifolds at their ends. The hole in the annular rods is slightly cooled to assure that the maximum temperature along the thermocouple wiring is at its end, where the measurement is desired.

To accomplish these temperature measurement goals, a total of 18 of the dummy-rods will be instrumented. Nine rods will be instrumented in the primary sector (including the centerline), six in the secondary sector, and three in tertiary sector. The thermocouples will be connected to their location of measurement via the inner annuli of the dummy rods as seen in Figure 3-5. These instrumentation rods will be modified to provide the thermocouples access to the coolant region along their axis. To measure

the bulk flow temperature of the gas, the thermocouple wiring will rise vertically from the bottom of the dummy rod to the desired height, and out horizontally through a small port in the rod, exposing the end-point to the channel gas.

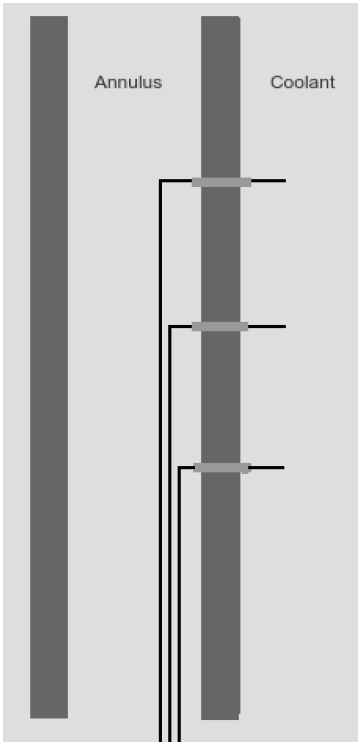

Figure 3-5. Thermocouple placement for coolant temperature measurement.

3.1.4. Primary System Design Considerations

The active hexagonal core will be surrounded by a reflector region, followed by a core barrel and pressure vessel. The RPV shell will consist of three flanged sections: the lower shell, the upper head and the cylindrical shell. Helium coolant will flow into the RPV through the inlet duct, down through the annulus between the core barrel and inner wall of the RPV, reverse direction in the lower plenum, flow up through the active core heater region into the upper plenum, and out through the outlet duct. To achieve similarity in flow resistance, the upper support plate will serve as a flow restrictor. An image of the core configuration can be seen in Figure 3-4.

At the existing HTTF, the cavity is modeled as a separate tank, the reactor cavity simulation tank, and is connected to the pressure vessel through break valves. For the EM^2-modeled design, the pressure vessel will sit inside a reactor cavity. The pressure vessel shell will have penetrations for the crossover ducts, an upper break valve, a lower break valve, control rod guide tubes, core heater elements, lower access, upper plenum visualization and instrumentation.

Using a new EM^2-modeled RPV will require a redesign of the concentric inlet/outlet duct due to geometric considerations and so that the RPV connects to the existing secondary system in a manner that preserves flow and heat transfer conditions during a LOFC event. The existing pressure vessel, which is the proposed reactor cavity, has an outside diameter of 166.4 cm and a height of 537.2 cm.

Due to the core's relatively small size and weight, the HTTF crane system may be capable of lifting the core in its entirety. The core will be designed with adequate structural support and lifting connection mechanisms such that its transport to and from the pressure vessel will not result in any structural damage. For maintenance and instrumentation needs, there will be an access port on the lower vessel head so that the lower plenum and core support floor can be accessed without having to remove the core from the pressure vessel.

While the helium coolant flows upward through the core in the EM^2 and proposed model, the HTTF helium circulator is currently configured to produce flow in the opposite direction, or downward through the core, during normal operations. The HTTF blower and piping configuration shall be modified such that the flow direction in the primary system during normal operating conditions will match the EM^2 flow direction. At the HTTF, the circulator coupling is a magnetic coupling in which the magnets are rated to a maximum operational limit of 300˚C. In order to implement the EM^2 primary loop temperatures, the coupling and its cooling system will likely need to be redesigned. This task will be revisited if this project is continued.

3.1.5. Direct Reactor Auxiliary Cooling System

Passive safety is a feature of Generation IV reactor designs. In order to accomplish passive safety with respect to decay heat removal, many designs rely on natural circulation with heat rejection to air during shutdown and accident scenarios. The Direct Reactor Auxiliary Cooling System is one such passive natural circulation cooling system, chosen for integration with several of the advanced reactor designs currently in development, such as the Fluoride-Salt Cooled High Temperature Reactor, the Advanced High Temperature Reactor, and the Energy Multiplier Module. Experimental validation of thermal hydraulic phenomena involving the DRACS during shutdown and accident scenarios is essential for licensing any reactor that relies on the DRACS for decay heat removal.

The DRACS is capable of removing heat directly from the reactor vessel to ambient using natural convection. The proposed project includes the use of a DRACS, analogous to the one used in the EM^2, to model decay heat removal during a LOFC event. Figure 3-6 shows a schematic of the proposed DRACS.

The prototype EM^2 design contains two independent DRACS modules. This project will model the behavior of one module due to constraints related to the current configuration of the HTTF and Advanced Nuclear System Engineering laboratory (ANSEL) building.

The DRACS consists of a direct and an intermediate loop, two heat exchangers, and a cooling tower. The DRACS will include loop valves on the direct and intermediate loops in order to control direct loop bypass flow and intermediate loop flow during normal plant operations.

This system can be integrated to the HTTF, but some limitations exist. The design of the existing HTTF pressure vessel limits the ability to construct a DRACS that is geometrically identical to the prototype, and replacing the pressure vessel to alleviate this design constraint will likely result in a significant increase in cost. Instead, the DRACS will use preexisting ports on the pressure vessel through which the direct loop will protrude.

Another constraint of this project is the existing cooling tower. The roof of the bay that houses the HTTF is unable to support the weight of another cooling tower. (Blake, 2016). There are two ways forward; (1) replace the existing cooling tower with one similar in design to the prototypical DRACS, or (2) use the existing cooling tower, but with proper modification. As part of the cost reduction strategy, it was opted to use the existing cooling tower.

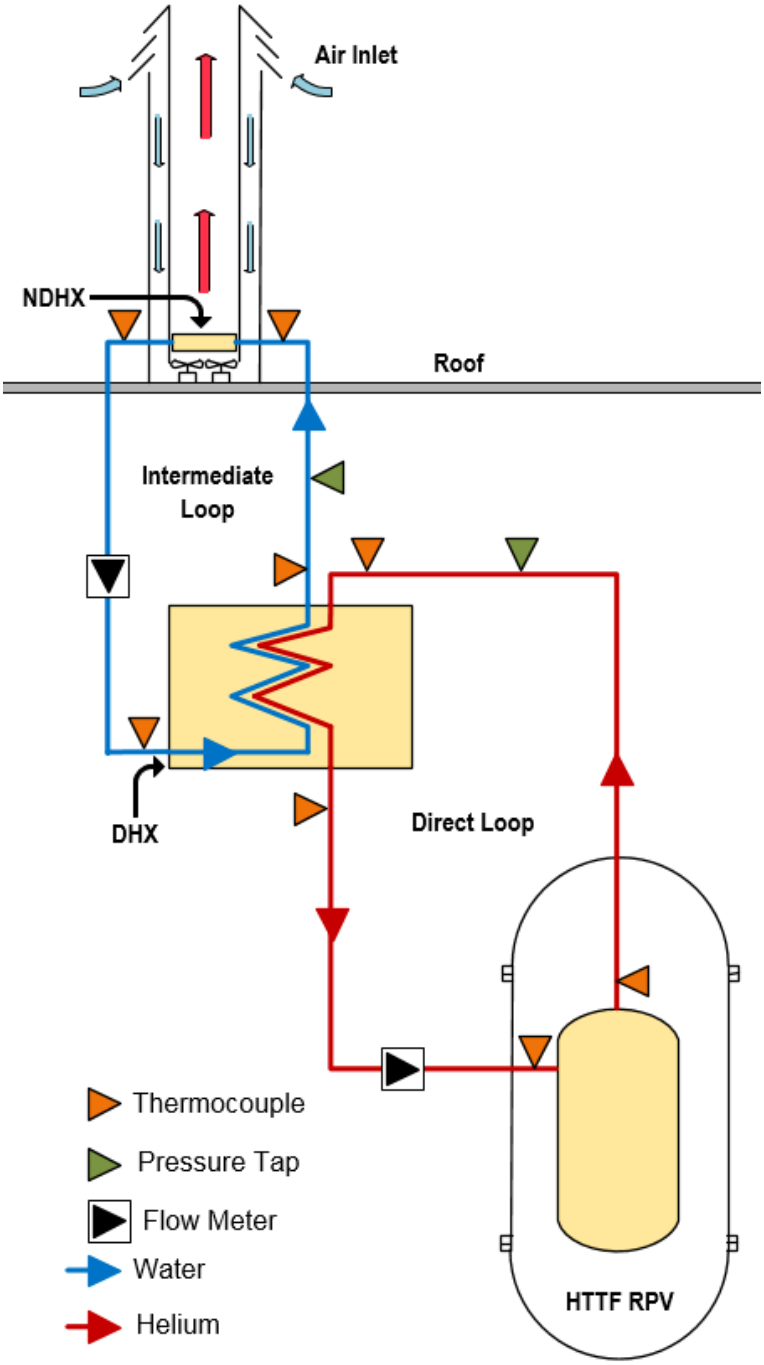

Figure 3-6. Schematic of proposed DRACS.

The DRACS Direct Heat Exchanger (DHX), which is shown in Figure 3-7, will be connected to the upper head of the existing reactor vessel, where the hot helium will move upwards by means of buoyancy driven flow. The height of the EM^2 DRACS direct loop is unknown; however, the distance between the intermediate loop and the Natural Draft Heat Exchanger (NDHX) is known, as shown in Figure 3-8. The NDHX will be placed right above the roof of the facility. By knowing the height of the intermediate loop, it is possible to know the height and calculate the length of the direct loop.

The heat generated in the core and absorbed by the coolant will be transferred from the direct loop to the intermediate loop through the DHX, after which the cooled helium will be driven back into the reactor due to buoyancy. The intermediate loop, which will use the cooling tower as heat sink, will contain water as the working fluid. The heat in the intermediate loop will be transferred to the ambient air through the NDHX fins. In order to model the EM^2 DRACS as closely as possible, it is important to keep in mind the scale-down parameters, which can be found in (Blake, 2016). Information about the equipment needed for the DRACS can be found in Appendix H.

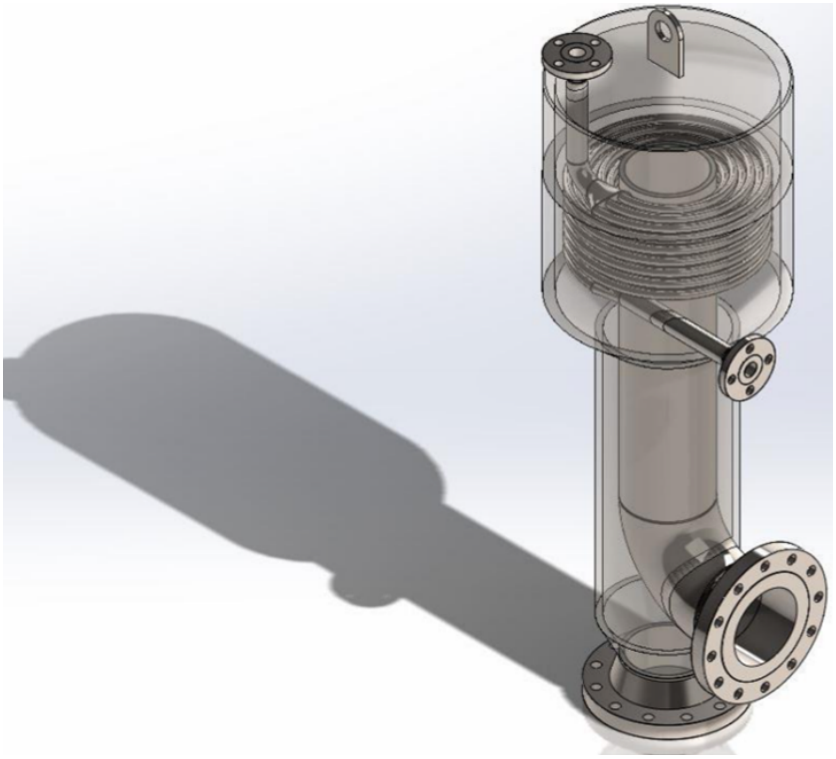

Figure 3-7. Scaled-down model of the DHX module (Blake, 2016)

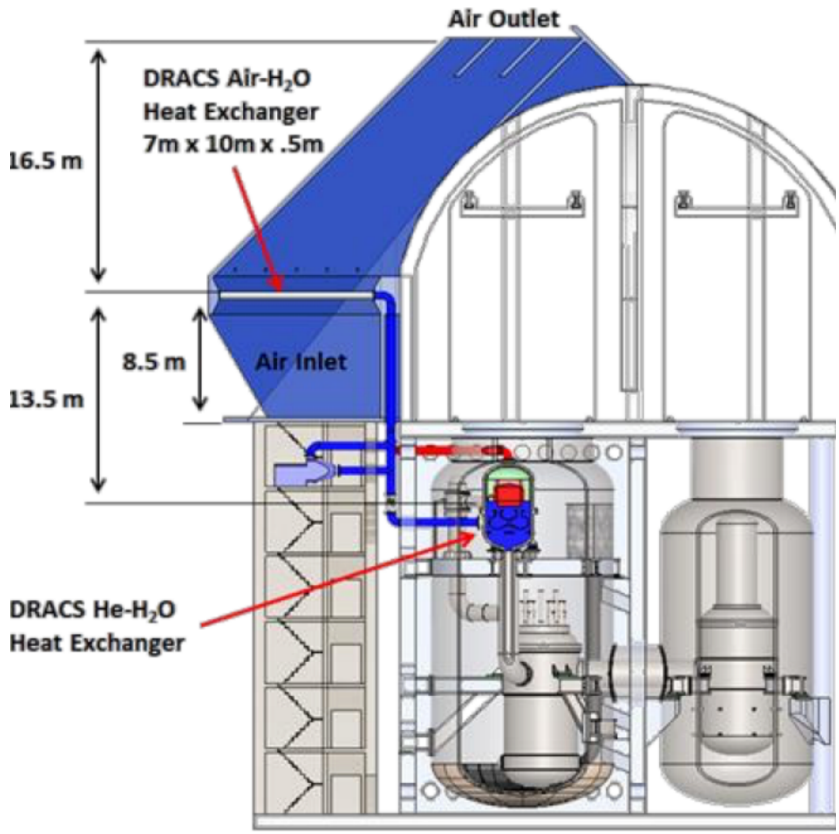

Figure 3-8. Prototypical EM² DRACS diagram with dimensions (Blake, 2016)

The equipment needed for the DRACS will be customized based on the scaling ratios. In order to integrate the DRACS with the HTTF, some modifications need to be completed, including:

1. The existing reactor pressure vessel of the HTTF will be used to simulate the reactor cavity. As a result, it is necessary to use the upper plenum ports and one of the rod drive nozzle ports as access points for the direct loop of the DRACS. Figure 3-9 shows how the DHX and the primary loop will be connected to the HTTF RPV.
2. The existing cooling tower has to be modified in order to model the NDHX and piping of the DRACS.

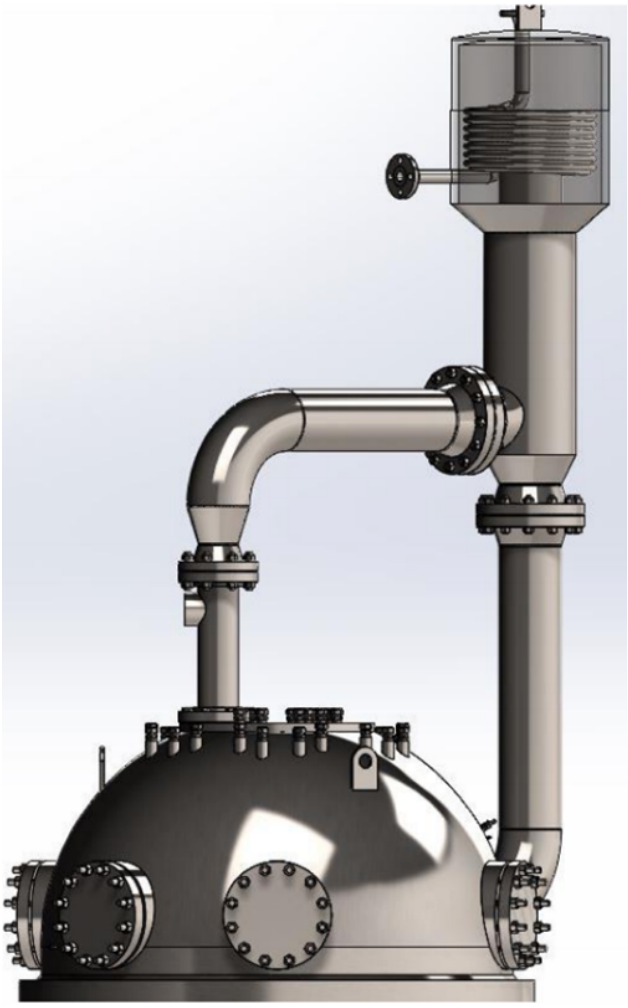

Figure 3-9. Direct loop model attached to upper head (Blake, 2016)

The following list includes all the components needed for the direct and intermediate loops.

Table 3-2. Components needed for HTTF DRACS Module.

Part	Location
Reducer	Direct loop inlet
Flange 5 in.	
Flange 8 in.	
90 degrees elbow 8 in. short	
Horizontal pipe	Direct loop inlet
Vertical pipe	Direct loop inlet
Plenum	DHX
Lift Lug	DHX
Reducer 1	Direct loop outlet
Reducer 2	Direct loop outlet
Concentric pipe	Direct loop outlet
Vertical pipe	Direct loop outlet
90 degrees elbow 1.5 in.	
DHX riser pipe	Intermediate loop outlet
Horizontal pipe	Intermediate DHX outlet
Vertical pipe	Intermediate NDHX inlet
NDHX tubes	NDHX
NDHX fins	NDHX
Vertical pipe	Intermediate NDHX outlet
Horizontal pipe	Intermediate NDHX outlet
Flange 1.5 in.	
Horizontal pipe	Intermediate DHX inlet
DHX manifold	DHX inlet
Valve 1	Direct loop valve
Valve 2	Intermediate loop valve
Helical coil tube bundle	DHX
DHX manifold	DHX outlet
Direct flow over DHX	Direct loop heat exchanger

Details regarding these components can be found in Appendix H.

The instrumentation required for the measurement of temperatures, pressures, and flow rates inside of the DRACS is shown in Table 3-3.

Table 3-3. Instrumentation for the HTTF DRACS model. (Blake, 2016)

Instrument type	Facility Tag	Loop	Location
Thermocouple	TK-7311	Direct	Loop inlet
Thermocouple	TK-7312	Direct	DHX shell side inlet
Thermocouple	TK-7313	Direct	DHX shell side outlet
Thermocouple	TK-7314	Direct	Loop outlet
Thermocouple	TK-7321	Intermediate	DHX tube side outlet
Thermocouple	TK-7322	Intermediate	NDHX tube side inlet
Thermocouple	TK-7323	Intermediate	NDHX tube side outlet
Thermocouple	TK-7324	Intermediate	DHX tube side inlet
Pressure Tap	PT-7312	Direct	DHX shell side inlet
Pressure Tap	PT-7321	Intermediate	DHX Outlet
Flow Transmitter	FT-7313	Direct	DHX Outlet
Flow Transmitter	FT-7324	Intermediate	DHX Inlet

Thermocouples needed for the DRACS will be installed at the inlet and outlet of the heat exchangers to determine the rate of heat removal of the heat exchangers. A flow transmitter and a pressure tap will be implemented in both the direct and intermediate loops. The pressure tap will be placed at a point where the pressure is highest, so it will be able to indicate if the loop over-pressurizes. By knowing the fluid pressure and temperature in the loop, calculations can be performed to determine the effectiveness of heat removal through the DRACS system. Finally, measurement of the flow rate will provide important information regarding the loops' ability to produce sustained-flow natural circulation.

3.1.6. Support Structure Design

The incorporation of another reactor pressure vessel inside of the existing vessel requires the use of a support structure that can be adapted to the vessel internals. The current core configuration has a lower support plate that is located at the bottom of the of the vessel.

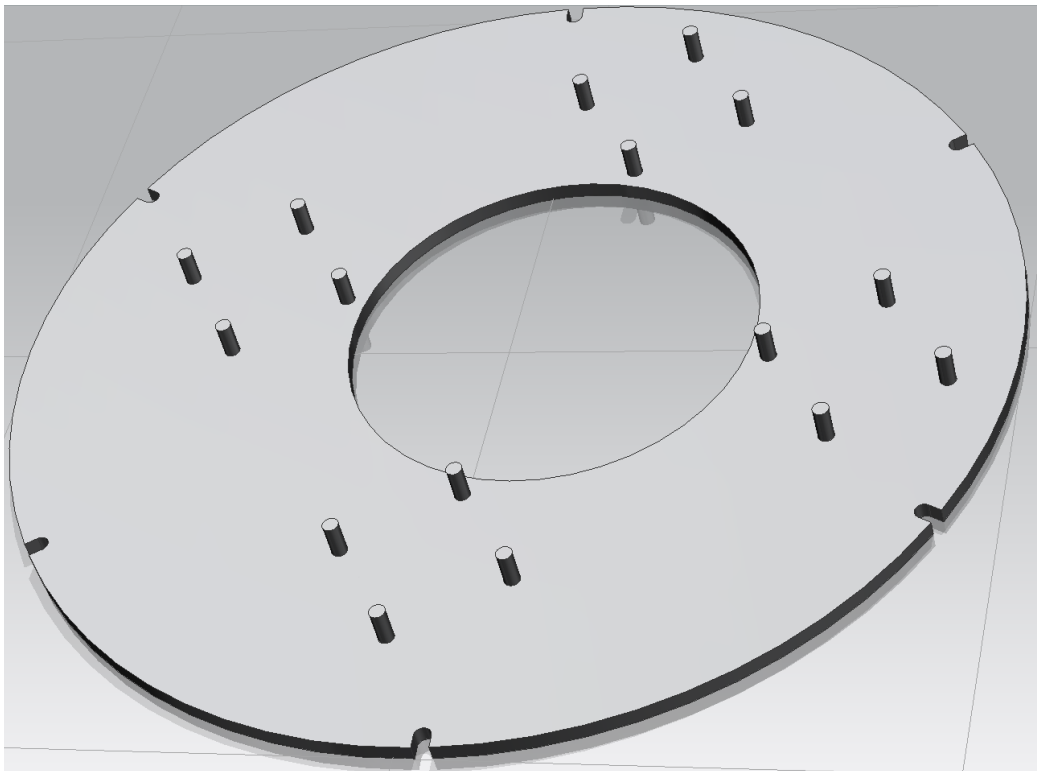

Figure 3-10. Lower support plate

The support plate remains in a fixed position due to the internal support ring and the alignment pins, which form part of the existing reactor pressure vessel. For the new vessel, a similar support plate will be used; however, the new plate, which is shown in Figure 3-10, will have bolts which will be used to keep the legs of the new RPV attached to the support plate. Figure 3-11 shows the location of the new lower plate, and how the new RPV will be placed inside the current reactor vessel.

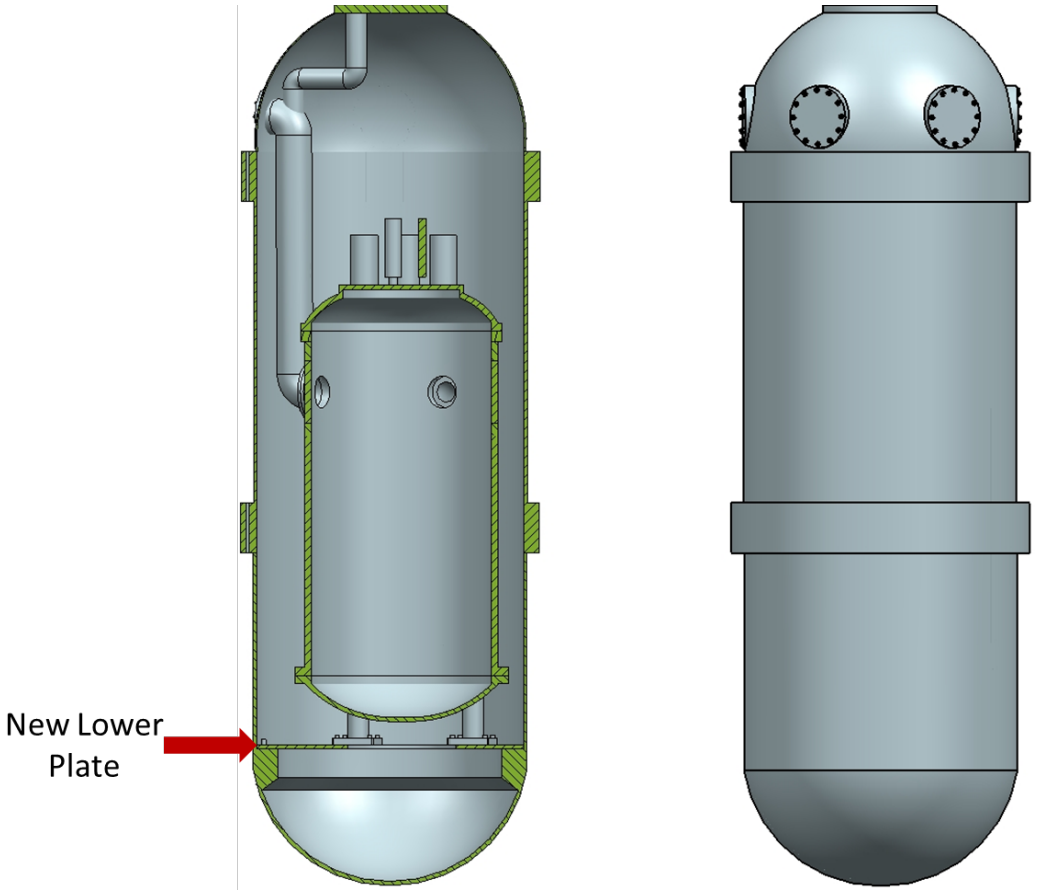

Figure 3-11. Revised configuration of the HTTF RPV.

A support structure will also be needed to keep the piping and the DRACS heat exchanger in place. The direct loop and the DRACS heat exchanger will be kept in place by a support structure that will be placed below the heat exchanger. The structure, which is shown in Figure 3-12, will be bolted to the existing HTTF support structure.

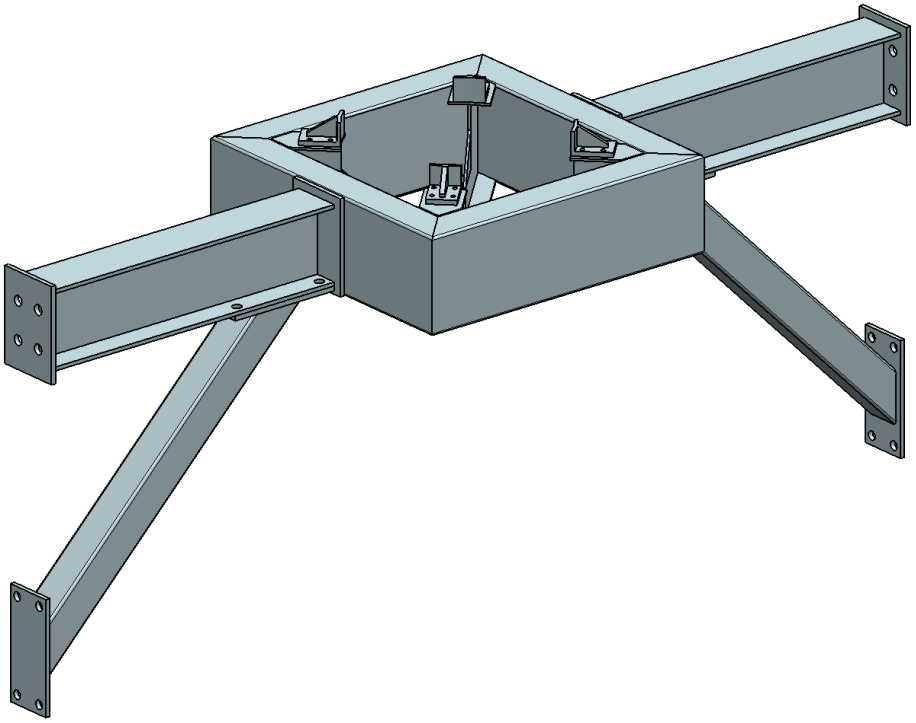

Figure 3-12. DHX support structure.

For the intermediate loop, multiple pipe clamps will be used to keep the pipes immobile.

During normal operations, it is anticipated that there will be bypass flow through the DRACS. Therefore, a bypass system will be required in order to model this bypass during normal operation but also allow for full DRACS operation during accident conditions. Natural circulation as a flow driver is relatively weak and it is more sensitive to friction and form loss. Thus, valves will be installed in the DRACS that will not have a considerable impact on the natural circulation while open. Ball valves were chosen due to their low minor loss coefficient. These two valves will be connected to the existing ports in the upper head that have been selected to serve as the inlet and outlet of the DRACS.

3.2. Characteristic Time and Scale Ratios

Modified as-built characteristic ratios for D-LOFC natural circulation, and P-LOFC natural circulation are shown in the following tables. These time and scale ratios were developed in the *Scaling and Design Requirements Technical Report* (Woods, 2017, 1). They were first presented in the *Test Facility Description Technical Report* (Woods, 2017, 2). Based on the changes to the temperature and heater rod scaling presented in this report, these characteristic ratios have been re-calculated. The as-built characteristic ratios for buoyancy-driven gas ingress presented in the *Test Facility Description Technical Report* have not changed due to the changes in temperature and heater rod diameter scaling. Scaling of molecular diffusion is not included due to the placement of the cross over ducts in relation to the core. Due to this placement it is likely that the buoyancy driven gas ingress will continue until the core is covered with the ingressing gas and natural circulation can be initiated.

Table 3-4. Characteristic ratios for DCC natural circulation.

Characteristic Ratio	Equation in Scaling Report	Ratio (HTTF/EM^2)	Distortion
$\left(\Pi_{G,NC}\right)_R$	(3-72)	1:1	0.00
$\left(\Pi_{Ri,NC}\right)_R$	(3-73)	1:1	0.00
$\left(\Pi_{F,NC}\right)_R$	(3-74)	1:1	0.00
$\left(\Pi_{Pe,NC}\right)_R$	(3-77)	1:4.4	0.77
$\left(\Pi_{core,NC}\right)_R$	(3-78)	1:1 *(core power ratio 1:36)*	0.0
$\left(t_{NC}\right)_R$	(3-79)	1:2	—
$\left(\Pi_{NuFo,NC,EM2}\right)_R$	(5-5)	1:8.6	0.88
$\left(\Pi_{Ra,channel,NC}\right)_R$	(5-10)	1:18	0.94

Table 3-5. Characteristic ratios for PCC natural circulation.

Characteristic Ratio	Equation in Scaling Report	Ratio (HTTF/EM^2)	Distortion
$\left(\Pi_{Ri,PCC}\right)_R$	(3-124)	1:1	0.00
$\left(\Pi_{F,PCC}\right)_R$	(3-125)	1:1 (*following HTTF loop valve closure*)	0.00
$\left(\Pi_{Pe,PCC}\right)_R$	(3-126)	1:5.3 (*following HTTF loop valve closure*)	0.81
$\left(\Pi_{core,PCC}\right)_R$	(3-127)	1:1 (core power ratio 1:532)	0.0
$\left(\Pi_{SG,PCC}\right)_R$	(3-128)	1:1 (*following HTTF loop valve closure*)	0.0
$\left(\Pi_{NuFo,PCC,EM2}\right)_R$	(5-11)	1:3.5	0.71
$\left(\Pi_{Ra,channel,PCC}\right)_R$	(5-16)	1:5500	~1.0

3.3. Project Implementation

Reconfiguring the HTTF to model EM^2-related thermal hydraulic phenomena will be a significant undertaking, requiring the installation of a new pressure vessel and internals, as well as a direct reactor auxiliary cooling system. This is proposed as a 5 year project, and it is expected that approximately 4 graduate and 4 undergraduate students will be involved. Successful integral effects testing will likely generate several high impact publications, as advanced gas reactor thermal hydraulic phenomena is an area with significant gaps in experimental research and code validation. Several of the students will likely formulate masters and PhD theses related to this project.

3.3.1. Project Overview

The modification of the HTTF to an EM^2 configuration and the conduct of the tests outlined in the *Test Plan Technical Report* (Gutowska, 2017) for the EM^2 configuration would be planned as a five-year project.

During the first year, the following tasks would be completed:

1. Finalize scaling analysis for HTTF reconfiguration
2. Complete detailed design and analysis
3. Finalize matrix test plans

4. Remove existing pressure vessel internals

During the second year, the following tasks would be completed:

1. Construct EM^2-modeled core
2. Install pressure vessel within reactor cavity
3. Install new core inside pressure vessel
4. Connect existing heater system to new core

During the third year, the following tasks will be completed:

1. Integrate dummy-rod cooling system within the core.
2. Construct and install the DRACS
3. Modify circulator configuration

During the fourth and fifth year, the following tasks will be completed:

1. Shakedown testing
2. Matrix testing

3.3.2. Risk Management

There are 3 primary risks that will be touched upon qualitatively in this report, to be returned to in further detail if this project is continued.

Failure of the DRACS to adequately remove decay heat and perform natural circulation.

Distortions that result from the scaling of the DRACS may result in reduced heat removal capabilities. There are geometric specifications of the prototypical DRACS design that are not publicly available, so design choices have been made that may not match the prototype.

Excessive corrosion of the heater elements in the core due to oxidation or steam-water ingress.

Oxidation is an unavoidable chemical reaction that will occur in the core region even if air or oxygen is not used as a working gas due to impurities. Some oxidation is acceptable and is not expected to effect the structural integrity of the core. Calculations will be performed to determine the expected quantity of oxidation over the course of the proposed matrix tests, and careful consideration will be made to prevent excessive oxidation.

One postulated test, the Steam Water Ingress (SWI) event, presents specific challenges. During a SWI event, a rupture in the DRACS DHX tubing may result in an ingress of water into the core. Water causes corrosion, and a failure to adequately remove the water injected into the core during such a test might result in high levels of oxidation. The reflector material may also absorb the moisture, making it harder to remove. The SWI event test may be cancelled if a more detailed risk assessment deems the injection of water to be too harmful for the test facility.

Unpredicted challenges due to very high temperatures encountered during testing.

The proposed test facility is a first of its kind, and will be operating at temperatures in excess of 1430°C during the D-LOFC tests. While tests under these conditions will be highly valuable for experimental code validation of HTGRs, there are heightened risks associated with the extreme temperatures and the accompanying stresses and strains that such a facility is susceptible to. A wealth of lessons learned from the existing HTTF have and will be applied to this project whenever possible in an effort to predict and mitigate any potential design concerns going forward.

It is important that the SiC heater rods retain sufficient strength over the entirely of testing at the HTTF. To prevent excessive mass loss and reduction in strength, the oxygen concentration, and PO2, shall be monitored and maintained at a level that prevents the onset of active oxidation. Preliminary testing will be performed to evaluate the strength of the SiC rods under varying loads and degrees of oxidative mass loss to determine the maximum rate of mass loss during matrix testing that does not compromise the structural integrity of the core.

3.3.3. Economic Analysis

The following are cost estimates for completing the work scope outlined in this report. These are estimates which have been developed through discussions with potential component vendors and past experience maintaining and operating the current configuration HTTF. Note that these figures are only estimates and do not represent a quote to get the applicable work completed. They are meant to provide an approximate cost for the completion of the subject work scope.

Table 3-6. EM² and DRACS testing program cost estimate (by item)

DRACS Construction and Installation	
DRACS components including instrumentation	$120,000
DRACS installation (mechanical and electrical)	$100,000
Total, DRACS Construction and Installation	**$220,000**
EM² Core Construction and Installation	
SiC heater rods	$60,000
Dummy rods	$75,000
Reflector ceramic	$18,000
Reflector molds	$15,000
Reflector casting	$50,000
Pressure vessel and support structure	$250,000
Core barrel and core support	$100,000
Dummy rod cooling system	$35,000
Instrumentation	$250,000
EM² core installation (mechanical and electrical)	$150,000
Total, EM² Core Construction and Installation	**$1,003,000**
Circulator Modification	
Total, Circulator Modification	**$75,000**
Design, Maintenance and Operation (annually)	
Professional Staff (salary & overhead) (includes 1.0 FTE principal investigator, 0.5 FTE technician, and 0.1 FTE program manager)	$350,000
Students (stipend, tuition and overhead) (includes 4 graduate students, and 2-4 undergraduate students)	$325,000
Separately metered electricity (years 4 and 5 only)	$100,000
Consumable materials (supplies and overhead)	$35,000

Table 3-7. EM² and DRACS testing program cost estimate (by year)

Year 1	$710,000
Year 2	$1,628,000
Year 3	$1,090,000
Year 4	$810,000
Year 5	$810,000
Total, Project	**$5,048,000**

4. STEAM-WATER INGRESS EVENT

This section considers the expansion of the utilization of the HTTF to the collection of validation data for the Steam-Water Ingress (SWI) event. A general scaling methodology for the SWI event is discussed in the *Scaling and Design Requirements Technical Report* (Woods, 2017, 1). An overview of the HTTF, the prototypical EM^2 and the prototypical DRACS designs is included in the *Test Facility Description Technical Report* (Woods, 2017, 2). The *Test Facility Description Technical Report* also includes a preliminary application of the scaling methodology outlined in the *Scaling and Design Requirements Technical Report*.

4.1. Facility Redevelopment Needs

4.1.1. Hardware

The following materials and components will be utilized under the scope of reconfiguring the HTTF for collection of SWI data. Component specifications can be seen in Appendix I.

ASME Steam Generator Tank

The increase of moisture can be accomplished by injecting high temperature and pressure steam into the cold leg of the HTTF. The cold leg already has a ¼" connection, which could be used to connect the steam-water injection system. It is known that the operational pressure of the HTTF is 0.8 MPa, and the core inlet temperature is estimated to be 259°C (Woods, 2017, 2). In order to inject the steam into the cold leg, it is necessary to increase the pressure of the steam higher than the pressure inside the cold leg, and the steam has to reach a temperature close to 259°C in order to reduce thermal stress.

The ASME steam generator tank will be used to create steam with the temperature and pressure required. It has the capability to withstand a maximum pressure of 150 psi and temperature of 550°F.

Centrifugal Pump

The steam-water injection system must operate at a pressure higher than 0.8 MPa in order to allow the steam to enter the cold leg. The local domestic water system reaches a pressure of 35 psi in the most remote points, and buildings should not exceed a pressure of 80 psi. (OSU Construction Standards, 2015) Because of this, it is required to install a centrifugal pump that will be connected to the steam generator tank and the city water supply system in order to have an uninterrupted water supply.

Immersion Heater 10" Flange

It is calculated that the thermal energy needed for the steam-water injection system is 223 kW. A flanged immersion heater of 250 kW will be able to provide the energy required for this system. The immersion heater will be connected to the steam generator tank along with a control system.

Differential Pressure Transmitter

The immersion heater must be fully submerged in order to avoid malfunction. The differential pressure transmitter will indicate if water needs to be pumped into the tank or not.

4.1.2. Sensors and Instrumentation

Absorption spectrometer

Real-time in-situ measurements of moisture concentration are possible by probing H_2O electronic transitions in the near-infrared (NIR) using absorption spectroscopy. The main components of such a device are a laser light source, optical transmission system, and photo-detector. Tunable diode laser absorption spectroscopy (TDLAS) is widely used in laboratories and industry for in-situ gas analysis, and off-the-shelf designs such as shown in Figure 4-1 are available.

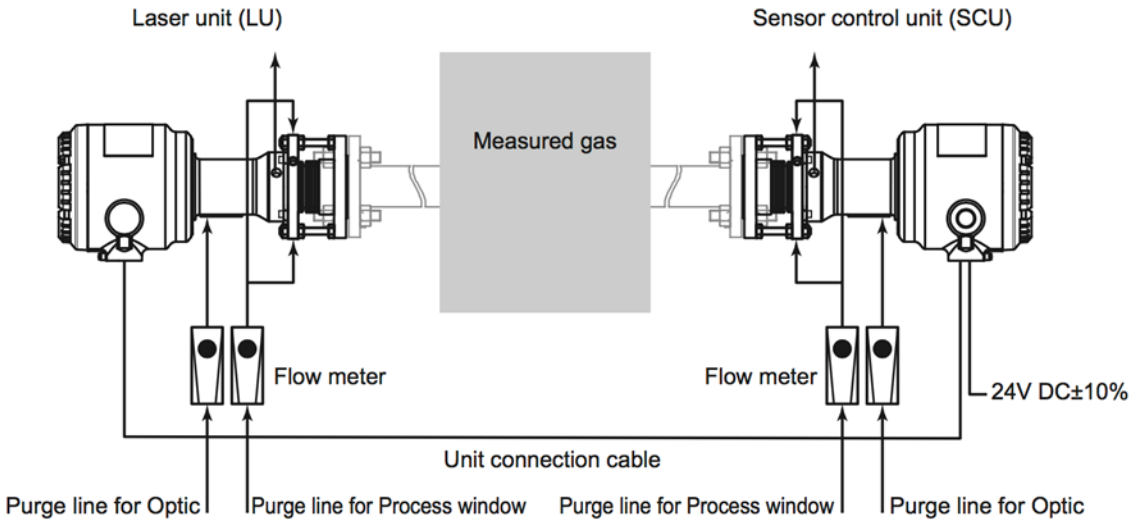

Figure 4-1. Standard TDLAS Configuration. (Yokogawa, 2015)

A spectrometer set-up can be installed across the upper plenum head of the RPV using the uninterrupted optical path in-between the control rod tubes shown in Figure 4-2. The device laser unit and sensor unit, each connected via short pipe flanges extending outward from the vessel head, can be aligned such that light absorption of a particular wavelength within the coolant can be measured to deduce the concentration of H_20 present.

The following types of instrumentation are currently installed at the HTTF.

1. Thermocouples to measure gas, heater, wall and ceramic temperatures. Due to the fact that many portions of the HTTF core will operate at very high temperatures, there is a mixture of K- and C-type thermocouples installed in the test facility. C-type thermocouples are capable of extended operation above the expected maximum temperature (1400°C) at the HTTF.
2. Pressure transducers to measure the static pressure in tanks and vessels.
3. Differential pressure transducers to measure flow induced pressure drops as well as liquid levels in tanks, vessels and piping.
4. Flow meters to measure various single-phase liquid flow rates.
5. Power meters to measure the core power and provide feedback for core power control.
6. Gas Concentration Instruments (GCIs). These devices measure the concentration of gases in a binary gas mixture. The GCIs measure the capacitance of a subject gas mixture and can use the measure of capacitance to determine the proportions of each gas in the mixture. The GCIs provide real-time measurement at high temperatures without the need for taking batch samples. These devices are being developed at OSU in support of the HTTF project.

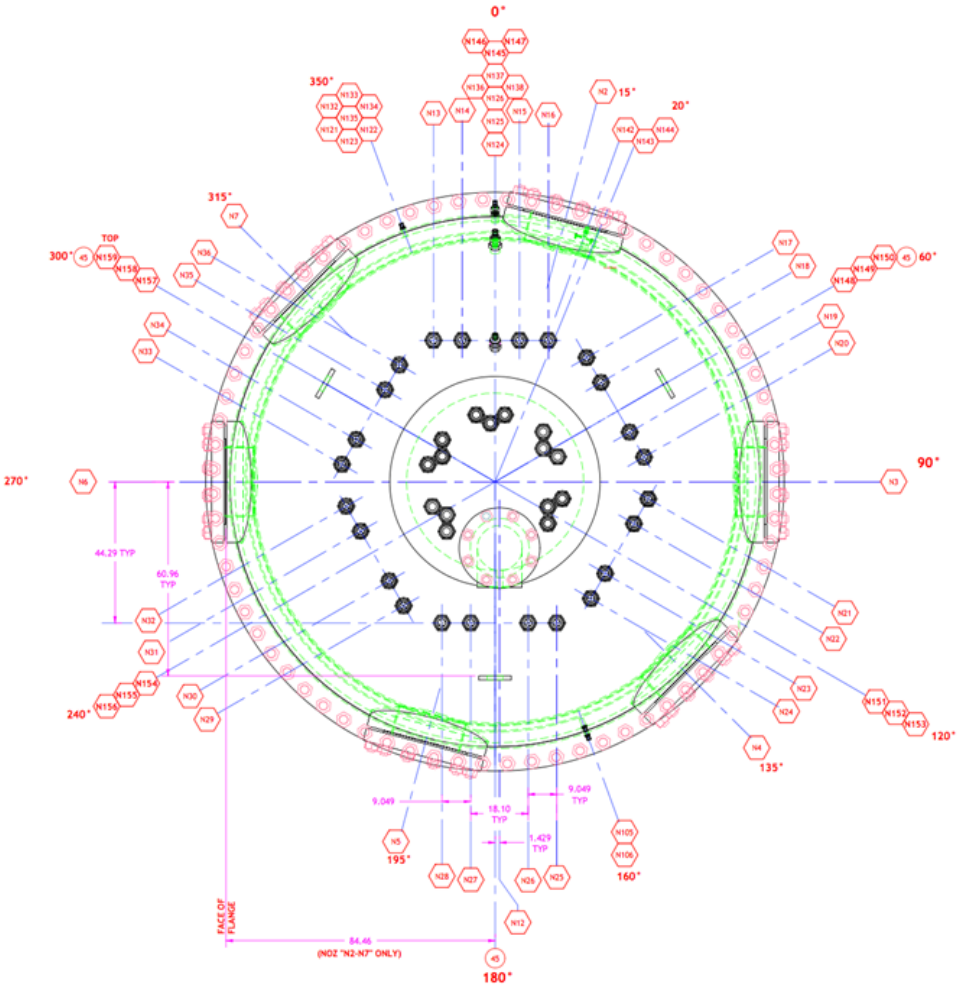

Figure 4-2. HTTF Schematic Displaying the Optical Path through the Upper Plenum, from N6 to N3.

The GCI detectors are ideal for moisture monitoring in regions of limited optical access, such as the core. Due to their compact and nonintrusive nature, capacitive-type detectors have been installed at various locations within the primary system. In the Primary Sector of the core, axial levels 1 through 9 and the Upper Plenum Floor are all instrumented with 1 GCI. However, GCI locations alternate between levels. In the upper plenum, three control rod guide tubes are instrumented with GCIs. Gas sensors are also placed in the lower plenum, attached to the support posts, as well as in the concentric inlet/outlet ducts, attached to the crossover duct rakes. Figure 4-3 shows multiple locations where the GCIs can be placed.

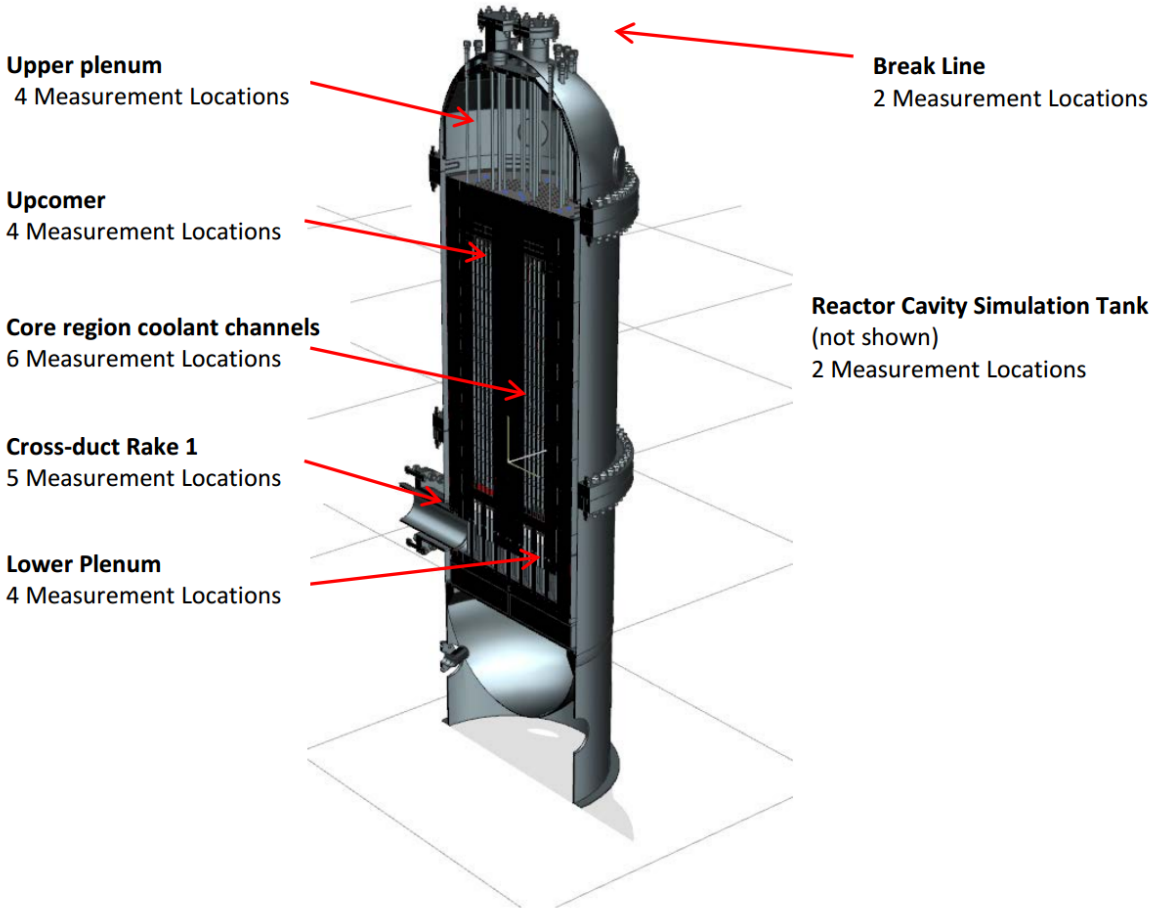

Figure 4-3. Possible locations of GCIs inside of the HTTF RPV.

4.2. Project Implementation

4.2.1. Schedule

This is planned as a one-year project. During the first six months, the following tasks will be completed:

1. Finalize matrix tests.
2. Install LAS device across upper vessel head.
3. Test and verify the successful installation of the LAS and GCIs.
4. Integrate water tank with immersion heater.
5. Install sensors and control panel.
6. Modify piping to include a narrow flange and valve for steam-water injection.

7. Connect centrifugal pump and steam generator tank to the municipal water system.

During the second six months, the following tasks will be completed:

1. Perform shakedown testing of the system.
2. Perform low ingress flow rate SWI matrix tests.
3. Perform high ingress flow rate SWI matrix tests.

4.2.2. Outcomes/Impacts

This project can directly provide understanding to fill in knowledge gaps identified in the DOE PIRT for the HTGR. The data obtained will be very useful for understanding steam-water transport and steam-water flow paths within the helium primary system during the steam-water ingress event of a conventional steam-cycle HTGR. It is anticipated that results from this project will be suitable for publication in journals within the field of nuclear engineering and gas reactor development.

The proposed project will require a team of at least 3 graduate and undergraduate students to perform the design work and construction efforts necessary to modify the HTTF to model the SWI event. Data generated through the successful operation of the SWI related equipment, as well as existing HTTF infrastructure, will need to be analyzed and processed, requiring additional collaboration between students. There will be uncertainty and error associated with the sensor technology (TDLAS and GCIs) that will be quantified as well.

4.2.3. Risk Management

There are five primary risks associated with the project.

Failure of absorption spectrometer

The laser absorption spectroscopy (LAS) technique has been tried and tested in laboratory and industry settings and can be observed in the literature as a go-to method for optical gas measurement. That being said, LAS technology is fairly complex and through its integration in this novel manner, unknown challenges may be encountered. Large temperature fluctuations across the path of the laser in the upper plenum may cause significant uncertainty in the concentration measurements.

Having two methods for moisture monitoring, with the GCIs being the second, will provide insurance that steam-water transport data collection will be possible by mitigating the risk associated with either method failing to operate adequately.

Failure of gas concentration instruments

While the GCI devices are designed to be installed directly within the primary coolant environment, they will be subjected to high temperatures, pressures, and in general, forces that may cause their structural degradation over time. In addition, the electronics needed to collect data using the GCIs is still under development. If GCIs are unavailable or fail, limited moisture monitoring could be performed by the laser absorption spectrometer. However, the investigation of local, in-situ moisture monitoring methods would need to be revisited since one laser absorption spectrometer may not be able to provide sufficient data required for code validation.

Long term corrosion effects in the core due to hydrolysis

In order to perform steam-water ingress event testing at the HTTF, the impact of steam and water vapor on the HTTF components must be addressed. The HTTF core blocks are composed of Greencast-94F ceramic, which is an absorber of water vapor. This absorption results in a sustained presence of water-moisture in the pores of the ceramic, and potentially other regions of the core. This may be a concern with regard to corrosion of the graphite heater elements via hydrolysis.

Graphite can oxidize and suffer mass loss in an oxidative environment at temperature in excess of 450 °C. (Mohanty, 2011) The steam introduced due to a steam-water ingress event poses a threat to the structural integrity of graphite components due to the heightened reaction rate of Carbon and H_20 at accident temperatures and steam concentrations. The graphite heater components of the HTTF are G-320; a nuclear-grade, fine grain, high density graphite with uniform structure (McEligot, 2016), such that oxidation is limited due to a limited reactive surface area. Despite this, oxidation damage will occur during sustained steam-water accident conditions.

The acute moisture ingress encountered during a SWI event will have minimal effects on the core components due to large difference between the amount of moisture introduced compared to the entire mass of the core, and the relatively short amount of time that high temperatures will be sustained in the core during testing. (Ball, 2011) The greater concern is of chronic oxidation due to a long term presence of water moisture introduced into the core due to its absorption in the ceramic while performing SWI tests.

There may be methods that could be employed to mitigate deleterious effects due to introducing water into the core while performing the steam-water ingress event tests. For example, currently at the HTTF, there are procedures in place to "bake" the core after the experiments are performed at a high enough temperature to vaporize the latent water moisture that has built up in the core, and purge it with the primary system gas.

Increase of pressure and temperature in the steam-water injection system tank

The steam generator tank will be operating at high pressure and temperature. The malfunction of the heater and/or sensors can cause a constant increase of temperature and pressure, and it can lead to shortage of liquid water inside of the tank, and leaks in the tank through the pipe connections and/or the immersion heater. In order to avoid these scenarios, a relief valve will be placed at the top of the tank which will limit the pressure of the system. In addition to this, the immersion heater will include a control system that will shut down the heater when the temperature of the liquid exceeds the preset limits.

Increase or decrease of the water level in the steam-water injection system tank

During normal operation of the steam-water injection system, the mass flow rate in should be almost equal to the flow rate leaving the system. The heater used for this system is required to be fully submerged in order to avoid any malfunction. That being said, the tank should contain enough liquid water to keep the heaters submerged. To avoid the damage of the equipment, a pressure differential sensor will be installed in the tank. If the water level decreases considerably, the differential pressure transmitter will activate the centrifugal pump, which it will keep pumping water into the tank until the water reaches a safe level. On the other hand, if the water level increases too much, which can cause thermal shock in the cold leg, the differential pressure transmitter will shut down the pump. As steam leaves the tank, the water level will decrease until safe levels are reached.

4.3. Economic Analysis

Table 4-1 and 4-2 shows an estimate of the total cost of the moisture sensors, and the equipment needed for the steam-water injection system.

Table 4-1. SWI testing program cost estimate (by item)

Instrumentation	
Tunable Diode Laser Absorption Spectroscopy	$50,000
Total, Instrumentation	**$50,000**
Steam Water Injection System	
Total, Steam Water Injection System	**$24,000**
Design, Maintenance and Operation (one year)	
Professional Staff (salary & overhead) (includes 1.0 FTE principal investigator, 0.5 FTE technician, and 0.1 FTE program manager)	$350,000
Students (stipend, tuition and overhead) (includes 3 graduate students)	$225,000
Consumable materials (supplies and overhead)	$30,000

Table 4-2. SWI testing program cost estimate (by year)

Year 1	$679,000
Total, Project	**$679,000**

5. REFERENCES

Abedrabbo, S. (1988). Emissivity Measurements and Modeling of Silicon Related Materials and Structures. PhD thesis, New Jersey Institute of Technology and Rutgers State University of New Jersey.

Ball, S. J., (2011). NGNP Moisture Ingress Assessment Committee, Assessment of NGNP Moisture Ingress Events, INL/EXT-11-21397.

Bergman, T. (2011). Fundamentals of Heat and Mass Transfer. Hoboken: John Wiley & Sons.

Blake, Grant. Scaling Analysis for the Direct Reactor Auxiliary Cooling System for Gas-cooled Fast Reactors during a Depressurized Loss of Forced Convection Event, Thesis, Oregon State University, 2016

Auerkari. P. (1996). Mechanical and Physical Properties of Engineering Alumina Ceramics. Number ISBN 951-38- 4987-2. Technical Research Centre of Finland (VTT).

Bruls, R. Hintzen, H. de With, G. Metselaar, R. van Miltenberg, J. (2001). The temperature dependence of the Grüneisen parameters of MgSiN2, AlN and β Si3N4. Journal of Physics and Chemistry of Solids, 62: 783–792.

Cadell, S. (2012). Development of a Binary Mixture Gas Composition Instrument for Use in a Confined High Temperature Environment. PhD Thesis. Oregon State University.

Cagran, C. Hanssen, L. Noorma, M. Gura, A. Mekhontsev, S. (2007). Temperature-resolved infrared spectral emissivity of SiC and Pt-10Rh for temperatures up to 900○C. International Journal of Thermophysics, 28 (2):581–597.

Ceramic Industry. (2015). Material Properties Charts. Online access (12/4/2017) at: https://www.ceramicindustry.com/ceramic-materials-properties-charts.

Choi, et al. (2013). "A Compact Gas-Cooled Fast Reactor with an Ultra-Long Fuel Cycle." Science and Technology of Nuclear Installations.

de Faoite, D. Browne, D. Chang-Diaz, F. Stanton, K. (2011). A review of the processing, composition, and temperature-dependent mechanical and thermal properties of dielectric technical ceramics. Journal of Material Science, 47(10):4211–4235.

de Klerk, A. (2003). Voidage variation in packed beds at small column to particle diameter ratio. American Institute of Chemical Engineers Journal, 49(8):2022–2029.

du Toit, C. (2008). Radial variation in porosity in annular packed beds. Nuclear Engineering and Design, 238: 3073–3079.

Dyson, B., Lohr, R. D, Morrell, R. (1989). UK High Temperature Mechanical Testing Committee, National Physical Laboratory, & Institute of Ceramics. Mechanical testing of engineering ceramics at high temperatures. Elsevier.

Franco Junior, A. Shanafield, D. (2004). Thermal conductivity of polycrystalline Aluminum Nitride (AlN) ceramics. Ceramica, 50:247–253.

Gutowska, I., Coddington, T., Louria, S. and Woods, B. G. (2017). Scaling Studies for Advanced High Temperature Reactor Concepts, Test Plan Technical Report

HC Starck, Product Information Molybdenum Alloys, URL: https://www.hcstarck.com/molybdenum_alloy.

HC Starck, High Performance Solutions with MoLa Alloys, URL: https://www.hcstarck.com/hcs-admin/file/ae23e4b248d030140149754c51d64a36.de.0/mola_alloys_hc_starck.pdf

Hegbom, T. (1997). Integrating electrical heating elements in appliance design (Electrical engineering and electronics; 101). New York: Marcel Dekker.

Idaho National Laboratory. (2007). NGNP Engineering White Paper: High Temperature Fluid Flow Test Facility. INL/EXT-07-13146.

Idaho National Laboratory. (2009). Evaluation of Integrated High Temperature Component testing Needs. INL/EXT-09-15620.

International Chemical Safety Cards (ICSC). (2000) Aluminum Oxide. International Labor Organization, 0351 edition.

International Chemical Safety Cards (ICSC). (2004). Silicon Carbide (non-fibrous). International Labor Organization, 1061 edition. Online access (12/4/2017) at: http://www.ilo.org/dyn/icsc/showcard.display?p lang=enp card id=1061p version=2.

I Squared R Elements, Co. Silicon Carbide Heating Elements (Starbar®) and Molybdenum Disilicide Heating Elements (Moly-D®), URL: http://heatingelements.isquaredrelement.com/viewitems/tarbar-silicon-carbide-heating-element-accessories/a-b-and-c-type-terminal-straps

Kosolapova, T. Y., (1971). Carbides: Properties, Production, and Applications. Chapter IV, Page 67.

KTA 3102.2 Safety Standards of the Nuclear Safety Standards Commission: Reactor Core Design for High-Temperature Gas-Cooled Reactors. Part 2: Heat Transfer in Spherical Fuel Elements, Germany, June 1983.

Lee, J. Radu, I. Alexe. M. (2002). Oxidation behavior of AIN substrate at low temperature. Journal of Materials Science: Materials in Electronics, 13:131–137.

Lieberman, M. A., Lichtenberg, A. J. (2005). Principles of plasma discharges and materials processing. Hoboken, NJ: Wiley-Interscience.

Liu, L. Edgar, J. H. (2002). A global growth rate model for Aluminum Nitride sublimation. Journal of the Electrochemical Society, 149(1):G12–G15.

McEligot D., Swank D., Cottle D., Valentin F., (2016). Thermal Properties of G-348 Graphite, INL/EXT-16-38241.

McEligot, Swank, D. W. Cottle, D. Valentin, F. (2017). Thermal properties of G-348 graphite. Technical Report INL/EXT-16-38241, Idaho National Laboratory.

Mohanty S., Majumdar S., (2011). HTGR Graphite Core Component Stress Analysis Research Program – Task 1 Technical Letter Report, ANL-11/04.

Mori, M. Komeya, K. Tsuge, A. Inoue, H. (1984). Silicon Nitride powder. Technical Report NASA TM-77731, National Aeronautic and Space Administration.

Munro, R. (1997). Material properties of a sintered α SiC. Journal of Physical and Chemical Reference Data, 26 (5):1195–1203.

MatWeb, Material Property Data, URL: http://www.matweb.com/search/datasheet.aspx?matguid=8ff1e57a64334d44afad7971e39e5a00&ckck=1

Omega Engineering, Inc. (2000). The electric heaters handbook. Stamford, CT: OMEGA Engineering.

OSU Construction Standards. (2015, December 02). Retrieved July 18, 2017, from http://fa.oregonstate.edu/cpd-standards/22-plumbing/section-22-30-00-plumbing-equipment

Panchula, M. (1999). Synthesis and Sintering of Nanocrystalline Alumina and Aluminum Nitride. PhD thesis, Massachusetts Institute of Technology.

Poco Graphite, Inc. (2015). Properties and Characteristics of Graphite. Technical Report. Retrieved from: http://poco.com/Portals/0/Literature/Semiconductor/IND-109441-0115.pdf

Poco Graphite. (2015). Properties and characteristics of graphite. Technical report, Poco Graphite.

Riou, O. Logerais, P. Froger, V. Durastanti, J. Bouteville. A. (2013). Thermal study of an Aluminum Nitride cermaic heater for spray cvd on glass substrates by quantitative thermography. Quantitative Infrared Thermography Journal, 10(2):159–171.

Rohm and Haas, 2000. Online access (12/4/2017) at: http://www.dow.com/assets/attachments/business/gt/advanced ceramics/ cvd silicon carbide/tds/cvd silicon carbide.pdf.

Schleicher, R. W., EM2 and Spinoff Technologies. 2011.<http://www.nuc.berkeley.edu/events/em2-and-spinoff-technologies>.

Schleicher, R. W., Choi, H., and Rawls, J. (2013). “The Energy Multiplier Module: Advancing the Nuclear Fuel Cycle Through Technology Innovations.” Nuclear Technology, **184**, 2, pp. 169-180.

Schleicher, R. W., and Bertch, T. (2014). “Design and Development of EM^2." Proc. SMR 2014.

Slack, G. Batrum, S. (1975). Thermal expansion of some diamond like crystals. Journal of Applied Physics, 46 (1):89–98.

Slack, G. Huseby, I. (1982). Thermal Grüneisen parameters of CdAl2O4, β Si3N4, and other phenacite type compounds. Journal of Applied Physics, 53(10):6817–6822.

Slack. G. Tanzilli, R. Pohl, R. Vandersande, J. (1987). The intrinsic thermal conductivity of AlN. Journal of Physics and Chemistry of Solids, 48(7):641–647.

Slade, P. G. (2014). Electrical contacts: principles and applications. Boca Raton: CRC Press, Taylor & Francis Group.

Tanigawa, G. Enoeda, M. Akiba, M. (2007). Measurement of thermal expansion for a Li2TiO3 pebble bed. Fusion Engineering and Design, 82:2259–2263, 2007.

Thorn, R. Simpson, O. (1953). Spectral emissivities of graphite and carbon. Journal of Applied Physics, 24(5): 633.

Woods, B., G. (2015). Scaling analysis for the very high temperature reactor test facility at Oregon State University. Technical Report, OSU-HTTF-TECH-001-R0. Oregon State University. School of Nuclear Science and Engineering.

Woods, B., G. (2015). OSU High Temperature Test Facility Design Technical Report. Revision 1. Technical Report, Oregon State University, School of Nuclear Science and Engineering.

Woods, B.G., Jackson, R.B., Utberg, J. E., Cox, J. T., Cadell, S. R., and Blake, G. C. (2015). Instrumentation Plan for the OSU High Temperature Test Facility, Technical Report, OSU-HTTF-TECH-002-R0. Oregon State University. School of Nuclear Science and Engineering.

Woods, B. G., Hertell, M. (2016). OSU HTTF Heater Design Technical Report. Internal Technical Report. Oregon State University. School of Nuclear Science and Engineering.

Woods, B. G., Cox, J., Blake, G. (2017). Scaling Studies for Advanced High Temperature Reactor Concepts, Scaling and Design Requirements Technical Report.

Woods, B. G., Gutowska, I., Blake, G., Coddington, T. and Louria, S. (2017). Scaling Studies for Advanced High Temperature Reactor Concepts, Test Facility Description Technical Report

Woods, B. (2017). OSU High Temperature Test Facility Program Quality Plan, OSU-HTTF-ADMIN-001.

Ximing, S. Fu, L. Minggang, L. (2014). Numerical simulation of flow patterns of fuel spheres in pebble bed reactors. Online access (12/4/2017) at: http://www.iaea.org/inis/collection/NCLCollectionStore/_Public/48/076/48076894.pdf

Yokogawa 2015, General Specifications, Model TDLS8000. < https://www.yokogawa.com/us/solutions/products-platforms/process-analyzers/gas-analyzers/oxygen-analyzers/tdls8000-tunable-diode-laser-spectrometer/ >

Zheng, Y, Shi, L., Dong, Y. (2009). Thermal-hydraulic Transient Studies of the Chinese 200 MWe HTR-PM for Loss of Forced Cooling Accidents. Annals of Nuclear Energy 36. p. 742-751.

Zheng, Y., Lapins, J., Laurien, E., Shi, L., & Zhang, Z. (2012). Thermal-hydraulic Analysis of a Pebble-bed Modular High Temperature Gas-cooled Reactor with ATTICA3D and THERMIX Codes. Nuclear Engineering and Design, 246, 286-297.

Zhou, Y., Zhou, K., Ma, Y., & Sui, Z. (2013). Thermal-hydraulic Simulation of Reactor of HTR-PM Based on Thermal-fluid Network and SIMPLE Algorithm. Progress in Nuclear Energy, 62, 83-93.

APPENDIX A: PB-HTTF STRUCTURAL MATERIAL PROPERTIES

G535

1. Typical Properties

Specific Gravity	g/cm^3	1.82	lb/ft^3	114
Specific Resistance	μΩm	17	μΩinch	669.29
Young's Modulus	GPa	10.8	MSI	1.57
Flexural Strength	MPa	63.7	PSI	9,240
Tensile Strength	MPa	45	PSI	6,572
Shore Hardness	sHD	72	sHD	72
C.T.E	$\times 10^{-6}$/°C	5.5	× 10-6/°F	3.06
Thermal Conductivity	W/mK	81	BTU / (hr-ft-°F)	47
Pore Size	mm	0.001	inch	0.00005
Porosity	%	12	%	12
Grain Size	mm	0.004	Inches	0.00016
Gas Permeability	cm^2/sec	0.05	Inch/sec	0.0078

All properties measured room temperatures except for C.T.E.
C.T.E. = Coefficient Thermal Expansion (R.T. to 1000°C)
Flexural Strength determined using third point loading

2 Additional Properties

2.1. Electrical Resistance

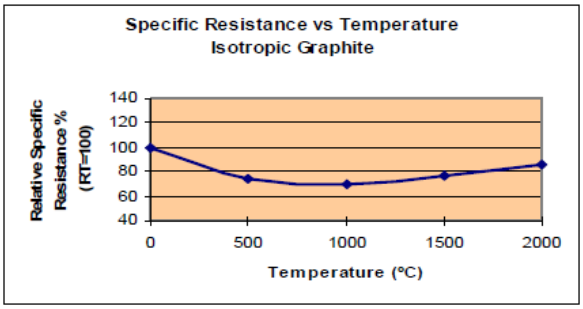

2.2 Ash Content

Designation	ppm
Standard	200 (max)
Purified (S type)	5 (max)

2.3 Metallic Impurities

	Impurity (ppm)												
Grade	Al	B	Ca	Co	Cr	Cu	Fe	Mg	Mn	Ni	Si	Ti	V
Standard	1	1	100	3	ND	1	40	1	ND	ND	100	30	3
Purified	ND	ND	ND	ND	ND	ND	<1	<1	ND	ND	<1	<1	ND

Note: All properties are typical values and are not to use for specification limits.

G540

1. Typical Properties

Specific Gravity	g/cm^3	1.85	lb/ft^3	116
Specific Resistance	μΩm	15	μΩinch	590.55
Young's Modulus	GPa	13.7	MSI	1.99
Flexural Strength	MPa	88.2	PSI	12,793
Tensile Strength	MPa	54	PSI	7,887
Shore Hardness	sHD	78	sHD	78
C.T.E	$\times 10^{-6}$/°C	5.5	× 10-6/°F	3.06
Thermal Conductivity	W/mK	93	BTU / (hr-ft-°F)	54
Pore Size	mm	0.001	inch	0.00003
Porosity	%	11	%	11
Grain Size	mm	0.002	Inches	0.00008
Gas Permeability	cm^2/sec	0.01	Inch/sec	0.0016

All properties measured room temperatures except for C.T.E.
C.T.E. = Coefficient Thermal Expansion (R.T. to 1000°C)
Flexural Strength determined using third point loading

2 Additional Properties

2.1. Electrical Resistance

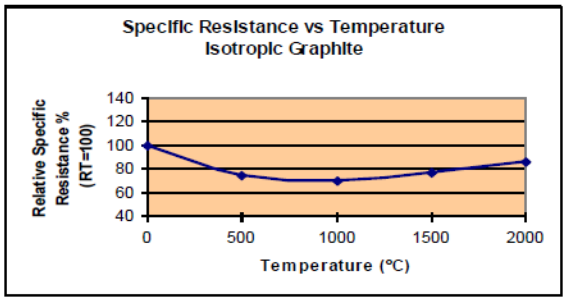

2.2 Ash Content

Designation	ppm
Standard	200 (max)
Purified (S type)	5 (max)

2.3 Metallic Impurities

	Impurity (ppm)												
Grade	Al	B	Ca	Co	Cr	Cu	Fe	Mg	Mn	Ni	Si	Ti	V
Standard	1	1	100	3	ND	1	40	1	ND	ND	100	30	3
Purified	ND	ND	ND	ND	ND	ND	<1	<1	ND	ND	<1	<1	ND

Note: All properties are typical values and are not to use for specification limits.

CeraMaterials

Extruded GH030 Graphite

Typical Physical Properties

	English Units	Metric Units
Maximum Particle Size	0.031 in.	0.8 mm
Apparent Density	108 lb/ft^3	1.72 gm/cc
Hardness Rockwell	80 R	80 R
Porosity	18 %	18%
Specific Resistance	32.5 x 10^{-5} ohm-in	8.5 Micro ohm-m
Flexural Strength	2300 psi	16 N/mm^2
Compressive strength	5100 psi	35 N/mm^2
Thermal Conductivity	90 BTU/ft.hr °F	160 W/m.°C
Coefficient of Thermal Expansion	1.4 x 10^{-6}/°F	2.5 x 10^{-6}°C
Tensile Strength	1900 psi	13 N/mm^2

The above values are typical and are not to be used as specification limits, unless otherwise noted.

Please contact: Jerry Weinstein (518) 701-6722
Email; jerryw@ceramaterials.com
For pricing; www.ceramaterials.com

Broad Base. Best Solutions.

SGL GROUP
THE CARBON COMPANY

SIGRAFINE® R7660

Material: Graphite
Forming: Isostatically pressed
Application: High-temperature application

SIGRAFINE® is the new brand name for our fine-grain graphites, previously known under the names RINGSDORFF®, SIGRAFORM®, SIGRAMENT® and CRYSTA-SIL®.

Material data of SIGRAFINE® R7660

Typical properties	Units	Test standards	Values*
Average grain size	µm	ISO 13320	10
Bulk density	g/cm³	DIN IEC 60413/204	1.75
Open porosity	Vol. %	DIN 66133	14
Medium pore entrance diameter	µm	DIN 66133	1.5
Coefficient of permeability (ambient temperature)	cm²/s	DIN 51935	0.25
Rockwell hardness $HR_{5/100}$		DIN IEC 60413/303	75
Resistivity	µΩm	DIN IEC 60413/402	23
Flexural strength	MPa	DIN IEC 60413/501	50
Compressive strength	MPa	DIN 51910	115
Dynamic modulus of elasticity	MPa	DIN 51915	10.5×10^3
Thermal expansion (20 – 200 °C)	K^{-1}	DIN 51909	3.7×10^{-6}
Thermal conductivity (20 °C)	$Wm^{-1}K^{-1}$	DIN 51908	45
Ash content	ppm	DIN 51903	200

* Value might be changed due to material size

08 2015/0 1NÄ Printed in Germany

Graphite Materials & Systems | SGL CARBON GmbH
Sales Europe/Middle East/Africa | iso-europe@sglgroup.com
Sales Americas | iso-americas@sglgroup.com
Sales Asia/Pacific | iso-asia@sglgroup.com
www.fine-grain-graphites.com | www.sglgroup.com/gms

TDS R7660.02

Grade: GR008GP

Manufacturer: Graphtek LLC
Method of Manufacturing: Extruded
Description: Superfine grain, high density, purified (less than 50ppm) extruded graphite

PROPERTY	US VALUE		METRIC VALUE	
Particle Size	**0.008**	in	**0.02032**	cm
Density	**0.060**	lb/in^3	**1.65**	gr/cm^3
Flexural Strength	**3700**	psi	**25.5**	MPa
Compressive Strength	**6000**	psi	**41.4**	MPa
Resistivity	**3.2**	$ohmXinX10^{-4}$		
CTE	**0.6**	$in/in\ °F \times 10^{-6}$	**1.1**	Microns/m °C
Temperature (Air)	**750**	°F	**399**	°C
Temperature (Inert)	**5000**	°F	**2760**	°C
Ash Content	**less than 50**	ppm		

GREENCAST®-94 PLUS

HarbisonWalker International

Product Data

6/10: 5477

Description: High-Alumina, Low-Silica Castable for Severe Abrasion	
Features:	• Fine grained. • Outstanding abrasion resistance from dust erosion, rubbing, and heavy impact. • High temperature resistance for hydrogen service.
Uses:	• Lining areas subjected to rubbing, grinding, or high-velocity, dust-laden gases. • Hydrogen transfer lines and secondary ammonia reformer linings. • High temperature burner blocks and high temperature thermal combustors. • Waste heat boiler high temperature boiler inlets. • Upper case sections of copper and iron vertical channel induction units.

Chemical Analysis: Approximate (Calcined Basis)	
Silica (SiO_2)	0.2%
Alumina (Al_2O_3)	94.1%
Iron Oxide (Fe_2O_3)	0.2%
Titania (TiO_2)	0.1%
Lime (CaO)	5.1%
Magnesia (MgO)	0.1%
Alkalies (Na_2O+K_2O)	0.2%

Physical Data (Typical)	Vibration Cast
Maximum Service Temperature	3400°F (1870°C)
Material Required	168 lb/ft³ (2.69 g/cm³)
Bulk Density	lb/ft³ (g/cm³)
After 220°F (105°C)	169 to 175 (2.71 to 2.80)
After 1500°F (815°C)	160 to 168 (2.56 to 2.69)
Modulus of Rupture	lb/in.² (MPa)
After 220°F (105°C)	1,400 (9.7)
After 1500°F (815°C)	1,750 (12.1)
After 2000°F (1095°C)	960 (6.6)
After 2500°F (1370°C)	1,510 (10.4)
Cold Crushing Strength	lb/in.² (MPa)
After 220°F (105°C)	7,000 to 18,000 (48.3 to 124.1)
After 1500°F (815°C)	7,000 to 11,000 (48.3 to 75.9)
After 2000°F (1095°C)	7,920 (54.6)
After 2500°F (1370°C)	9,830 (67.8)
Permanent Linear Change	
After 220°F (105°C)	None
After 1500°F (815°C)	0.0 to -0.2%
After 2000°F (1095°C)	+0.4%
After 2500°F (1370°C)	-0.6%
After 2900°F (1595°C)	-0.7%
After 3200°F (1760°C)	-0.5%
Abrasion Loss	
After 1500°F (815°C)	< 12.0 cc

Thermal Conductivity	Btu·in./hr·ft²·°F (W/m·°C)
At 400°F (205°C)	30.6 (4.41)
At 800°F (425°C)	21.1 (3.04)
At 1200°F (650°C)	16.3 (2.35)
At 1600°F (870°C)	14.1 (2.03)
At 2000°F (1095°C)	13.6 (1.96)
At 2400°F (1315°C)	14.5 (2.09)

Note: The test data shown are based on average results on production samples and are subject to normal variation on individual tests. The test data cannot be taken as establishing minimum or maximum specification purposes. ASTM test procedures used when applicable.

Mixing and Using Information (Water calculated at 8.337 lb/gallon)	55 lb bag	1000 lb bag	1500 lb bag
Water Required—Vibration Casting (Weight 8.3%)			
Pounds	4.6	83.0	124.5
Gallons	0.5	10.0	14.9
Liters	2.1	37.6	56.4
Water Required—Hand Casting (Weight 9.1%)			
Pounds	5.0	91.0	136.5
Gallons	0.6	10.9	16.4
Liters	2.3	41.2	61.9
Working Time		20 minutes	
For detailed mixing and using instructions, contact your HWI representative or visit www.thinkHWI.com.			
Heatup/Dryout Schedule			
See HWI Dryout Schedule 2—PLUS Rated Castables and Gunning Castables.			
Installation Guidelines			
See HWI Installation Guidelines CC-1—Conventional Castables—Standard.			
Shelf Life (Under Proper Storage Conditions)		365 days	

APPENDIX B: PB-HTTF INSTRUMENT LOCATIONS

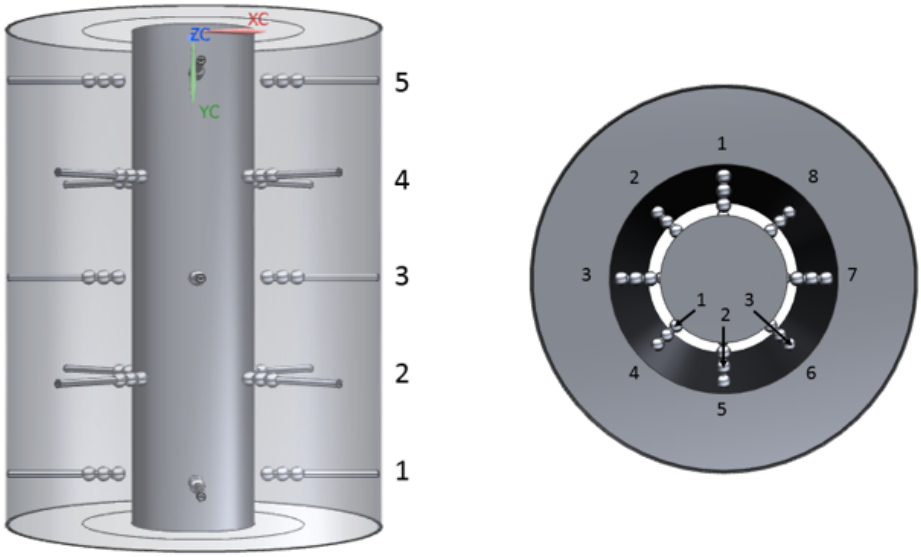

Figure 41 PB-HTTF core detailed instruments location.

High Temperature Thermocouples	Axial Level	Azimuthal Position	Radial Position
1	1	3	1
2	1	5	1
3	1	5	2
4	1	7	2
5	2	4	1
6	2	6	1
7	2	6	2
8	2	8	2
9	3	5	1
10	3	7	1
11	3	7	2
12	3	1	2
13	4	6	1
14	4	8	1
15	4	8	2

16	4	2	2
17	5	7	1
18	5	1	1
19	5	1	2
20	5	3	2
K-Type Thermocouples	Axial Level	Azimuthal Position	Radial Position
1	1	1	3
2	1	7	3
3	2	2	3
4	2	8	3
5	3	3	3
6	3	1	3
7	4	4	3
8	4	2	3
9	5	5	3
10	5	3	3
Gas Concentration Instruments	Axial Level	Azimuthal Position	Radial Position
1	1	1	1
2	1	3	2
3	1	5	3
4	2	2	1
5	2	4	2
6	2	6	3
7	3	3	1
8	3	5	2
9	3	7	3
10	4	4	1
11	4	6	2
12	4	8	3
13	5	5	1

14	5	7	2
15	5	1	3
MEMs Anemometer Clusters	Axial Level	Azimuthal Position	Radial Position
1	1	7	1
2	1	1	2
3	1	3	3
4	2	8	1
5	2	2	2
6	2	4	3
7	3	1	1
8	3	3	2
9	3	5	3
10	4	2	1
11	4	4	2
12	4	6	3
13	5	3	1
14	5	5	2
15	5	7	3

APPENDIX C: THERMAL EXPANSION MATLAB CALCULATIONS

```
%  This code calculates the Radial and Axial Thermal Expansion
% for PB-HTTF using the average core temperatures during DCC, PCC
% and Normal Operation given by (Zheng 2009) with reference to the HTR-PM
clc
close all
% Nominal Dimensions of PB-HTTF
L = 1.98; %Length
R = .75/2; % Radius for equivalent flow area
T_r = [600 775 975]; %HTR-PM Ref Temp for [NO PCC DCC] Celsius
T_0 = 25; %RT Celsius
%
% Graphite Calculation
% Uses G-348 from INL/EXT-16-38421 R1
%
b_g = 4.812E-6;
c_g = 1.145E-9;
del_Lg = L*(b_g*(T_r-T_0)+c_g*(T_r.^2-T_0^2));
del_Rg = R*(b_g*(T_r-T_0)+c_g*(T_r.^2-T_0^2));
L_g = L+del_Lg;
R_g = R+del_Rg;
%
% Aluminum Nitride Calculation
% Uses AlN from (Bruhls 2000)
%
alpha_aln =[250 2.24E-6
            300 2.77E-6
            350 3.25E-6
            400 3.68E-6
            450 4.07E-6
            500 4.42E-6
            550 4.72E-6
            600 4.98E-6
            650 5.21E-6
            700 5.41E-6
            750 5.58E-6
            800 5.73E-6
            900 5.98E-6
            1000 6.17E-6
            1100 6.32E-6
            1200 6.43E-6
            1300 6.53E-6]; %Kelvin, Alpha
 for i= 1:3
    k = 1;
    L_aln(i) = L;
    R_aln(i) = R;
    for j = (T_0+273+1):(T_r(i)+273)
        if j > alpha_aln(k+1,1)
            k = k+1;
        end
        alpha_temp              =              alpha_aln(k,2)+(alpha_aln(k+1,2)-alpha_aln(k,2))/(alpha_aln(k+1,1)-
alpha_aln(k,1))*(j-alpha_aln(k,1));
        del_Laln = alpha_temp*L_aln(i);
        del_Raln = alpha_temp*R_aln(i);
        L_aln(i) = L_aln(i)+del_Laln;
        R_aln(i) = R_aln(i)+del_Raln;
    end
```

```
end
%
% Aluminum Oxide Calculations
% Calculated Using the Greencast Expansion in (Woods 2015) Tech-003
%
alpha_alo =[   25 1.1725
              563 1.5650
              643 1.6333
              758 1.7403
              971 1.9350
              1026 1.9838]; %Celsius, % Linear Change
 for i= 1:3
    k = 1;
    for j = 1:5
       if T_r(i) > alpha_alo(k,1) && T_r(i) < alpha_alo(k+1,1)
          k = j;
       end
    end
    alpha_temp              =              alpha_alo(k,2)+(alpha_alo(k+1,2)-alpha_alo(k,2))/(alpha_alo(k+1,1)-
alpha_alo(k,1))*(T_r(i)-alpha_alo(k,1))-alpha_alo(1,2);
    L_alo(i) = L*(1+alpha_temp/100);
    R_alo(i) = R*(1+alpha_temp/100);
 end
%
% Silicon Carbide Calculations
% Calculated Using (Munro 1997)
%
alpha_temp = (4.22+8.33*10^-4*T_0-3.51*exp(-.00527*T_0))*10^-6;
L_0 = (alpha_temp*T_0+1)^-1*L;
R_0 = (alpha_temp*T_0+1)^-1*R;
for i =1:3
    alpha_temp = (4.22+8.33*10^-4*T_r(i)-3.51*exp(-.00527*T_r(i)))*10^-6;
    L_sic(i)= L_0*(alpha_temp*T_r(i)+1);
    R_sic(i)= R_0*(alpha_temp*T_r(i)+1);
end
%
% Silicon Nitride Calculations
% Calculate Using (Bruhls 2000)
%
alpha_sin =[300 1.19E-6
           350 1.59E-6
           400 1.94E-6
           450 2.23E-6
           500 2.47E-6
           550 2.66E-6
           600 2.83E-6
           650 2.96E-6
           700 3.07E-6
           750 3.17E-6
           800 3.25E-6
           900 3.37E-6
           1000 3.47E-6
           1100 3.54E-6
           1200 3.59E-6
           1300 3.64E-6]; %Kelvin, Alpha
for i= 1:3
```

```
    k = 1;
    L_sin(i) = L;
    R_sin(i) = R;
    for j = (T_0+273+1):(T_r(i)+273)
        if j > alpha_sin(k+1,1)
            k = k+1;
        end
        alpha_temp = alpha_sin(k,2)+(alpha_sin(k+1,2)-alpha_sin(k,2))/(alpha_sin(k+1,1)-alpha_sin(k,1))*(j-
alpha_sin(k,1));
        del_Lsin = alpha_temp*L_sin(i);
        del_Rsin = alpha_temp*R_sin(i);
        L_sin(i) = L_sin(i)+del_Lsin;
        R_sin(i) = R_sin(i)+del_Rsin;
    end
 end
```

APPENDIX D: AL_2O_3 EMISSIVITY MATLAB CODE

```
% This is for determining appropriate emissivity values for al2o3
format long
clc
close all
h= 6.626E-34; %j/s
k = 1.3806E-23; %j/k
c_0 = 2.99E+8; %m/s
lam_disc = 1E-8;
lam_min = 5E-7;
lam_max = 5E-5;
mat_num = ceil(((lam_max-lam_min)/lam_disc));
wave = zeros(1,mat_num);
rad = zeros(3,mat_num);
rad_rat = zeros(3,mat_num);
rad_em = zeros(3,mat_num);
em = zeros(3,mat_num);
tot_em = zeros(1,3);
T = [850 1050 1250];
em_1 = [9.60E-07    0.529790991
1.95154E-06 0.283393817
2.98238E-06 0.20613635
3.97357E-06 0.308637854
4.92511E-06 0.688695686
7.89868E-06 0.977697995
1.09119E-05 0.87548759
1.39251E-05 0.572396126];
em_2 = [9.60E-07    0.397632401
1.99119E-06 0.214648062
3.06167E-06 0.187587572
4.92511E-06 0.720413748
7.89868E-06 0.977697995
1.09119E-05 0.909848823
1.39251E-05 0.604114188];
em_3 = [0.000001    0.313027616
1.99119E-06 0.190859516
3.06167E-06 0.187587572
4.88546E-06 0.752155097
7.93833E-06 0.969745192
1.09119E-05 0.923064682
1.38458E-05 0.680812746];
T_em_alo = [814 1055 1127];

for i = 1:3
    for j = 1:mat_num
        wave(j) = lam_min+(j-1)*lam_disc;
        rad(i,j) = (2*h*c_0^2)/(wave(j)^5)*(1/(exp((h*c_0)/(k*T(i)*wave(j)))-1));
    end
end
for i = 1:3
    rad_rat(i,:) = rad(i,:)/sum(rad(i,:));
    if i == 1
        c = 1;
        for j = 1:mat_num
            if wave(j) < em_1(1,1)
                em(i,j) = em_1(1,2);
            elseif wave(j) >= em_1(8,1)
```

```
            em(i,j) = em_1(8,2);
        else
            if wave(j) >= em_1(c,1)
              c = c+1;
            end
            em(i,j)   =   em_1(c-1,2)+   (wave(j)-em_1(c-1,1))/(em_1(c,1)-em_1(c-1,1))*(em_1(c,2)-em_1(c-
1,2));
        end
      end
   elseif i == 2
      c = 1;
      for j = 1:mat_num
        if wave(j) < em_2(1,1)
            em(i,j) = em_2(1,2);
        elseif wave(j) >= em_2(7,1)
            em(i,j) = em_2(7,2);
        else
            if wave(j) >= em_2(c,1)
              c = c+1;
            end
            em(i,j)   =   em_2(c-1,2)+   (wave(j)-em_2(c-1,1))/(em_2(c,1)-em_2(c-1,1))*(em_2(c,2)-em_2(c-
1,2));
        end
      end
   else
      c = 1;
      for j = 1:mat_num
        if wave(j) < em_3(1,1)
            em(i,j) = em_3(1,2);
        elseif wave(j) >= em_3(7,1)
            em(i,j) = em_3(7,2);
        else
            if wave(j) >= em_3(c,1)
              c = c+1;
            end
            em(i,j)   =   em_3(c-1,2)+   (wave(j)-em_3(c-1,1))/(em_3(c,1)-em_2(c-1,1))*(em_3(c,2)-em_3(c-
1,2));
        end
      end
   end
   rad_em(i,:) = times(rad_rat(i,:),em(i,:));
   tot_em(i) = sum(rad_em(i,:));
end
semilogx(wave,rad)
title('Thermal Radiation Intensity vs. Wavelength')
ylabel('Radiation Intensity(W sr-1 m-3)')
xlabel('Wavelength (m)')
legend('DCC Air Ingress & Normal Operation','PCC Natural Circulation','DCC Natural Circulation')
figure
semilogx(wave,rad_rat)
title('Normalized Radiation Intensity vs. Wavelength')
ylabel('Radiation Intensity (unitless)')
xlabel('Wavelength (m)')
legend('DCC Air Ingress & Normal Operation','PCC Natural Circulation','DCC Natural Circulation')
figure
plot(wave,em)
```

APPENDIX E: SIC EMISSIVITY MATLAB CODE

```
% This is for determining appropriate emissivity values for SiC
format long
clc
close all
h= 6.626E-34; %j/s
k = 1.3806E-23; %j/k
c_0 = 2.99E+8; %m/s
lam_disc = 1E-8;
lam_min = 5E-7;
lam_max = 5E-5;
mat_num = ceil(((lam_max-lam_min)/lam_disc));
wave = zeros(1,mat_num);
rad = zeros(3,mat_num);
rad_rat = zeros(3,mat_num);
rad_em = zeros(3,mat_num);
em = zeros(1,mat_num);
tot_em = zeros(1,3);
T = [850 1050 1250];
em_1 = [2.00449E-06 0.822391414
3.97303E-06 0.826624182
4.56629E-06 0.829535469
5.24045E-06 0.835421768
5.99551E-06 0.848760691
6.96629E-06 0.859087708
7.55955E-06 0.86946168
8.12584E-06 0.879839007
8.66517E-06 0.896189837
9.15056E-06 0.914039913
9.47416E-06 0.934895187
9.82472E-06 0.955747107
1.00404E-05 0.976615797
1.03101E-05 0.976582257
1.0418E-05  0.936270334
1.04719E-05 0.857159148
1.05528E-05 0.760134161
1.05798E-05 0.663115881
1.06876E-05 0.533251719
1.07685E-05 0.430256582
1.09303E-05 0.322773772
1.13079E-05 0.218249203
1.16045E-05 0.152540667
1.18472E-05 0.118182123
1.21169E-05 0.092775449
1.24404E-05 0.097212812
1.26562E-05 0.127036726
1.2791E-05  0.164333389
1.28719E-05 0.22402482
1.29798E-05 0.304608419
1.30607E-05 0.377732685
1.32225E-05 0.443384203
1.34112E-05 0.486644307
1.37079E-05 0.531383532
1.41663E-05 0.586550394
1.47056E-05 0.623796747
```

```
1.52989E-05 0.65058863
0.000016    0.672889485
1.6836E-05  0.692188496
1.78067E-05 0.70400805
1.89124E-05 0.712825759
0.0000196   0.722441724
2.0018E-05  0.721643468];

for i = 1:3
   for j = 1:mat_num
      wave(j) = lam_min+(j-1)*lam_disc;
      rad(i,j) = (2*h*c_0^2)/(wave(j)^5)*(1/(exp((h*c_0)/(k*T(i)*wave(j)))-1));
   end
   rad_rat(i,:) = rad(i,:)/sum(rad(i,:));
   if i == 1
      c = 1;
      for j = 1:mat_num
         if wave(j) < em_1(1,1)
            em(i,j) = em_1(1,2);
         elseif wave(j) >= em_1(43,1)
            em(i,j) = em_1(43,2);
         else
            if wave(j) >= em_1(c,1)
              c = c+1;
            end
            em(i,j)   =   em_1(c-1,2)+   (wave(j)-em_1(c-1,1))/(em_1(c,1)-em_1(c-1,1))*(em_1(c,2)-em_1(c-
1,2));
         end
      end
   end
   rad_em(i,:) = times(rad_rat(i,:),em);
   tot_em(i) = sum(rad_em(i,:));
end
semilogx(wave,rad)
title('Thermal Radiation Intensity vs. Wavelength')
ylabel('Radiation Intensity(W sr-1 m-3)')
xlabel('Wavelength (m)')
legend('DCC Air Ingress','PCC Natural Circulation','DCC Natural Circulation')
figure
semilogx(wave,rad_rat)
title('Normalized Radiation Intensity vs. Wavelength')
ylabel('Radiation Intensity (unitless)')
xlabel('Wavelength (m)')
legend('DCC Air Ingress','PCC Natural Circulation','DCC Natural Circulation')
figure
semilogx(wave,em)
```

APPENDIX F: Si_3N_4 EMISSIVITY LATLAB CODE

```
% This is for determining appropriate emissivity values for Si3N4
format long
clc
close all
h= 6.626E-34; %j/s
k = 1.3806E-23; %j/k
c_0 = 2.99E+8; %m/s
lam_disc = 1E-8;
lam_min = 5E-7;
lam_max = 5E-5;
mat_num = ceil(((lam_max-lam_min)/lam_disc));
wave = zeros(1,mat_num);
rad = zeros(3,mat_num);
rad_rat = zeros(3,mat_num);
rad_em = zeros(3,mat_num);
em = zeros(1,mat_num);
tot_em = zeros(1,3);
T = [850 1050 1250];
em_1 = [1.43275E-06 0.897005988
2.02958E-06 0.900598802
2.8057E-06  0.900598802
3.49227E-06 0.900598802
4.20833E-06 0.907784431
4.95424E-06 0.91497006
5.81929E-06 0.92754491
6.68433E-06 0.94011976
7.37036E-06 0.950898204
7.87693E-06 0.968862275
8.26446E-06 0.979640719
8.59317E-06 0.97245509
8.74403E-06 0.94011976
8.83591E-06 0.893413174
8.96032E-06 0.792814371
9.11529E-06 0.677844311
9.26848E-06 0.598802395
9.41952E-06 0.562874251
9.54017E-06 0.537724551
9.69032E-06 0.519760479
9.80794E-06 0.555688623
9.98668E-06 0.562874251
1.01106E-05 0.473053892
1.02943E-05 0.379640719
1.04461E-05 0.329341317
1.06268E-05 0.297005988
1.08361E-05 0.289820359
1.1015E-05  0.293413174
1.11934E-05 0.307784431
1.13705E-05 0.347305389
1.15763E-05 0.411976048
1.17824E-05 0.469461078
1.19892E-05 0.51257485
1.22257E-05 0.559281437
1.2433E-05  0.591616766
1.27001E-05 0.623952096
1.29374E-05 0.652694611
1.32345E-05 0.681437126
```

```
1.34722E-05 0.702994012
1.37699E-05 0.720958084
1.40378E-05 0.735329341
1.43654E-05 0.749700599
1.46931E-05 0.764071856
1.50214E-05 0.764071856
1.53793E-05 0.771257485
1.57666E-05 0.785628743
1.61838E-05 0.8
1.66005E-05 0.825149701
1.70188E-05 0.817964072
1.74712E-05 0.724550898
1.79815E-05 0.667065868
1.84874E-05 0.699401198
1.90229E-05 0.735329341
1.95588E-05 0.764071856
2.01846E-05 0.785628743];
 for i = 1:3
   for j = 1:mat_num
      wave(j) = lam_min+(j-1)*lam_disc;
      rad(i,j) = (2*h*c_0^2)/(wave(j)^5)*(1/(exp((h*c_0)/(k*T(i)*wave(j)))-1));
   end
   rad_rat(i,:) = rad(i,:)/sum(rad(i,:));
   if i == 1
      c = 1;
      for j = 1:mat_num
         if wave(j) < em_1(1,1)
            em(i,j) = em_1(1,2);
         elseif wave(j) >= em_1(55,1)
            em(i,j) = em_1(55,2);
         else
            if wave(j) >= em_1(c,1)
              c = c+1;
            end
            em(i,j)   =   em_1(c-1,2)+   (wave(j)-em_1(c-1,1))/(em_1(c,1)-em_1(c-1,1))*(em_1(c,2)-em_1(c-
1,2));
         end
      end
   end
   rad_em(i,:) = times(rad_rat(i,:),em);
   tot_em(i) = sum(rad_em(i,:));
end
semilogx(wave,rad)
title('Thermal Radiation Intensity vs. Wavelength')
ylabel('Radiation Intensity(W sr-1 m-3)')
xlabel('Wavelength (m)')
legend('DCC Air Ingress & Normal Operation','PCC Natural Circulation','DCC Natural Circulation')
figure
semilogx(wave,rad_rat)
title('Normalized Radiation Intensity vs. Wavelength')
ylabel('Radiation Intensity (unitless)')
xlabel('Wavelength (m)')
legend('DCC Air Ingress & Normal Operation','PCC Natural Circulation','DCC Natural Circulation')
figure
semilogx(wave,em)
```

APPENDIX G: MATLAB PEBBLE BED POROSITY MATLAB CODE

```
%This is a code to calculate the radial porosity for the PB-HTTF with
%R_o =.45 and R_i = .25 referencing methodology of du Toit (2008)

%bulk porosity determined from du Toit 2008 fig 1 since our dimensions are
%identical to those listed. IE ~14 pebble diameters across the annulus

clc
ep_b = .364;
%
%1.5 cm
%
% For the exponential formation
n = 6;
r_o = .45;
r_i = .25;
d_p = .015;
c = (1/ep_b-1);
del = .001;
num = (r_o-r_i)/del + 1;
r = zeros(1,num);
ep_r = zeros(3,num);
for i = 1:num
    r(i) = r_i+(i-1)*del;
    if r(i) <= (r_o+r_i)/2
        ep_r(1,i) = ep_b*(1+c*exp(-n*(r(i)-r_i)/d_p));
    else
        ep_r(1,i) = ep_b*(1+c*exp(-n*(-r(i)+r_o)/d_p));
    end
end

% For the oscillatory formation
ep_m = .245 ;%from document
ep_x = zeros(3,num);
x = zeros(1,num);
c_e = .876;
for i = 1:num
    if r(i) < (r_o+r_i)/2
        x(i) = 2*(r(i)-r_i)/d_p-1;
        if x(i) < -1
            error = 1
        elseif x(i) <= 0
            ep_x(1,i) = ep_m+(1-ep_m)*x(i)^2;
        else
            ep_x(1,i) = ep_b +(ep_m-ep_b)*exp(-x(i)/4)*cos(pi/c_e*x(i));
        end
    else
        x(i) = 2*(r_o-r(i))/d_p-1;
        if x(i) < -1
            error = 2
        elseif x(i) <= 0
            ep_x(1,i) = ep_m+(1-ep_m)*x(i)^2;
        else
            ep_x(1,i) = ep_b +(ep_m-ep_b)*exp(-x(i)/4)*cos(pi/c_e*x(i));
        end
    end
```

```
end
figure(1)
hold on
plot(r,ep_r(1,:),r,ep_x(1,:))

%Averaging the wall effect
da = zeros(1,num-1);
ep_ave = zeros(2,num-1);
ep_ar = zeros(2,num-1);
for i = 1:num-1
   da(i) = (pi()*(r(i+1)^2-r(i)^2))/(pi()*(r_o^2-r_i^2)); %Normalized Differential Area
   ep_ave(1,i) =  (ep_r(1,i)+ep_r(1,i+1))/2; %Porosity averaged from start and end for expo
   ep_ave(2,i) =  (ep_x(1,i)+ep_x(1,i+1))/2; %Porosity averaged for oscil
   ep_ar(1,i) = da(i)*ep_ave(1,i); %Average Porosity weighted by area
   ep_ar(2,i) = da(i)*ep_ave(2,i); %Average Porosity weighted by area
end
ep_tot(1,1) = sum(ep_ar(1,:));
ep_tot(1,2) = sum(ep_ar(2,:));
%
% 5cm
%
% For the exponential formation
d_p = .05;
for i = 1:num
   r(i) = r_i+(i-1)*del;
   if r(i) <= (r_o+r_i)/2
      ep_r(2,i) = ep_b*(1+c*exp(-n*(r(i)-r_i)/d_p));
   else
      ep_r(2,i) = ep_b*(1+c*exp(-n*(-r(i)+r_o)/d_p));
   end
end

% For the oscillatory formation

for i = 1:num
   if r(i) < (r_o+r_i)/2
      x(i) = 2*(r(i)-r_i)/d_p-1;
      if x(i) < -1
         error = 1
      elseif x(i) <= 0
         ep_x(2,i) = ep_m+(1-ep_m)*x(i)^2;
      else
         ep_x(2,i) = ep_b +(ep_m-ep_b)*exp(-x(i)/4)*cos(pi/c_e*x(i));
      end
   else
      x(i) = 2*(r_o-r(i))/d_p-1;
      if x(i) < -1
         error = 2
      elseif x(i) <= 0
         ep_x(2,i) = ep_m+(1-ep_m)*x(i)^2;
      else
         ep_x(2,i) = ep_b +(ep_m-ep_b)*exp(-x(i)/4)*cos(pi/c_e*x(i));
      end
   end
end
figure(1)
```

```
plot(r,ep_r(2,:),r,ep_x(2,:))

%Averaging the wall effect

for i = 1:num-1
    da(i) = (pi()*(r(i+1)^2-r(i)^2))/(pi()*(r_o^2-r_i^2)); %Normalized Differential Area
    ep_ave(1,i) =  (ep_r(2,i)+ep_r(2,i+1))/2; %Porosity averaged from start and end for expo
    ep_ave(2,i) =  (ep_x(2,i)+ep_x(2,i+1))/2; %Porosity averaged for oscil
    ep_ar(1,i) = da(i)*ep_ave(1,i); %Average Porosity weighted by area
    ep_ar(2,i) = da(i)*ep_ave(2,i); %Average Porosity weighted by area
end
ep_tot(2,1) = sum(ep_ar(1,:));
ep_tot(2,2) = sum(ep_ar(2,:));
%
% 6cm
%
% For the exponential formation
d_p = .06;
for i = 1:num
    r(i) = r_i+(i-1)*del;
    if r(i) <= (r_o+r_i)/2
        ep_r(3,i) = ep_b*(1+c*exp(-n*(r(i)-r_i)/d_p));
    else
        ep_r(3,i) = ep_b*(1+c*exp(-n*(-r(i)+r_o)/d_p));
    end
end

% For the oscillatory formation

for i = 1:num
    if r(i) < (r_o+r_i)/2
        x(i) = 2*(r(i)-r_i)/d_p-1;
        if x(i) < -1
            error = 1
        elseif x(i) <= 0
            ep_x(3,i) = ep_m+(1-ep_m)*x(i)^2;
        else
            ep_x(3,i) = ep_b +(ep_m-ep_b)*exp(-x(i)/4)*cos(pi/c_e*x(i));
        end
    else
        x(i) = 2*(r_o-r(i))/d_p-1;
        if x(i) < -1
            error = 2
        elseif x(i) <= 0
            ep_x(3,i) = ep_m+(1-ep_m)*x(i)^2;
        else
            ep_x(3,i) = ep_b +(ep_m-ep_b)*exp(-x(i)/4)*cos(pi/c_e*x(i));
        end
    end
end
figure(1)
plot(r,ep_r(3,:),r,ep_x(3,:))
xlabel('Radial Position (m)')
ylabel('Porosity (unitless)')
title('Radial Porosity Variation for PB-HTTF')
```

```
legend('Exp 1.5','Osc 1.5','Exp 5.0','Osc 5.0','Exp 6.0','Osc 6.0','Location','best')
%Averaging the wall effect

for i = 1:num-1
   da(i) = (pi()*(r(i+1)^2-r(i)^2))/(pi()*(r_o^2-r_i^2)); %Normalized Differential Area
   ep_ave(1,i) =  (ep_r(3,i)+ep_r(3,i+1))/2; %Porosity averaged from start and end for expo
   ep_ave(2,i) =  (ep_x(3,i)+ep_x(3,i+1))/2; %Porosity averaged for oscil
   ep_ar(1,i) = da(i)*ep_ave(1,i); %Average Porosity weighted by area
   ep_ar(2,i) = da(i)*ep_ave(2,i); %Average Porosity weighted by area
end
ep_tot(3,1) = sum(ep_ar(1,:));
ep_tot(3,2) = sum(ep_ar(2,:));
%
%
% This section is for HTR-PM Comparison
%
%
n = 6;
r_pm = 1.5;
d_p = .06;
c = (1/ep_b-1);
del = .001;
num = r_pm/del + 1;
r = zeros(1,num);
ep_r_pm = zeros(1,num);
for i = 1:num
   r(i) = (i-1)*del;
   ep_r_pm(i) = ep_b*(1+c*exp(-n*(-r(i)+r_pm)/d_p));
end

% For the oscillatory formation
ep_m = .245 ;%from document
ep_x_pm = zeros(1,num);
x = zeros(1,num);
c_e = .876;
for i = 1:num
   x(i) = 2*(r_pm-r(i))/d_p-1;
   if x(i) < -1
      error = 2
   elseif x(i) <= 0
      ep_x_pm(i) = ep_m+(1-ep_m)*x(i)^2;
   else
      ep_x_pm(i) = ep_b +(ep_m-ep_b)*exp(-x(i)/4)*cos(pi/c_e*x(i));
   end
end
figure(2)
plot(r,ep_r_pm,r,ep_x_pm)
xlabel('Radial Position (m)')
ylabel('Porosity (unitless)')
title('Radial Porosity Variation for HTR-PM')
legend('Exp 6.0','Osc 6.0','Location','best')

%Averaging the wall effect
da = zeros(1,num-1);
ep_ave = zeros(2,num-1);
ep_ar = zeros(2,num-1);
```

```
for i = 1:num-1
    da(i) = (pi()*(r(i+1)^2-r(i)^2))/(pi()*r_pm^2); %Normalized Differential Area
    ep_ave(1,i) =  (ep_r_pm(i)+ep_r_pm(i+1))/2; %Porosity averaged from start and end for expo
    ep_ave(2,i) =  (ep_x_pm(i)+ep_x_pm(i+1))/2; %Porosity averaged for oscil
    ep_ar(1,i) = da(i)*ep_ave(1,i); %Average Porosity weighted by area
    ep_ar(2,i) = da(i)*ep_ave(2,i); %Average Porosity weighted by area
end
ep_pm(1,1) = sum(ep_ar(1,:));
ep_pm(1,2) = sum(ep_ar(2,:));
```

APPENDIX H: EM^2 HTTF COMPONENTS

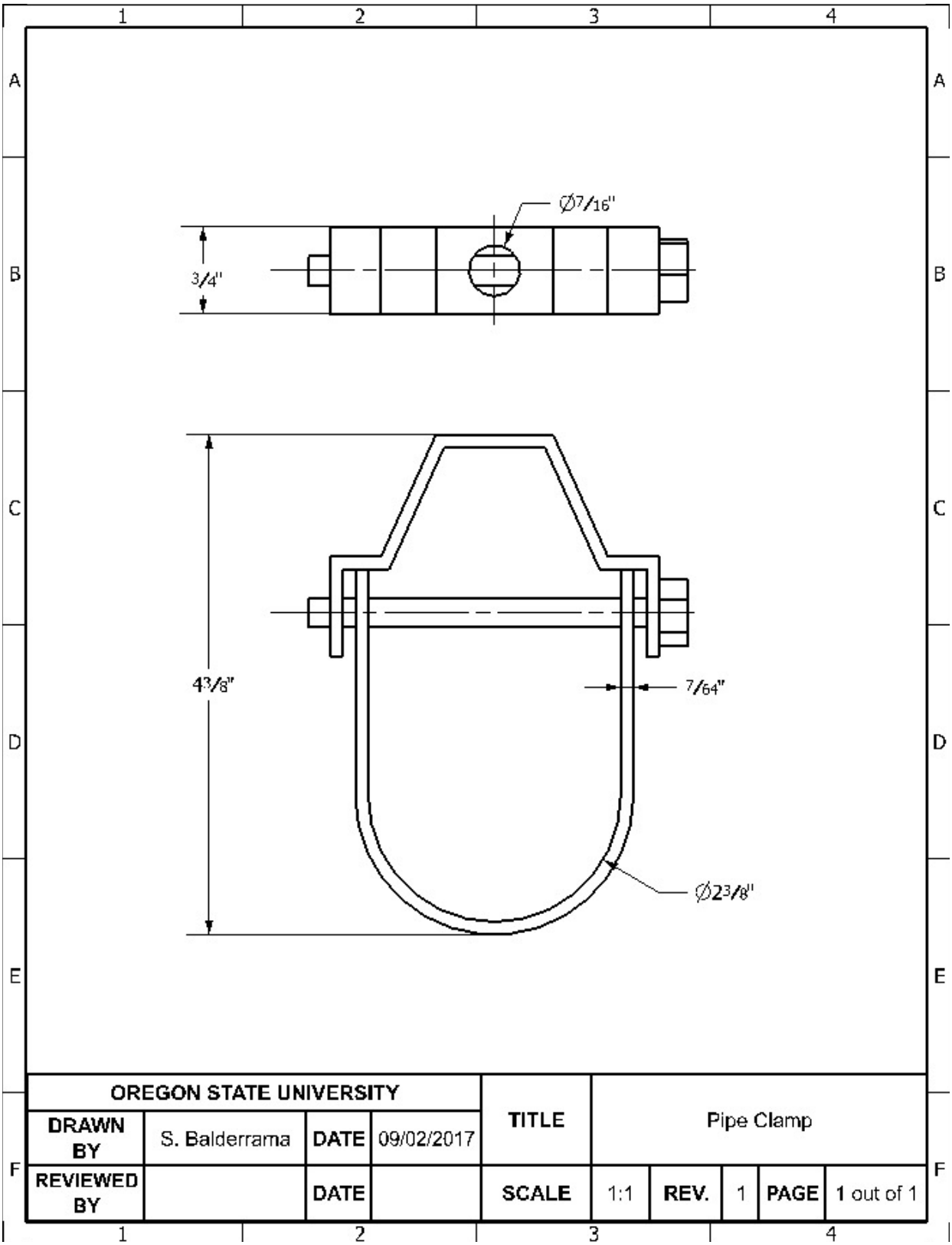

OREGON STATE UNIVERSITY				TITLE	Pipe Clamp				
DRAWN BY	S. Balderrama	DATE	09/02/2017						
REVIEWED BY		DATE		SCALE	1:1	REV.	1	PAGE	1 out of 1

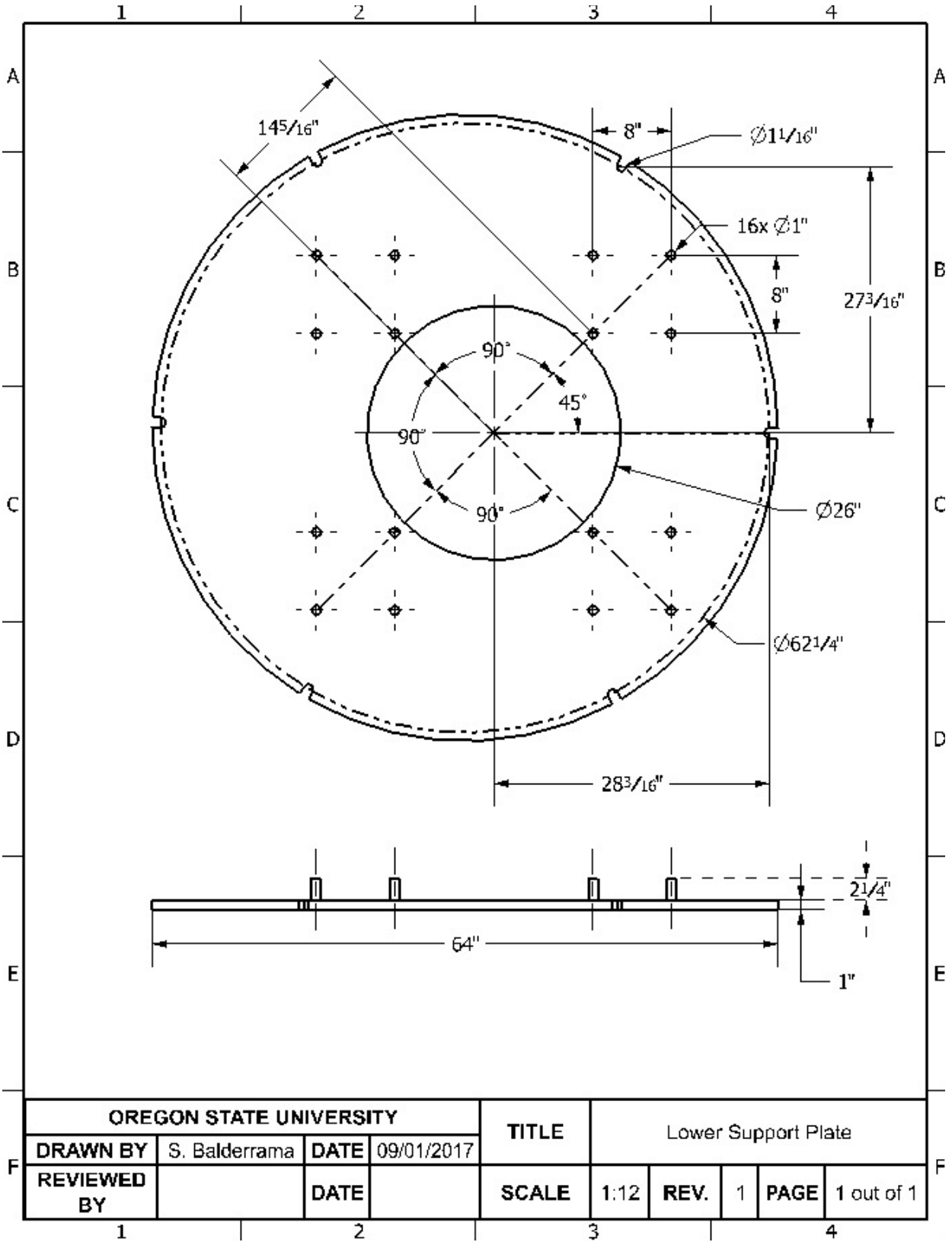

OREGON STATE UNIVERSITY				TITLE	Lower Support Plate				
DRAWN BY	S. Balderrama	DATE	09/01/2017						
REVIEWED BY		DATE		SCALE	1:12	REV.	1	PAGE	1 out of 1

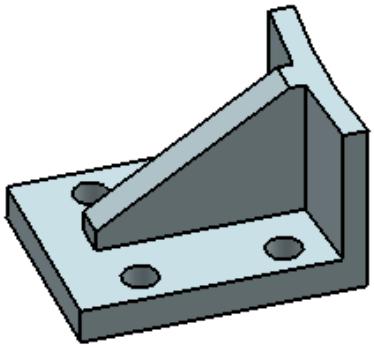

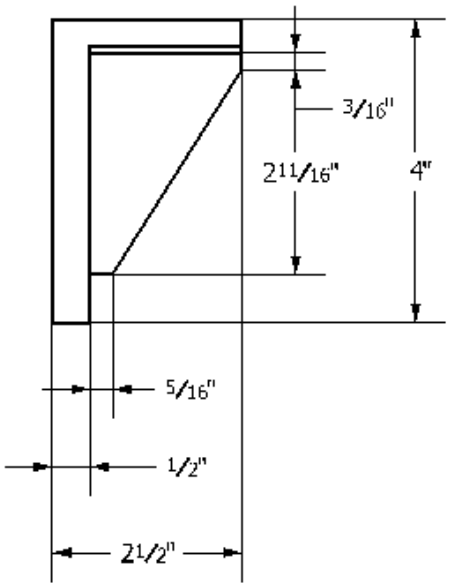

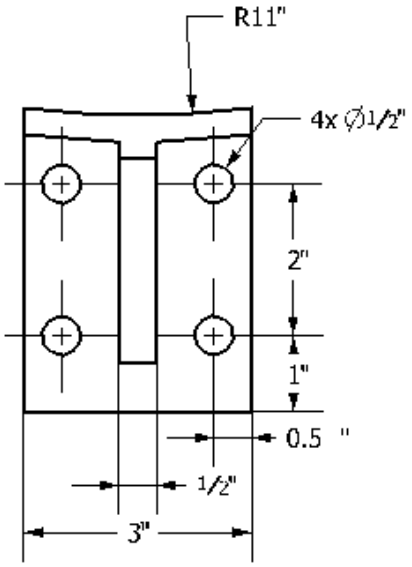

OREGON STATE UNIVERSITY				TITLE	Heat Exchanger Bracket				
DRAWN BY	S. Balderrama	DATE	09/03/2017						
REVIEWED BY		DATE		SCALE	1:2	REV.	1	PAGE	1 out of 1

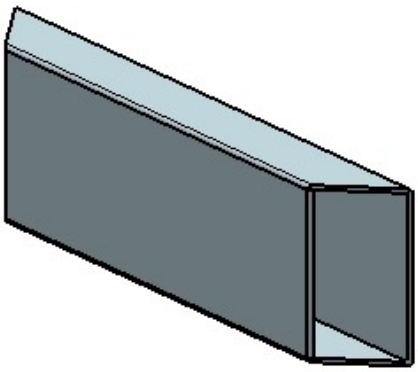

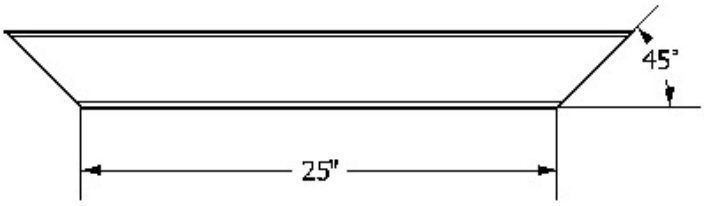

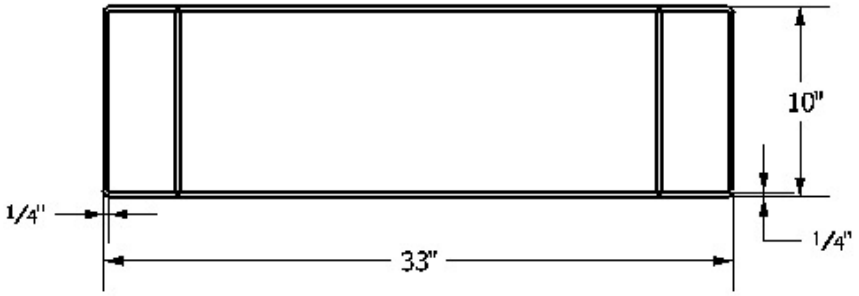

OREGON STATE UNIVERSITY				TITLE	DHX Support Structure				
DRAWN BY	S. Balderrama	DATE	09/10/2017						
REVIEWED BY		DATE		SCALE	1:8	REV.	1	PAGE	1 out of 1

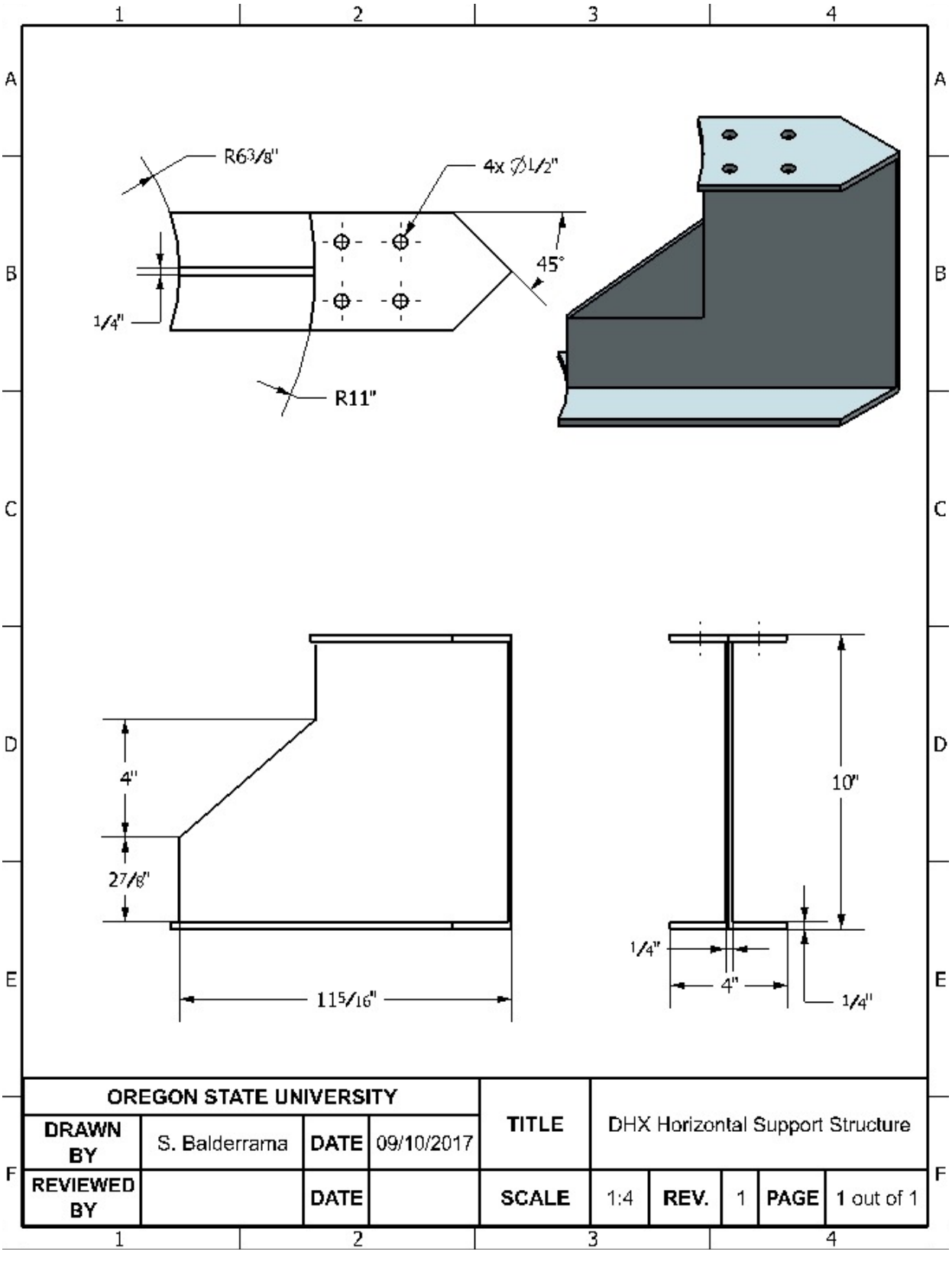

OREGON STATE UNIVERSITY				TITLE	DHX Horizontal Support Structure				
DRAWN BY	S. Balderrama	DATE	09/10/2017						
REVIEWED BY		DATE		SCALE	1:4	REV.	1	PAGE	1 out of 1

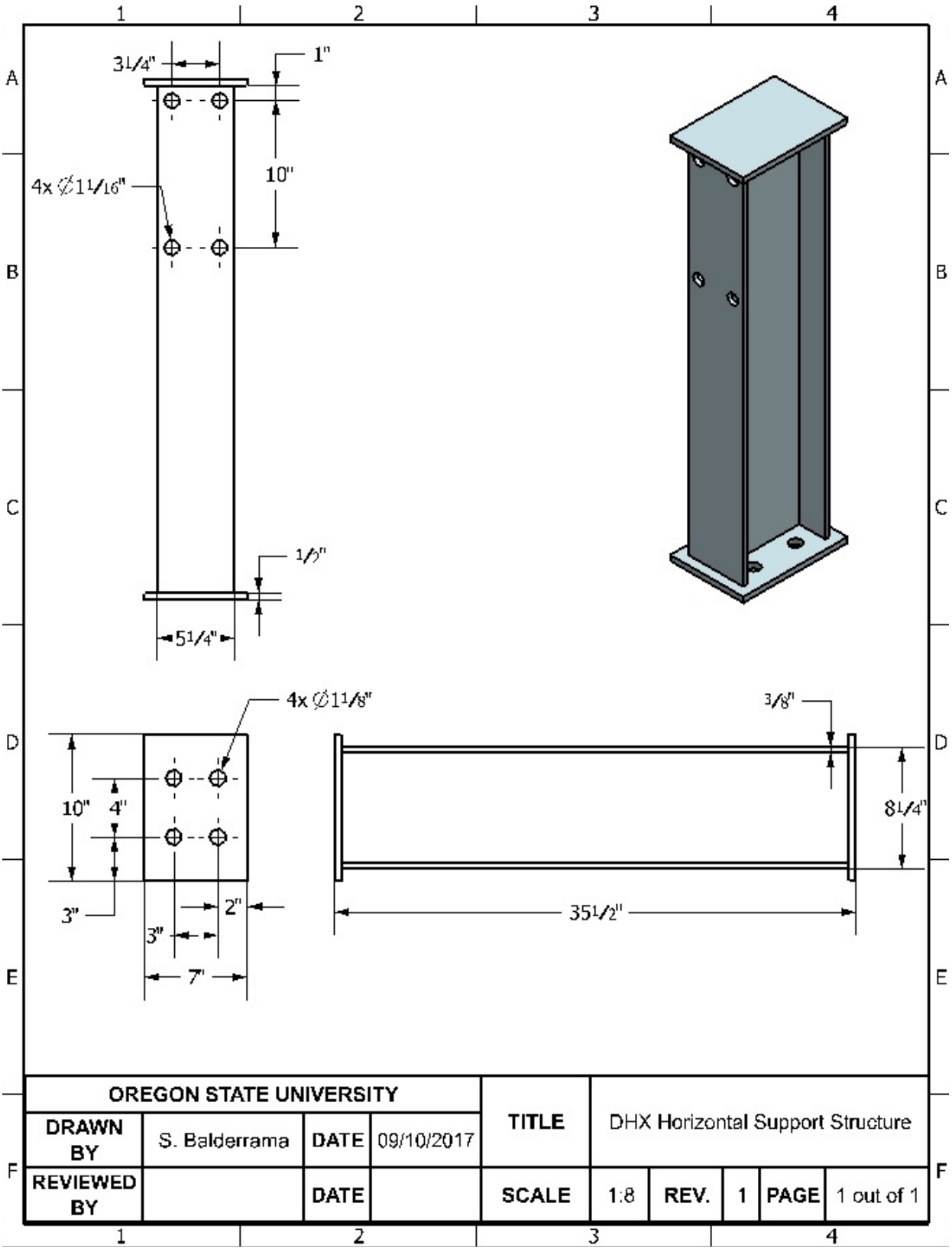
3 1/4"
1"
10"
4x ∅1 1/16"
1/2"
5 1/4"
4x ∅1 1/8"
3/8"
10"
4"
3"
2"
3"
7"
8 1/4"
35 1/2"
OREGON STATE UNIVERSITY
DRAWN BY
S. Balderrama
DATE
09/10/2017
TITLE
DHX Horizontal Support Structure
REVIEWED BY
DATE
SCALE
1:8
REV.
1
PAGE
1 out of 1

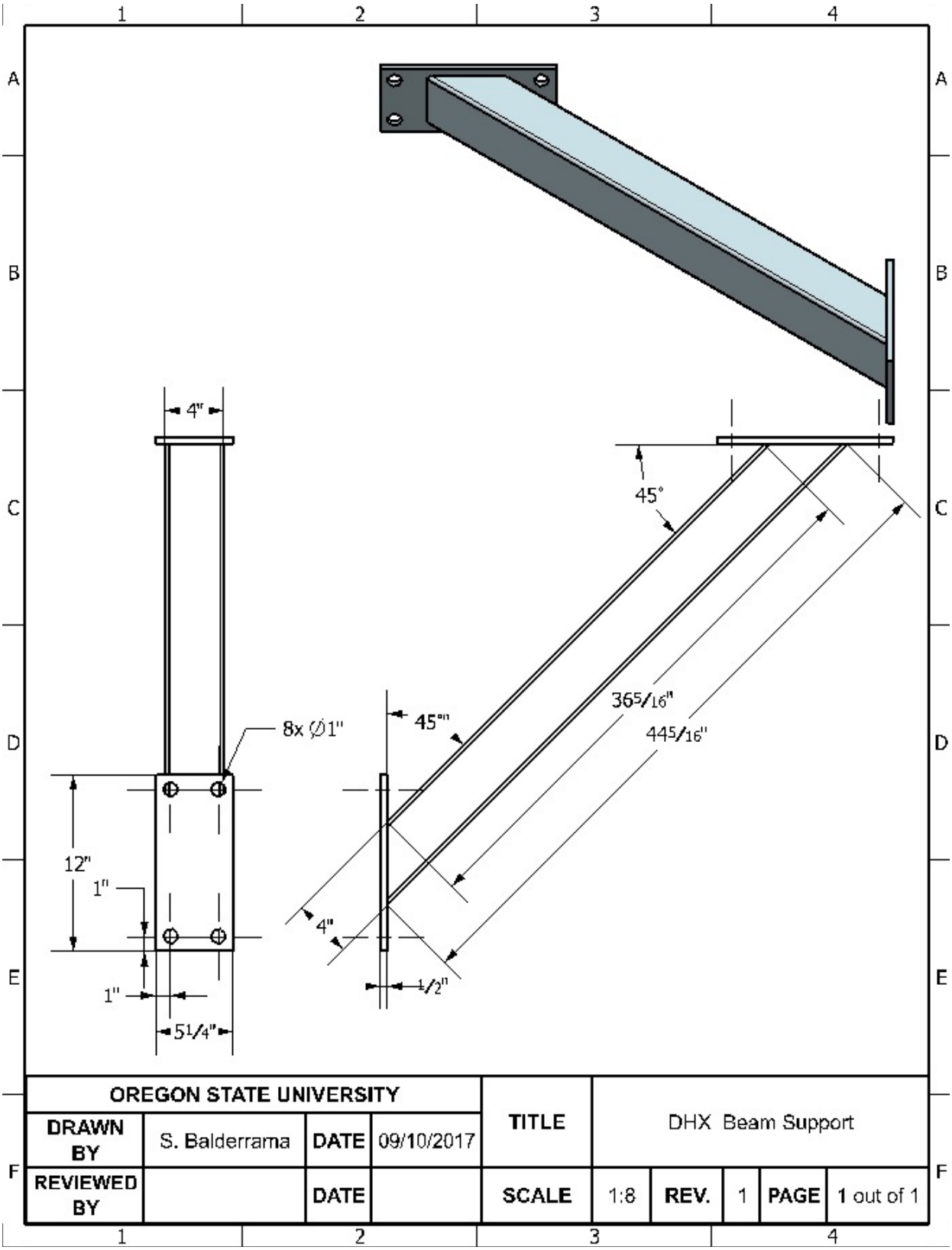

OREGON STATE UNIVERSITY				TITLE	DHX Beam Support				
DRAWN BY	S. Balderrama	DATE	09/10/2017						
REVIEWED BY		DATE		SCALE	1:8	REV.	1	PAGE	1 out of 1

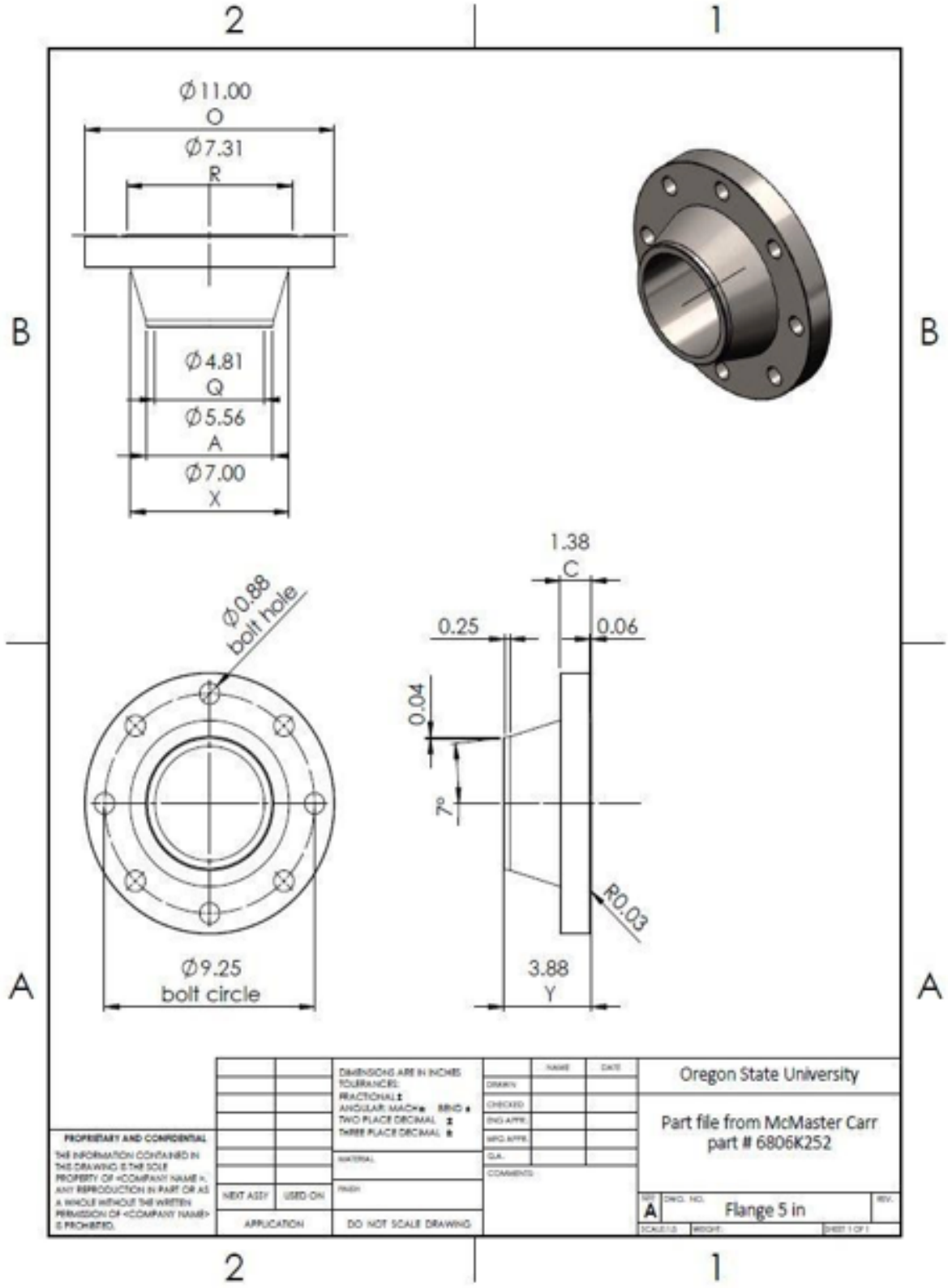
2
1
B
A
Ø11.00
O
Ø7.31
R
Ø4.81
Q
Ø5.56
A
Ø7.00
X
Ø0.88
bolt hole
Ø9.25
bolt circle
1.38
C
0.25
0.06
0.04
7°
R0.03
3.88
Y
PROPRIETARY AND CONFIDENTIAL
THE INFORMATION CONTAINED IN THIS DRAWING IS THE SOLE PROPERTY OF <COMPANY NAME >. ANY REPRODUCTION IN PART OR AS A WHOLE WITHOUT THE WRITTEN PERMISSION OF <COMPANY NAME> IS PROHIBITED.
NEXT ASSY
USED ON
APPLICATION
DIMENSIONS ARE IN INCHES
TOLERANCES:
FRACTIONAL ±
ANGULAR: MACH ± BEND ±
TWO PLACE DECIMAL ±
THREE PLACE DECIMAL ±
MATERIAL
FINISH
DO NOT SCALE DRAWING
NAME
DATE
DRAWN
CHECKED
ENG APPR.
MFG APPR.
Q.A.
COMMENTS
Oregon State University
Part file from McMaster Carr
part # 6806K252
SIZE
A
DWG. NO.
Flange 5 in
REV.
SCALE: 1:3
WEIGHT:
SHEET 1 OF 1

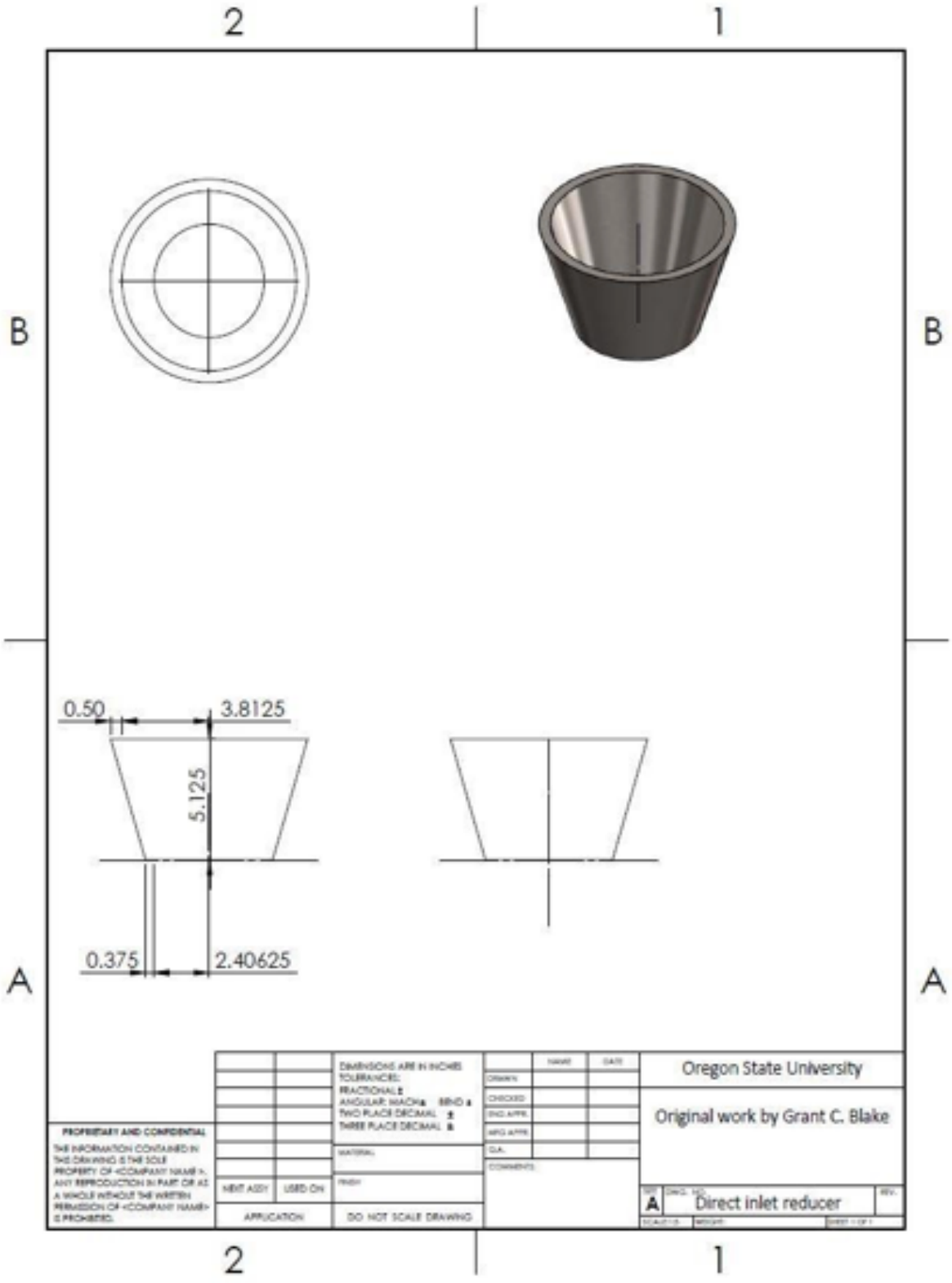
2
1
B
B
0.50
3.8125
5.125
0.375
2.40625
A
A
PROPRIETARY AND CONFIDENTIAL
THE INFORMATION CONTAINED IN THIS DRAWING IS THE SOLE PROPERTY OF <COMPANY NAME >. ANY REPRODUCTION IN PART OR AS A WHOLE WITHOUT THE WRITTEN PERMISSION OF <COMPANY NAME> IS PROHIBITED.
NEXT ASSY
USED ON
APPLICATION
DIMENSIONS ARE IN INCHES
TOLERANCES:
FRACTIONAL ±
ANGULAR: MACH ± BEND ±
TWO PLACE DECIMAL ±
THREE PLACE DECIMAL ±
MATERIAL
FINISH
DO NOT SCALE DRAWING
NAME
DATE
DRAWN
CHECKED
ENG APPR.
MFG APPR.
Q.A.
COMMENTS:
Oregon State University
Original work by Grant C. Blake
SIZE
A
DWG. NO.
Direct inlet reducer
REV.
SCALE: 1:5
WEIGHT
SHEET 1 OF 1
2
1

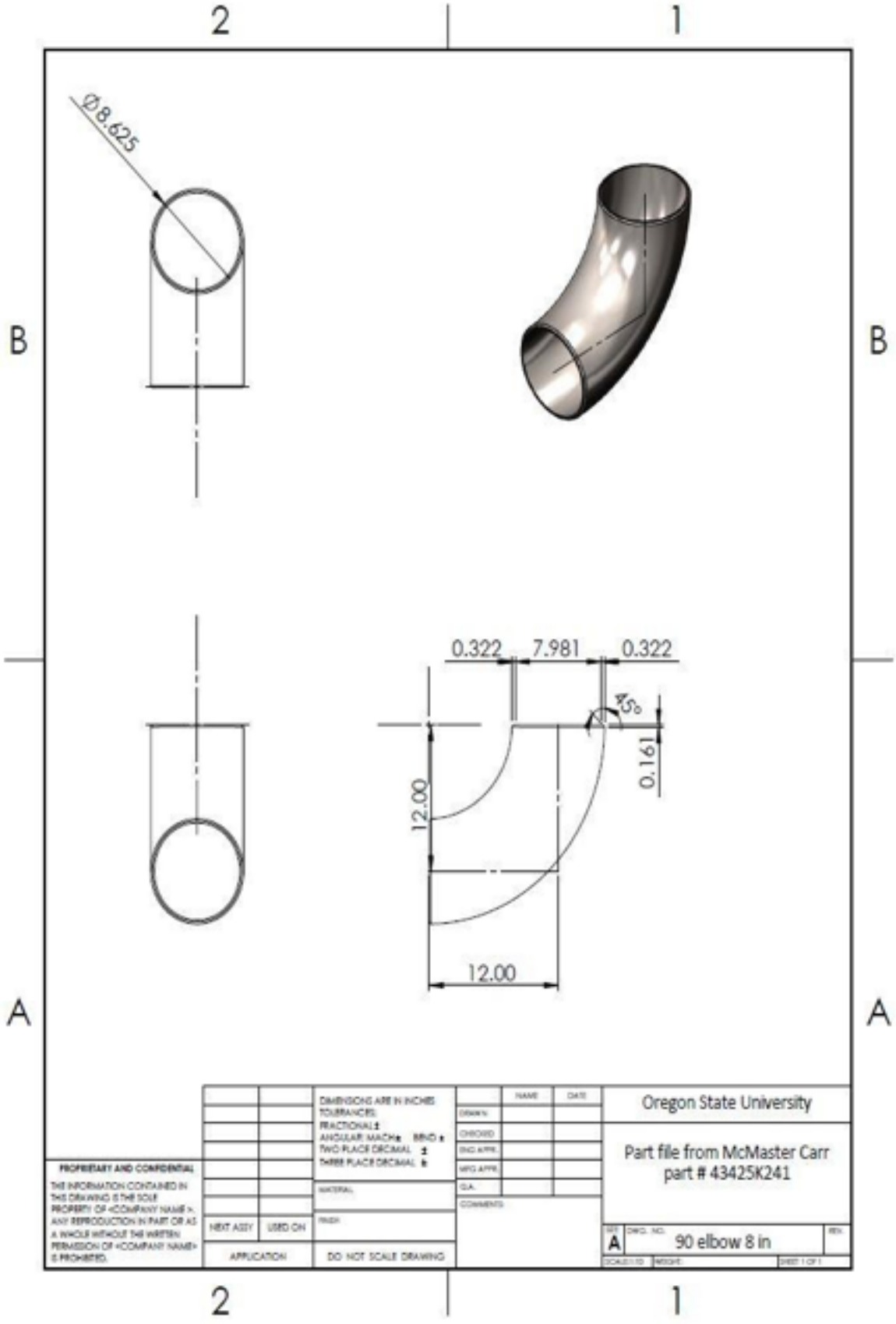
2
1
B
A
Ø8.625
0.322
7.981
0.322
45°
0.161
12.00
12.00
PROPRIETARY AND CONFIDENTIAL
THE INFORMATION CONTAINED IN THIS DRAWING IS THE SOLE PROPERTY OF <COMPANY NAME >. ANY REPRODUCTION IN PART OR AS A WHOLE WITHOUT THE WRITTEN PERMISSION OF <COMPANY NAME> IS PROHIBITED.
DIMENSIONS ARE IN INCHES
TOLERANCES:
FRACTIONAL ±
ANGULAR: MACH ± BEND ±
TWO PLACE DECIMAL ±
THREE PLACE DECIMAL ±
MATERIAL
FINISH
NEXT ASSY
USED ON
APPLICATION
DO NOT SCALE DRAWING
NAME
DATE
DRAWN
CHECKED
ENG APPR.
MFG APPR.
Q.A.
COMMENTS
Oregon State University
Part file from McMaster Carr
part # 43425K241
SIZE
A
DWG. NO.
90 elbow 8 in
REV
SCALE: 1:10
WEIGHT:
SHEET 1 OF 1

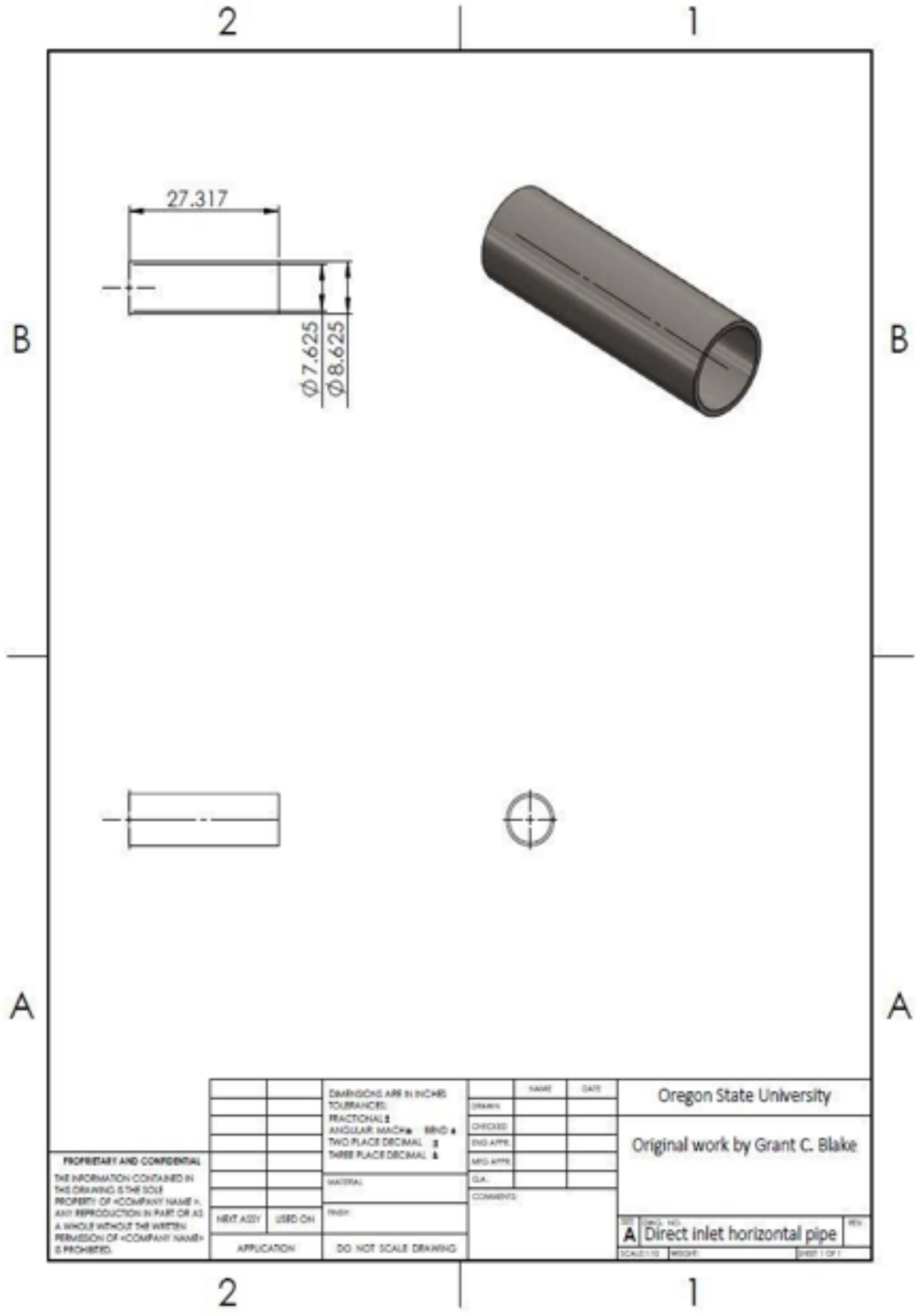
2
1
B
A
27.317
Ø7.625
Ø8.625
Oregon State University
Original work by Grant C. Blake
Direct inlet horizontal pipe
PROPRIETARY AND CONFIDENTIAL
DO NOT SCALE DRAWING

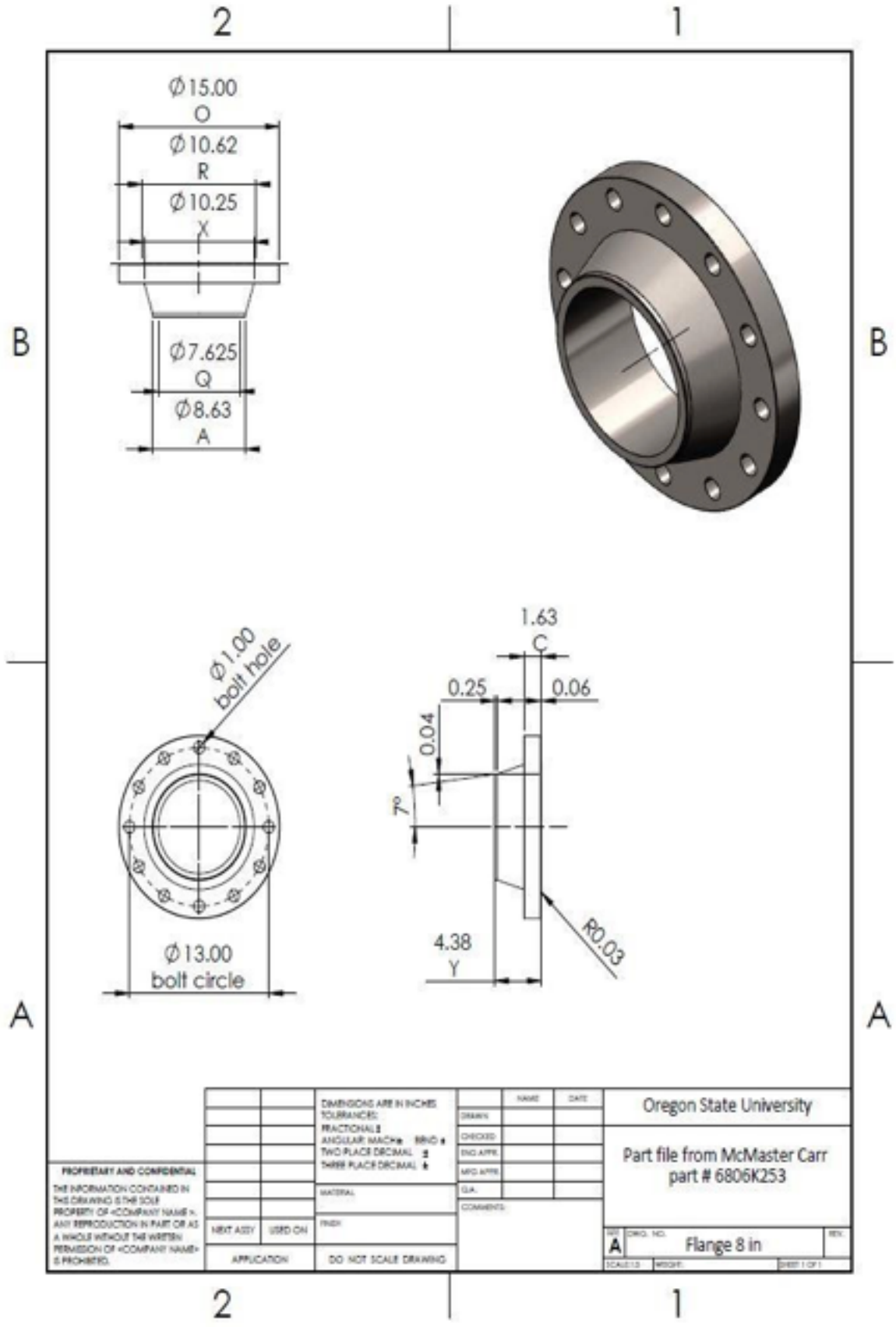
2
1
B
A
Ø15.00
O
Ø10.62
R
Ø10.25
X
Ø7.625
Q
Ø8.63
A
Ø1.00
bolt hole
Ø13.00
bolt circle
1.63
C
0.25
0.06
0.04
7°
4.38
Y
R0.03
PROPRIETARY AND CONFIDENTIAL
THE INFORMATION CONTAINED IN THIS DRAWING IS THE SOLE PROPERTY OF <COMPANY NAME>. ANY REPRODUCTION IN PART OR AS A WHOLE WITHOUT THE WRITTEN PERMISSION OF <COMPANY NAME> IS PROHIBITED.
DIMENSIONS ARE IN INCHES
TOLERANCES:
FRACTIONAL ±
ANGULAR: MACH ± BEND ±
TWO PLACE DECIMAL ±
THREE PLACE DECIMAL ±
MATERIAL
FINISH
NEXT ASSY
USED ON
APPLICATION
DO NOT SCALE DRAWING
NAME
DATE
DRAWN
CHECKED
ENG APPR.
MFG APPR.
Q.A.
COMMENTS:
Oregon State University
Part file from McMaster Carr
part # 6806K253
SIZE
A
DWG. NO.
Flange 8 in
REV.
SCALE: 1:3
WEIGHT:
SHEET 1 OF 1

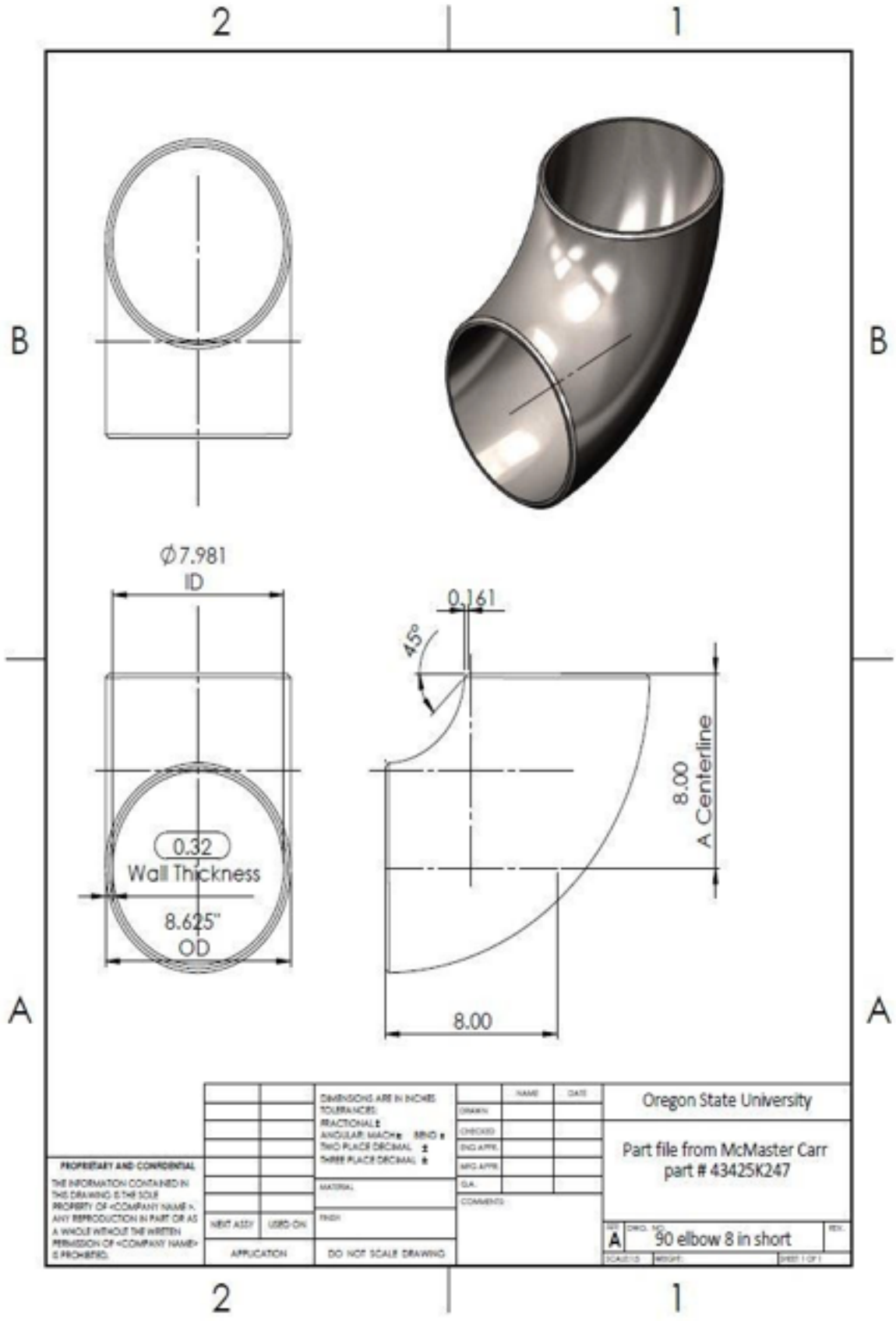
2
1
B
A
Ø7.981
ID
0.161
45°
8.00
A Centerline
0.32
Wall Thickness
8.625"
OD
8.00
DIMENSIONS ARE IN INCHES
TOLERANCES:
FRACTIONAL ±
ANGULAR: MACH ± BEND ±
TWO PLACE DECIMAL ±
THREE PLACE DECIMAL ±
MATERIAL
FINISH
NEXT ASSY
USED ON
APPLICATION
DO NOT SCALE DRAWING
NAME
DATE
DRAWN
CHECKED
ENG APPR.
MFG APPR.
Q.A.
COMMENTS:
Oregon State University
Part file from McMaster Carr
part # 43425K247
SIZE
A
DWG. NO.
90 elbow 8 in short
REV.
SCALE: 0.5
WEIGHT:
SHEET 1 OF 1
PROPRIETARY AND CONFIDENTIAL
THE INFORMATION CONTAINED IN THIS DRAWING IS THE SOLE PROPERTY OF <COMPANY NAME >. ANY REPRODUCTION IN PART OR AS A WHOLE WITHOUT THE WRITTEN PERMISSION OF <COMPANY NAME> IS PROHIBITED.

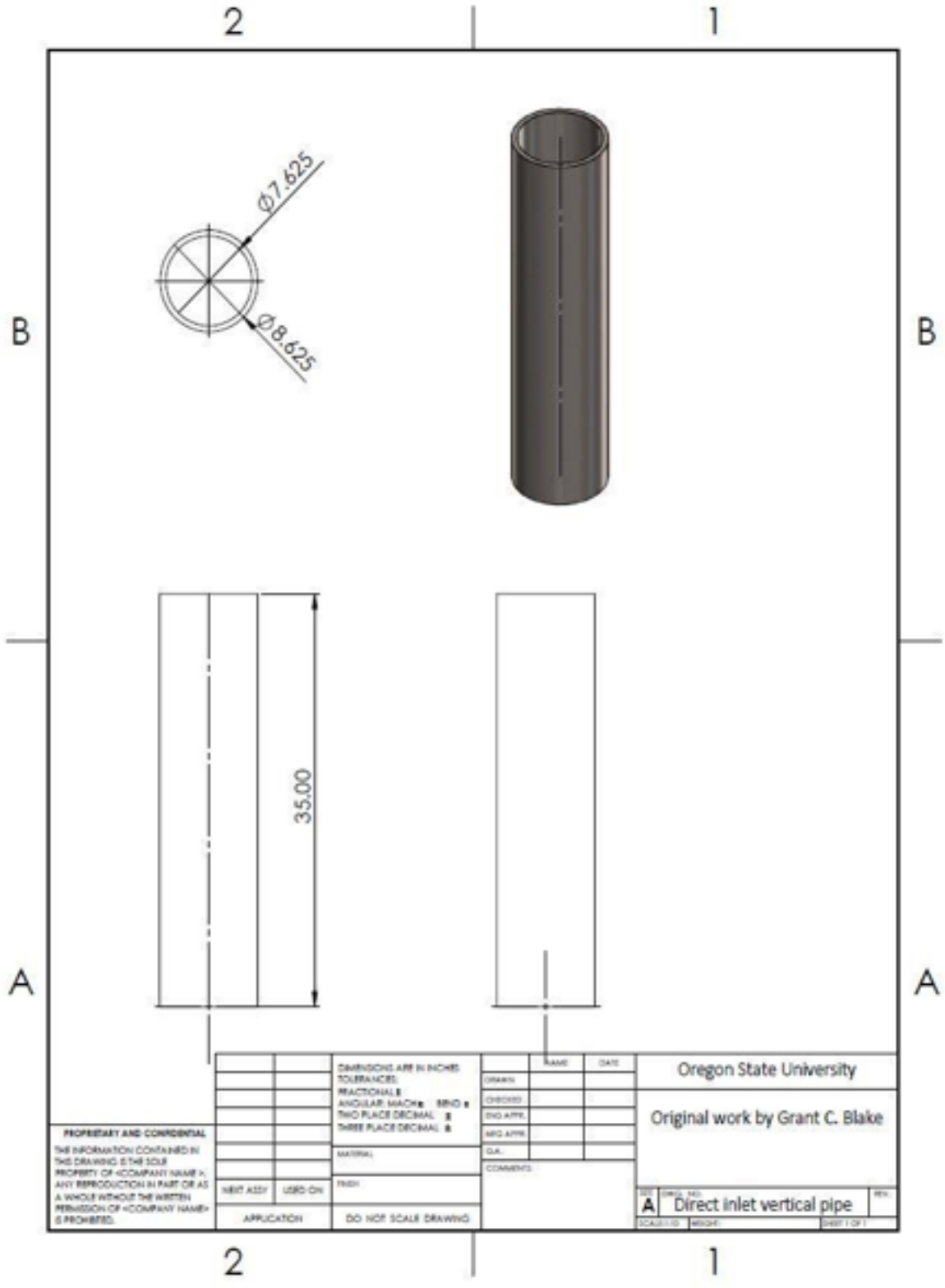
2
1
B
A
Ø7.625
Ø8.625
35.00
Oregon State University
Original work by Grant C. Blake
Direct inlet vertical pipe
PROPRIETARY AND CONFIDENTIAL

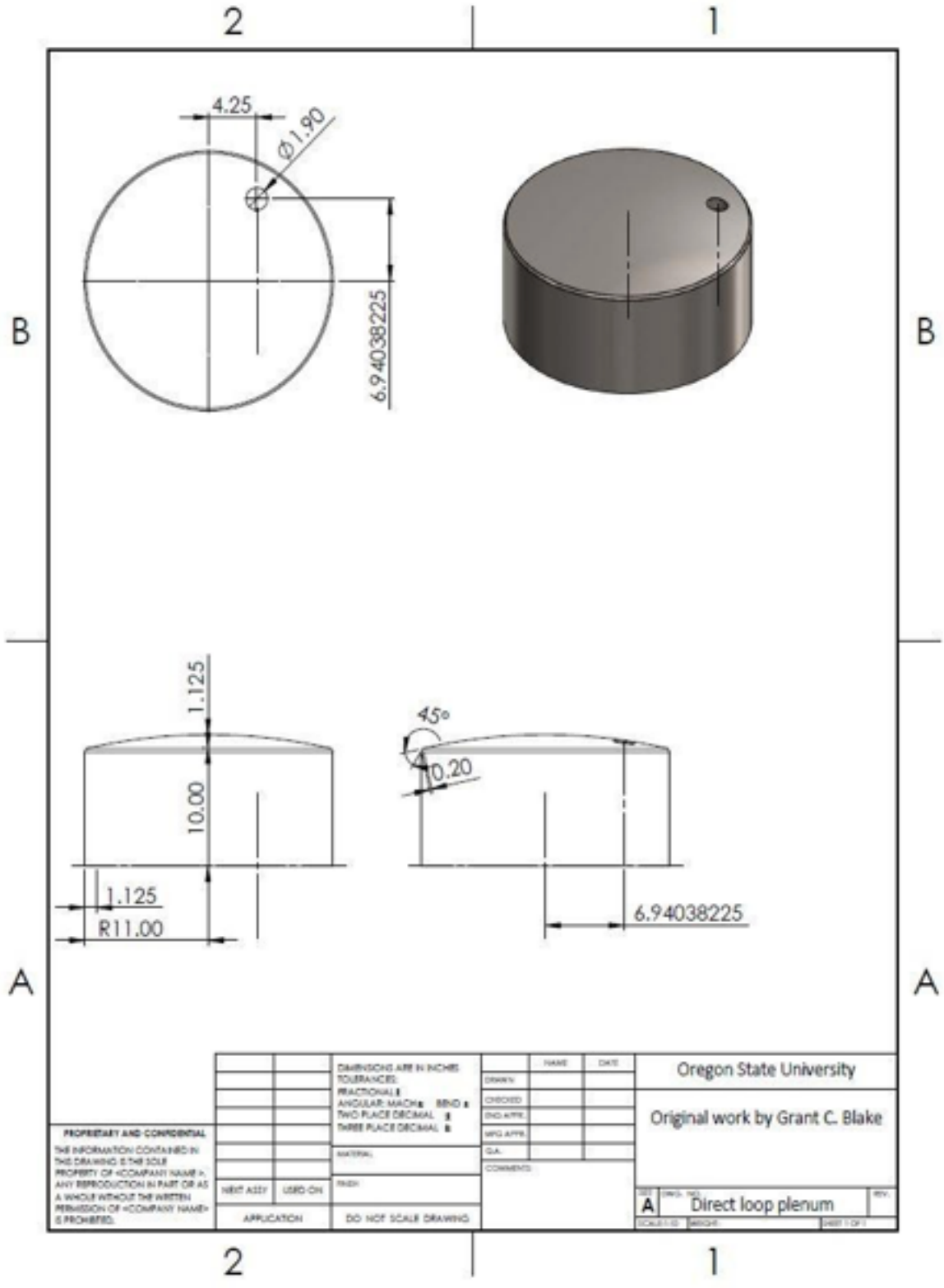
2
1
B
A
4.25
Ø1.90
6.94038225
1.125
10.00
1.125
R11.00
45°
0.20
6.94038225
DIMENSIONS ARE IN INCHES
TOLERANCES:
FRACTIONAL ±
ANGULAR: MACH ± BEND ±
TWO PLACE DECIMAL ±
THREE PLACE DECIMAL ±
NAME
DATE
DRAWN
CHECKED
ENG APPR.
MFG APPR.
Q.A.
COMMENTS:
MATERIAL
NEXT ASSY
USED ON
FINISH
APPLICATION
DO NOT SCALE DRAWING
PROPRIETARY AND CONFIDENTIAL
THE INFORMATION CONTAINED IN THIS DRAWING IS THE SOLE PROPERTY OF <COMPANY NAME>. ANY REPRODUCTION IN PART OR AS A WHOLE WITHOUT THE WRITTEN PERMISSION OF <COMPANY NAME> IS PROHIBITED.
Oregon State University
Original work by Grant C. Blake
SIZE
A
DWG. NO.
Direct loop plenum
REV.
SCALE: 1:10
WEIGHT
SHEET 1 OF 1

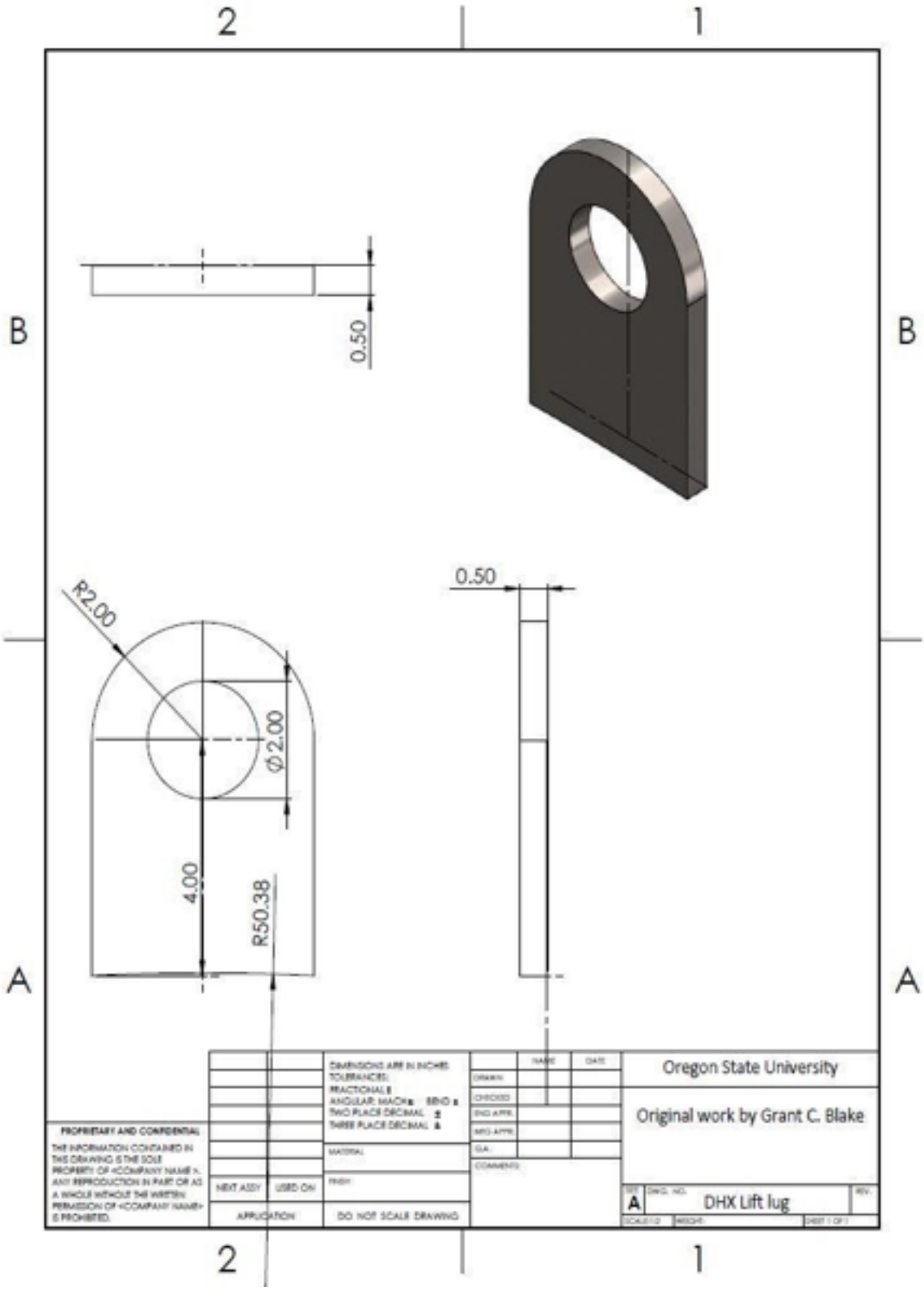
2
1
B
B
0.50
R2.00
Ø2.00
4.00
R50.38
0.50
A
A
Oregon State University
Original work by Grant C. Blake
DHX Lift lug
A
2
1

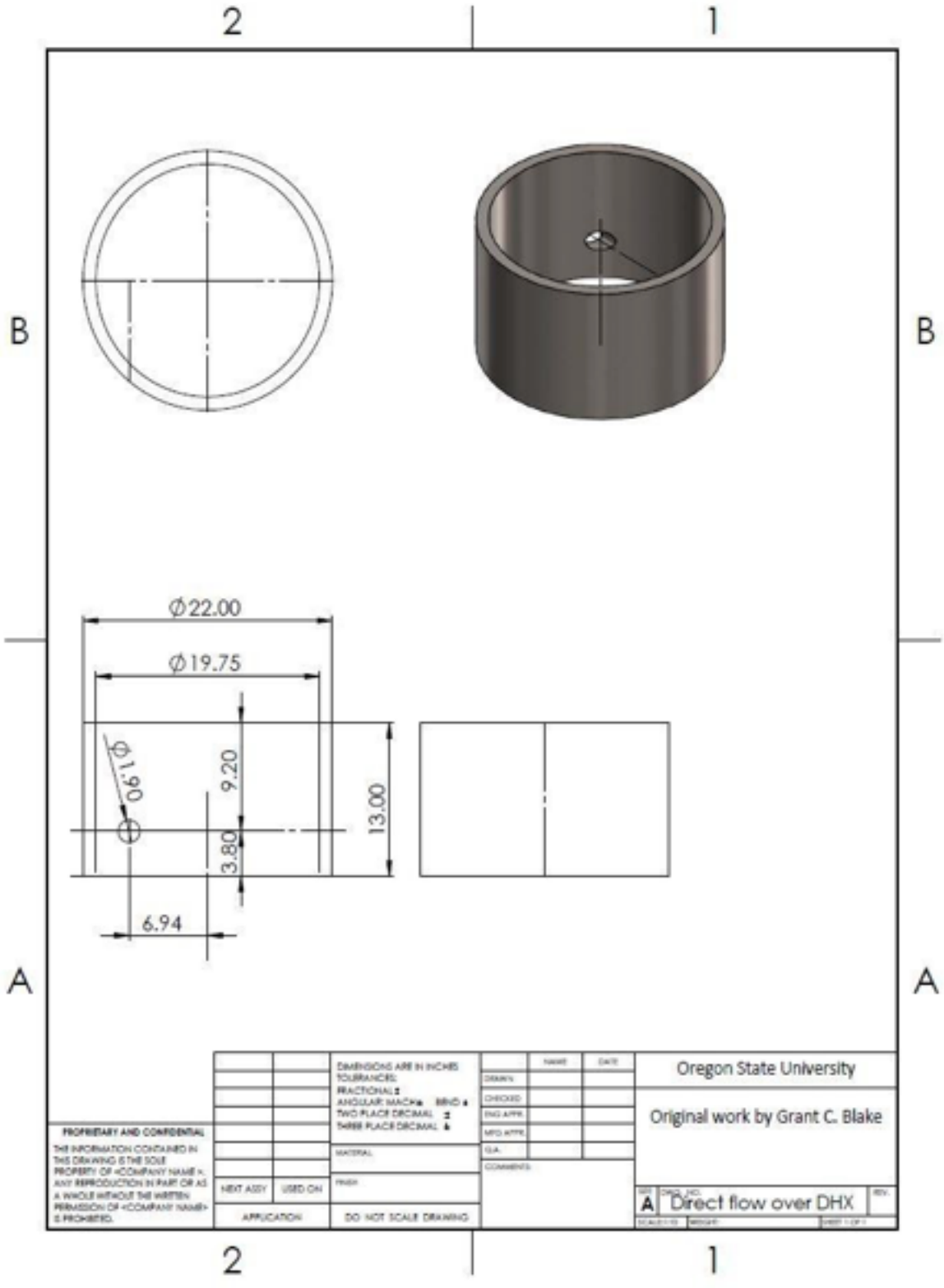
2
1
B
B
A
A
Ø22.00
Ø19.75
Ø1.90
9.20
13.00
3.80
6.94
Oregon State University
Original work by Grant C. Blake
Direct flow over DHX
PROPRIETARY AND CONFIDENTIAL
DIMENSIONS ARE IN INCHES
TOLERANCES:
FRACTIONAL ±
ANGULAR: MACH ± BEND ±
TWO PLACE DECIMAL ±
THREE PLACE DECIMAL ±
MATERIAL
FINISH
NEXT ASSY
USED ON
APPLICATION
DO NOT SCALE DRAWING
DRAWN
CHECKED
ENG APPR.
MFG APPR.
Q.A.
COMMENTS:
NAME
DATE
SIZE
A
DWG. NO.
REV.
SCALE: 1:10
WEIGHT
SHEET 1 OF 1

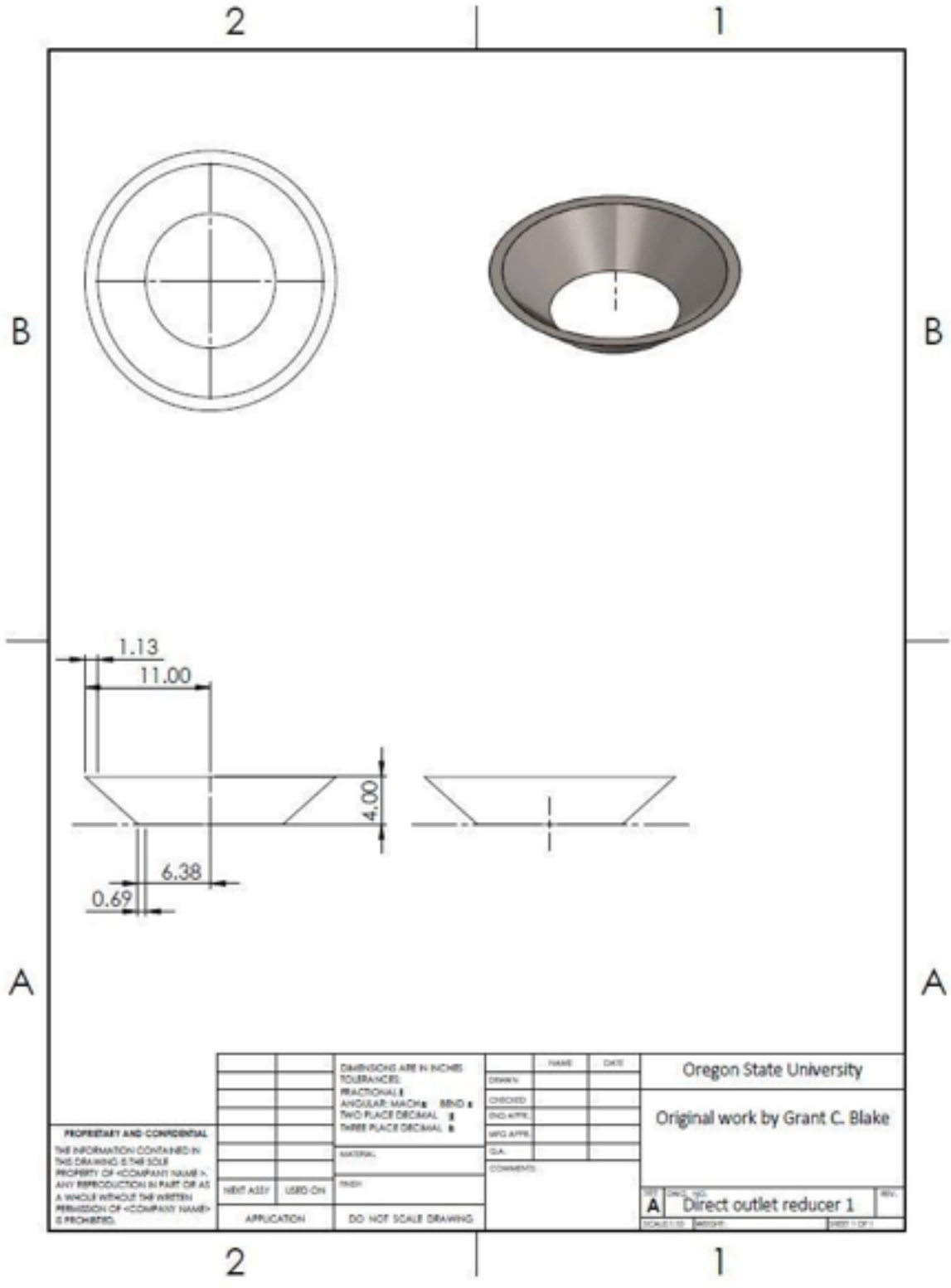
2
1
B
B
1.13
11.00
4.00
6.38
0.69
A
A
PROPRIETARY AND CONFIDENTIAL
THE INFORMATION CONTAINED IN THIS DRAWING IS THE SOLE PROPERTY OF <COMPANY NAME >. ANY REPRODUCTION IN PART OR AS A WHOLE WITHOUT THE WRITTEN PERMISSION OF <COMPANY NAME> IS PROHIBITED.
NEXT ASSY
USED ON
APPLICATION
DIMENSIONS ARE IN INCHES
TOLERANCES:
FRACTIONAL ±
ANGULAR: MACH ± BEND ±
TWO PLACE DECIMAL ±
THREE PLACE DECIMAL ±
MATERIAL
FINISH
DO NOT SCALE DRAWING
NAME
DATE
DRAWN
CHECKED
ENG APPR.
MFG APPR.
Q.A.
COMMENTS:
Oregon State University
Original work by Grant C. Blake
SIZE
A
Direct outlet reducer 1
REV.
2
1

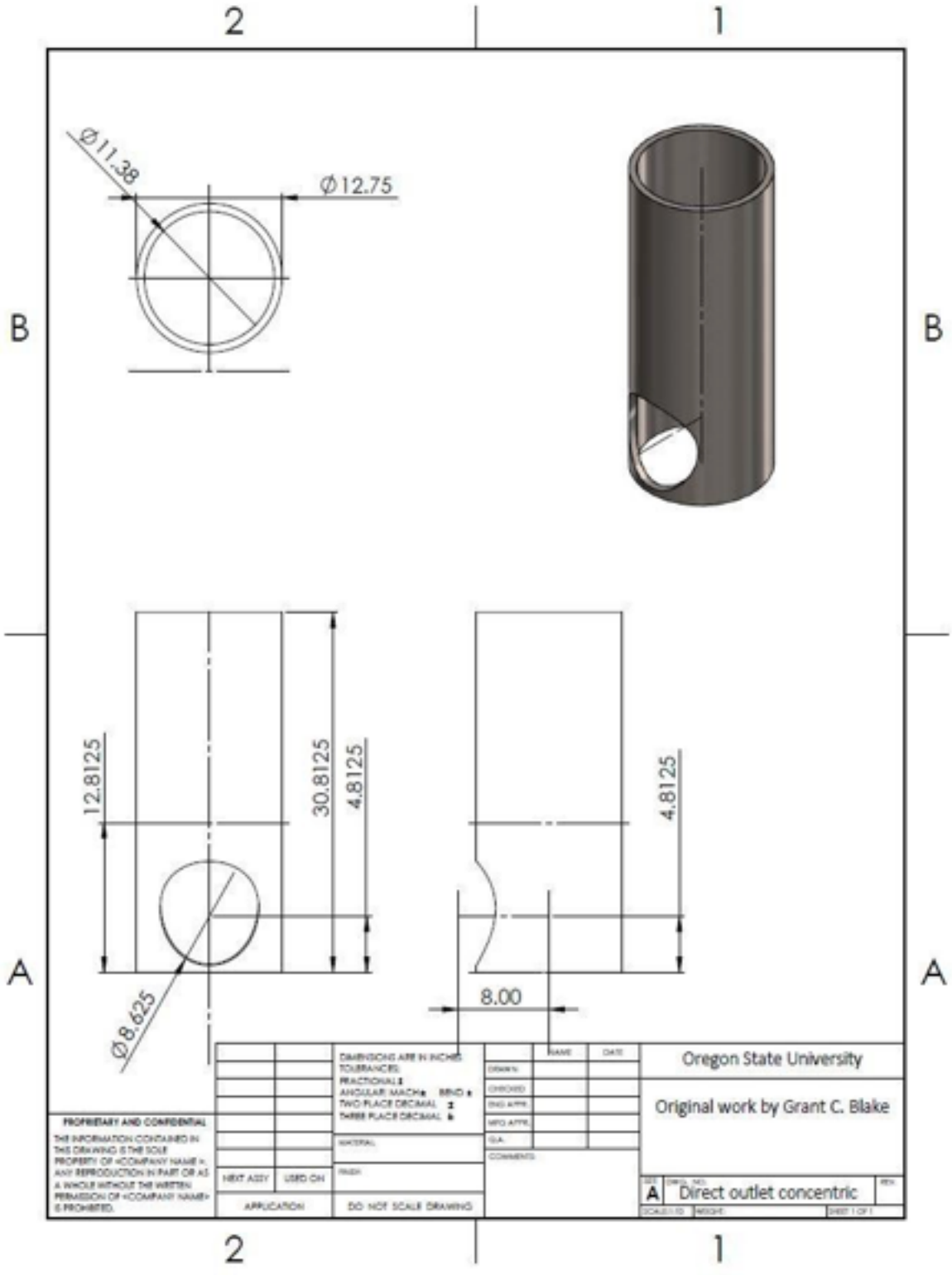
2
1
B
A
Ø11.38
Ø12.75
12.8125
30.8125
4.8125
4.8125
8.00
Ø8.625
Oregon State University
Original work by Grant C. Blake
Direct outlet concentric
PROPRIETARY AND CONFIDENTIAL
THE INFORMATION CONTAINED IN THIS DRAWING IS THE SOLE PROPERTY OF <COMPANY NAME>. ANY REPRODUCTION IN PART OR AS A WHOLE WITHOUT THE WRITTEN PERMISSION OF <COMPANY NAME> IS PROHIBITED.
NEXT ASSY
USED ON
APPLICATION
DO NOT SCALE DRAWING
NAME
DATE
DRAWN
CHECKED
ENG APPR.
MFG APPR.
Q.A.
COMMENTS
SIZE
A
SCALE: 1:10
WEIGHT
SHEET 1 OF 1

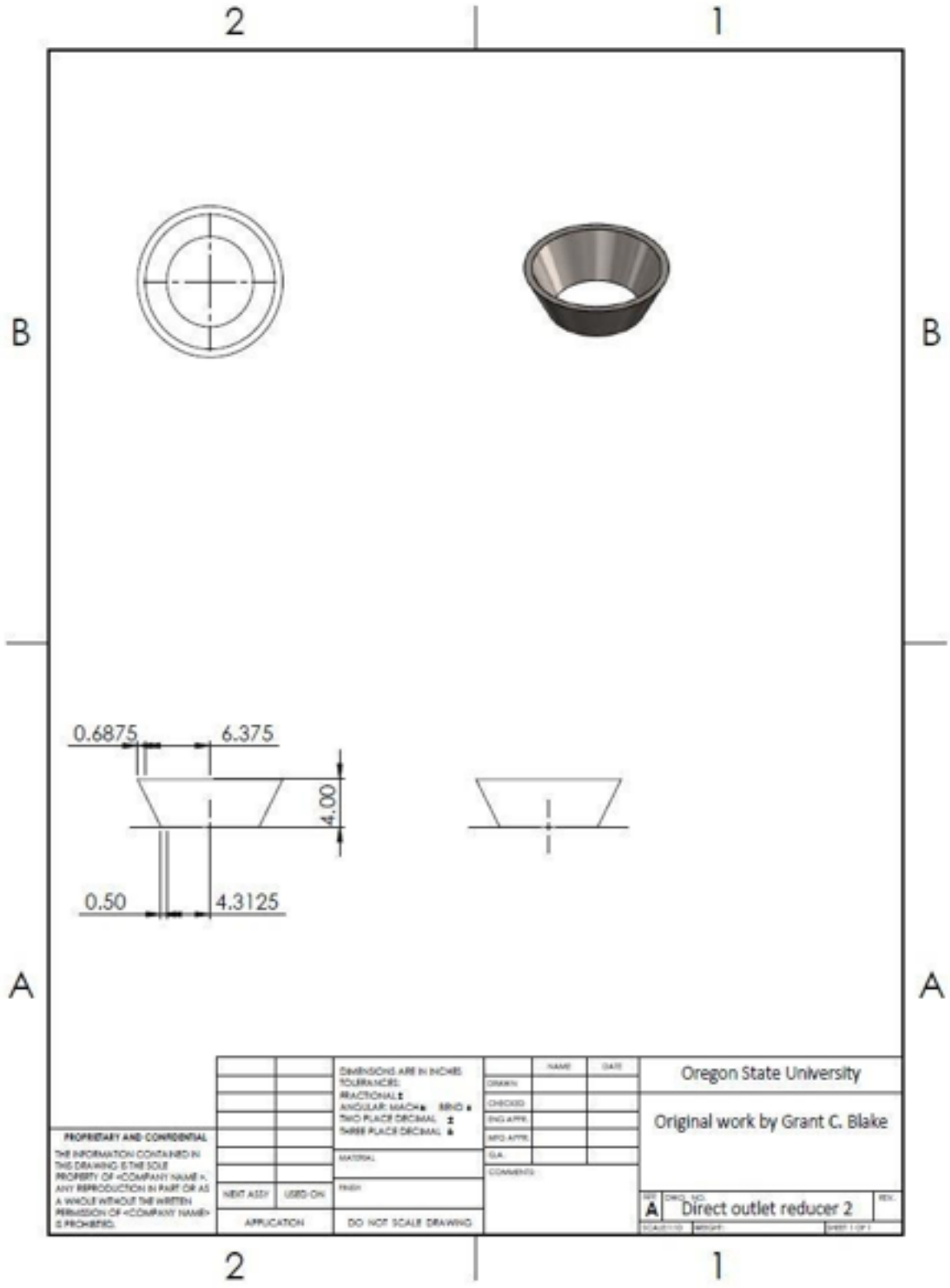
2
1
B
B
A
A
0.6875
6.375
4.00
0.50
4.3125
Oregon State University
Original work by Grant C. Blake
Direct outlet reducer 2
PROPRIETARY AND CONFIDENTIAL
DO NOT SCALE DRAWING
APPLICATION

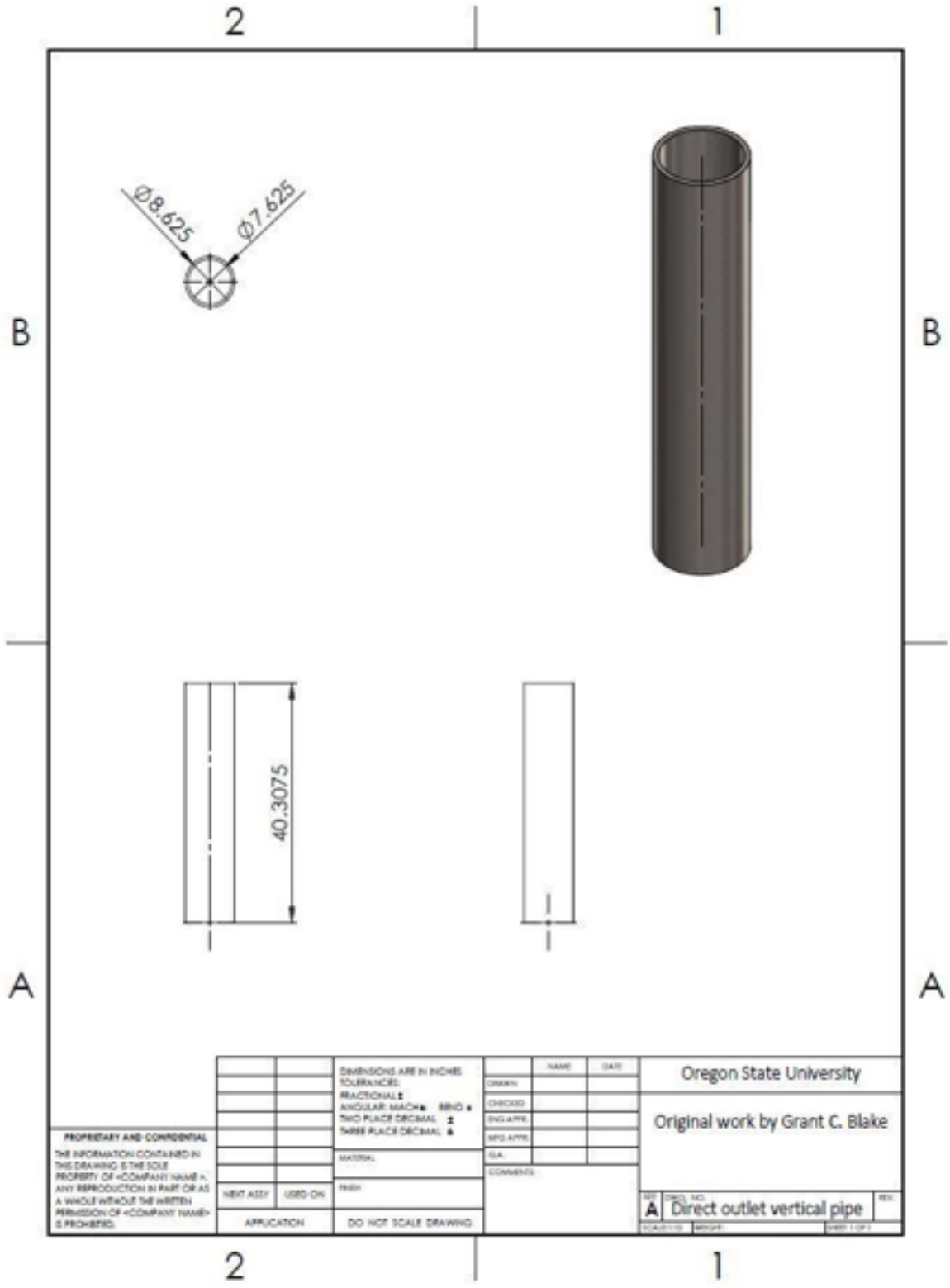
2
1
B
A
Ø8.625
Ø7.625
40.3075
PROPRIETARY AND CONFIDENTIAL
THE INFORMATION CONTAINED IN THIS DRAWING IS THE SOLE PROPERTY OF <COMPANY NAME>. ANY REPRODUCTION IN PART OR AS A WHOLE WITHOUT THE WRITTEN PERMISSION OF <COMPANY NAME> IS PROHIBITED.
NEXT ASSY
USED ON
APPLICATION
DIMENSIONS ARE IN INCHES
TOLERANCES:
FRACTIONAL ±
ANGULAR: MACH ± BEND ±
TWO PLACE DECIMAL ±
THREE PLACE DECIMAL ±
MATERIAL
FINISH
DO NOT SCALE DRAWING
NAME
DATE
DRAWN
CHECKED
ENG APPR.
MFG APPR.
QA
COMMENTS
Oregon State University
Original work by Grant C. Blake
SIZE
A
DWG. NO.
Direct outlet vertical pipe
REV.
SCALE: 1:10
WEIGHT:
SHEET 1 OF 1

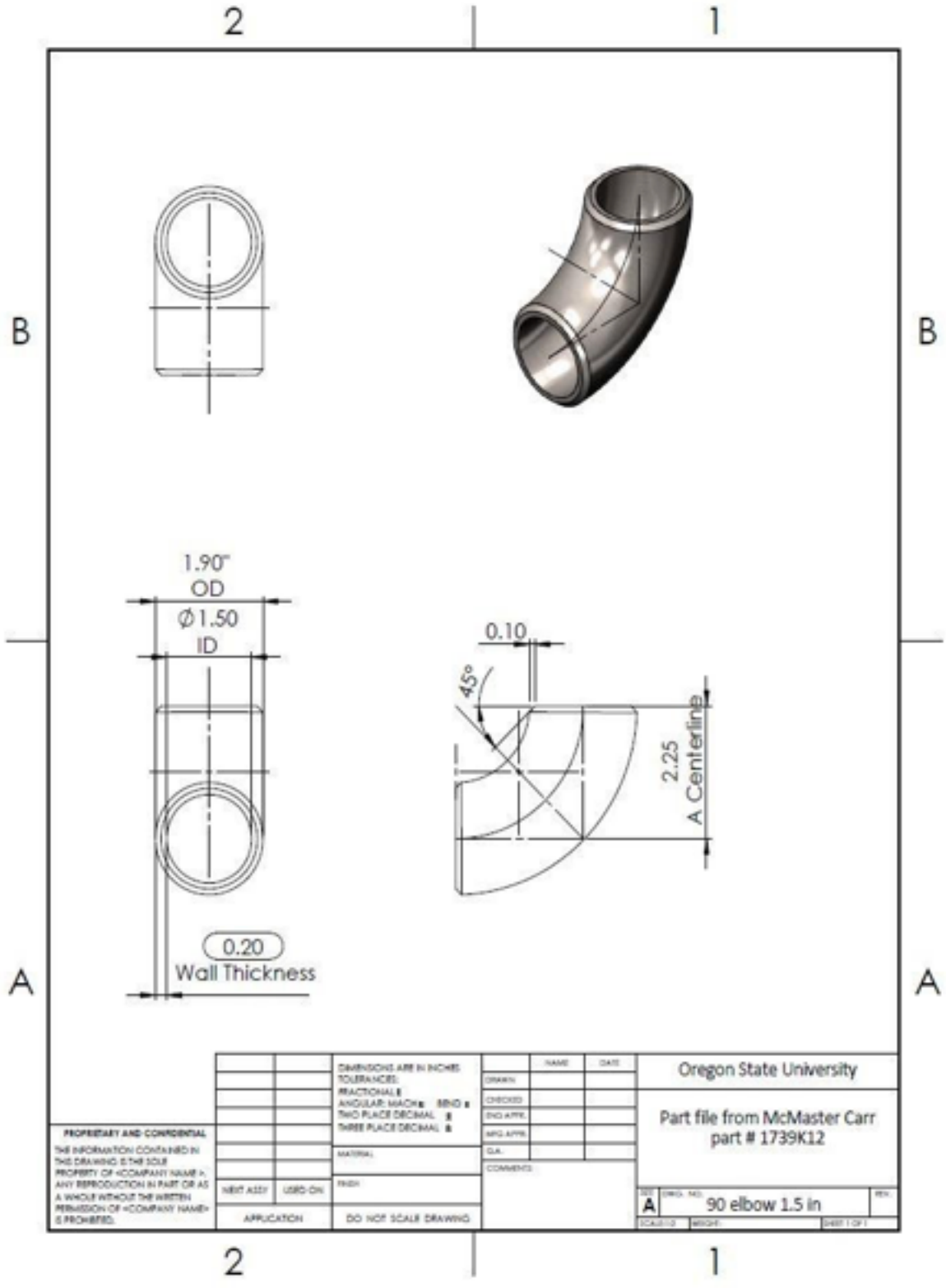
2
1
B
A
1.90"
OD
Ø1.50
ID
0.20
Wall Thickness
0.10
45°
2.25
A Centerline
Oregon State University
Part file from McMaster Carr
part # 1739K12
90 elbow 1.5 in
PROPRIETARY AND CONFIDENTIAL
DO NOT SCALE DRAWING

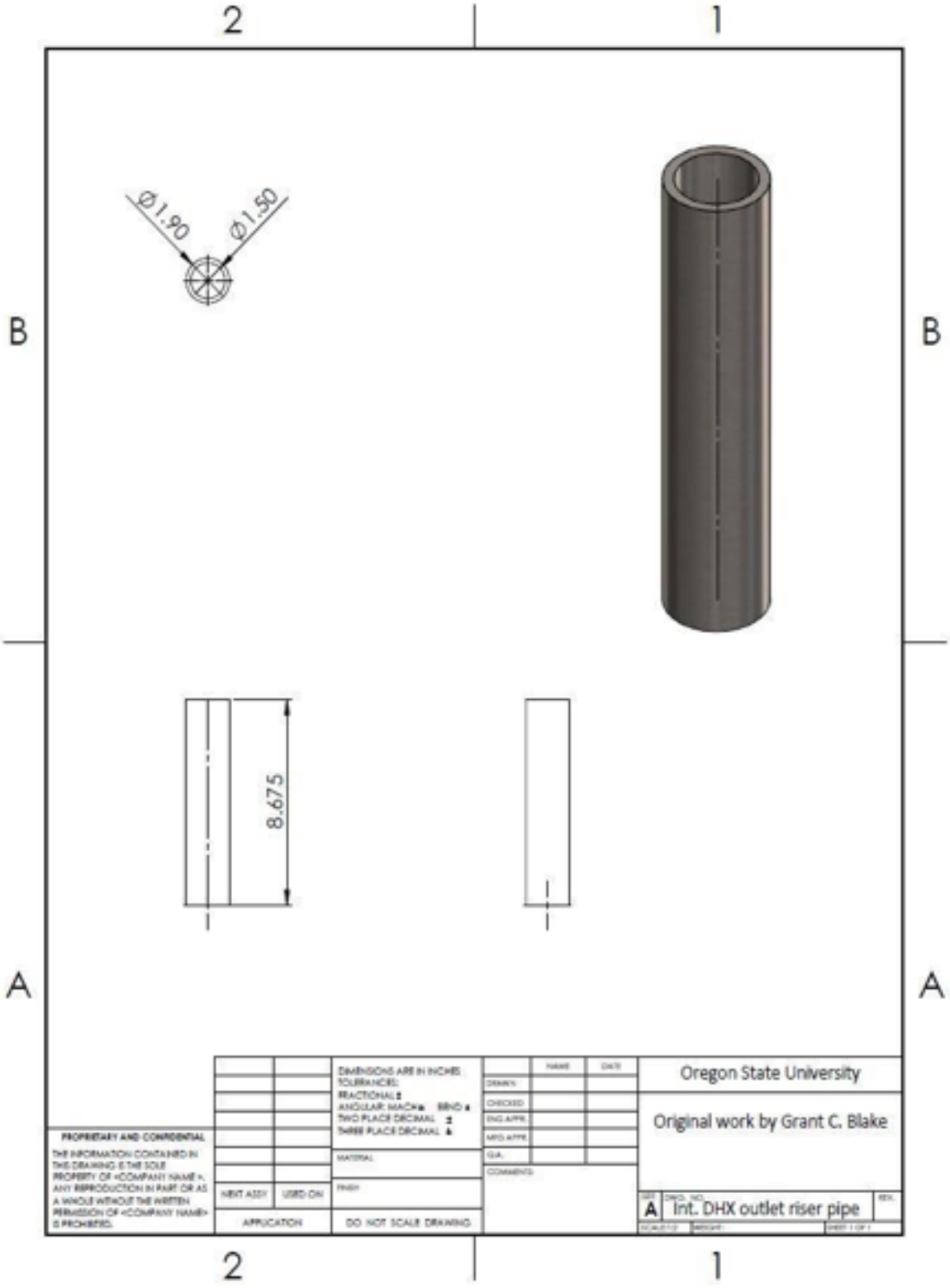
2
1
B
B
A
A
Ø1.90
Ø1.50
8.675
DIMENSIONS ARE IN INCHES
TOLERANCES:
FRACTIONAL ±
ANGULAR: MACH ± BEND ±
TWO PLACE DECIMAL ±
THREE PLACE DECIMAL ±
MATERIAL
NEXT ASSY
USED ON
FINISH
APPLICATION
DO NOT SCALE DRAWING
DRAWN
CHECKED
ENG APPR.
MFG APPR.
QUA.
COMMENTS
NAME
DATE
Oregon State University
Original work by Grant C. Blake
PROPRIETARY AND CONFIDENTIAL
THE INFORMATION CONTAINED IN THIS DRAWING IS THE SOLE PROPERTY OF «COMPANY NAME». ANY REPRODUCTION IN PART OR AS A WHOLE WITHOUT THE WRITTEN PERMISSION OF «COMPANY NAME» IS PROHIBITED.
SIZE
A
DWG. NO.
Int. DHX outlet riser pipe
REV.
SCALE: 1:2
WEIGHT:
SHEET 1 OF 1

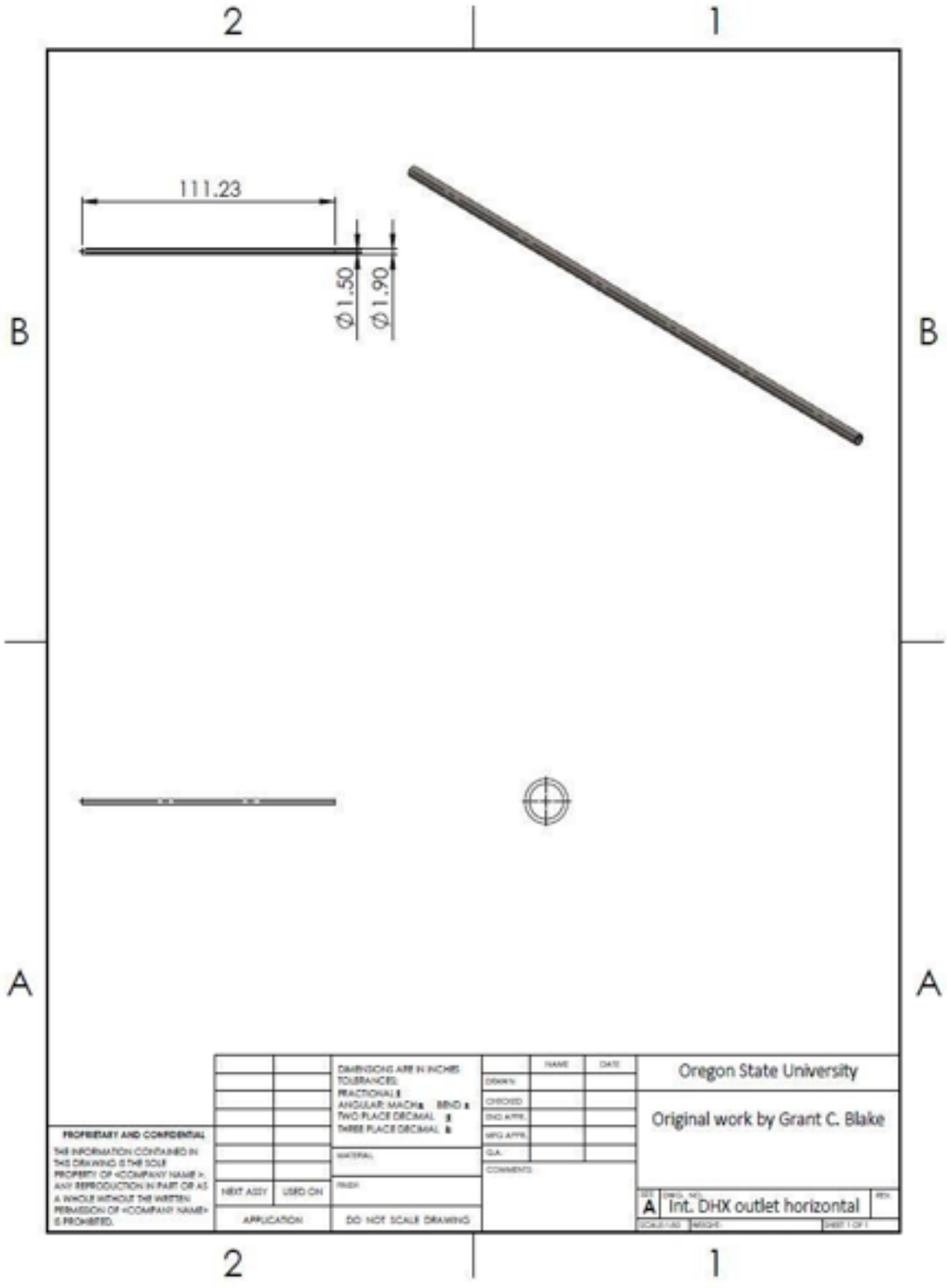
2
1
B
A
111.23
Ø1.50
Ø1.90
PROPRIETARY AND CONFIDENTIAL
THE INFORMATION CONTAINED IN THIS DRAWING IS THE SOLE PROPERTY OF <COMPANY NAME>. ANY REPRODUCTION IN PART OR AS A WHOLE WITHOUT THE WRITTEN PERMISSION OF <COMPANY NAME> IS PROHIBITED.
NEXT ASSY
USED ON
APPLICATION
DIMENSIONS ARE IN INCHES
TOLERANCES:
FRACTIONAL ±
ANGULAR: MACH ± BEND ±
TWO PLACE DECIMAL ±
THREE PLACE DECIMAL ±
MATERIAL
FINISH
DO NOT SCALE DRAWING
NAME
DATE
DRAWN
CHECKED
ENG APPR.
MFG APPR.
Q.A.
COMMENTS:
Oregon State University
Original work by Grant C. Blake
SIZE
A
DWG. NO.
Int. DHX outlet horizontal
REV
SCALE: NO
WEIGHT
SHEET 1 OF 1

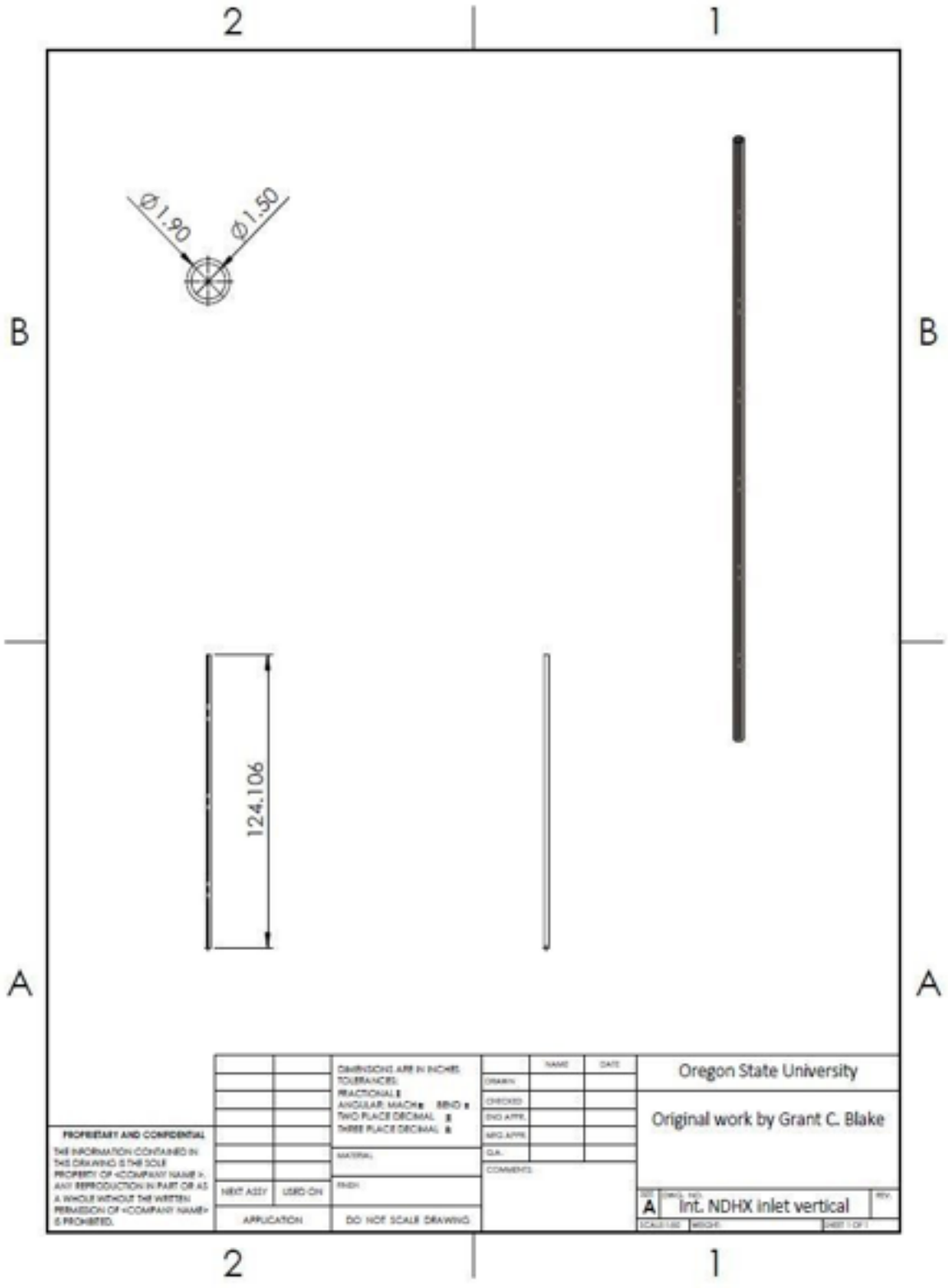
2
1
B
A
Ø1.90
Ø1.50
124.106
PROPRIETARY AND CONFIDENTIAL
THE INFORMATION CONTAINED IN THIS DRAWING IS THE SOLE PROPERTY OF <COMPANY NAME >. ANY REPRODUCTION IN PART OR AS A WHOLE WITHOUT THE WRITTEN PERMISSION OF <COMPANY NAME> IS PROHIBITED.
NEXT ASSY
USED ON
APPLICATION
DIMENSIONS ARE IN INCHES
TOLERANCES:
FRACTIONAL ±
ANGULAR: MACH ± BEND ±
TWO PLACE DECIMAL ±
THREE PLACE DECIMAL ±
MATERIAL
FINISH
DO NOT SCALE DRAWING
NAME
DATE
DRAWN
CHECKED
ENG APPR.
MFG APPR.
Q.A.
COMMENTS:
Oregon State University
Original work by Grant C. Blake
SIZE
A
DWG. NO.
Int. NDHX inlet vertical
REV.
SCALE: 1:50
WEIGHT:
SHEET 1 OF 1

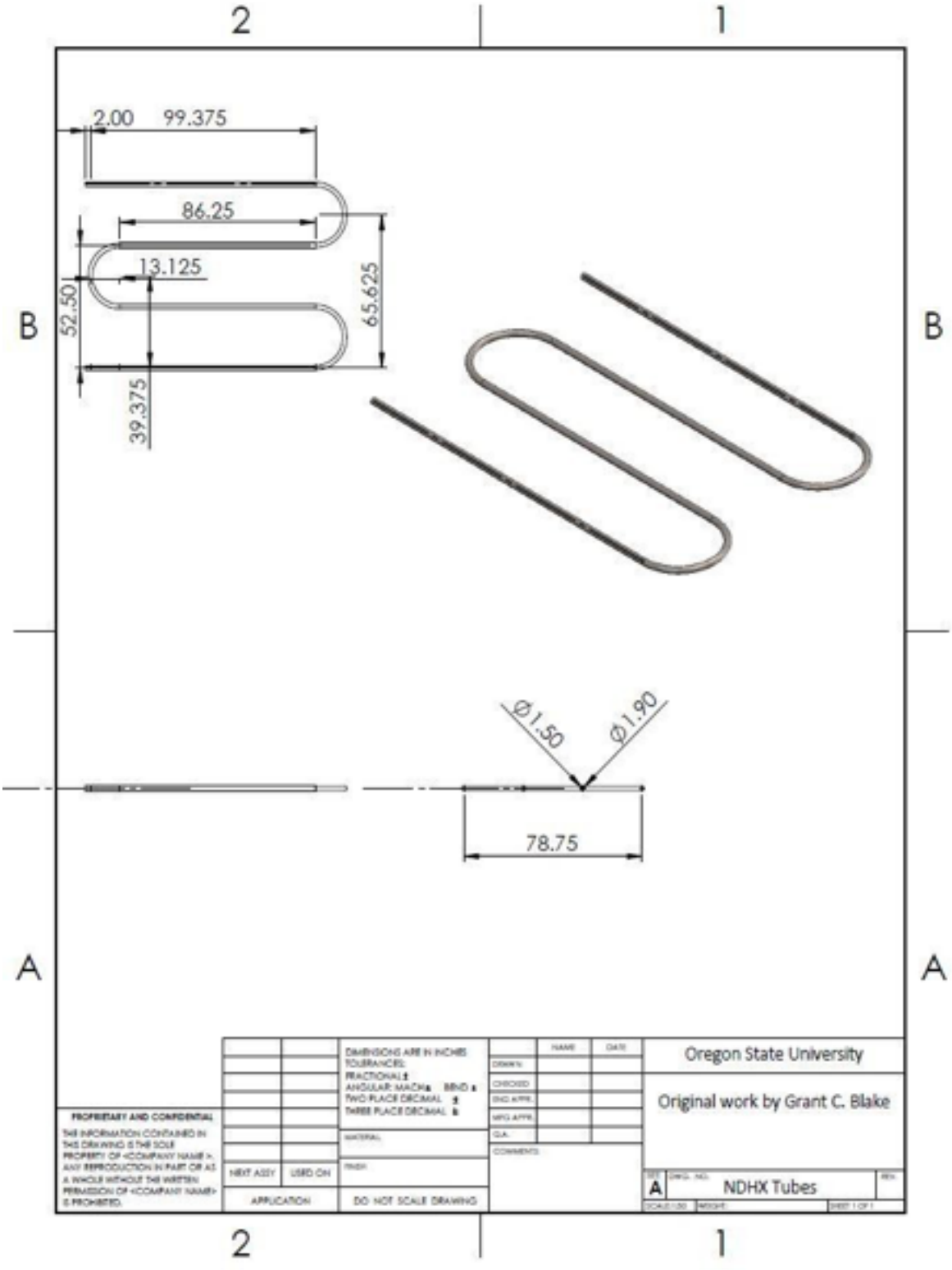
2
1
B
A
2.00
99.375
86.25
13.125
52.50
65.625
39.375
Ø1.50
Ø1.90
78.75
Oregon State University
Original work by Grant C. Blake
NDHX Tubes
PROPRIETARY AND CONFIDENTIAL
THE INFORMATION CONTAINED IN THIS DRAWING IS THE SOLE PROPERTY OF <COMPANY NAME>. ANY REPRODUCTION IN PART OR AS A WHOLE WITHOUT THE WRITTEN PERMISSION OF <COMPANY NAME> IS PROHIBITED.
DO NOT SCALE DRAWING

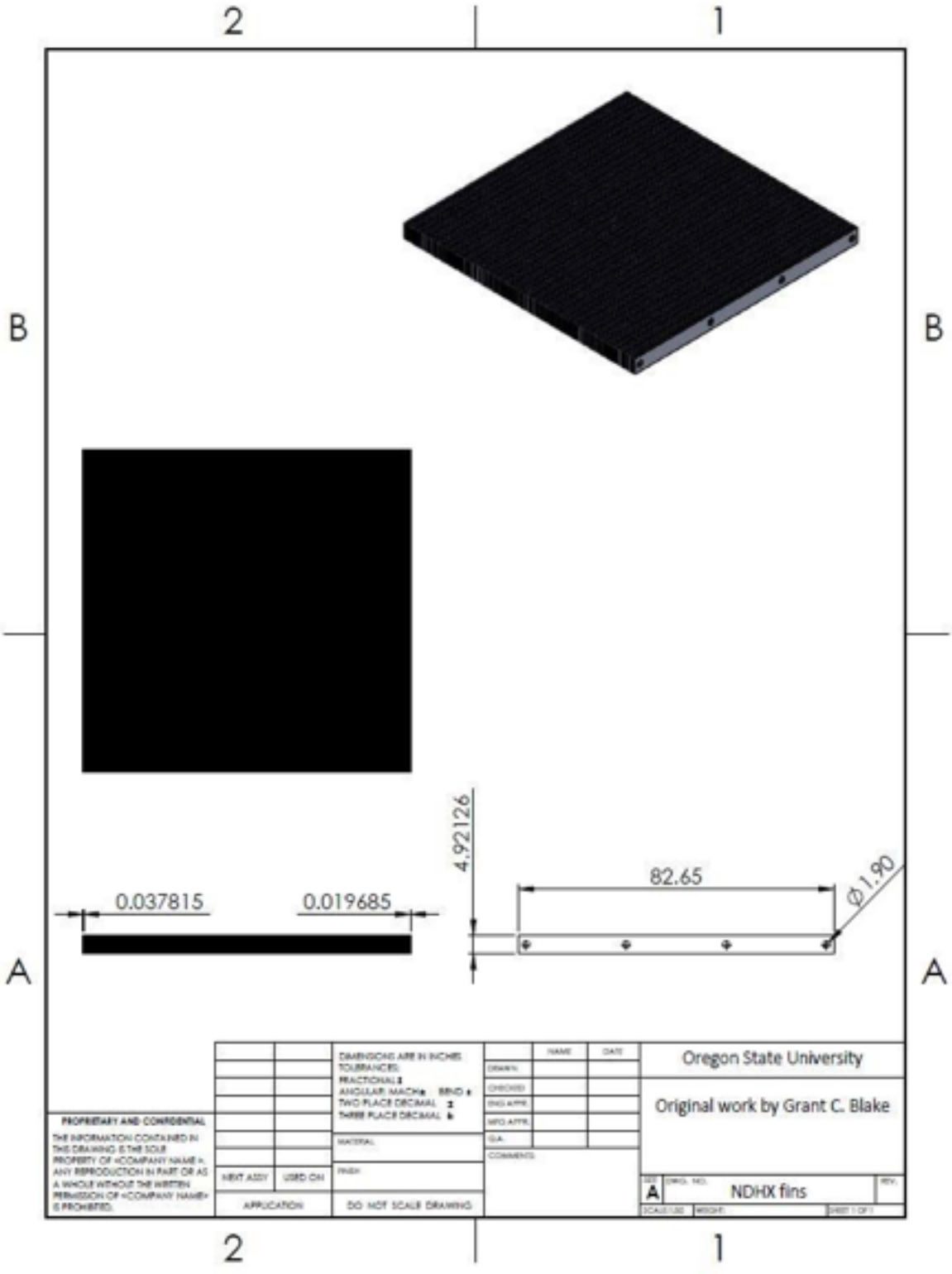
2
1
B
B
A
A
4.92126
82.65
Ø1.90
0.037815
0.019685
Oregon State University
Original work by Grant C. Blake
NDHX fins
A
PROPRIETARY AND CONFIDENTIAL
DO NOT SCALE DRAWING

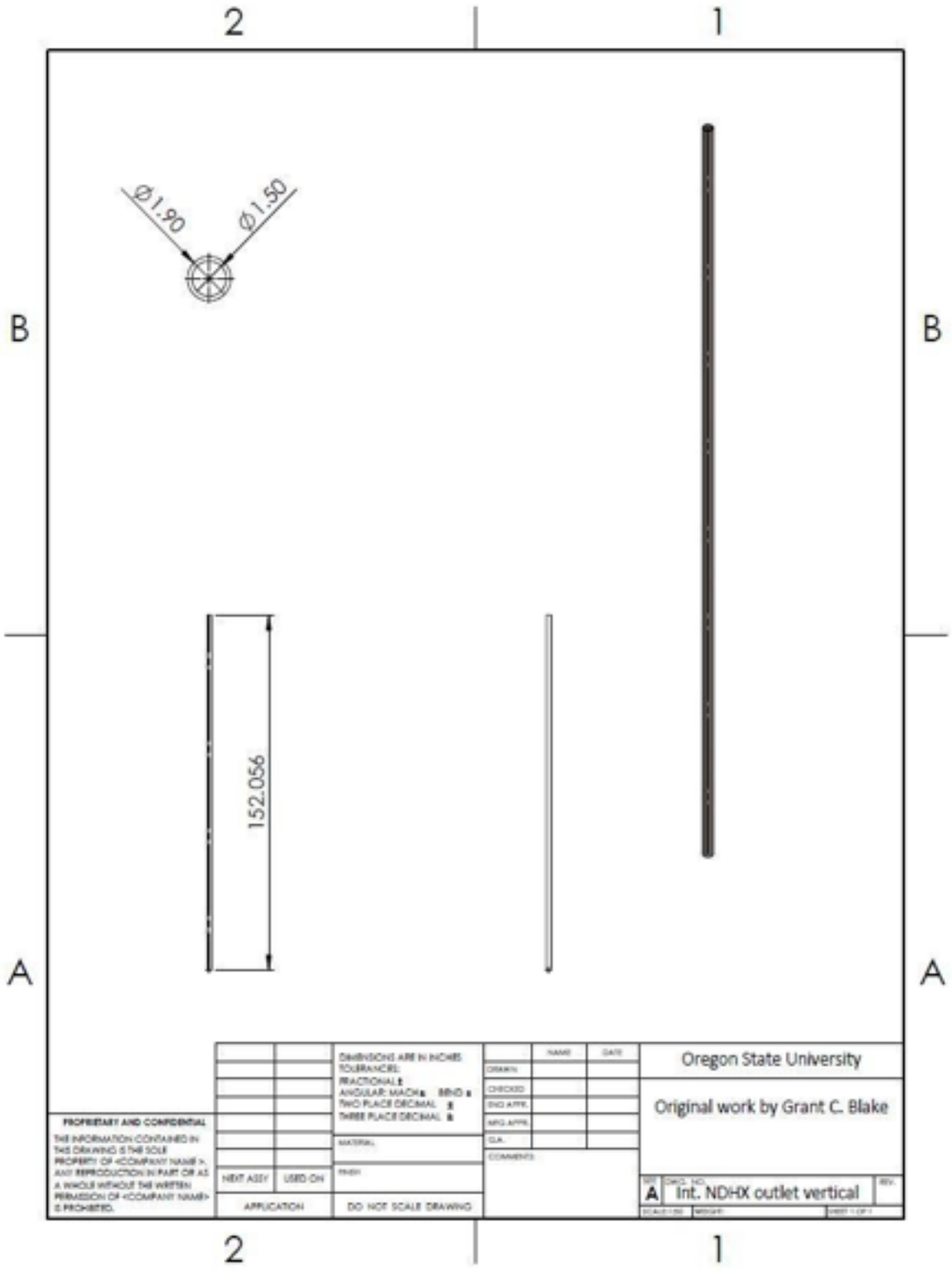
2
1
B
A
Ø1.90
Ø1.50
152.056
PROPRIETARY AND CONFIDENTIAL
THE INFORMATION CONTAINED IN THIS DRAWING IS THE SOLE PROPERTY OF <COMPANY NAME >. ANY REPRODUCTION IN PART OR AS A WHOLE WITHOUT THE WRITTEN PERMISSION OF <COMPANY NAME> IS PROHIBITED.
NEXT ASSY
USED ON
APPLICATION
DIMENSIONS ARE IN INCHES
TOLERANCES:
FRACTIONAL ±
ANGULAR: MACH ± BEND ±
TWO PLACE DECIMAL ±
THREE PLACE DECIMAL ±
MATERIAL
FINISH
DO NOT SCALE DRAWING
NAME
DATE
DRAWN
CHECKED
ENG APPR.
MFG APPR.
QA
COMMENTS
Oregon State University
Original work by Grant C. Blake
SIZE
A
DWG. NO.
Int. NDHX outlet vertical
REV.
SCALE: 1/50
WEIGHT:
SHEET 1 OF 1

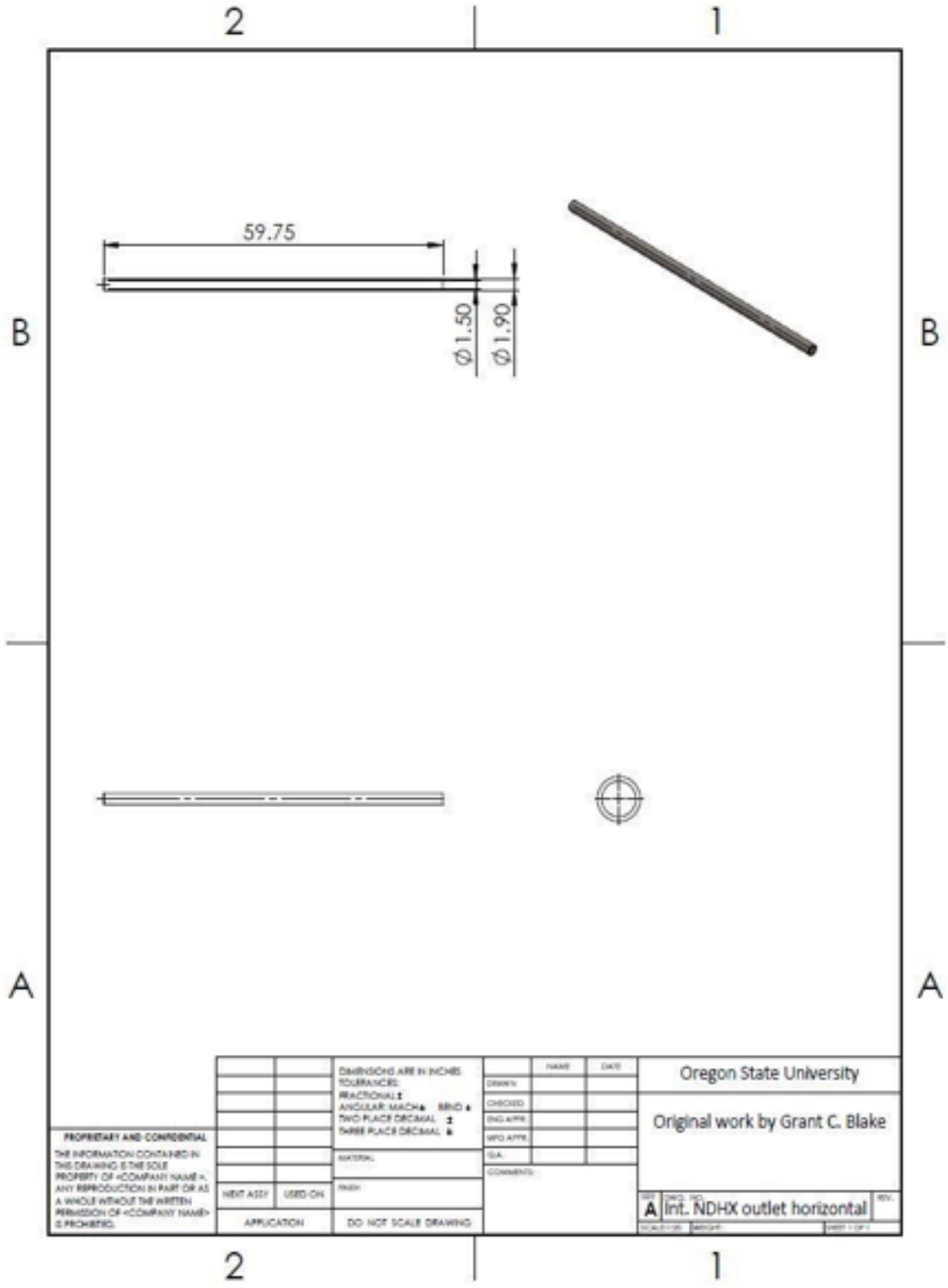
2
1
B
A
59.75
Ø1.50
Ø1.90
PROPRIETARY AND CONFIDENTIAL
THE INFORMATION CONTAINED IN THIS DRAWING IS THE SOLE PROPERTY OF <COMPANY NAME>. ANY REPRODUCTION IN PART OR AS A WHOLE WITHOUT THE WRITTEN PERMISSION OF <COMPANY NAME> IS PROHIBITED.
NEXT ASSY
USED ON
APPLICATION
DIMENSIONS ARE IN INCHES
TOLERANCES:
FRACTIONAL ±
ANGULAR: MACH ± BEND ±
TWO PLACE DECIMAL ±
THREE PLACE DECIMAL ±
MATERIAL
FINISH
DO NOT SCALE DRAWING
NAME
DATE
DRAWN
CHECKED
ENG APPR.
MFG APPR.
Q.A.
COMMENTS:
Oregon State University
Original work by Grant C. Blake
SIZE
A
DWG. NO.
Int. NDHX outlet horizontal
REV.
SCALE: 1:20
WEIGHT:
SHEET 1 OF 1

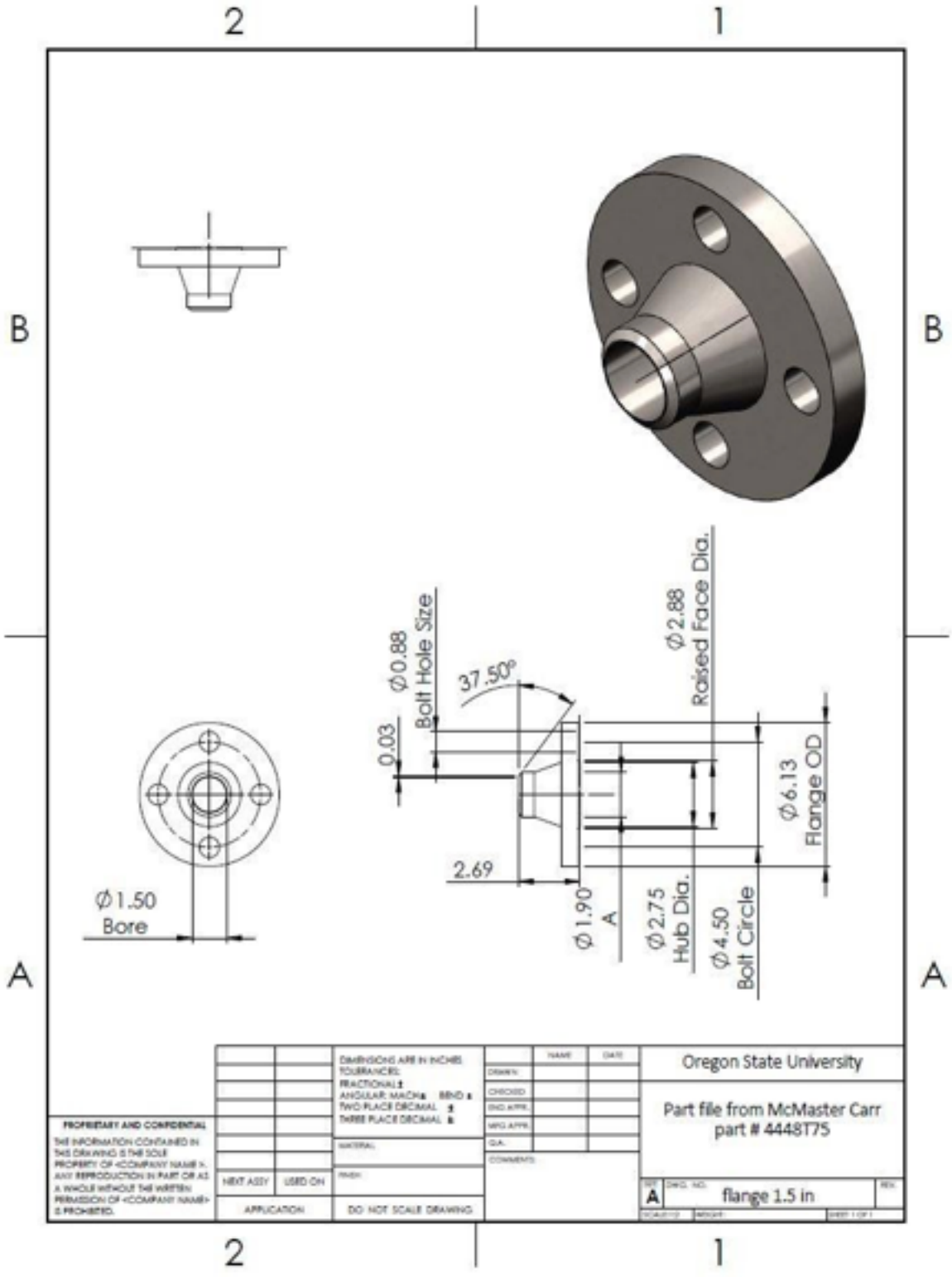
2
1
B
A
Ø0.88
Bolt Hole Size
37.50°
Ø2.88
Raised Face Dia.
0.03
Ø6.13
Flange OD
2.69
Ø1.50
Bore
Ø1.90
A
Ø2.75
Hub Dia.
Ø4.50
Bolt Circle
PROPRIETARY AND CONFIDENTIAL
THE INFORMATION CONTAINED IN THIS DRAWING IS THE SOLE PROPERTY OF <COMPANY NAME >. ANY REPRODUCTION IN PART OR AS A WHOLE WITHOUT THE WRITTEN PERMISSION OF <COMPANY NAME> IS PROHIBITED.
NEXT ASSY
USED ON
APPLICATION
DIMENSIONS ARE IN INCHES
TOLERANCES:
FRACTIONAL ±
ANGULAR: MACH ± BEND ±
TWO PLACE DECIMAL ±
THREE PLACE DECIMAL ±
MATERIAL
FINISH
DO NOT SCALE DRAWING
NAME
DATE
DRAWN
CHECKED
ENG APPR.
MFG APPR.
Q.A.
COMMENTS
Oregon State University
Part file from McMaster Carr
part # 4448T75
SIZE
A
DWG. NO.
flange 1.5 in
REV
SCALE: 1:2
WEIGHT
SHEET 1 OF 1

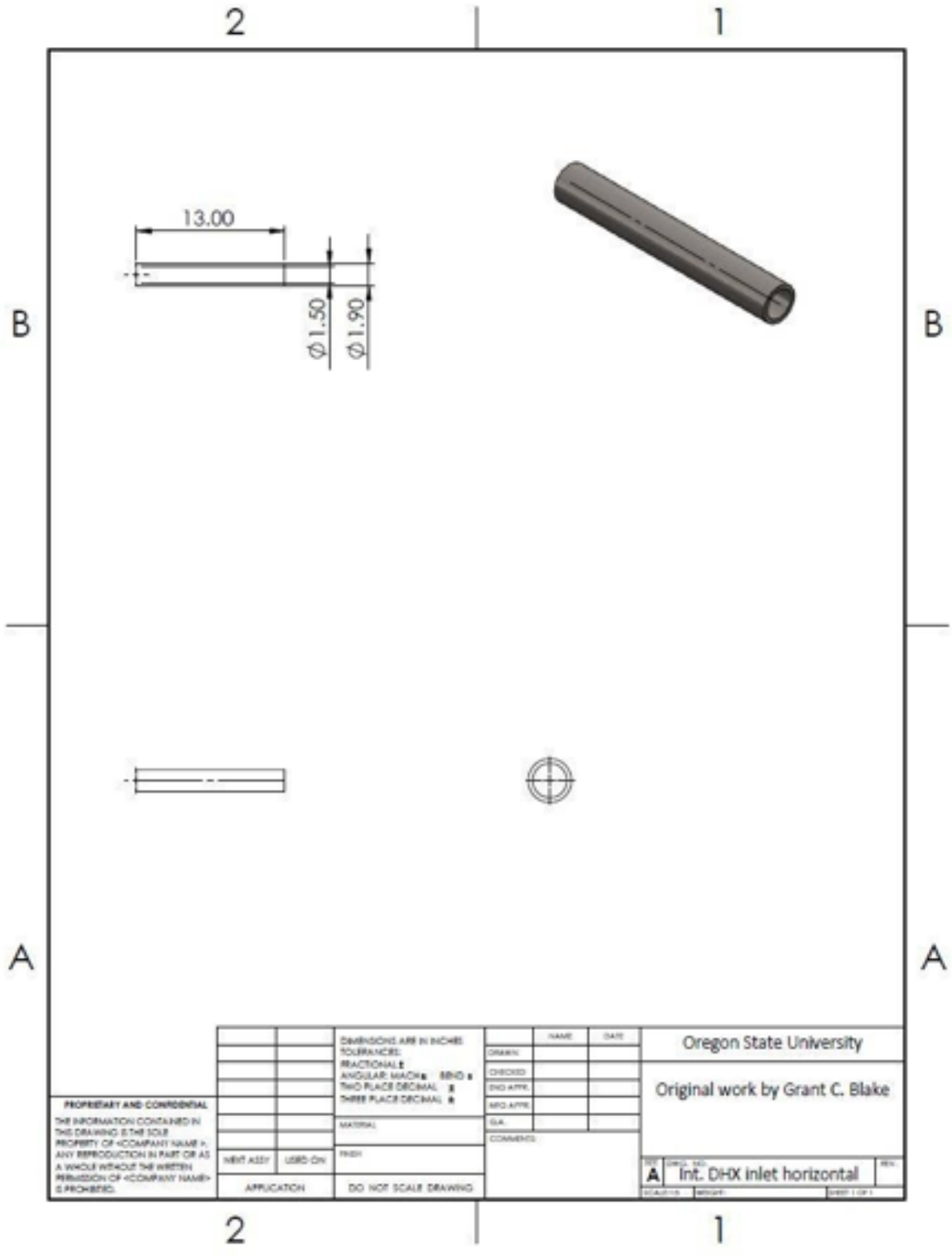
2
1
B
A
13.00
Ø1.50
Ø1.90
PROPRIETARY AND CONFIDENTIAL
THE INFORMATION CONTAINED IN THIS DRAWING IS THE SOLE PROPERTY OF <COMPANY NAME>. ANY REPRODUCTION IN PART OR AS A WHOLE WITHOUT THE WRITTEN PERMISSION OF <COMPANY NAME> IS PROHIBITED.
NEXT ASSY
USED ON
APPLICATION
DIMENSIONS ARE IN INCHES
TOLERANCES:
FRACTIONAL ±
ANGULAR: MACH ± BEND ±
TWO PLACE DECIMAL ±
THREE PLACE DECIMAL ±
MATERIAL
FINISH
DO NOT SCALE DRAWING
NAME
DATE
DRAWN
CHECKED
ENG APPR.
MFG APPR.
Q.A.
COMMENTS:
Oregon State University
Original work by Grant C. Blake
SIZE
A
DWG. NO.
Int. DHX inlet horizontal
REV
SCALE: 1:5
WEIGHT:
SHEET 1 OF 1

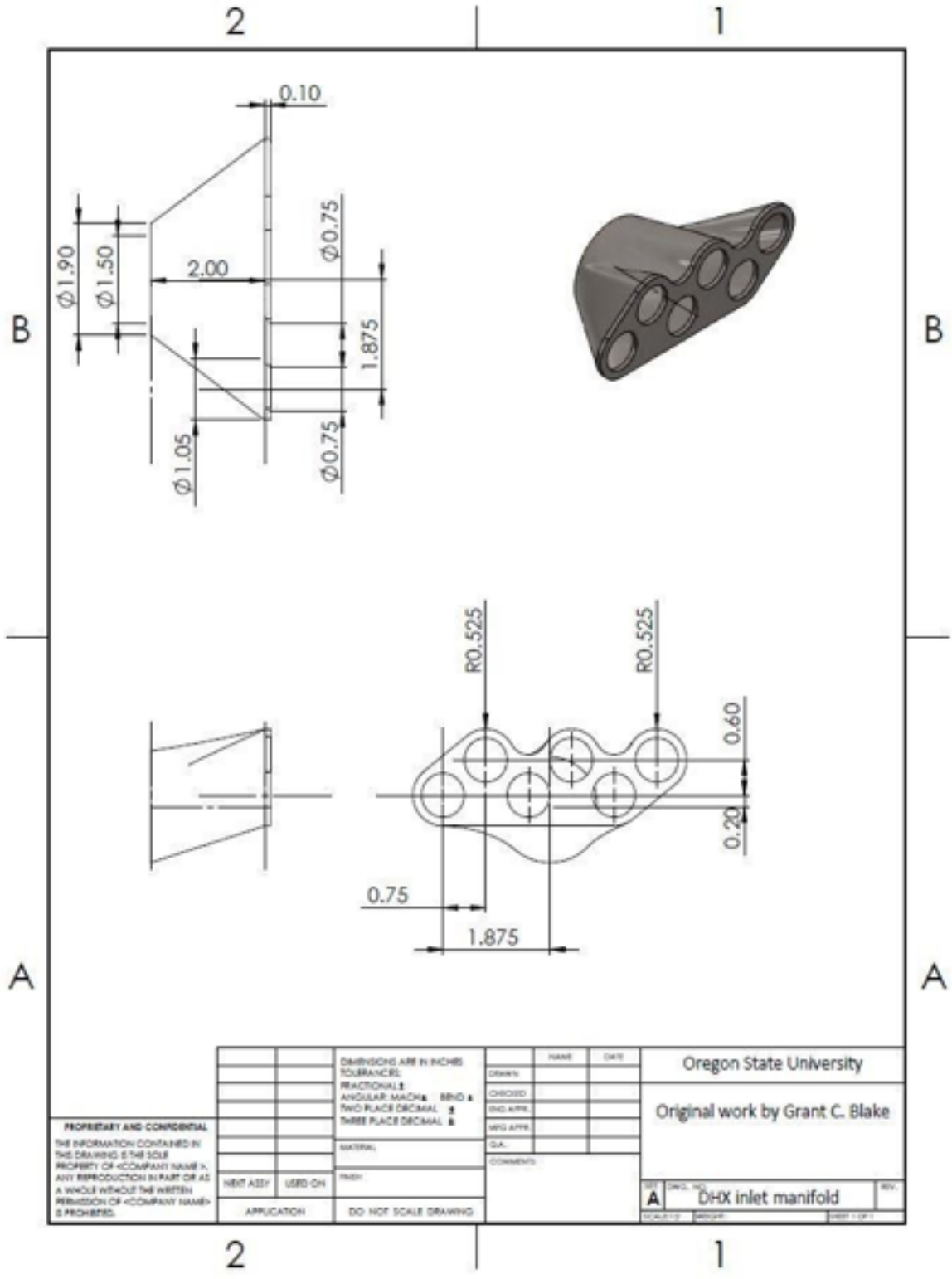
2
1
B
A
0.10
Ø1.90
Ø1.50
2.00
Ø0.75
1.875
Ø1.05
Ø0.75
R0.525
R0.525
0.60
0.20
0.75
1.875
Oregon State University
Original work by Grant C. Blake
DHX inlet manifold
PROPRIETARY AND CONFIDENTIAL
DO NOT SCALE DRAWING

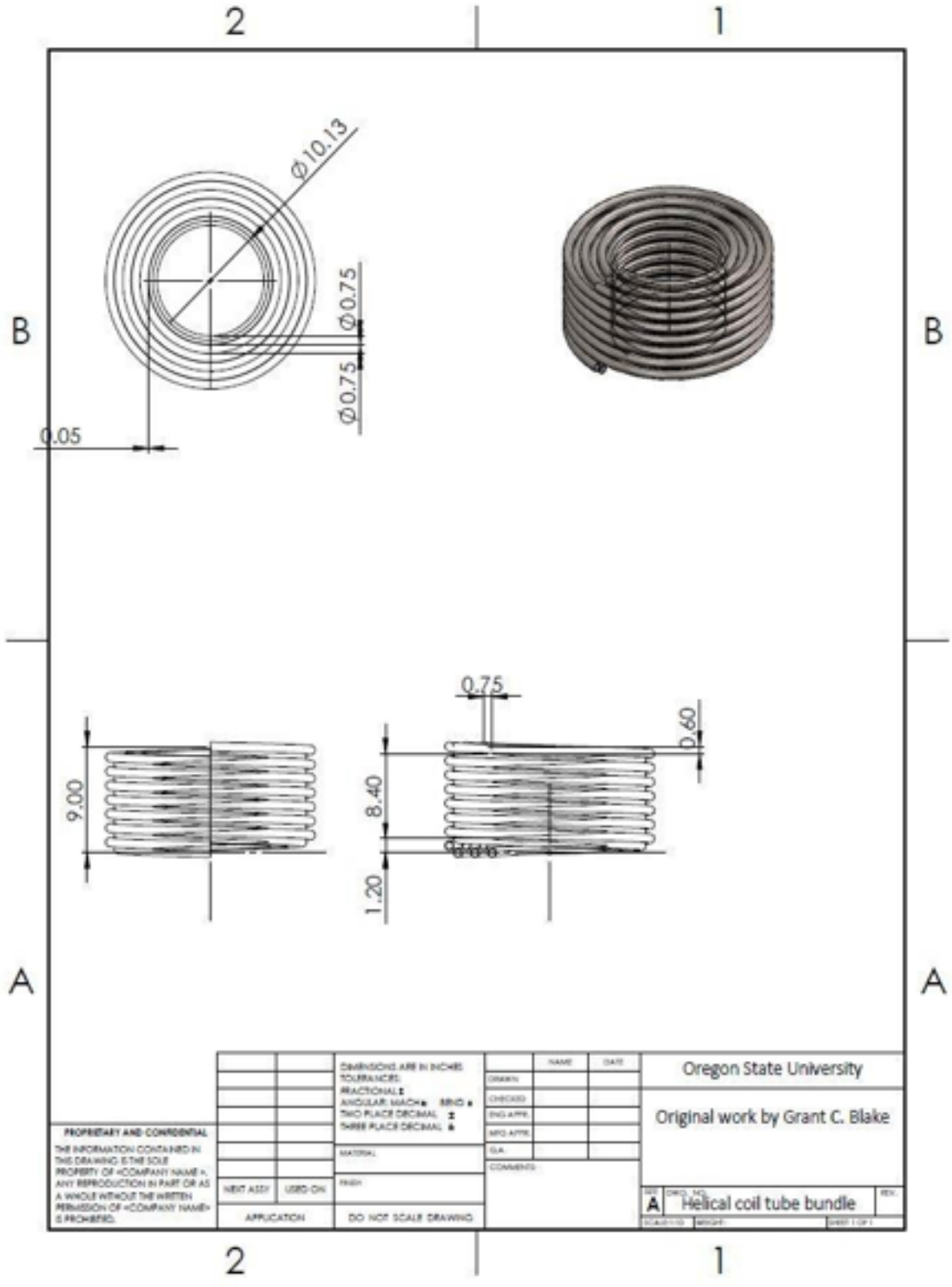
2
1
B
B
A
A
Ø10.13
Ø0.75
Ø0.75
0.05
0.75
0.60
9.00
8.40
1.20
Oregon State University
Original work by Grant C. Blake
Helical coil tube bundle
PROPRIETARY AND CONFIDENTIAL
THE INFORMATION CONTAINED IN THIS DRAWING IS THE SOLE PROPERTY OF <COMPANY NAME>. ANY REPRODUCTION IN PART OR AS A WHOLE WITHOUT THE WRITTEN PERMISSION OF <COMPANY NAME> IS PROHIBITED.
DIMENSIONS ARE IN INCHES
TOLERANCES:
FRACTIONAL ±
ANGULAR: MACH ± BEND ±
TWO PLACE DECIMAL ±
THREE PLACE DECIMAL ±
MATERIAL
FINISH
NEXT ASSY
USED ON
APPLICATION
DO NOT SCALE DRAWING
NAME
DATE
DRAWN
CHECKED
ENG APPR.
MFG APPR.
QA
COMMENTS
SIZE
A
DWG. NO.
REV.
SCALE: 1:1
WEIGHT
SHEET 1 OF 1

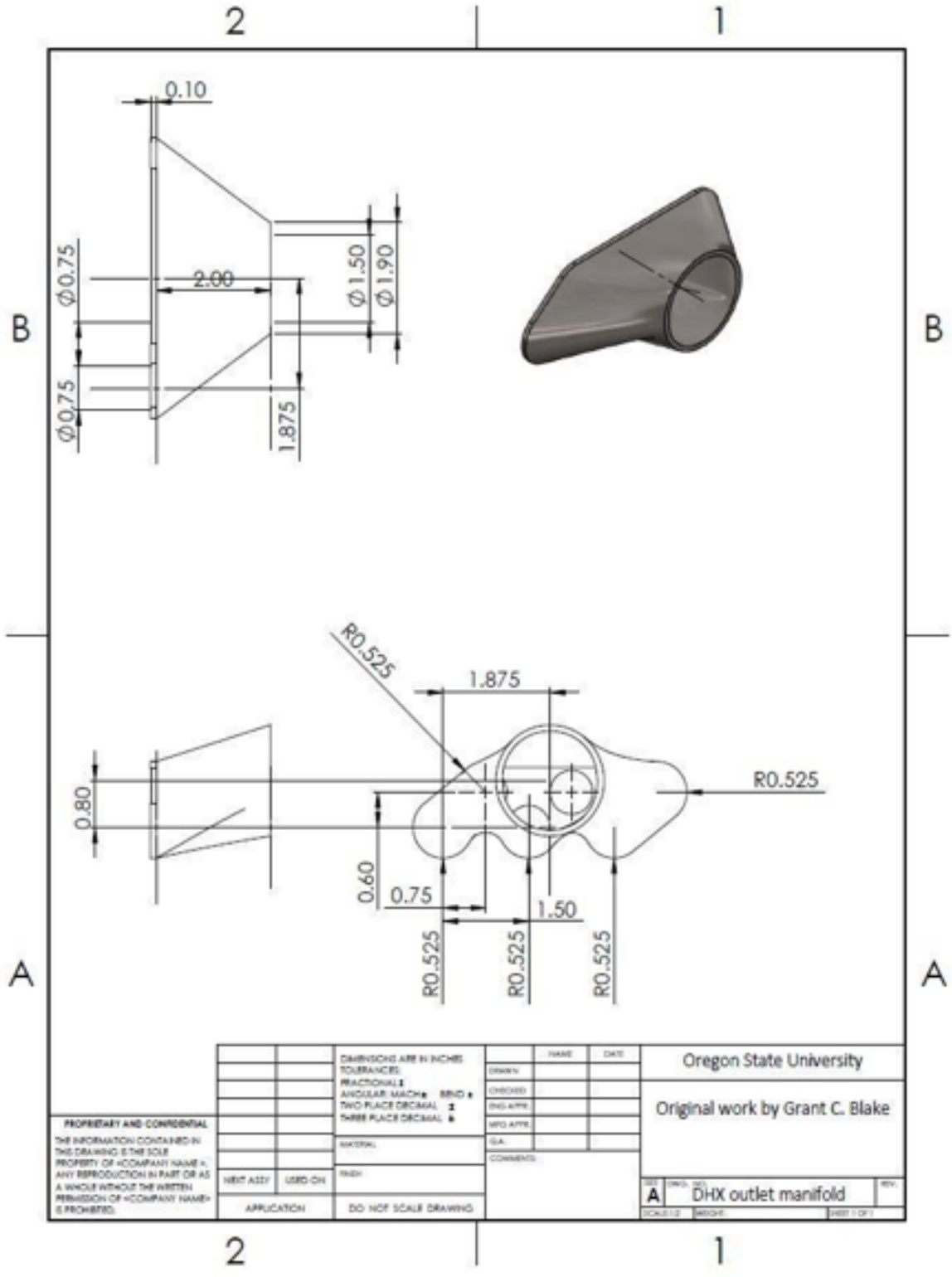
2
1
B
A
0.10
2.00
1.875
1.875
0.80
0.60
0.75
1.50
R0.525
R0.525
R0.525
R0.525
R0.525
Oregon State University
Original work by Grant C. Blake
DHX outlet manifold
PROPRIETARY AND CONFIDENTIAL
DO NOT SCALE DRAWING

APPENDIX I: SWI HTTF COMPONENTS

- ASME Steam Generator Tank with a 10” 150# Flange
  30” Diameter x 72” Length, 155 psi ASME, 201 Gallon Capacity, Horizontal with Attached Saddles, misc. FNPT Connections, Unlined Interior, Primer Painted Exterior.

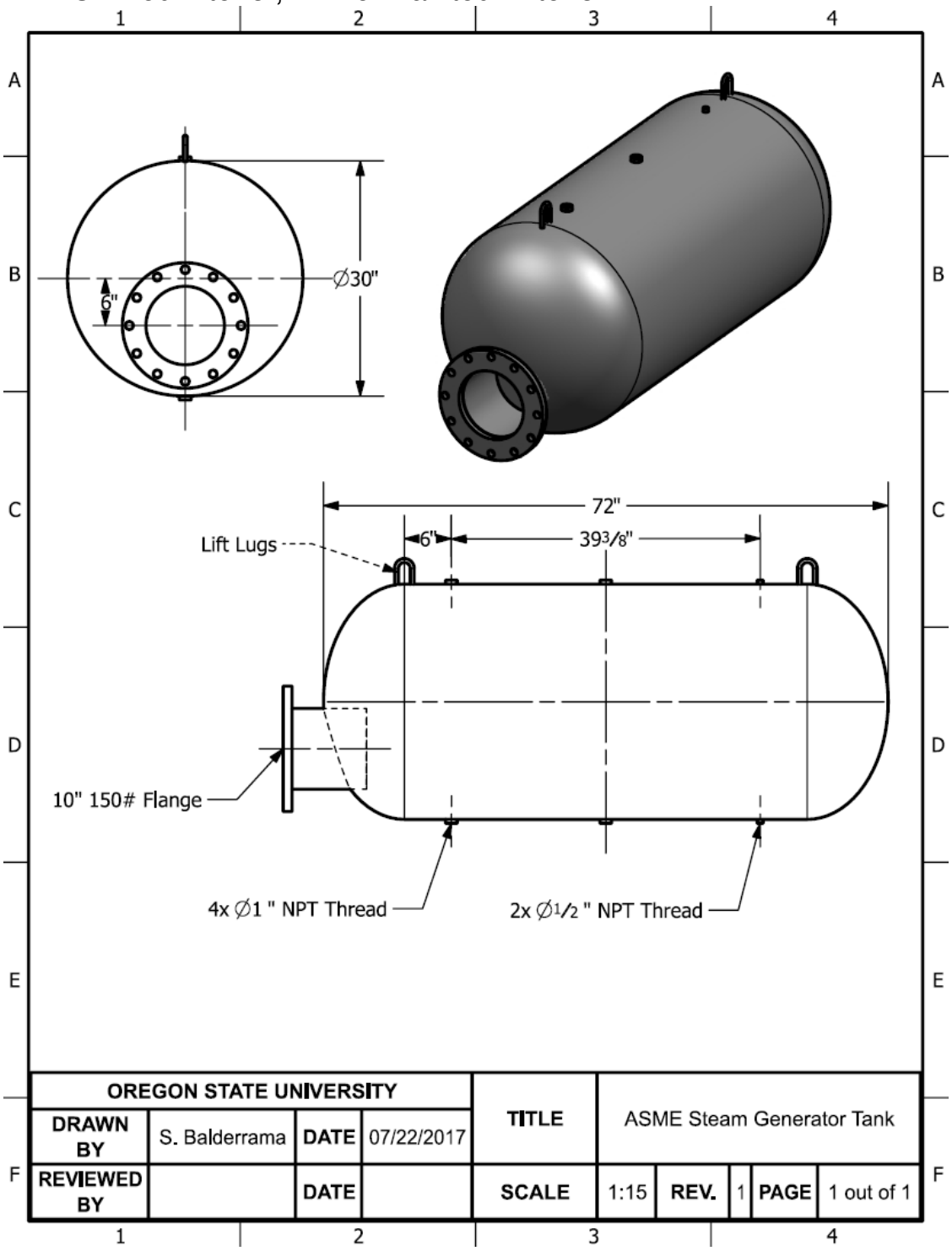

- High-Flow Backflow-Prevention Valve

McMaster-Carr, Check Valve, Bronze Seal, 1” NPT Female, Pressure Class 300, 3-11/16” End-to-End Length.

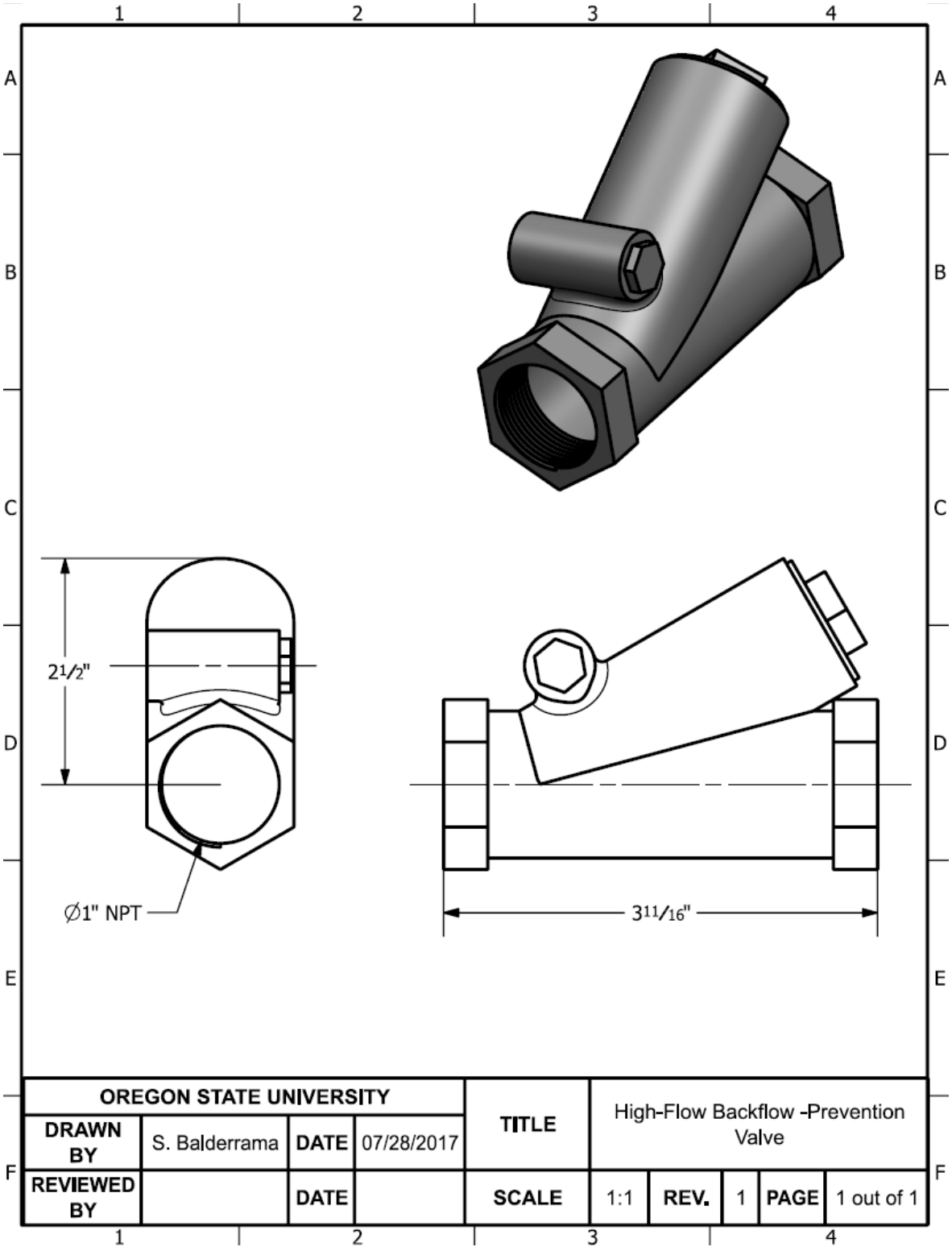

OREGON STATE UNIVERSITY				TITLE	High-Flow Backflow -Prevention Valve				
DRAWN BY	S. Balderrama	DATE	07/28/2017						
REVIEWED BY		DATE		SCALE	1:1	REV.	1	PAGE	1 out of 1

- Bronze Flow-Adjustment Valve, Pressure Class 300

McMaster-Carr, Globe Valve, Straight, 420 Stainless Steel Disc, 1 NPT Female, 3-5/8” End-to-End Length.

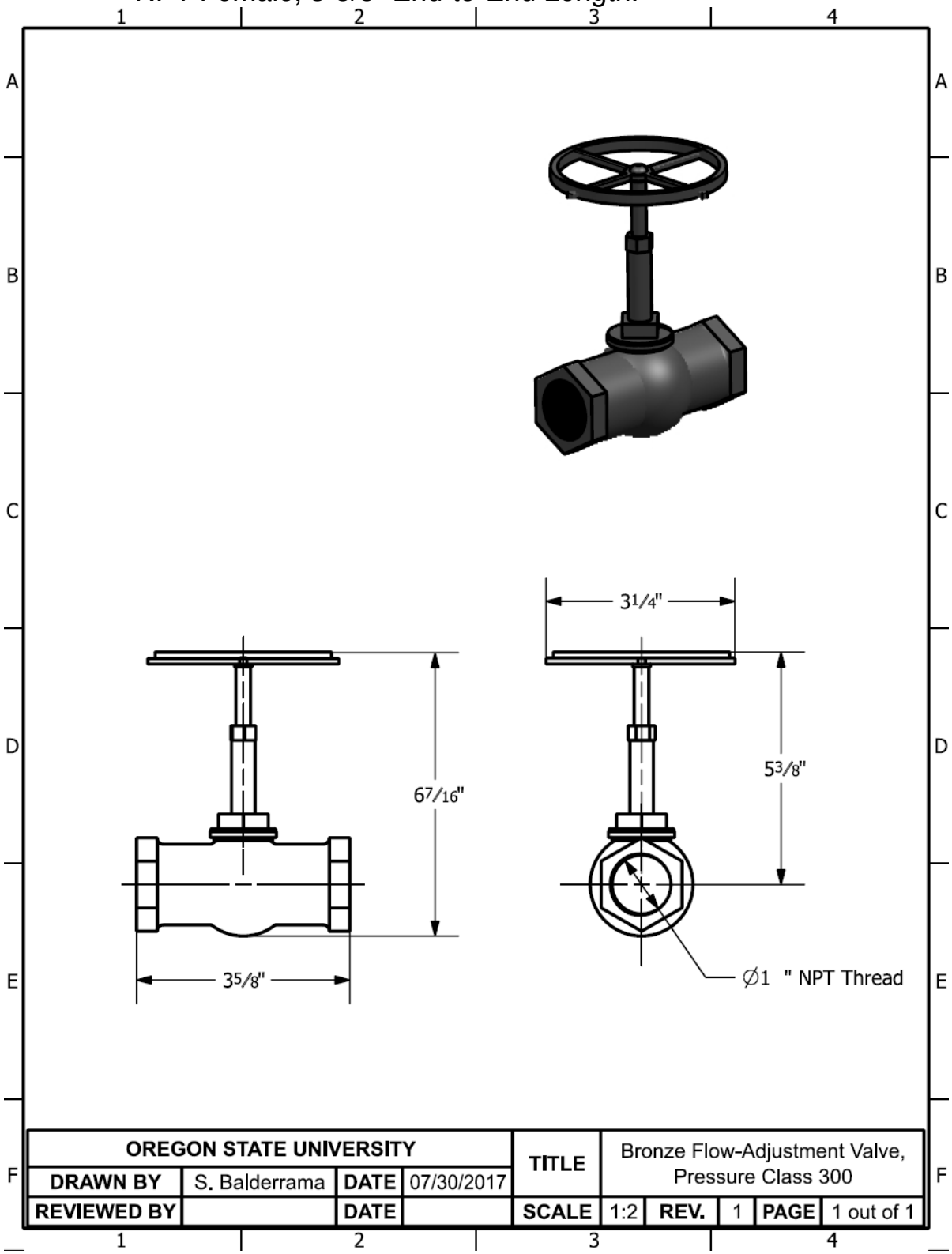

- Bronze Flow-Adjustment Valve, Pressure Class 125

McMaster-Carr, Globe Valve, Straight, 1 NPT Female, 2-15/16” End-to-End Length.

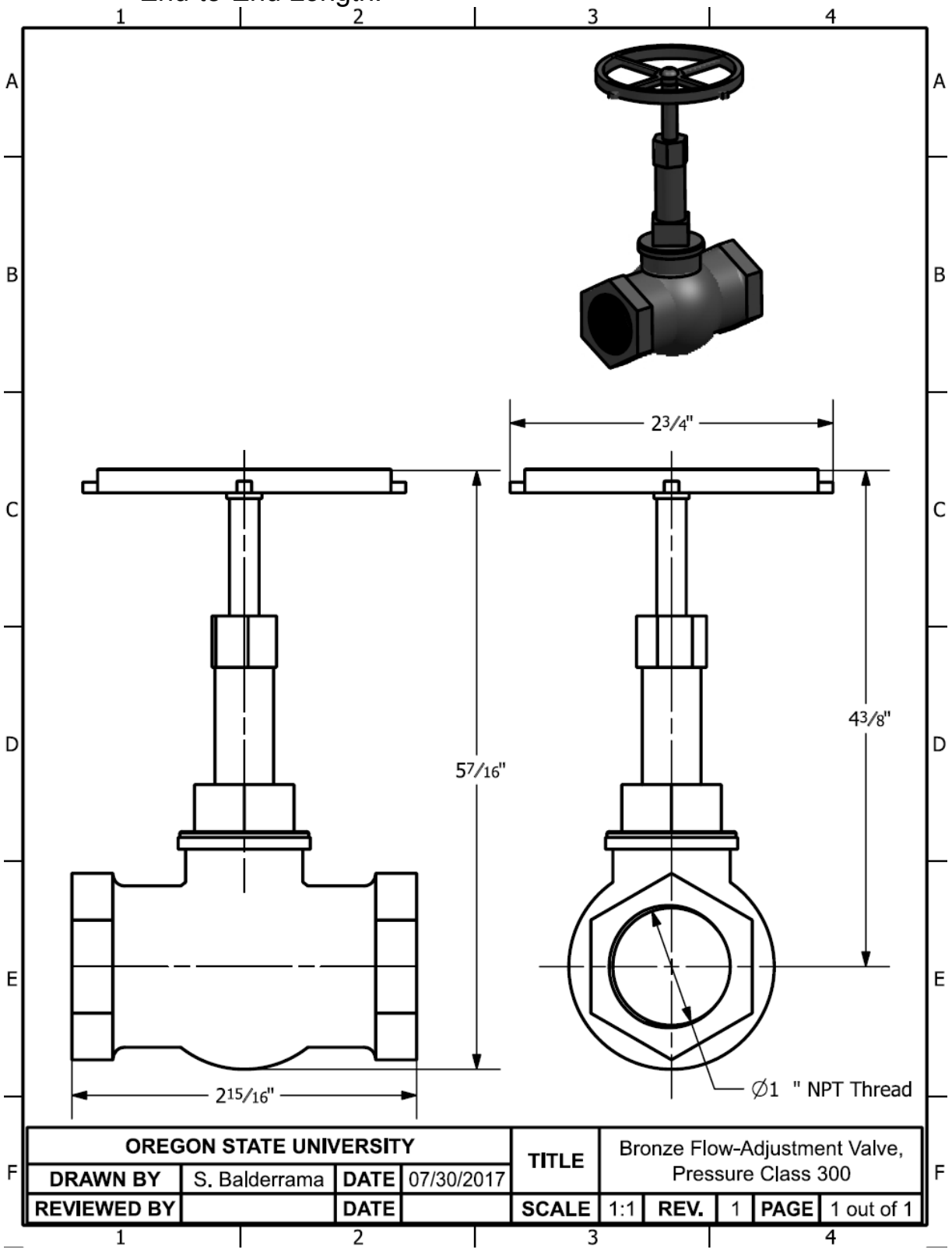

- 90° Elbow Connector

  McMaster-Carr, 90° Elbow Connector, 1 NPT Female, Maximum Steam Pressure 300 psi at 550˚F, Material: Steel, Schedule 80.

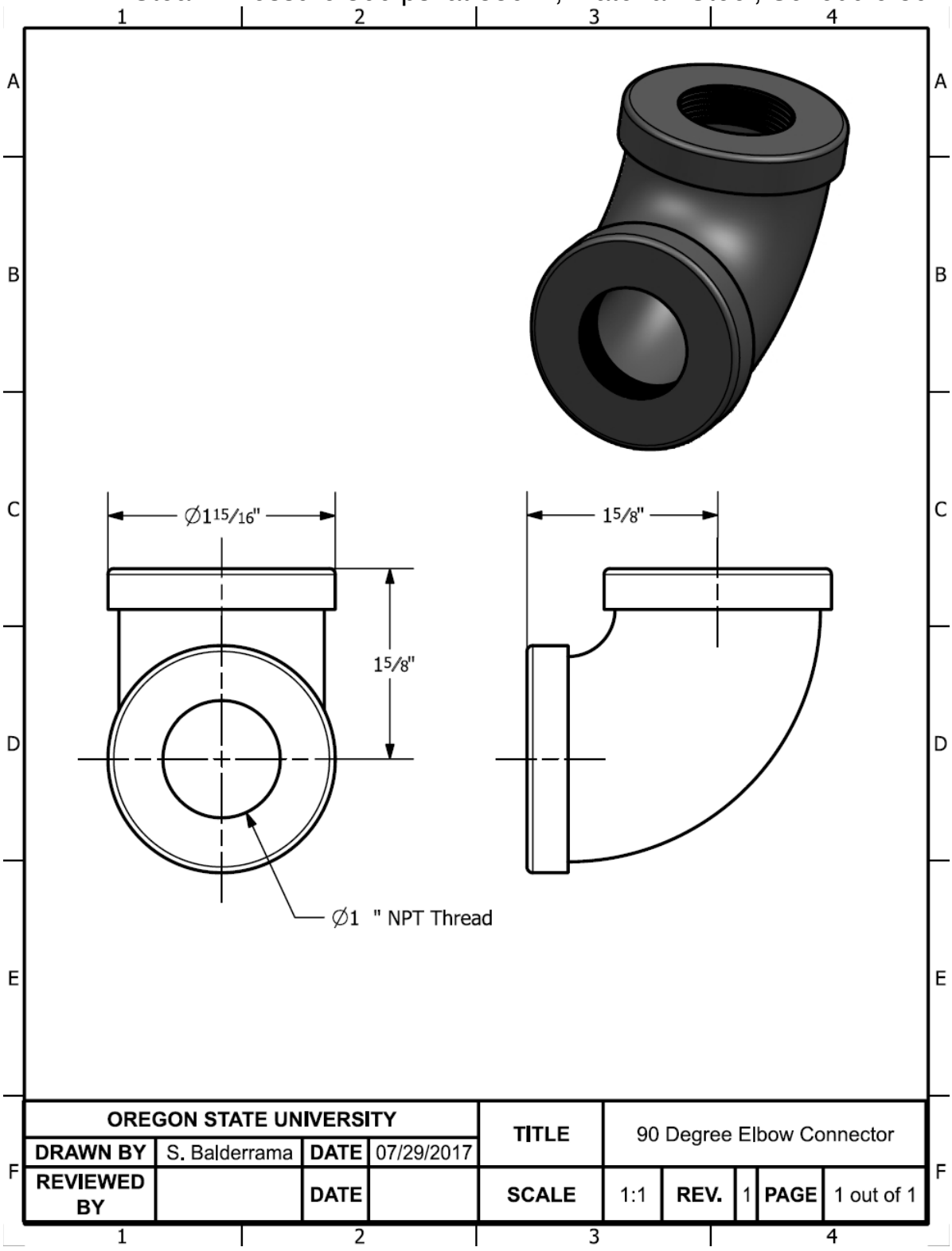

OREGON STATE UNIVERSITY				TITLE	90 Degree Elbow Connector				
DRAWN BY	S. Balderrama	DATE	07/29/2017						
REVIEWED BY		DATE		SCALE	1:1	REV.	1	PAGE	1 out of 1

- Black Steel Pipe

  Grainger, Black Steel Schedule 80 Seamless Pipe, Pipe Size: 1”, Overall Pipe Length: 5 ft., Pipe Thread Type: MNPT x MNPT.

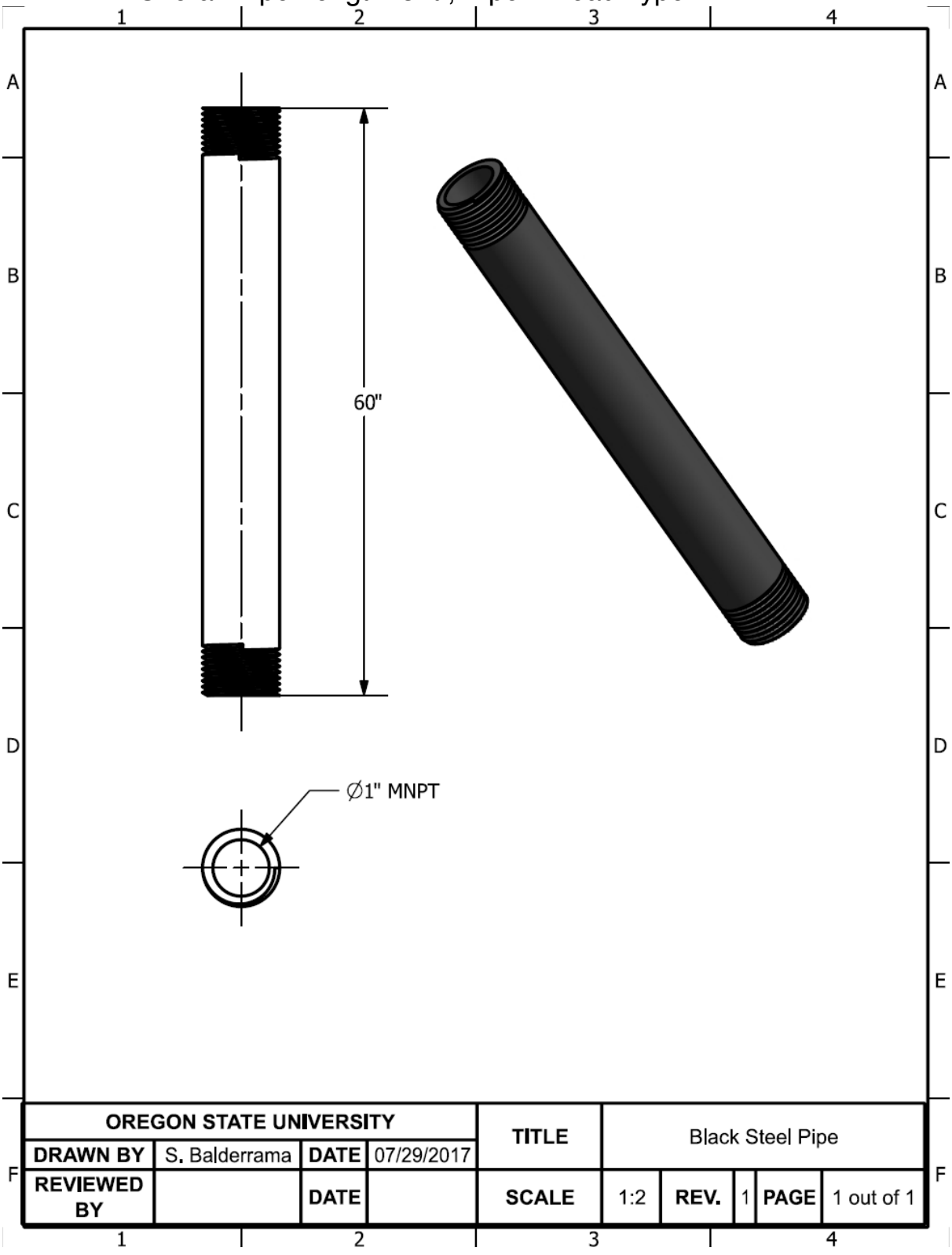

OREGON STATE UNIVERSITY				TITLE	Black Steel Pipe				
DRAWN BY	S. Balderrama	DATE	07/29/2017						
REVIEWED BY		DATE		SCALE	1:2	REV.	1	PAGE	1 out of 1

- Immersion Heater 10” 150# Flange

  250 kW, 480V, 3 PH (301.1 Amps), Density 39 W/in2, Water Steam Application, 3 Circuits, ANSI 150 Lbs., (Stainless Steel Material), Flange 0.475” O.D. Tube Diameter, Incoloy 800 Sheath Material, 68” Immersed Length, 8” Cold Section, Thermocouple Type J for Temperature Control, Themrocouple Type J for High Limit Control, NEMA 7 (Explosion Proof – Class 1, Div. 2, GR. B, C & D Hazloc Classification) Model #FLI36250X1468-TX. 500°F Operating Temperature/ 125 psig Operating Pressure

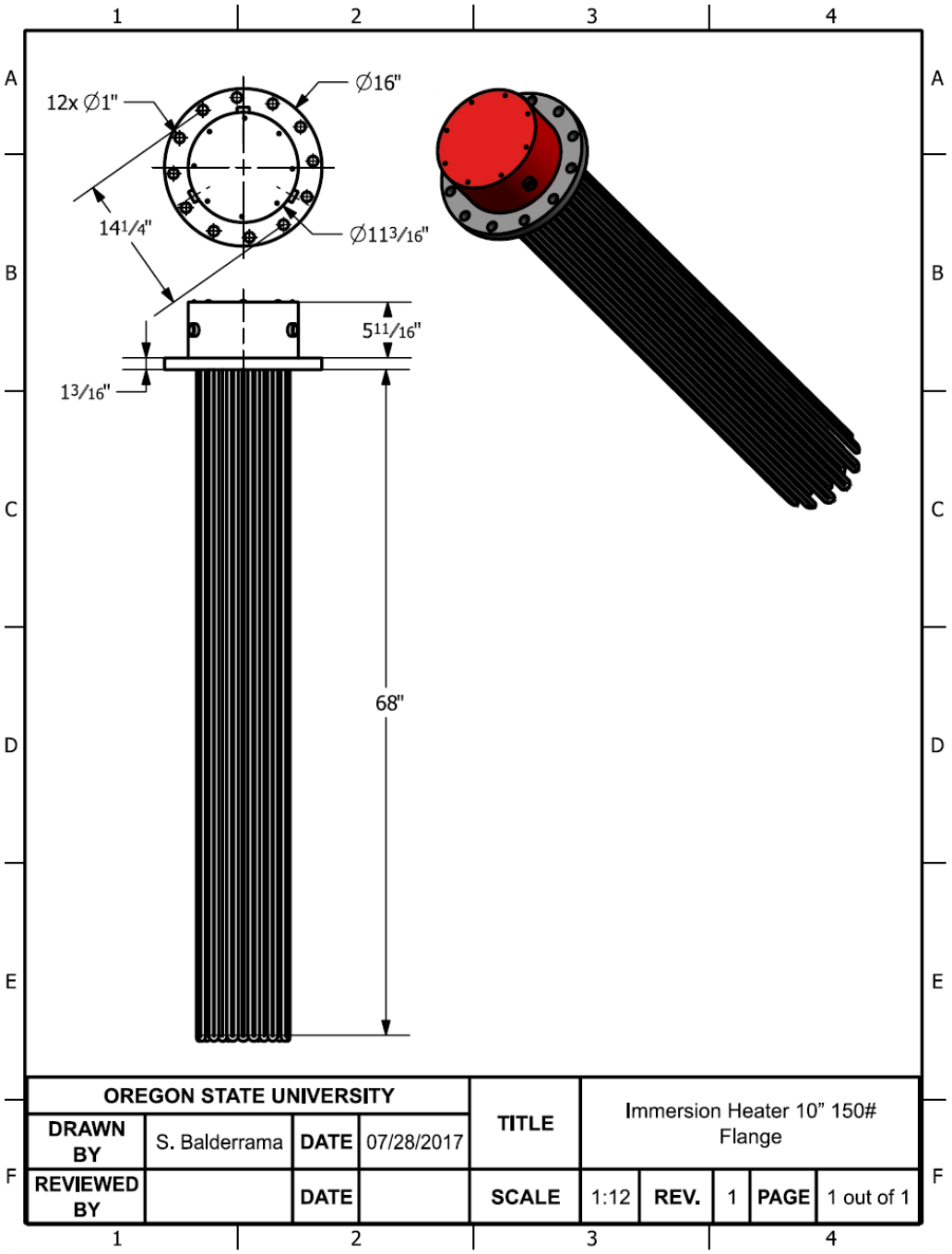

- High-Head Circulation Pump for Water
  McMaster-Carr, Centrifugal Pump, 6 Impeller Stages, 3 HP, 208-240/440-480V AC, Maximum Flow Rate: 20 gpm at 150 ft. of head.

- Differential Pressure Transmitter

Pressure Range: -300 to 300 psi, Output: 4-20 mA with digital signal based on HART protocol, SST Coplanar Flange, Conduit Entry Size: ½-14 NPT.

- Relief Valve

  Grainger, Safety Relief Valve, Material: Bronze, 1” MNPT Inlet, 1-1/4” FNPT Outlet, Factory Set Pressure: 125 psi, Overall Length 1-3/4”.

- Pipe Fitting 1” FNPT to ¼” FNPT

- Control Panel Terminal Box

  WATTCO, Control Panel: Terminal Box Type (Water Resistant), Include: Main Disconnect, Control Transformer, 3 Connectors and Fuses for 3 Loads of 83.33 kW 480V 3PH, 1 Temperature Controller, 2 Position Selector Switch “On-Off”, 3 Greenn Light “Heater On”, Junction Terminals for Thermocouple Type J, Wiring Diagram